Quynh Nhu, Feb 2025

# Micro- and nanoplastics in soil: Analytical methods and environmental fate


**Quynh Nhu Phan Le (MSc. Chem)**

This dissertation is submitted for the degree of

Doctor of Philosophy

**March 2025**

**Lancaster Environment Centre**

This PhD is funded by European Union's Horizon 2020, SOPLAS ITN, grant agreement No 955334.

Quynh Nhu, Feb 2025

# Declaration

I declare that the work in this thesis is my own and has not been submitted for another degree or qualification at any other institution. Many of the ideas in this thesis were the product of discussion with my supervisor Prof. Crispin Halsall, Prof. John Quinton, Dr. Ben Surridge and Dr. Lorna Ashton. Any collaborators involved in this research are properly acknowledged.

Quynh Nhu Phan Le (MSc. Chem)

Lancaster Environment Centre, Lancaster University, UK

# Statement of authorship

This thesis is presented in an alternative format, comprising a collection of seven papers. Three have been published in peer-reviewed journals, while a fourth is currently under review. The remaining three papers have been prepared for submission to journals and are included here in an alternative format. All papers have multiple authors, including co-authors from outside my supervisory team. The details of these papers are outlined below. Chapters 1 and 7 serve as the introduction and conclusion for the thesis and are not intended for submission.

**Chapter 2** is an adapted version of a manuscript currently under review at Analytical and Bioanalytical chemistry.

Phan Le, Q.N., Halsall, C., Peneva, S., Wrigley, O., Braun, M., Amelung, W., Quinton, J., Surridge, B. "Towards quality-assured measurements of microplastics in soils using fluorescence microscopy" (ready for submission)

Q.N.P.L. contributed to the Conceptualisation, Formal Analysis, Investigation, Methodology, Visualisation, Writing – Original Draft Preparation and Writing – Review and Editing.

**Chapter 3** is published as:

Peneva, S.[1], Phan Le, Q.N.[1], Munhoz, D. R.[1], Wrigley, O., Wille, F., Doose, H., Halsall, C., Harkes, P., Sander, M., Braun, M., Amelung, W. "Microplastic analysis in soils: A comparative assessment". Ecotoxicology and Environmental Safety, Volume 289, 2025, 117428, ISSN 0147-6513, https://doi.org/10.1016/j.ecoenv.2024.117428.

[1] shared co-first authorship

Q.N.P.L. contributed to the Conceptualisation, Formal Analysis, Investigation, Methodology, Visualisation, Writing – Review and Editing.

**Chapter 4**: is intended for submission as:

Phan Le, Q.N., Halsall, C., Kunaschk, M., Surridge, B., Ashton, L., Quinton, J., "Transfer of microplastics from sewage sludge to farmland: A case study in the UK"

Q.N.P.L. contributed to the Conceptualisation, Formal Analysis, Investigation, Methodology, Visualisation, Writing – Original Draft Preparation and Writing – Review and Editing.

**Chapter 5:** is intended for submission as:

Phan Le, Q.N., Halsall, C., Kunaschk, M., Surridge, B., Ashton, L., Quinton, J., "Biosolid Amendments as Drivers for Microplastic Pollution in Soils: Measurements and Insights from Multiple Analytical Methods in an agricultural field study"

Q.N.P.L. contributed to the Conceptualisation, Formal Analysis, Investigation, Methodology, Visualisation, Writing – Original Draft Preparation and Writing – Review and Editing.

**Chapter 6:** is intended for submission as:

Phan Le, Q.N., Evangeliou, N., Halsall, C., Quinton, J., Surridge B., Ashton, L., Eckhardt, S., Ruggiero, L., Sciarra, A., Florindo, F., Zaccone, C., Materić, D. "First evidence of nanoplastics in Antarctica soil"

Q.N.P.L. contributed to the Conceptualisation, Formal Analysis, Investigation, Methodology, Visualisation, Writing – Original Draft Preparation and Writing – Review and Editing.

**Appendix 1** is published as

Peneva, S., Phan Le, Q.N., Munhoz, D. R., Wrigley, O., Macan, G. P.F., Doose, H., Amelung, W., Braun, M. "Plastic input and dynamics in industrial composting". Waste Management, Volume 193, 2025, Pages 283-292, ISSN 0956-053X, https://doi.org/10.1016/j.wasman.2024.11.043.

Q.N.P.L. contributed to the Formal Analysis and Writing – Review and Editing.

**Appendix 2** is published as

G. P.F. Macan, M. Anguita-Maeso, C. Olivares-García, Q.N. Phan Le, C. Halsall, B. B. Landa. "Unravelling the plastisphere-soil and plasticplane microbiome of plastic mulch residues in agricultural soils". Applied Soil Ecology, Volume 206, 2025, 105900, ISSN 0929-1393, https://doi.org/10.1016/j.apsoil.2025.105900.

Q.N.P.L. contributed to Methodology, Data curation, and Writing – review & editing.

# Statement of Confirmation

I hereby agree with the above statements:

Professor Crispin Halsall
Lancaster Environment Centre, Lancaster University, UK

# Abstract

Microplastics (MPs) and nanoplastics (NPs) are emerging pollutants in various environments, with soil identified as their largest reservoir. However, their sources, environmental fate, transport mechanisms, and impacts remain poorly understood, primarily due to challenges in analysing MPs and NPs within complex soil matrices. While several analytical approaches exist for microplastic analysis in soil, standardized approaches are lacking, and research on nanoplastic is extremely limited despite their higher toxicity potential.

To address these gaps, this PhD study first developed and optimized a quick and efficient extraction method for MPs from soil, followed by quantification with Nile red staining-fluorescence microscopy for its speed, cost-effectiveness, and high sample throughput (Chapter 2). This method was then compared with digital microscopy, Fourier-transformed infrared and Raman micro-spectroscopies, pyrolysis gas chromatography coupled with mass spectrometry, and quantitative proton nuclear magnetic resonance spectroscopy, each employing tailored extraction protocols (Chapter 3). Testing with spiked MPs of various types, sizes, and soil types (clayey, loamy and sandy) revealed significant impacts of extraction and analytical methods on recovery rates. Fluorescence microscopy was particularly effective for detecting small conventional plastics, while proton nuclear magnetic resonance spectroscopy excelled in analysing biodegradable MPs. Organic matter and clay in the soil matrix were identified as key complicating factors.

Fluorescence microscopy, combined with Raman and Fourier-transformed infrared micro-spectroscopies for chemical identification, was further applied to investigate agricultural soil organic amendments as a major source of soil plastics (Chapter 4 and 5). This included investigation of MPs in sewage sludge and anaerobic digestate from biogas plants, as well as soils treated with these materials. Microplastics as small as 25 µm were detected, with concentrations reaching 3650 MPs/g in sewage sludge and 1050 MPs/g in anaerobic digestate. Amended soils exhibited significantly higher MPs concentrations than control fields, with detailed analyses confirming the transfer of plastics by type, size, and shape.

Additionally, this study developed a novel nanoplastic extraction method coupled with thermal desorption proton transfer reaction mass spectrometry for highly sensitive NPs analysis (Chapter 6). Applying this approach to Antarctic soils revealed NPs concentrations of up to 300 ng/g, with atmospheric source modelling indicating contributions from both local and long-range deposition, alongside clear seasonal patterns.

This PhD research marks a significant advancement in analytical methods for microplastics and nanoplastics in soil, provides critical evidence of agricultural practices and atmospheric transport as plastic contamincation sources, and ultimately delivers essential data for risk assessment and policy development to tackle plastic pollution—one of the most pressing environmental challenges of our time.

# Acknowledgements

I want to sincerely thank my supervisors, Prof. Crispin Halsall, Prof. John Quinton, Dr. Ben Surridge, and Dr. Lorna Ashton, for their continuous support throughout my PhD. I am especially grateful to Cris and John for their invaluable guidance and encouragement. Their belief in me has made a huge difference, and I could not have completed this work without them.

I also deeply appreciate my colleagues at LEC, my officemates, and the Soil Group, as well as my SOPLAS colleagues and supervisors. Their support, kindness, and teamwork have made this PhD journey not only academically fulfilling but also a truly enjoyable and memorable experience. I feel lucky to have made such wonderful friends along the way.

To my best friend, Emilee, thank you for always being there during my PhD. Your support and friendship have been a constant source of strength and joy, and I couldn't have done this without you.

Finally, I want to dedicate this achievement to my family—my mom, dad, and brother—whose love and encouragement have shaped who I am. To my boyfriend, Viet, thank you for standing by my side through it all. Your love and support have been my biggest motivation, and I am forever grateful.

This thesis is a reflection of the incredible people who have supported me, and I dedicate this milestone to all of you.

# Table of Contents

**1 AN INTRODUCTION TO SOIL PLASTIC POLLUTION: SOURCES, ENVIRONMENTAL FATE AND EFFECTS AND ANALYTICAL APPROACHES 19**
1.1 Plastic pollution ..... 20
1.2 Overview of micro- and nanoplastics ..... 21
1.3 Sources of microplastics and nanoplastics in soil ..... 22
*1.3.1 Agricultural practices ..... 22*
*1.3.2 Runoff from the surroundings and atmospheric deposition ..... 23*
1.4 Environmental fate and behaviours of plastics in soil ..... 24
*1.4.1 Degradation of plastics ..... 24*
*1.4.2 Release behaviours of plastic additives in agricultural soil ..... 25*
*1.4.3 The sorption behaviours of pollutants onto plastics ..... 26*
*1.4.4 Transport of microplastics and nanoplastics ..... 26*
1.5 Environmental effects of microplastics and nanoplastics in soil ..... 27
*1.5.1 Effects of microplastics and nanoplastics on soil properties ..... 27*
*1.5.2 Effects of microplastics and nanoplastics on soil organisms ..... 28*
*1.5.3 Effects of microplastics and nanoplastics on soil $CO_2$ emissions ..... 29*
1.6 Plastic analysis in soil: state of the arts and challenges ..... 30
*1.6.1 Soil sampling for microplastics and nanoplastics analysis ..... 31*
*1.6.2 Extraction of microplastics and nanoplastics in soil ..... 31*
*1.6.3 Identification and quantification of microplastics and nanoplastics in soil ..... 33*
1.7 Knowledge gap and thesis aim ..... 36
References ..... 39

**OVERVIEW TO THE THESIS ..... 49**

**2 TOWARD QUALITY-ASSURED MEASUREMENTS OF MICROPLASTICS IN SOIL USING FLUORESCENCE MICROSCOPY ..... 51**
Abstract ..... 53
2.1 Introduction ..... 54
2.2 Materials and methods ..... 55
*2.2.1 Preparation of soil and microplastic standards ..... 55*
*2.2.2 Extraction of microplastics from soils ..... 56*
*2.2.3 Fluorescence microscopy and image analysis ..... 56*
*2.2.4 Quality assurance and quality control ..... 57*
2.3 Results and discussion ..... 58
*2.3.1 Recovery of various large microplastic particles ..... 58*
*2.3.2 Recovery of small microplastics ..... 61*
*2.3.3 Comparison of fluorescence microscopy with FTIR microspectroscopy ..... 66*
2.4 Conclusions ..... 67
References ..... 68
Supporting information ..... 73

**3 MICROPLASTIC ANALYSIS IN SOIL: A COMPARATIVE ASSESSMENT 88**
Abstract ..... 90

3.1 Introduction ..... 91
3.2 Materials and methods ..... 93
*3.2.1 Soil used for spike-recovery experiments.* ..... *93*
*3.2.2 Plastic materials used for recovery experiments.* ..... *94*
*3.2.3 Spiking of soil samples* ..... *94*
*3.2.4 Data Analysis* ..... *98*
3.3 Results ..... 98
*3.3.1 Recovery of large microplastics* ..... *98*
*3.3.2 Recovery of small microplastics* ..... *101*
3.4 Discussion ..... 103
*3.4.1 Microplastic properties as affected by the extraction method* ..... *103*
*3.4.2 Implications for the extraction of large microplastics* ..... *105*
*3.4.3 Implications for the extraction of small microplastics* ..... *108*
3.5 Conclusions ..... 110
References ..... 112
Supporting Information ..... 117

**4 TRANSFER AND LOADING OF MICROPLASTICS IN SEWAGE-SLUDGE AMENDED AGRICULTURAL SOIL ..... 133**
Abstract ..... 134
4.1 Introduction ..... 135
4.2 Materials and methods ..... 136
*4.2.1 Sewage sludge and soil sampling* ..... *136*
*4.2.2 Microplastic extraction from sewage sludge and soil matrices* ..... *137*
*4.2.3 Identification and characterisation of microplastics* ..... *138*
*4.2.4 Quality assurance and quality control* ..... *138*
*4.2.5 Statistical analysis* ..... *139*
4.3 Results ..... 139
*4.3.1 Microplastics in digested sewage sludge* ..... *139*
*4.3.2 Microplastics in sludge-amended and background soils* ..... *140*
4.4 Discussion ..... 143
*4.4.1 Microplastics in sewage sludge* ..... *143*
*4.4.2 Microplastics in sludge-amended soil* ..... *145*
*4.4.3 Wider implications* ..... *149*
4.5 Conclusions ..... 150
References ..... 151
Supporting information ..... 155

**5 BIOSOLID AMENDMENTS AS DRIVERS FOR MICROPLASTIC POLLUTION IN SOILS: MEASUREMENTS AND INSIGHT FROM MULTIPLE ANALYTICAL METHODS IN AN AGRICULTURAL FIELD STUDY ..... 171**
Abstract ..... 172
5.1 Introduction ..... 173
5.2 Materials and methods ..... 174
*5.2.1 Anaerobic digestate and soil sampling* ..... *174*
*5.2.2 Microplastic extraction* ..... *175*
*5.2.3 Identification and characterisation of microplastics* ..... *177*
*5.2.4 Quality assurance and quality control* ..... *178*
*5.2.5 Statistical analysis* ..... *178*
5.3 Results ..... 178

*5.3.1 Microplastics in anaerobic digestate* ..... *178*
*5.3.2 Microplastics in digestate-amended soil* ..... *179*
*5.3.3 Comparison between fluorescence microscopy and FTIR* ..... *180*
*5.3.4 Comparison between Raman and FTIR for fibre analysis* ..... *182*
5.4 Discussion ..... 183
*5.4.1 Microplastics in anaerobic digestate* ..... *183*
*5.4.2 Microplastics in biosolid-amended soils* ..... *184*
*5.4.3 Variation in microplastic concentrations based on analytical methods* ..... *185*
5.5 Conclusions ..... 187
References ..... 188
Supporting information ..... 192

**6 FIRST EVIDENCE OF NANOPLASTIC IN ANTARCTICA SOIL ..... 195**
Abstract ..... 197
6.1 Introduction ..... 198
6.2 Materials and methods ..... 199
*6.2.1 Site description* ..... *199*
*6.2.2 Soil sampling* ..... *199*
*6.2.3 Microplastic analysis* ..... *200*
*6.2.4 Nanoplastic analysis* ..... *201*
*6.2.5 Quality assurance and quality control* ..... *202*
*6.2.6 Lagrangian dispersion modelling* ..... *203*
6.3 Results ..... 204
*6.3.1 Microplastics concentration in Antarctica soil* ..... *204*
*6.3.2 Nanoplastic concentration in Antarctica soil* ..... *205*
*6.3.3 Potential plastic emission sources* ..... *206*
6.4 Discussion ..... 207
*6.4.1 Occurrence of microplastics in Antarctica* ..... *207*
*6.4.2 Occurrence of nanoplastics in Antarctica* ..... *208*
*6.4.3 Source of microplastics and nanoplastics to Antarctica* ..... *210*
*6.4.4 Analytical limitations of the present study* ..... *212*
6.5 Conclusions ..... 213
References ..... 215
Supporting information ..... 221

**7 CONCLUSION ..... 229**
7.1 Synopsis of results ..... 229
7.2 Concluding remarks ..... 230
*7.2.1 Environmental aspects: sources and behaviour of plastic in soil* ..... *230*
*7.2.2 Analytical aspect: challenges and advance* ..... *234*
*Key takeaways and recommendations* ..... *234*
7.3 Future research ..... 235
*7.3.1 Analytical advancement* ..... *235*
*7.3.2 Environmental aspects* ..... *235*
7.4 Addressing plastic contamination in agricultural soils ..... 236

**8 APPENDICES ..... 1**

# List of Tables

**Table 1.1.** An overview of commonly used of plastics and their characteristics ..... 19

**Table 3.1.** Physicochemical properties of soils used for comparative method assessment ..... 94

**Table 3.2.** Characteristics of plastics used for method testing .....96

**Table 3.3.** Mean recoveries (%) with standard error (SE) of large MPs (0.5 - 1 mm) for all types of soils; all using microscopical techniques. .....100

# List of Figures

**Figure 1.1.** A schematic showing the extraction and separation steps of the MPs-soil measurement procedure.....56

**Figure 2.2.** Fluorescence image of different polymer types (from left to right: nylon, PS, PET, PVC, PBAT/PLA, PP, LDPE, HDPE) with dia. 500-1000 µm after being extracted from the soil matrix. The MPs were stained with NR, illuminated under 470 nm, and observed through a green filter set. Black PBAT/PLA, which exhibited no fluorescence signal, was captured and analysed in brightfield mode. .....60

**Figure 2.3**. Bright-field (a, c) and fluorescence images (b, d) of nylon before and after extraction from soil, respectively.....61

**Figure 2.4.** MPs recovery for different polymers and MPs size classes across the three soil types. Percent recoveries are reported as a mean of three replicates with standard deviation error bars.....63

**Figure 2.5.** Box and whisker plot displaying the MPs number concentrations in soil samples (n=6) collected from the Hazelrigg field station, as measured by fluorescence microscopy and FTIR spectroscopy methods.....66

**Figure 3.1.** Illustration of main approaches used for microplastic extraction (SOM = soil organic matter; for additional information on the methods, see also Table S3, Supplementary Materials). .....97

**Figure 3.2** Recoveries in percent of added number of particles on the y-axis, of small particles, for LDPE and PBAT/ PLA with methods using particle counting, i.e., method B – Fluorescence microscopy, method C2 – FPA-µ-FTIR and method C3 - µ-Raman microscopy and methods assessing bulk polymer amounts, i.e., method C4 - Py-GC-MS and method D - $^{1}$H-NMR. Note that $^{1}$H-NMR allowed a differentiation of PBAT and PLA from the added Mulch-derived MPs; hence, both polymers are displayed separately. The solvent used for the Soxhlet-extraction was chosen exclusively for PBAT/PLA and Py-GC-MS failed to identify PLA. Error bars represent standard errors.....104

**Figure 4.1.** Characterization of SMPs in digested sludge cake, including polymer mean compositions for total SMPs (a), the size distribution for both particle like

and elongated (fibre-like) SMPs, errors bars represent the standard deviation of size distribution of sewage sludge samples (n=3) (b) and the mean proportion of each shape for each polymer type (c). ..... 140

**Figure 4.2.** Mean of total SMPs, particle-like and elongated SMPs in sludge-amended agricultural soil, non-amended agricultural and non-agricultural soils. Each boxplot indicates the median (central mark) and 25th and 75th percentiles, with whiskers outside the box indicating the 10th and 90th percentiles. Points outside the whiskers indicate outliers..... 141

**Figure 4.3.** Polymer composition (a), proportion (%) of shape for each polymer (with number on each bar represent the actual concentration (MPs/g) (b) and size distribution for each shape for sludge-amended agricultural, non-amended agricultural and non-agricultural background soil, errors bars represent the standard deviation of size distribution of sewage sludge samples (c) ..... 142

**Figure 4.4.** Comparison between expected MPs concentration for each polymer type in soil based on two sewage sludge applications, and the MPs concentration within sludge-amended soil measured in this study. ..... 146

**Figure 5.1.** A schematic of the extraction protocol for MPs from digestate and soil samples, along with the analytical methods used for comparison. The bottom panel showcases images obtained using different techniques—colour, fluorescence, and u-FTIR—along with an overlay of these images for the same sample filter. ..... 174

**Figure 5.2.** MPs characteristics of AD measured by FPA-µ-FTIR. Figure 1a presents the proportion of each polymer detected. Figure 1b illustrates the distribution of particle shapes for each polymer type, with the numbers on the columns representing the concentration (MPs/g) for each shape. Figure 1c shows the proportion of each size class based on the Feret diameter of the detected MPs.... 167

**Figure 5.3.** Polymer composition, shape, and size distribution of microplastics in biosolid-amended soil (a, c, e) and background soil (b, d, f). Pie charts (a, b) show the proportion of polymers detected. Bar charts (c, d) illustrate the proportion of elongated versus particle-like microplastics across polymer types, with the numbers on the columns representing the concentration (MPs/g) for each shape. Pie charts (e, f) represent the size distribution of the detected MPs based on their Feret diameters. ..... 179

**Figure 5.4.** Comparison of MPs detection results using FM and FTIR spectroscopy on a single Anodisc filter (25 mm diameter). The central image shows an overlay of RGB, fluorescence, and FTIR images of the sample filter with highlighted regions. Insets illustrate: (a) MPs detected by both FTIR and FM, (b) MPs detected by FM but not FTIR, (c) MPs not detected by either method, and (d) MPs detected by FTIR but not FM. Individual panels display FM, FTIR, RGB, and overlay images to compare detection performance across methods ..... 180

**Figure 5.5.** Comparison of MPs concentrations obtained by different methods on a subset of biosolid amended samples. Total MPs concentrations (a) and particle-like MPs (b) were measured using µ-FTIR and FM, while elongated MPs (c) were

quantified using µ-Raman, µ-FTIR, and FM. Raman spectra (d) confirm the identification of PP, PE, and PEST. Microscopic images (e) show representative PP, PE, and PEST fibres with scale bar ..... 182

**Figure 6.1.** Sampling locations in the McMurdo Dry Valleys, Antarctica. The main map shows the proximity of Taylor Valley and Wright Valley to the Ross Ice Shelf, Ross Sea and some research stations, with detailed views of sampling points (red dots) in both valleys. The inset map provides the broader geographical context of the McMurdo Dry Valleys within Antarctica. ..... 200

**Figure 6.2.** Workflow for MPs and NPs extraction from soil ..... 202

**Figure 6.3.** Morphological diversity of MPs visualized under GFP Filter fluorescence microscopy using Nile Red staining ..... 204

**Figure 6.4.** NPs concentration (ng/g) and composition across different sites in Taylor and Wright Valleys. The bar chart illustrates NPs concentrations at individual sampling sites (Site ID; see **Figure** 6.1.), categorized by polymer type. The # symbol indicates sites where deeper soil samples were collected. Uncertainty bars represent general PTR-MS quantification associated uncertainty of 30%. The pie chart shows the overall NPs composition across all sites. ..... 205

**Figure 6.5.** Footprint emission sensitivity for deposited NPs in Antarctic summer (left) and in all other months (right) expressed in mg $m^2$ $month^{-1}$ per kg $s^{-1}$. At each grid cell, the colours show the simulated accumulated monthly deposition flux ($mg/m^2$) at the receptor (white diamond) for a unit emission source (kg $s^{-1}$) in this respective grid cell. ..... 207

# List of Abbreviations and Acronyms

| | |
|---|---|
| ABS | Acrylonitrile Butadiene Styrene |
| AD | Anaerobic Digestate |
| $Al_2O_3$ | Aluminium Oxide |
| ANOVA | Analysis of Variance |
| ATR | Attenuated Total Reflectance |
| dia. | Diameter |
| DOC | Dissolved Organic Carbon |
| FM | Fluorescence Microscopy |
| FTIR | Fourier Transform Infrared Spectroscopy |
| $FeSO_4$ | Iron (II) Sulphate |
| $H_2O$ | Water |
| $H_2O_2$ | Hydrogen Peroxide |
| $H_2SO_4$ | Sulphuric acid |
| HDPE | High-Density Polyethylene |
| HPLC | High-Performance Liquid Chromatography |
| LDPE | Low-Density Polyethylene |
| LMP | Large Microplastics (≥ 500 µm) |
| LOD | Limit of Detection |
| LOQ | Limit of Quantification |
| MPs | Microplastic |
| NPs | Nanoplastic |
| NR | Nile Red |
| NaCl | Sodium Chloride |
| PA | Polyamide |
| PBAT | Polybutylene Adipate Terephthalate |
| PC | Polycarbonate |
| PE | Polyethylene |
| PEST | Polyester |
| PET | Polyethylene Terephthalate |
| PLA | Polylactic Acid |
| PMMA | Polymethyl Methacrylate |
| PP | Polypropylene |
| PS | Polystyrene |
| PUR | Polyurethane |
| PVC | Polyvinyl Chloride |
| Py-GCMS | Pyrolysis-Gas Chromatography/Mass Spectrometry |
| SBS | Styrene-Butadiene-Styrene |
| SD | Standard Deviation |
| SMP | Small Microplastics (25-500 µm) |
| SOM | Soil Organic Matter |
| TD-PTR-MS | Thermal Desorption-Proton Transfer Reaction-Mass Spectrometry |
| TOC | Total Organic Carbon |
| TOF | Time Of Flight |
| TWP | Tire Wear Particles |

| | |
|---|---|
| $ZnCl_2$ | Zinc Chloride |
| rpm | Rounds Per Minute |
| RSD | Relative Standard deviation |
| $^1$H-NMR | Proton Nuclear Magnetic Resonance Spectroscopy |
| $\rho$ | Density (g/cm$^3$) |
| $\Theta$ | Pore Width |
| WWTP | Wastewater treatment plant |

# List of Appendices

Appendix 1: Plastic input and dynamic in industrial composting ..... 2

Appendix 2: Unravelling the plasticsphere-soil and plasticplane microbiome of plastic mulch residues in agricultural soils .....13

# List of Outputs

## Publication

1. Phan Le, Q.N., Halsall, C., Peneva, S., Wrigley, O., Braun, M., Amelung, W., Ashton, L., Surridge, W.J.B., Quinton, J. Towards quality-assured measurements of microplastics in soil using fluorescence microscopy. *Analytical Bioanalytical Chemistry* (2025). https://doi.org/10.1007/s00216-025-05810-6
2. Peneva, S., Phan Le, Q.N., Munhoz, R.D., Wrigley, O., Macan P.F.G., Doose, H., Amelung, W., Braun, M., Plastic input and dynamics in industrial composting, Waste Management, Volume 193, 2025, Pages 283-292, ISSN 0956-053X, https://doi.org/10.1016/j.wasman.2024.11.043.
3. Peneva, S., Phan Le, Q.N., Munhoz, R.D., Wrigley, O., Wille, F., Doose, H., Halsall, C., Harkes, P., Sander, M., Braun, M., Amelung, W., Microplastic analysis in soils: A comparative assessment, Ecotoxicology and Environmental Safety, Volume 289, 2025, 117428, ISSN 0147-6513, https://doi.org/10.1016/j.ecoenv.2024.117428.
4. Macan, P.F.G., Anguita-Maeso, M., Olivares-García, C., Phan Le, Q.N., Halsall, C., Landa, B.B., Unravelling the plastisphere-soil and plasticplane microbiome of plastic mulch residues in agricultural soils, Applied Soil Ecology, Volume 206, 2025, 105900, ISSN 0929-1393, https://doi.org/10.1016/j.apsoil.2025.105900.

## Conferences

1. **Main convener** at EGU conference (2024). Session title: Plastics in arable soils: Where do we stand?
2. Poster presentation at EGU conference (2024): Phan Le, Q.N., Halsall, C., Kunaschk, M., Surridge, B., Ashton, L., Quinton, J., "Sewage sludge in farmland: A gateway to microplastic pollution?"
3. Oral presentation at EGU conference (2023). Phan Le, Q.N., Halsall, C., Peneva, S., Wrigley, O., Braun, M., Amelung, W., Quinton, J., Surridge, B. "Towards quality-assured measurements of microplastics in soils using fluorescence microscopy"
4. Poster presentation at SETAC conference (2023): Phan Le, Q.N., Halsall, C., Peneva, S., Wrigley, O., Braun, M., Amelung, W., Quinton, J., Surridge,

B. “Towards quality-assured measurements of microplastics in soils using fluorescence microscopy”

# 1 An introduction to soil plastic pollution: sources, environmental fate and effects and analytical approaches

*This chapter provides an overview of plastic pollution, introducing microplastics and nanoplastics as emerging contaminants before focusing on soil as one of the largest reservoirs of plastic accumulation. It presents a literature review on the fate of plastics in soil and their ecological impacts, followed by a discussion on analytical approaches, highlighting key challenges and advancements in detection and quantification. Finally, the chapter transitions into the thesis's aims and objectives, positioning the research within the broader context of soil plastic pollution, analytical advancements, and environmental significance.*

## 1.1 Plastic pollution

Plastic, a versatile and transformative material, emerged as a ground-breaking innovation in the early 20th century, with the first fully synthetic plastic, Bakelite, invented in 1907 (Geyer et al., 2017). Its development marked the beginning of a new era, enabling the creation of lightweight, durable, and cost-effective products. Post-World War II, the "plastic boom" revolutionized industries, from packaging and construction to healthcare and transportation. By the 1960s, plastic production surged, driven by its ability to replace traditional materials like wood, metal, and glass (Geyer et al., 2017).

Plastics are synthetic organic polymers thermo-plastics or thermo-set properties (synthesized from hydrocarbon or biomass raw materials), elastomers (e.g., butyl rubber), material fibres, monofilament lines, coatings and ropes (Uhrin & Kershaw, 2020). Many plastics are manufactured as composites of multiple polymers, often combined with additives such as plasticizers, colorants, stabilizers, and other functional substances. Plastics are broadly categorized into two primary types: thermoplastics, which soften and can be reshaped when heated, including materials like polyethylene, polypropylene, and polystyrene; and thermosets, which are rigid and cannot be reformed after curing, such as polyurethane, paints, and epoxy resins. Approximately 15% of total synthetic polymer production is dedicated to fibres like polyester and acrylic (UNEP, 2021).

**Table 1:** An overview of commonly used of plastics (Lassen et al., 2015).

| Plastic Type | Abbreviation | Chemical Structure | Common Uses |
|---|---|---|---|
| Low-Density Polyethylene | LDPE | (-$CH_2$-$CH_2$-) n | Plastic bags, squeeze bottles, film wraps |
| High-Density Polyethylene | HDPE | (-$CH_2$-$CH_2$-) n | Containers, pipes, cutting boards |
| Polypropylene | PP | (-$CH(CH_3)$-$CH_2$-) n | Food containers, automotive parts, textiles |
| Polyvinyl Chloride | PVC | (-$CH_2$-CHCl-) n | Pipes, medical devices, flooring, cables |
| Polyethylene Terephthalate | PET | (-CO-$C_6H_4$-CO-O-$CH_2$-$CH_2$-O-) n | Beverage bottles, food packaging, fibres for textiles |
| Polystyrene | PS | (-$CH(C_6H_5)$-$CH_2$-) n | Disposable cutlery, insulation, foam packaging |
| Polymethyl Methacrylate | PMMA | (-$CH_2$-$C(CH_3)$ ($COOCH_3$)-) n | Acrylic glass, lenses, signage, lighting covers |
| Polyamide | PA | (-NH-($CH_2$) x-CO-)n | Textiles, ropes, gears, automotive parts |
| Polylactic Acid | PLA | (-$C(CH_3)(COOCH_3)$-O-)n | Food packaging, disposable utensils, medical implants |
| Polybutylene Adipate Terephthalate | PBAT | (-O-($CH_2$)$_4$-OCO-$C_6H_4$-CO-)n | Compostable bags, food wraps, agricultural films |

The very qualities that make plastics so valuable—durability and resistance to degradation—have also created a significant environmental challenge: plastic pollution. To date, an estimated 8,300 million tonnes of virgin plastics have been produced (Geyer et al., 2017). By 2015, approximately 6,300 million tonnes of plastic waste had been generated, of which only 9% was recycled, 12% was incinerated, with 79% (by far the largest fraction) deposited in landfills or the natural environment. If current production and waste management trends persist, it is projected that 12,000 million tonnes of plastic waste will have accumulated in landfills or the environment by 2050 (Geyer et al., 2017). The economic costs of marine plastic pollution, including its impacts on tourism, fisheries, aquaculture, and cleanup efforts, were estimated at US$6–19 billion globally in 2018 (UNEP, 2021). Moreover, by 2040, businesses could face an annual financial risk of US$100 billion if governments mandate them to cover waste management costs based on projected plastic volumes and recyclability (UNEP, 2021). Beyond these economic implications, the long-term effects of plastic-associated chemicals on human health remain a critical area of concern. Growing evidence highlights risks such as endocrine disruption and carcinogenicity (UNEP, 2021), emphasizing the urgent need for sustainable strategies to address the pervasive issue of plastic pollution.

## 1.2 Overview of micro- and nanoplastics

'Plastic' covers a very wide range of compositions, size, shape and other properties which all influence the distribution, fate and effects in the environment and need to be accounted for where possible. Microplastics (MPs), defined as plastic particles less than 5 mm in size, are categorized into primary and secondary microplastics (Andrady, 2011). Primary MPs are intentionally manufactured and released into the environment in the form of small particles. Examples include microbeads added to personal care products like exfoliating scrubs and shower gels. They also arise from the wear and tear of larger plastic items, such as tire erosion during driving or the shedding of synthetic fibres from textiles during washing. Secondary MPs result from the fragmentation of larger plastic debris into smaller particles after exposure to environmental conditions, particularly in marine ecosystems. Processes like photodegradation and weathering break down improperly managed waste, such as discarded plastic bags or lost fishing nets, into MP fragments (Andrady, 2011). MPs are pervasive in terrestrial, freshwater, and marine environments, where they are ingested by a wide range of organisms, often leading to bioaccumulation and biomagnification (Thompson et al., 2024).

Nanoplastics (NPs), a subcategory of MPs formed through degradation, are defined as extremely small particles typically ranging from 1 to 1,000 nm in size (UNEP, 2021). Gigault et al. (Gigault et al., 2018) describe NPs as "particles unintentionally produced from the degradation or manufacturing of plastic objects, exhibiting colloidal behaviour." Their high surface area-to-volume ratio enhances their ability to adsorb organic pollutants and hazardous contaminants. Due to their minute size, NPs can enter the food chain when ingested by unicellular and multicellular marine organisms (UNEP, 2021). Additionally, they are highly polydisperse and often form hetero aggregates with natural or anthropogenic materials, which further influences their colloidal behaviour (Gigault et al., 2018). Despite their environmental prevalence, the environmental and health impacts of NPs on organisms, including humans, remain poorly understood. Further research is essential to uncover their ecological and toxicological effects.

MPs and NPs have emerged as a significant threat to terrestrial ecosystems, with soils potentially representing the largest global reservoirs of MPs (Hurley, Rachel R. & Nizzetto, 2018). However, research on plastics in soil remains limited due to unique challenges. The inherent heterogeneity of soil complicates sampling and quantification, while the absence of standardized methods for isolating and identifying MPs and NPs from complex soil matrices hampers comparability across studies. This gap underscores the urgent need for targeted research on soil systems to better understand the distribution, persistence, and ecological impacts of plastic pollution in terrestrial environments.

## 1.3 Sources of microplastics and nanoplastics in soil

Hurley and Nizzetto and Nizzetto *et al.* (Hurley, Rachel R. & Nizzetto, 2018) separated MPs sources into three categories: (1) inputs from agricultural practices; (2) runoff from the surroundings and deposition (e.g., from air and precipitation) and (3) the fragmentation of larger discarded plastic debris.

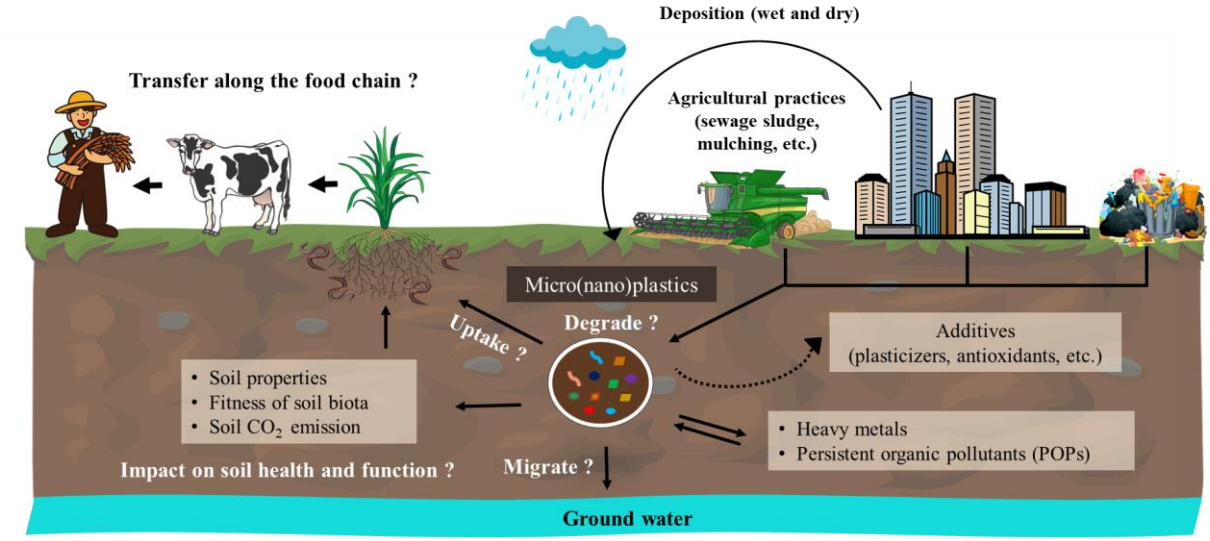


**Figure 2:** A simplified illustration of input pathways, environmental fate and impact of MPs and NPs in soils.

### 1.3.1 Agricultural practices

Plastics have greatly improved agricultural productivity and profitability, e.g., through the use of greenhouse cultivation and mulch films. However, their deliberate use in farming leads to direct plastic contamination of soils. Additionally, plastics entering soils indirectly through application of wastewater irrigation, sewage sludge, and municipal compost produced from biological waste collected in our growing cities, raising environmental concerns (Bläsing & Amelung, 2017a). While these practices promote a Circular Economy and benefit farmers, they also introduce plastics of various sizes and compositions, now recognized as a significant environmental issue in the European Strategy for Plastics in a Circular Economy (EC, 2018a) and the European Plastic Waste Strategy (EC, 2018b).

Sewage sludge is commonly repurposed as agricultural fertilizer, with around 50% recycled for this use in Europe and North America (Nizzetto et al., 2016). Wastewater

treatment plants efficiently trap MPs, primarily in the solid sludge phase (Murphy et al., 2016). For example, Mahon et al. found up to 15,800 microplastic particles $kg^{-1}$ and demonstrated that pre-treatment methods like lime stabilization, anaerobic digestion, and thermal drying do not effectively remove microplastics. Sources of MPs and NPs in WWTPs include cosmetic microbeads, synthetic garment fibres, tire debris, fragmented plastics from urban runoff, and NPs from cosmetics (da Costa et al., 2016a; Murphy et al., 2016). Polymeric flocculants used in wastewater treatment may also contribute to MP contamination (Hurley, Rachel R. & Nizzetto, 2018).

Compost, a common agricultural fertilizer, is a potential source of plastic contamination. In the EU, compost production reached 18 million tons in 2008, with a projected 37% increase by 2020 (ARCADIS, 2010). Bio-waste compost often contains plastic due to improper disposal and insufficient waste separation. Studies at composting facilities revealed residual plastics in final products, despite sieving and manual sorting. Visible plastic concentrations ranged from 2.38 to 180 mg $kg^{-1}$, with smaller particles also detected. Annual plastic inputs to fields from compost may range from 0.016–1.2 kg $ha^{-1}$ (7 t $ha^{-1}$) to 0.08–6.3 kg $ha^{-1}$ (35 t $ha^{-1}$) (Bläsing & Amelung, 2017b).

Plastic mulching, a widespread agricultural technique, boosts harvests and crop quality by increasing soil temperature and enhancing water efficiency (Zhao et al., 2016). Covering 4,270 $km^2$, it is the largest agricultural surface application in Europe (Scarascia-Mugnozza et al., 2012), with global use projected to grow 5.7% annually until 2019 (Transparency Market Research, 2013). Common polymers include LDPE and HDPE, with 700,000 t of LDPE used yearly in East Asia (Espí et al., 2006). While effective for yields, plastic mulching contributes to soil contamination. Studies found meso- and macroplastic residues (e.g., 3 g PE/$m^2$ soil) in horticultural fields (Ramos et al., 2015). Harmful additives like phthalates, present at 50–120 mg/kg in mulches, result in significantly higher soil concentrations compared to non-mulched soils (Kong et al., 2012).

Irrigation is another agricultural pathway for plastic entry into soil, particularly for MPs and smaller plastic fragments. Globally, irrigation covers 270 Mha, accounting for 18% of total agricultural land (FAO, 2013), utilising groundwater and wastewater in many regions. Groundwater irrigation likely contributes minimal plastic due to filtration through soil layers, though nanoparticles and colloids may infiltrate. In contrast, untreated wastewater contains up to 627,000 MP items/$m^3$, contributing billions of particles to fields per cropping season, depending on crop type and irrigation volume (Bläsing & Amelung, 2017b). Treated wastewater, though lower in plastic concentration (0–125,000 items/$m^3$), can still deposit millions of particles annually (Bläsing & Amelung, 2017b).

However, current analytical methods are limited to tracking larger particles from these agricultural sources, especially sewage sludge and compost, with no protocols to measure nanoscale plastics in these soil amendments or soil, creating challenges for accurate exposure assessments. NPs and tire debris are likely significant but under-quantified pollutants in terrestrial environments (Hurley, Rachel R. & Nizzetto, 2018).

### 1.3.2 Runoff from the surroundings and atmospheric deposition

Uncaptured runoff from roads and urban areas can contaminate nearby soils, and atmospheric transport facilitates the long-distance movement of smaller plastic particles,

as evidenced in urban environments. Urban runoff, including overland flow from rainfall, snowmelt, and stormwater, is a major pathway for MP transfer to aquatic environments, mobilizing large quantities of land-based MPs and pollutants(Wang, Chengqian et al., 2022). It significantly contributes to MP pollution in waterbodies, with 42% of MPs in European rivers being tire and road wear particles (Siegfried et al., 2017), 43% of MPs in Germany's Warnow estuary originating from stormwater, and 62% of MPs in the Baltic Sea entering via stormwater runoff, including sewer overflow.

Due to their small size and lightweight properties, MPs and NPs particles can become suspended and transported as urban dust (Su et al., 2022). Atmospheric transport is common in urban air and has been observed in remote, pristine areas (Allen et al., 2021). Additionally, MPs are ubiquitous in dry and wet depositions, predominantly fibres, though fragments dominate in some areas. Fibres are typically <1000 μm long, with the longest at 5 mm, and fragments are often <100 μm (Allen et al., 2019). MP abundance varies from 2 to 600 particles per m²/day between urban and remote areas, depending on sampling methods, with differences driven by sources, pathways, and environmental reservoirs (Su et al., 2022).

## 1.4 Environmental fate and behaviours of plastics in soil

The environmental fate, transport, and impact of micro(nano)plastics (MN Ps) in soil are complex and influenced by various physical, chemical, and biological processes. Their fate is governed by factors such as particle size, shape, density, and surface chemistry, which influence interactions with soil components and environmental conditions.

### 1.4.1 Degradation of plastics

MPs undergo various degradation processes once they enter agricultural soils, influenced by both anthropogenic activities and environmental factors. MPs are modified through photodegradation, microbial degradation, and other oxidative pathways, with their fate largely dependent on soil properties and the inherent characteristics of the plastics.

#### 1.4.1.1 Photodegradation

MPs on the soil surface are exposed to solar radiation, triggering physicochemical changes (Bonyadinejad et al., 2022). This photodegradation processes involve molecular chain breakage, oxidative transformations, and structural rearrangements within the polymer matrix (Mao et al., 2020). For instance, low-density polyethylene (LDPE) undergoes photodegradation, with selective breakdown of non-crystalline regions, thereby increasing crystallinity, and reduced molecular weight (Bonyadinejad et al., 2022). Polymers like PVC lose chlorine, forming polyenes, while PE, PP, and PS produce free radicals that initiate photo-oxidative reactions and microcrack formation (Yousif & Haddad, 2013).

#### 1.4.1.2 Microbial degradation

When MPs infiltrate deeper soil layers, they are shielded from UV radiation but remain susceptible to microbial degradation. Key processes include enzymatic hydrolysis, microbial colonization, enzymatic depolymerization, and the microbial assimilation of polymer-derived carbon (Sander 2019). Natural polymers like cellulose are more easily

hydrolysed by microbial enzymes into monosaccharides, which are then mineralized into $CO_2$ and $H_2O$ due to their hydrophilic nature (Brodhagen et al., 2015). Modern biodegradable mulch films, composed of blends of natural polymers, degrade rapidly due to enzyme-labile functional groups in their main chains (Sander et al 2019). In contrast, conventional MPs such as PE, PP and PS exhibit high resistance to microbial degradation (Wu et al., 2024a). However, environmental aging processes, such as photooxidation and physical stressors (e.g., rainwater and wind), can enhance their hydrophilicity, promoting microbial adherence and subsequent degradation (Karlsson et al., 2018).

#### 1.4.1.3 Other pathways

Soil redox fluctuations, driven by microbial activity, water vapor condensation on iron minerals, and the transformation of Fe (II)-bearing clay minerals into ferrihydrite, generate reactive oxygen species (ROS) such as hydroxyl radicals (·OH) and hydrogen peroxide ($H_2O_2$), which can accelerate oxidative degradation (Wu et al., 2024a). Additionally, freeze–thaw cycles in soil (Tian, C. et al., 2022) and ingestion by soil fauna, including earthworms (Wang, Jie et al., 2020b), amoebas (Zhang, Siyi et al., 2022) and springtails (Kim & An, 2020), further contribute to MP fragmentation and degradation.

### 1.4.2 Release behaviours of plastic additives in agricultural soil

Global agriculture utilizes over 12.5 million tons of plastics annually, with 6.1 million tons used specifically for plastic films (European Commission, 2021). These films often contain additives such as functional enhancers, colorants, and reinforcing agents. Many of these additives that are physically bonded to the polymer matrix, are potentially carcinogenic, mutagenic, or endocrine-disrupting and can migrate into the environment through mechanical abrasion, volatilization, leaching, or dissolution during use (Groh et al., 2019). While the presence of these additives in agricultural soils is well-documented, studies investigating their release behaviours in soil systems remain limited compared to research in aquatic environments (Wu et al., 2024a).

Field studies, including Gong et al. (Gong et al., 2021), identify agricultural mulch films as major sources of organophosphate antioxidants and their oxidized derivatives in soils. Experimental simulations have shown significant leaching of these additives—such as tris (2,4-di-tert-butylphenyl) phosphite—from plastic films into agricultural soils (Gong et al., 2021). Environmental factors, such as freeze–thaw cycles, have been demonstrated to accelerate the migration of plasticizers like phthalates into soil environments (Tun et al., 2022; Wu et al., 2022). Additive leaching is primarily driven by diffusion and partitioning, with the partition coefficient between the plastic and its surrounding medium being a key determinant (Endo et al., 2013; Lee et al., 2018; Sun et al., 2019). However, these dynamics remain poorly characterized, hindering a full understanding of additive release in agricultural settings.

Natural soil conditions, including temperature, moisture, pH, organic matter content, and texture, significantly influence additive migration. Existing aquatic models, such as diffusion and linear free energy models (Xu et al., 2023), often fail to capture the complexities of soil environments. Developing soil-specific release models is critical for accurately predicting and mitigating the environmental impacts of plastic additives in agricultural soils.

## 1.4.3 The sorption behaviours of pollutants onto plastics

Wang et al. (Wang, Yanhua et al., 2021) identified key mechanisms driving pollutant adsorption on MPs in aquatic environments, including electrostatic interactions, hydrophobic interactions, hydrogen bonding, van der Waals forces, microporous filling, and π-π bonding, with the first three being dominant. In soils, these mechanisms are more complex and can be categorized into three stages: partition, diffusion, and adsorption (Lan et al., 2021).

### 1.4.3.1 Partition

MPs interact with soil organic matter and pore water, primarily through hydrophobic partitioning. Hydrophobic MPs such as PE, PS, PA, and PP effectively sorb organic pollutants, including pesticides (e.g., carbendazim, diflubenzuron, malathion), with sorption positively correlating with LogKow values, indicating spontaneous exothermic reactions (Lan et al., 2021; Šunta et al., 2020; Wang, Ting et al., 2020).

### 1.4.3.2 Diffusion

Pollutants undergo external diffusion on MP surfaces before migrating into internal pores to reach equilibrium, a process enhanced by aging-induced surface cracking and microporosity (Li, Hui et al., 2021; Li, Zhiwei et al., 2020). Additional chemical diffusion mechanisms, such as dissolution and reaction diffusion, can also contribute under specific conditions (Wang, Jie et al., 2020b).

### 1.4.3.3 Adsorption

Adsorption depends on charges and functional groups of MPs and pollutants. Negatively charged MPs adsorb positively charged pollutants (such as trace metals like Ag, Cd, Co, Cr, Cu, Hg, Ni, Pb, Zn, etc.) via electrostatic interactions, though salinized soils with high $Ca^{2+}/Na^{+}$ levels can neutralize these charges, reducing adsorption capacity (Wang, Han et al., 2022; Wu, et al., 2024b).

Furthermore, biofilm formation on MP surfaces enables interactions with microbial debris and dissolved organic matter, which adsorb pollutants through complexation (Wu et al., 2024b). Incorporation of MPs into soil has been shown to increase DOM content (0.75–74.29% for conventional inert MPs), further facilitating pollutant adsorption (Wang, Yuan et al., 2021). This underscores the multifaceted and dynamic nature of MP-mediated pollutant adsorption in soil systems.

## 1.4.4 Transport of microplastics and nanoplastics

Most plastic particles enter soil through surface deposition (Bläsing & Amelung, 2017a). Processes like tillage, bioturbation (e.g., in Chernozems, Kastanozems, Phaozems and Luvisols), and the presence of large cracks in soils (e.g., such as in Vertisols) can incorporate plastics into deeper layers. Earthworms have been shown to transport polyethylene (PE) beads (710–2800 µm) to depths of 10 cm within 21 days (Rillig et al., 2017). Similar observations were made for low density PE b 400 µm (Huerta Lwanga et al., 2017). Both studies reported a size-dependent translocation, i.e. smaller microplastic particles were preferred for bioturbated transport.

Leaching, the downward movement of particles driven by percolating water and hydraulics, occurs mainly for particles smaller than soil pore diameters. McGechan et al. (McGechan, 2002) found that particles smaller than 1.91 μm are likely to leach, although larger particles (up to 20 μm) have also been reported to migrate under certain conditions (Wang, Jun et al., 2013). Plastic colloids (2.6–5 μm) showed leaching potential in sandy soils but were better retained in denser soils (Morales et al., 2009; Zhang, Wei et al., 2010). Nanoparticles (<100 nm), while small enough to fit through meso- and macropores, are often retained in soil due to properties like size, coating, and interactions with soil chemistry, such as Fe-oxide content and pH (Jaisi & Elimelech, 2009; Pachapur et al., 2016).

Erosion, influenced by land use, slope, and vegetation cover, can transport plastic particles laterally to other ecosystems. Vineyards with high slopes and partly missing vegetation cover are particularly susceptible (Cerdan et al., 2010), while other arable lands also contribute through sheet and rill erosion. Additionally, larger plastic items may be blown off the soil surface, leading to wind-driven transport (Bläsing & Amelung, 2017a). Despite the recognized risks, data on plastic movement through erosion are still limited.

# 1.5 Environmental effects of microplastics and nanoplastics in soil

## 1.5.1 Effects of microplastics and nanoplastics on soil properties

Studies since 2017 have shown that large plastic film fragments disrupt soil properties, including moisture content, bulk density, porosity, and water distribution (Jiang, X. J. et al., 2017). Smaller MPs (<2 mm) have been found to increase soil water movement and evaporation, negatively impacting soil structure integrity (Wan et al., 2019). Field experiments reveal that MPs can alter soil physical attributes depending on their polymer type, concentration, and density (de Souza Machado et al., 2018). For instance, MPs like PP fibres, PA beads, PET fibres, and HDPE fragments reduce soil bulk density due to their lower density compared to soil particles (de Souza Machado et al., 2018). Fibrous MPs strongly interact with amphiphilic and hydrophobic soil compounds, affecting water retention and aggregate stability (de Souza Machado et al., 2019). In contrast, MPs resembling natural soil particles in size and shape have minimal impact on soil structure and hydrodynamics (de Souza Machado et al., 2019; Zhang, G. S. et al., 2019).

#### 1.5.1.1 Dissolved Organic Matter (DOM)

The presence of MPs has been shown to increase soil DOM content, particularly by enriching labile components, while the concentration of recalcitrant DOM elements varies depending on environmental conditions (Wu et al., 2024b). For example, Sun et al. (Sun et al., 2022) observed that both PE and PBS MPs (1% w/w) significantly increased soil DOM after a 30-day incubation, with labile components such as carbohydrate-like, protein/amino sugar-like, and lipid-like compounds. Biodegradable MPs (e.g., PLA, PBS) contribute more to DOM enrichment compared to inert MPs (e.g., PE, PP) (Wu et al., 2024b).

#### 1.5.1.2 Other soil properties

MPs can affect soil pH, cation exchange capacity (CEC), and mineral interactions. Recent studies show that PE MPs affect soil pH differently, increasing it in Cd-contaminated soil but lowering it in Cd-free soil (Wang, Fangli et al., 2021; Wang, Jie et al., 2020a). These pH changes can influence CEC, which typically rises with higher pH (Ma et al., 2023). However, larger PE MPs may reduce soil porosity, potentially lowering CEC (Ma et al., 2023). Additionally, PS MPs interact with soil mineral colloids through electrochemical processes like charge neutralization, double-layer compression, van der Waals forces, and aggregation (Vu et al., 2022). These interactions alter soil properties, including electrostatic interactions, cation bridging, hydrogen bonding, ligand exchange, and hydrophobicity (Lu et al., 2023; Shu et al., 2023), highlighting the complex effects of MPs on soil physicochemical characteristics.

### 1.5.2 Effects of microplastics and nanoplastics on soil organisms

#### 1.5.2.1 Soil fauna

MPs have been shown to significantly impact soil fauna. Early studies revealed that earthworms (Oligochaetes) ingest MPs, favouring smaller particles (<50 μm) (Chen et al., 2020). Through natural activities like burrowing and excretion, earthworms fragment MPs into finer particles and transport them deeper into the soil (Heinze et al., 2021; Rillig et al., 2017). High MP concentrations (≥1% by weight) impair earthworm immunity, alter feeding habits, and hinder growth, while lower concentrations (<0.5% by weight) have minimal effects (Cao et al., 2017; Ding et al., 2021). MPs also facilitate the bioaccumulation of heavy metals (e.g., Cd (Zhou, Yanfei et al., 2020), Cu (Li, Ming et al., 2021), Pb (Li, Ming et al., 2023) and organic pollutants (e.g., phenanthrene (Xu, G. et al., 2021), dufulin (Sun, W. et al., 2021) (Liu, Yang et al., 2022), and perfluorooctanoic acid (Sobhani et al., 2021), impeding growth and inducing oxidative stress in earthworms. However, debates persist regarding MP ingestion preferences, effects on metal accumulation, and their influence on earthworm gut microbiota (Yang, Yang et al., 2022).

#### 1.5.2.2 Soil flora

In recent years, research has increasingly focused on the toxic effects of MPs on plants. Van Kleunen et al. (Van Kleunen et al., 2019) reported that low concentrations of ethylene-propylene-diene-monomer MPs slightly enhanced spruce growth, while concentrations of 5% or higher significantly hindered tree survival and development. Similarly, Yu et al. (Yu, H. et al., 2021) demonstrated that MPs elevated ROS levels in Bacopa sp. tissues, triggering lipid peroxidation and antioxidant defences. This oxidative stress negatively impacted seed germination and reduced chlorophyll b synthesis in seedlings. Furthermore, Kaur et al. (Kaur et al., 2022) found that PS MPs induced cellular toxicity and nuclear damage in onion root tip cells, disrupting spindle apparatus formation and leading to micronuclei generation.

MPs affect soil flora directly and indirectly. MPs can infiltrate plant tissues via root uptake, with smaller particles (<30 μm) being more readily absorbed through endocytosis and aquaporins (Rillig, 2020). Functional group charges influence uptake efficiency, e.g., amino-functionalized MPs more readily penetrating root tissues than carboxyl-functionalized counterparts (Wang, Yu et al., 2022). Indirectly, fibrous MPs enhance soil aeration, promoting root penetration, while larger MPs may encase roots, reducing

nutrient absorption (Lozano & Rillig, 2020). However, the long-term implications of these changes on plant health require further investigation.

#### 1.5.2.3 Soil microbial communities

MPs transform soil microbial communities by providing new ecological niches on their surfaces and altering soil structure and organic matter composition (Chai et al., 2020; Khalid et al., 2020). These changes influence microbial dynamics, as reflected in variations in abundance, diversity, functional gene expression, and enzymatic activities, which are shaped by habitat conditions, survival strategies, and nutrient availability. Generally, the introduction of MPs into soil reduces overall microbial diversity (Qiang et al., 2023). However, certain microbial taxa capable of degrading specific MP types thrive. For example, β-Proteobacteriales and Clostridiales degrade PP (Zhang, Mengjun et al., 2019), Cyanobacteria and Zygomycota for PS (Li, Hong-Zhe et al., 2021) while Actinobacteria, Bacillus, and Pseudomonas target PE (Zhang, Mengjun et al., 2019). Fungal communities are particularly sensitive to MP presence, with their responses depending on MP concentrations (Li, Hong-Zhe et al., 2021). The interaction between MPs and soil microbes is complex, varying with MP type, concentration, and soil conditions. Further research is essential to fully understand the ecological implications of these interactions.

### 1.5.3 Effects of microplastics and nanoplastics on soil $CO_2$ emissions

MPs, composed primarily of carbon-based polymers (~80% carbon content) (Rillig, 2018), have the potential to contribute to the soil carbon pool upon incorporation. However, studies show that dissolved organic matter (DOM) derived from MPs accounts for only 0.11%–0.48% of the total carbon content of the original plastic (Zhu et al., 2020). This limited contribution is due to the environmental and microbial resilience of common agricultural soil MPs, such as PE, PP, PS, which are categorized as part of a “recalcitrant carbon pool” (Seeley et al., 2020).

MPs predominantly influence soil carbon dynamics by affecting $CO_2$ emissions, with minimal impact on methane or nitrous oxide emissions (Gao, B. et al., 2022). High MP concentrations (≥1% by weight) are significantly correlated with increased $CO_2$ emissions ($r = 0.816$, $p < 0.01$), while concentrations ≤0.5% show no significant impact ($r = -0.592$, $p > 0.05$) (Wu, J. et al., 2024c). This threshold corresponds to approximately $10^5$–$10^7$ particles/kg of soil, a level rarely exceeded in agricultural soils except in regions like Xinjiang (Jia et al., 2022) and Wuhan (Zhou, Yanfei et al., 2019). MPs influence $CO_2$ emissions through several mechanisms: (1) enhancing DOM content and microbial activity, which improves soil aeration and metabolic processes; (2) altering microbial communities, including fungi, that impact soil organic carbon (SOC) stabilization and degradation; (3) modifying genes associated with microbial carbon degradation and fixation; and (4) affecting soil fauna, such as earthworms, which play key roles in carbon cycling (Wu, J. et al., 2024c).

However, most current studies are conducted under controlled conditions using single MP types (e.g., PE or PP) of specific sizes (≤630 μm), limiting their applicability to real-world soils with diverse MP types and sizes (Wu, J. et al., 2024c). Further research is essential to explore the complex interactions between MPs, soil properties, and biota under natural conditions.

## 1.6 Plastic analysis in soil: state of the arts and challenges

To accurately assess the risks posed by MPs and NPs in soil, reliable data on their occurrence is essential. Such data, obtained through robust analytical approaches, are critical for effectively monitoring plastic pollution levels, designing targeted mitigation measures, and supporting adaptive management strategies. However, MPs and NPs are among the most challenging analytes to study in environmental matrices due to their inherent diversity and complexity. The variability of plastic sources, usage patterns, emission pathways, and material properties contributes to a wide range of physical, chemical, and biological characteristics, including size, shape, density, polymer type, and surface properties. Consequently, advancing analytical methods are indispensable for the reliable identification, quantification, and characterization of MPs and NPs.

MPs and NPs are inherently complex due to their diverse characteristics, which span five key dimensions:

1. **Broad size range**: MPs vary significantly in size, from 1 µm to 1 mm, and up to 5 mm for larger particles. For NPs, sizes range from 1µm to 1nm.
2. **Varied polymer types**: MPs and NPs include conventional and biopolymers with different chemical compositions, structures, and densities.
3. **Different shapes:** MPs and NPs exhibit a variety of forms, such as spheres, irregular particles, fibres, films, and foams.
4. **Chemical diversity:** MPs and NPs may contain additives (e.g., antioxidants, plasticizers, pigments), weathering products, or sorbed contaminants like persistent organic pollutants, antibiotics, and heavy metals.
5. **Aging states:** MPs and NPs can range from primary to secondary particles, with varying degrees of degradation and biofouling leading to physiochemical changes such as changes in surface charge, and hydrophobicity, etc.

Given these dimensions and the wide concentration range of MPs and NPs in environmental samples, several challenges arise:

- **Sample size and representativeness**: The pollution level of different media (e.g., water, soil, air) and the desired information (e.g., MP mass, particle count, size range) dictate sample size. Smaller samples may suffice for detecting small particles, but larger samples are necessary for analysing larger particles or mass contributions.
- **Method validation and standardization**: Ensuring reliable results demands validated, harmonized, and standardized methods. However, suitable reference materials that mirror real-world MPs in terms of polymer type, size, shape, and aging state are still lacking.
- **Contamination prevention:** The ubiquity of plastics necessitates rigorous measures to prevent contamination during sampling, storage, preparation, and detection.

Additionally, soil is a highly complex and heterogeneous matrix, which further complicates microplastic analysis. Effective analysis requires careful consideration of the soil profile, soil type, and constituents such as soil solutes, silicates, (swellable) clay minerals, and soil organic matter (SOM), all of which vary in quantity, grain and aggregate sizes, and densities (Thomas et al., 2020a). SOM itself is a dynamic and highly

heterogeneous mixture derived from plant and animal litter at various stages of decomposition. The labile SOM fraction contains easily degradable molecules like peptides, lipids, and carbohydrates, while the more stable humic fraction comprises complex, polymeric macromolecules (Bronick & Lal, 2005). Certain soil constituents are suspected or have been shown to interfere with microplastic analysis, necessitating their removal or reduction during sample preparation (Thomas et al., 2020a). However, the selected purification methods must preserve the integrity of the polymer analytes, which is especially crucial for the analysis of small MPs, NPs, especially of biodegradable polymers. Currently, no standardized analytical protocols exist for soil. Reliable, quantitative analytical tools for these materials are still under development.

### 1.6.1 Soil sampling for microplastics and nanoplastics analysis

A robust soil sampling method is crucial for reliably and representatively studying the occurrence and characteristics of microplastics (MPs) in the environment. However, no standardized method for MP sampling currently exists. Most studies on soil MPs focus on pre-analysis and laboratory techniques, often neglecting field sampling (Chia et al., 2024).Where documented, sampling approaches are frequently random and lack proper justification, failing to account for the discrete nature of plastics and leading to significant sampling errors (Yu & Flury, 2021).

Plastic particles in soil occur as distinct entities with variable sizes and discontinuous distributions. Uniform distributions arise from biosolid applications or tillage, while spatial dependence occurs near point or line sources (e.g., waste sites, roadsides) or due to weathering, leading to significant variability and "nugget variance"—short-scale randomness in concentrations (Yu & Flury, 2021). The challenge for soil sampling is ensuring representative samples given the discrete spatial distribution of plastics and the wide range of reported concentrations in terrestrial ecosystems. Unlike continuous variables (e.g., nitrate concentrations in fields (Hofman & Brus, 2021), sampling errors for discrete plastics cannot rely on established concepts for continuous variables. Instead, the size or "support" of samples—the total volume or area—must be explicitly considered, as it strongly affects measured concentrations (Yu & Flury, 2021).

A recent study (Yu & Flury, 2021) simulated sampling strategies to quantify plastic particles in terrestrial environments. It modelled randomly distributed particles to determine the representative elementary volume (REV) and the number of samples needed for accurate measurements. The results revealed a non-linear relationship: low concentrations required numerous small cores, while high concentrations needed fewer. The study also recommends using large area replicated samples (e.g., 1 m × 1 m) and reducing soil volume through the quartering method.

### 1.6.2 Extraction of microplastics and nanoplastics in soil

Currently, standard methods to study NPs have not been established. For MPs, depending on the soil matrix and MPs in question, different protocols have been proposed and applied among laboratories (Thomas et al., 2020a). The overall process for soil MPs analysis involves three main stages: 1) Sampling and pre-processing, 2) MPs and NPs-soil separation, and 3) MPs and NPs identification and quantification. Soils are commonly sampled at the surface, to shallow depths (5 cm) and to greater depth with cores and soil

augers. After that, general sample pre-treatment procedure to reduce matrix interferences involves drying (either freeze-drying or heating in the oven at 40°C), homogenizing, sieving and sorting (macroplastics with size ≥ 5mm and MPs), followed by dispersion of soil aggregates. Next, density separation and digestion of soil organic matter (SOM) combined with filtration are performed, the order of which depends on the proportion of clay and organic matter in soils.

While initial steps for the sample preparation of MPs in soils, such as soil treatment techniques for characterizing the presence of MPs (e.g., drying, sorting, etc.), are generally agreed upon among laboratories and research groups (Thomas et al., 2020a), pre-concentration and matrix removal methods remain somewhat inconsistent and require further study and development.

#### 1.6.2.1 Density separation

Density separation is currently the most common technique to pre-concentrate or isolate MPs from soils. It exploits the buoyancy of plastic particles in solutions of a higher density, while the soil mineral fraction settles at the bottom. In principle, floating plastic particles from soil samples are collected after a certain amount of time following thorough mixing with a high-density salt solution (Hidalgo-Ruz et al., 2012). However, studies vary greatly in terms of sample amounts, applied density solutions, and the technical setup (Thomas et al., 2020a).

Generally, the recovery rates of various MP types increased with the density of the solutions. Deionized water ($\rho$ = 1.0 g $cm^{-3}$) and saturated sodium chloride (NaCl) solution ($\rho$= 1.2 g $cm^{-3}$) are suitable for separating low-density polymers like PE, PP, and PS from soil mineral matrices, while being cheap, easily available, and environmentally friendly (Liu, Mengting et al., 2018; Zubris & Richards, 2005). For denser polymers like PET or PVC, current studies recommend high-density salt solutions such as zinc chloride ($ZnCl_2$, $\rho$ = 1.5–1.7 g $cm^{-3}$), sodium iodine (NaI, $\rho$ = 1.6–1.8 g $cm^{-3}$) or sodium polytungstate (SPT, $\rho$ = 1.4–1.8 g $cm^{-3}$) (Horton et al., 2017; Thomas et al., 2020a).

#### 1.6.2.2 Digestion of soil organic matter

SOM can be only partially removed by density separation as the density of SOM ($\rho$ <1.6 g $cm^{-3}$, (Cerli et al., 2012) is similar to that of MPs and NPs ($\rho$ = 0.9–1.9 g $cm^{-3}$) (Thomas et al., 2020a). The removal of SOM is therefore required as SOM constituents may interfere with subsequent MPs and NPs analysis. For example, in Raman, SOM induced auto-fluorescence, thus show artifacts and hide MPs signals (Schrank et al., 2022).

Hydrogen peroxide ($H_2O_2$) and Fenton's reagent (an acidified solution (pH 3–5) of $H_2O_2$ and a $Fe^{2+}$ catalyst) are among the most commonly used reagent for removal of SOM, offering high removal efficiencies and good MP recoveries (Möller et al., 2020; Radford et al., 2021). Fenton's reagent significantly reduces degradation time compared to 30% $H_2O_2$, decreasing processing from several days to under 10 minutes without damaging the MPs in samples (Tagg et al., 2017). Alkaline solutions, such as sodium hydroxide (NaOH) and potassium hydroxide (KOH) remove from 35–68% of SOM from loamy sand soils (5.8% SOM) (Hurley, Rachel R. et al., 2018). However, NaOH caused significant PET and PC degradation (up to 30%), while KOH partially degraded PC, with even greater effects on biodegradable plastics like PLA (Kühn et al., 2017). Similarly, hydrochloric acid (HCl) and nitric acid ($HNO_3$) can digest SOM, with concentrated $HNO_3$

(65%) removing over 30% of SOM, while 96% $H_2SO_4$ and 13% potassium hypochlorite left minimal residues. However, ABS, PA, and PET were partially degraded or fragmented during treatment (Scheurer & Bigalke, 2018). Additionally, various enzymes, such as lipases, amylases, proteinases, chitinases, and cellulases, have been used for SOM digestion. However, these processes are often time-consuming and less cost-effective. Certain enzymes, like protease, can also have detrimental effects on biodegradable plastics (Löder et al., 2017; Möller et al., 2020).

## 1.6.3 Identification and quantification of microplastics and nanoplastics in soil

The choice of an appropriate method or combination of methods for MP analysis largely depends on the specific research questions and objectives of the study. For monitoring and modelling purposes, information on MP mass may suffice. In such cases, destructive mass-based methods are suitable, as they provide data on the polymer content in a sample without considering particle number, size, or shape. However, it is important to note that these methods are biased toward larger particles, as a few large particles can disproportionately influence the total mass, while smaller particles contribute minimally.

For studies requiring detailed insights—such as understanding the transport and fate of MPs or their environmental and human health impacts—non-destructive, particle-based methods are preferred. These techniques offer information on particle number, size, or size distribution (limited by the detection range of the method), and shape. Additionally, characterizing specific properties or compounds often necessitates specialized methods tailored to those attributes.

A comprehensive analysis of MPs with diverse characteristics typically requires a combination of analytical approaches, as no single method can capture all relevant data. Moreover, the choice of detection methods must consider the complexity of the sample matrix, the level of MP contamination, and the required sampling and preparation techniques to ensure representative and reliable results.

### 1.6.3.1 Particle-based approaches

#### *1.6.3.1.1 Optical microscopy*

Stereomicroscopy provides researchers with the ability to identify polymer types and measure their morphology and colour. However, visual identification has significant limitations, particularly in distinguishing pigmented microplastics or co-polymers from other materials, especially when analysing small particles. The potential for human error in visual identification can exceed 50%, highlighting its role as a supplementary method rather than a standalone technique. Furthermore, the classification of certain semi-synthetic celluloses (e.g., cellophane, viscose/rayon, and nitrocellulose) as MP (Bergmann et al.; Suaria et al.) has added to the challenges and uncertainties associated with visual identification.

#### *1.6.3.1.2 Fluorescence microscopy*

Fluorescence-based methods are widely used for the visual inspection of polymers. By employing dyes with an affinity for synthetic polymers, MPs can be observed under specific emission wavelengths (Maes et al., 2017a). For example, Nile Red staining induces green fluorescence in various polymers, offering high specificity and good recoveries for detecting synthetic plastic particles. However, this method cannot chemically identify plastics and is susceptible to false positives due to SOM interference. Furthermore, environmental surface contamination can alter the hydrophobicity of plastics, affecting the fluorescence colour of Nile Red (Lv et al., 2019; Maes et al., 2017a; Nel et al., 2021; Shruti et al., 2022; Tarafdar et al., 2022). In complex soil environments, this limitation significantly hinders the utility of Nile Red staining.

#### *1.6.3.1.3 Fourier Transform Infrared micro-spectroscopy*

FTIR spectroscopy is a non-destructive technique based on the analysis of molecular vibrations excited by the absorption of radiation in the mid-infrared region (4000–400 $cm^{-1}$) of the electromagnetic spectrum. The resulting characteristic vibrational fingerprint spectra allow for the accurate identification of the polymer type for MP as well as for the assignment of non-plastic particles using spectral databases or other chemometric methods (Moses et al., 2023).

FTIR spectroscopy offers versatility through modes like transmission, reflection, and attenuated total reflection (ATR). ATR-FTIR is particularly effective for larger MPs and weathered particles, requiring minimal sample preparation. For smaller MPs (10–20 μm), micro-FTIR (μ-FTIR) paired with optical microscopy delivers diffraction-limited spatial resolution, with imaging techniques like focal plane array (FPA) detectors enhancing its efficiency for large filter areas (Ivleva, 2021).

#### *1.6.3.1.4 Raman micro-spectroscopy*

Raman micro-spectroscopy, which combines spectroscopy with confocal optical microscopy, achieves superior spatial resolution (down to 300 nm) compared to FTIR-based methods, making it ideal for analysing particles smaller than 20 μm. This method is based on the effect of inelastic or Raman light scattering on molecules and (similar to IR spectroscopy) provides vibrational fingerprint spectra. Therefore, proper identification of plastic particles and some of additives (e.g., pigments, oxides) as well as other (in)organic and (micro)biological compounds can be performed using homemade and commercial spectral databases (Ivleva, 2021).

A major advantage of Raman spectroscopy is its insensitivity to water, unlike FTIR, enabling effective analysis of MPs in aqueous and biological samples. It has also proven efficient in distinguishing synthetic from natural fibres and identifying pigmented plastic particles. However, challenges like fluorescence interference from sample impurities often require pre-treatment steps such as density separation and chemical or enzymatic digestion.

### 1.6.3.2 Mass-based approaches

Mass spectrometry-based methods play a vital role in analysing MPs and NPs by providing detailed insights into their chemical composition and molecular structure. Techniques such as pyrolysis gas chromatography-mass spectrometry (Py-GC-MS), thermal desorption-proton transfer reaction mass spectrometry (TD-PTR-MS), matrix-assisted laser desorption ionization time-of-flight mass spectrometry (MALDI-TOF MS), etc. have been developed for this purpose (Ivleva, 2021). These approaches offer notable advantages, including high sensitivity, the ability to identify polymers and additives, and suitability for analysing complex environmental matrices. However, they also have limitations: they are destructive, require labour-intensive sample preparation, and face challenges with highly heterogeneous samples. Furthermore, accurate identification heavily depends on comprehensive polymer and additive databases.

#### *1.6.3.2.1 Pyrolysis–gas chromatography tandem mass spectrometry*

This technique employs a pyrolysis and thermal desorption unit to thermally break down samples in an inert atmosphere (Primpke, Sebastian et al., 2020). Py-GC/MS is a destructive technique based on the degradation products generated at defined temperatures under the exclusion of oxygen, which are then separated via gas chromatography, and their mass is determined using mass spectrometry. Polymers are identified and quantified by analysing their distinct degradation products and indicator ions through the resulting pyrograms (Ivleva, 2021). This method also allows for the detection of plastic-associated additives as well as of degradation by-products and, hence, they deliver the data necessary for reliable risk assessment of MP for the environment and human health. However, these mass-related data must be considered as bulk values of a given plastic type, e.g., PS, disregarding if it is a pure polymer or a share of a copolymer, and are independent from any kind of particle characteristics such as size, shape, form, etc. Its sample capacity ranges from 100 to 1000 µg, limiting its applicability to uniform samples. The detection sensitivity of Py-GC/MS varies from pg to µg, depending on the polymer and the environmental matrix (Ivleva, 2021).

#### *1.6.3.2.2 Quantitative proton nuclear magnetic resonance*

NMR characterizes and quantifies MPs by leveraging the magnetic properties of hydrogen nuclei in the plastic. When a prepared sediment sample undergoes proton NMR analysis, the hydrogen nuclei resonate at specific frequencies, revealing the composition, structure, and concentration of MPs based on signal intensity (Papini et al., 2024).

Peez et al. demonstrated qNMR's effectiveness for analysing LDPE, PET, and PS using deuterated toluene and chloroform, with detection limits of 19–21 µg/mL and quantification limits of 74–85 µg/mL (Peez et al., 2018). The method showed high recovery rates in spiked matrices: sediment (~97%), freshwater (~94%), biofilm (~95%), invertebrates (~72%), and non-matrix samples (~90%) (Peez et al., 2019). It was later extended to analyse PVC, ABS, and PA, achieving detection limits of 40–84 µg/mL and quantification limits of 132–281 µg/mL (Peez & Imhof, 2020). Nelson et al. applied qNMR to soil, quantifying polyester PBAT from biodegradable mulch films with detection and quantification limits of 1.3 and 4.4 µg/mL, respectively (Nelson et al., 2020).

#### *1.6.3.2.3 Thermal desorption-proton transfer reaction-mass spectrometry*

Recently, a novel method for the chemical characterization of NPs based on thermal desorption–proton transfer reaction-mass spectrometry (TD-PTR-MS) has been proposed by Materić et al. (Materić et al., 2020). This technique utilizes hydronium ions ($H_3O^+$), generated from water vapor, for the soft ionization of volatile organic fragments released during the thermal desorption of plastics. Characterized by sub-ppb sensitivity, sub-second time resolution, and a mass resolving power in the range of several thousand, TD-PTR/MS has already been widely applied to analyse various complex organic mixtures in the environment, including plastics.

The authors reported a limit of detection (LOD) of <1 ng for polystyrene (PS) in samples and applied this method for the (semi)quantification of NMPs in Alpine snow. The method's high sensitivity enabled the use of small sample volumes (1 mL) and eliminated the need for extensive preconcentration steps. Unique features in the high-resolution mass spectrum of synthetic polymers allowed for reliable fingerprinting, even in the presence of mixed organic compounds. For instance, a distinct fingerprint was detected for as little as 10 ng of PS within the DOM of snow samples. Although recovery rates were estimated at only 15% for PS, and minor impurities from various sources may cause interference, the TD-PTR/MS method demonstrates significant potential for the sensitive analysis of NMPs (Materić et al., 2020).

## 1.7 Knowledge gap and thesis aim

Although several extraction and analytical approaches are available for microplastic (MP) analysis in soil, their efficiency and applicability to soil samples have not been thoroughly tested. This is particularly relevant given the diversity of plastics in terms of size, shape, and polymer types in the environment, as well as the complex and heterogeneous nature of soil. Several methods, including particle-based techniques like fluorescence microscopy, FTIR, and Raman spectroscopy, as well as mass-based techniques like pyrolysis-GC/MS, are available. However, a comprehensive comparative assessment of these analytical methods with their respective extraction procedure for soil samples is still lacking.

Among the available methods for analysing MPs and NPs, fluorescence microscopy has gained attention as a fast and cost-effective option. Its high-throughput capability makes it particularly appealing for monitoring MPs across various environments. However, its application to soil samples remains underexplored, raising concerns about its reliability and accuracy in complex and heterogeneous matrices. Furthermore, it is unclear how the results obtained through fluorescence microscopy compare to those from other particle-based techniques, such as FTIR and Raman spectroscopy, when analysing the same samples. The analysis of MPs and NPs in soil using these techniques is indeed complicated by challenges like false positives and false negatives. Conducting a systematic evaluation of these methods to critically assess their strengths, limitations, and suitability for various research objectives is essential. Such an assessment would provide researchers with a clearer understanding of the most effective techniques for analysing specific sample types, ultimately improving the reliability and accuracy of MPs and NPs studies in soil environments.

Additionally, further research is crucial to better understand how MPs and NPs enter soil, particularly through agricultural practices, which are thought to be the largest contributors. This understanding is vital for developing effective mitigation measures and adaptive management strategies. While some studies have investigated MP presence in agricultural soil amendments such as sewage sludge and compost, research on plastic transfer and loading, supported by field evidence of soil contamination, remains limited. Moreover, most research has focused on larger plastic fragments, often overlooking smaller particles that are more environmentally significant and potentially more harmful. This gap likely stems from challenges in current analytical methods. Advancing these methods is essential to improving our understanding of MPs and NPs sources and, ultimately, their impacts.

Finally, analytical methods for detecting NPs in soil remain underdeveloped, leaving a significant gap in our understanding of their presence and behaviour in terrestrial environments. Studies have shown that NPs are prevalent in soils, where they can accumulate due to agricultural activities, industrial processes, and atmospheric deposition. However, existing techniques struggle to reliably detect and quantify these particles, particularly in complex and heterogeneous soil matrices. This limitation hinders our ability to assess their distribution, potential ecological risks, and long-term impacts. Advancing and standardizing analytical approaches is critical to enable accurate detection and comprehensive monitoring of NPs in soils, paving the way for data-driven mitigation strategies and environmental protection efforts.

**Thesis aim**:

Anchoring earlier studies and recent advances in analytical techniques, the aim of this PhD is to develop and advance analytical methodologies to detect and quantify microplastics and nanoplastics in soils and measure their input, presence and fate in different soil types.

**The specific objectives are:**

1. Develop and evaluate fluorescence microscopy with tailored extraction procedure as a high-throughput method for microplastic analysis in soil, ensuring its reliability and efficiency (Chapter 2).

2. Conduct a comparative assessment of various analytical techniques including optical microscopy, Fourier-transformed infrared and Raman micro-spectroscopies, pyrolysis gas chromatography mass spectrometry and quantitative proton nuclear magnetic resonance spectroscopy to identify, quantify, and characterize microplastics, both with and without the presence of a complex soil matrix (Chapter 3).

3. Apply fluorescence microscopy and vibrational spectroscopy to measure microplastic occurrence in soil organic amendments, assess their transfer to soil, and critically evaluate the strengths and limitations of these methods (Chapter 4 and 5).

4. Develop a novel nanoplastic extraction protocol for soil, enabling subsequent analysis using thermal desorption proton transferred reaction mass spectrometry. Apply this method to study nanoplastics in Antarctica, one of the most remote regions, to advance understanding of atmospheric microplastic and nanoplastic transport (Chapter 6).

# References

Allen, S., Allen, D., Baladima, F., Phoenix, V. R., Thomas, J. L., Le Roux, G., & Sonke, J. E. (2021). Evidence of free tropospheric and long-range transport of microplastic at Pic du Midi Observatory. Nature Communications, 12(1)10.1038/s41467-021-27454-7

Allen, S., Allen, D., Phoenix, V. R., Le Roux, G., Durántez Jiménez, P., Simonneau, A., Binet, S., & Galop, D. (2019). Atmospheric transport and deposition of microplastics in a remote mountain catchment. Nature Geoscience, 12(5), 339. 10.1038/s41561-019-0335-5

Andrady. (2011). Microplastics in the marine environment. Marine Pollution Bulletin, 62(8), 1596–1605. 10.1016/j.marpolbul.2011.05.030

ARCADIS. (2010). Assessment of the Options to Improve the Management of bio-Waste in the European Union-Final Report. .

Bergmann, M., Mützel, S., Primpke, S., Tekman, M. B., Trachsel, J., & Gerdts, G.White and wonderful? Microplastics prevail in snow from the Alps to the Arctic.

Bläsing, M., & Amelung, W. (2017a). Plastics in soil: Analytical methods and possible sources. Science of the Total Environment, 612, 422. 10.1016/j.scitotenv.2017.08.086

Bonyadinejad, G., Salehi, M., & Herath, A. (2022). Investigating the sustainability of agricultural plastic products, combined influence of polymer characteristics and environmental conditions on microplastics aging. Science of the Total Environment, 839, 156385. 10.1016/j.scitotenv.2022.156385

Brodhagen, M., Peyron, M., Miles, C., & Inglis, D. A. (2015). Biodegradable plastic agricultural mulches and key features of microbial degradation. Applied Microbiology and Biotechnology, 99(3), 1039–1056. 10.1007/s00253-014-6267-5

Bronick, C. J., & Lal, R. (2005). Soil structure and management : a review. Geoderma, 124(1), 3–22. 10.1016/j.geoderma.2004.03.005

Cerdan, O., Govers, G., Le Bissonnais, Y., Van Oost, K., Poesen, J., Saby, N., Gobin, A., Vacca, A., Quinton, J., Auerswald, K., Klik, A., Kwaad, F. J. P. M., Raclot, D., Ionita, I., Rejman, J., Rousseva, S., Muxart, T., Roxo, M. J., & Dostal, T. (2010). Rates and spatial variations of soil erosion in Europe : A study based on erosion plot data. Geomorphology, 122(1), 167–177. 10.1016/j.geomorph.2010.06.011

Cerli, C., Celi, L., Kalbitz, K., Guggenberger, G., & Kaiser, K. (2012). Separation of light and heavy organic matter fractions in soil — Testing for proper density cut-off and dispersion level. Geoderma, 170, 403–416. 10.1016/j.geoderma.2011.10.009

Chai, B., Li, X., Liu, H., Lu, G., Dang, Z., & Yin, H. (2020). Bacterial communities on soil microplastic at Guiyu, an E-Waste dismantling zone of China. Ecotoxicology and Environmental Safety, 195, 110521. 10.1016/j.ecoenv.2020.110521

Chen, Y., Liu, X., Leng, Y., & Wang, J. (2020). Defense responses in earthworms (Eisenia fetida) exposed to low-density polyethylene microplastics in soils. Ecotoxicology and Environmental Safety, 187, 109788. 10.1016/j.ecoenv.2019.109788

Chia, R. W., Lee, J., Cha, J., & Rodríguez-Seijo, A. (2024). Methods of soil sampling for microplastic analysis: a review. Environmental Chemistry Letters, 22(1), 227–238. 10.1007/s10311-023-01652-9

da Costa, J. P., Santos, P. S. M., Duarte, A. C., & Rocha-Santos, T. (2016). (Nano)plastics in the environment – Sources, fates and effects. Science of the Total Environment, 566-567, 15–26. 10.1016/j.scitotenv.2016.05.041

de Souza Machado, A. A., Lau, C. W., Kloas, W., Bergmann, J., Bachelier, J. B., Faltin, E., Becker, R., Görlich, A. S., & Rillig, M. C. (2019). Microplastics Can Change Soil

Properties and Affect Plant Performance. Environmental Science & Technology, 53(10), 6044–6052. 10.1021/acs.est.9b01339

de Souza Machado, A. A., Lau, C. W., Till, J., Kloas, W., Lehmann, A., Becker, R., & Rillig, M. C. (2018). Impacts of Microplastics on the Soil Biophysical Environment. Environmental Science & Technology, 52(17), 9656–9665. 10.1021/acs.est.8b02212

Endo, S., Yuyama, M., & Takada, H. (2013). Desorption kinetics of hydrophobic organic contaminants from marine plastic pellets. Marine Pollution Bulletin, 74(1), 125–131. 10.1016/j.marpolbul.2013.07.018

Espí, E., Salmerón, A., Fontecha, A., García, Y., & Real, A. I. (2006). PLastic Films for Agricultural Applications. Journal of Plastic Film & Sheeting, 22(2), 85–102. 10.1177/8756087906064220

European Commission. (2021). Assessment of agricultural plastics and their sustainability: a call for action. . https://knowledge4policy.ec.europa.eu/publication/assessment-agricultural-plastics-their-sustainability-call-action_en

FAO. (2013). World Agriculture: Towards 2015/2030: An FAO Perspective.

Gao, B., Li, Y., Zheng, N., Liu, C., Ren, H., & Yao, H. (2022). Interactive effects of microplastics, biochar, and earthworms on CO2 and N2O emissions and microbial functional genes in vegetable-growing soil. Environmental Research, 213, 113728. 10.1016/j.envres.2022.113728

Geyer, G., Jambeck, J., & Law, L. (2017). Production, use, and fate of all plastics ever made. Science Advances, 3(7), e1700782. 10.1126/sciadv.1700782

Gigault, J., Halle, A. T., Baudrimont, M., Pascal, P., Gauffre, F., Phi, T., El Hadri, H., Grassl, B., & Reynaud, S. (2018). Current opinion: What is a nanoplastic? Environmental Pollution, 235, 1030. 10.1016/j.envpol.2018.01.024

Gong, X., Zhang, W., Zhang, S., Wang, Y., Zhang, X., Lu, Y., Sun, H., & Wang, L. (2021). Organophosphite Antioxidants in Mulch Films Are Important Sources of Organophosphate Pollutants in Farmlands. Environmental Science & Technology, 55(11), 7398–7406. 10.1021/acs.est.0c08741

Groh, K. J., Backhaus, T., Carney-Almroth, B., Geueke, B., Inostroza, P. A., Lennquist, A., Leslie, H. A., Maffini, M., Slunge, D., Trasande, L., Warhurst, A. M., & Muncke, J. (2019). Overview of known plastic packaging-associated chemicals and their hazards. Science of the Total Environment, 651, 3253–3268. 10.1016/j.scitotenv.2018.10.015

Heinze, W. M., Mitrano, D. M., Lahive, E., Koestel, J., & Cornelis, G. (2021). Nanoplastic Transport in Soil via Bioturbation by Lumbricus terrestris. Environmental Science & Technology, 55(24), 16423–16433. 10.1021/acs.est.1c05614

Hidalgo-Ruz, V., Gutow, L., Thompson, R. C., & Thiel, M. (2012). Microplastics in the Marine Environment: A Review of the Methods Used for Identification and Quantification. Environmental Science & Technology, 46(6), 3060–3075. 10.1021/es2031505

Hofman, S. C. K., & Brus, D. J. (2021). How many sampling points are needed to estimate the mean nitrate-N content of agricultural fields? A geostatistical simulation approach with uncertain variograms. Geoderma, 385, 114816. 10.1016/j.geoderma.2020.114816

Horton, A. A., Svendsen, C., Williams, R. J., Spurgeon, D. J., & Lahive, E. (2017). Large microplastic particles in sediments of tributaries of the River Thames, UK – Abundance, sources and methods for effective quantification. Marine Pollution Bulletin, 114(1), 218–226. 10.1016/j.marpolbul.2016.09.004

Huerta Lwanga, E., Mendoza Vega, J., Ku Quej, V., Chi, J. D. L. A., Sanchez Del Cid, L., Chi, C., Escalona Segura, G., Gertsen, H., Salánki, T., Van Der Ploeg, M., Koelmans,

A. A., & Geissen, V. (2017). Field evidence for transfer of plastic debris along a terrestrial food chain. Scientific Reports, 7(1)10.1038/s41598-017-14588-2

Hurley, R. R., & Nizzetto, L. (2018). Fate and occurrence of micro(nano)plastics in soils: Knowledge gaps and possible risks. Current Opinion in Environmental Science & Health, 1, 6–11. 10.1016/j.coesh.2017.10.006

Hurley, R. R., Lusher, A. L., Olsen, M., & Nizzetto, L. (2018). Validation of a Method for Extracting Microplastics from Complex, Organic-Rich, Environmental Matrices. American Chemical Society (ACS). 10.1021/acs.est.8b01517

Ivleva, N. P. (2021). Chemical Analysis of Microplastics and Nanoplastics: Challenges, Advanced Methods, and Perspectives. American Chemical Society (ACS). 10.1021/acs.chemrev.1c00178

Jaisi, D. P., & Elimelech, M. (2009). Single-Walled Carbon Nanotubes Exhibit Limited Transport in Soil Columns. Environmental Science & Technology, 43(24), 9161–9166. 10.1021/es901927y

Jia, W., Karapetrova, A., Zhang, M., Xu, L., Li, K., Huang, M., Wang, J., & Huang, Y. (2022). Automated identification and quantification of invisible microplastics in agricultural soils. Science of the Total Environment, 844, 156853. 10.1016/j.scitotenv.2022.156853

Jiang, X. J., Liu, W., Wang, E., Zhou, T., & Xin, P. (2017). Residual plastic mulch fragments effects on soil physical properties and water flow behavior in the Minqin Oasis, northwestern China. Soil and Tillage Research, 166, 100–107. 10.1016/j.still.2016.10.011

Karlsson, T. M., Hassellöv, M., & Jakubowicz, I. (2018). Influence of thermooxidative degradation on the in situ fate of polyethylene in temperate coastal waters. Marine Pollution Bulletin, 135, 187–194. 10.1016/j.marpolbul.2018.07.015

Kaur, M., Xu, M., & Wang, L. (2022). Cyto–Genotoxic Effect Causing Potential of Polystyrene Micro-Plastics in Terrestrial Plants. Nanomaterials, 12(12)10.3390/nano12122024

Khalid, N., Aqeel, M., & Noman, A. (2020). Microplastics could be a threat to plants in terrestrial systems directly or indirectly. Environmental Pollution, 267, 115653. 10.1016/j.envpol.2020.115653

Kim, S. W., & An, Y. (2020). Edible size of polyethylene microplastics and their effects on springtail behavior. Environmental Pollution, 266, 115255. 10.1016/j.envpol.2020.115255

Kong, S., Ji, Y., Liu, L., Chen, L., Zhao, X., Wang, J., Bai, Z., & Sun, Z. (2012). Diversities of phthalate esters in suburban agricultural soils and wasteland soil appeared with urbanization in China. Environmental Pollution, 170, 161–168. 10.1016/j.envpol.2012.06.017

Kühn, S., van Werven, B., van Oyen, A., Meijboom, A., Bravo Rebolledo, E. L., & van Franeker, J. A. (2017). The use of potassium hydroxide (KOH) solution as a suitable approach to isolate plastics ingested by marine organisms. Marine Pollution Bulletin, 115(1), 86–90. 10.1016/j.marpolbul.2016.11.034

Lan, T., Wang, T., Cao, F., Yu, C., Chu, Q., & Wang, F. (2021). A comparative study on the adsorption behavior of pesticides by pristine and aged microplastics from agricultural polyethylene soil films. Ecotoxicology and Environmental Safety, 209, 111781. 10.1016/j.ecoenv.2020.111781

Lassen, C., Hansen, S. F., Magnusson, K., Hartmann, N. B., Rehne Jensen, P., Nielsen, T. G., & Brinch, A. (2015). Microplastics: Occurrence, effects and sources of releases to the environment in Denmark. Danish Environmental Protection Agency. http://mst.dk/service/publikationer/publikationsarkiv/2015/nov/rapport-ommikroplast

Lee, H., Byun, D., Kim, J. M., & Kwon, J. (2018). Desorption modeling of hydrophobic organic chemicals from plastic sheets using experimentally determined diffusion coefficients in plastics. Marine Pollution Bulletin, 126, 312–317. 10.1016/j.marpolbul.2017.11.032

Li, H., Zhu, D., Lindhardt, J. H., Lin, S., Ke, X., & Cui, L. (2021). Long-Term Fertilization History Alters Effects of Microplastics on Soil Properties, Microbial Communities, and Functions in Diverse Farmland Ecosystem. Environmental Science & Technology, 55(8), 4658–4668. 10.1021/acs.est.0c04849

Li, H., Wang, F., Li, J., Deng, S., & Zhang, S. (2021). Adsorption of three pesticides on polyethylene microplastics in aqueous solutions: Kinetics, isotherms, thermodynamics, and molecular dynamics simulation. Chemosphere, 264, 128556. 10.1016/j.chemosphere.2020.128556

Li, M., Jia, H., Gao, Q., Han, S., Yu, Y., & Sun, L. (2023). Influence of aged and pristine polyethylene microplastics on bioavailability of three heavy metals in soil: Toxic effects to earthworms (Eisenia fetida). Chemosphere, 311, 136833. 10.1016/j.chemosphere.2022.136833

Li, M., Liu, Y., Xu, G., Wang, Y., & Yu, Y. (2021). Impacts of polyethylene microplastics on bioavailability and toxicity of metals in soil. Science of the Total Environment, 760, 144037. 10.1016/j.scitotenv.2020.144037

Li, Z., Hu, X., Qin, L., & Yin, D. (2020). Evaluating the effect of different modified microplastics on the availability of polycyclic aromatic hydrocarbons. Water Research, 170, 115290. 10.1016/j.watres.2019.115290

Liu, M., Lu, S., Song, Y., Lei, L., Hu, J., Lv, W., Zhou, W., Cao, C., Shi, H., Yang, X., & He, D. (2018). Microplastic and mesoplastic pollution in farmland soils in suburbs of Shanghai, China. Environmental Pollution, 242, 855–862. 10.1016/j.envpol.2018.07.051

Liu, Y., Xu, G., & Yu, Y. (2022). Effects of polystyrene microplastics on accumulation of pyrene by earthworms. Chemosphere, 296, 134059. 10.1016/j.chemosphere.2022.134059

Löder, Imhof, Ladehoff, Löschel, Lorenz, Mintenig, Piehl, Primpke, Schrank, Laforsch, & Gerdts. (2017). Enzymatic Purification of Microplastics in Environmental Samples. Environmental Science &Amp; Technology, 51(24), 14283–14292. 10.1021/acs.est.7b03055

Lozano, Y. M., & Rillig, M. C. (2020). Effects of Microplastic Fibers and Drought on Plant Communities. Environmental Science & Technology, 54(10), 6166–6173. 10.1021/acs.est.0c01051

Lu, X., Hu, H., Li, J., Li, J., Wang, L., Liu, L., & Tang, Y. (2023). Microplastics existence affected heavy metal affinity to ferrihydrite as a representative sediment mineral. Science of the Total Environment, 859, 160227. 10.1016/j.scitotenv.2022.160227

Lv, L., Qu, J., Yu, Z., Chen, D., Zhou, C., Hong, P., Sun, S., & Li, C. (2019). A simple method for detecting and quantifying microplastics utilizing fluorescent dyes - Safranine T, fluorescein isophosphate, Nile red based on thermal expansion and contraction property. Elsevier BV. 10.1016/j.envpol.2019.113283

Ma, J., Xu, M., Wu, J., Yang, G., Zhang, X., Song, C., Long, L., Chen, C., Xu, C., & Wang, Y. (2023). Effects of variable-sized polyethylene microplastics on soil chemical properties and functions and microbial communities in purple soil. Science of the Total Environment, 868, 161642. 10.1016/j.scitotenv.2023.161642

Maes, Jessop, Wellner, Haupt, & Mayes. (2017). A rapid-screening approach to detect and quantify microplastics based on fluorescent tagging with Nile Red. Scientific Reports, 7(1), 44501. 10.1038/srep44501

Mao, R., Lang, M., Yu, X., Wu, R., Yang, X., & Guo, X. (2020). Aging mechanism of microplastics with UV irradiation and its effects on the adsorption of heavy metals. Journal of Hazardous Materials, 393, 122515. 10.1016/j.jhazmat.2020.122515

Materić, D., Kasper-Giebl, A., Kau, D., Anten, M., Greilinger, M., Ludewig, E., Van Sebille, E., Röckmann, T., & Holzinger, R. (2020). Micro- and Nanoplastics in Alpine Snow: A New Method for Chemical Identification and (Semi)Quantification in the Nanogram Range. Environmental Science &Amp; Technology, 54(4), 2353. 10.1021/acs.est.9b07540

McGechan, M. B. (2002). SW—Soil and Water: Transport of Particulate and Colloid-sorbed Contaminants through Soil, Part 2: Trapping Processes and Soil Pore Geometry. Biosystems Engineering, 83(4), 387–395. 10.1006/bioe.2002.0136

Möller, Löder, & Laforsch. (2020). Finding Microplastics in Soils: A Review of Analytical Methods. Environmental Science &Amp; Technology, 54(4), 2078–2090. 10.1021/acs.est.9b04618

Morales, V. L., Gao, B., & Steenhuis, T. S. (2009). Grain Surface-Roughness Effects on Colloidal Retention in the Vadose Zone. Vadose Zone Journal, 8(1), 11. 10.2136/vzj2007.0171

Moses, S. R., Roscher, L., Primpke, S., Hufnagl, B., Löder, M. G. J., Gerdts, G., & Laforsch, C. (2023). Comparison of two rapid automated analysis tools for large FTIR microplastic datasets. Springer Science and Business Media LLC. 10.1007/s00216-023-04630-w

Murphy, F., Ewins, C., Carbonnier, F., & Quinn, B. (2016). Wastewater Treatment Works (WwTW) as a Source of Microplastics in the Aquatic Environment. Environmental Science & Technology, 50(11), 5800–5808. 10.1021/acs.est.5b05416

Nel, H. A., Chetwynd, A. J., Kelleher, L., Lynch, I., Mansfield, I., Margenat, H., Onoja, S., Goldberg Oppenheimer, P., Sambrook Smith, G. H., & Krause, S. (2021). Detection limits are central to improve reporting standards when using Nile red for microplastic quantification. Chemosphere (Oxford), 263, 127953. 10.1016/j.chemosphere.2020.127953

Nelson, T. F., Remke, S. C., Kohler, H. E., McNeill, K., & Sander, M. (2020). Quantification of Synthetic Polyesters from Biodegradable Mulch Films in Soils. Environmental Science & Technology, 54(1), 266–275. 10.1021/acs.est.9b05863

Nizzetto, L., Futter, M., & Langaas, S. (2016). Are Agricultural Soils Dumps for Microplastics of Urban Origin? Environmental Science &Amp; Technology, 50(20), 10777. 10.1021/acs.est.6b04140

Pachapur, V. L., Dalila Larios, A., Cledón, M., Brar, S. K., Verma, M., & Surampalli, R. Y. (2016). Behavior and characterization of titanium dioxide and silver nanoparticles in soils. Science of the Total Environment, 563-564, 933–943. 10.1016/j.scitotenv.2015.11.090

Papini, G., Petrella, G., Cicero, D. O., Boglione, C., & Rakaj, A. (2024). Identification and quantification of polystyrene microplastics in marine sediments facing a river mouth through NMR spectroscopy. Marine Pollution Bulletin, 198, 115784. 10.1016/j.marpolbul.2023.115784

Peez, N., Becker, J., Ehlers, S. M., Fritz, M., Fischer, C. B., Koop, J. H. E., Winkelmann, C., & Imhof, W. (2019). Quantitative analysis of PET microplastics in environmental model samples using quantitative 1H-NMR spectroscopy: validation of an optimized and consistent sample clean-up method. Analytical and Bioanalytical Chemistry, 411(28), 7409–7418. 10.1007/s00216-019-02089-2

Peez, N., & Imhof, W. (2020). Quantitative 1H-NMR spectroscopy as an efficient method for identification and quantification of PVC, ABS and PA microparticles. Analyst, 145(15), 5363–5371. 10.1039/D0AN00879F

Peez, N., Janiska, M., & Imhof, W. (2018). The first application of quantitative 1 H NMR spectroscopy as a simple and fast method of identification and quantification of microplastic particles (PE, PET, and PS)10.1007/s00216-018-1510

Primpke, S.; Christiansen, S. H.; Cowger, W.; De Frond, H.; Deshpande, A.; Fischer, M.; Holland, E. B.; Meyns, M.; O'Donnell, B. A.; Ossmann, B. E.Critical Assessment of Analytical Methods for the Harmonized and Cost-Efficient Analysis of Microplastics. *Appl. Spectrosc.* 2020, *74*, 1012– 1047, DOI: 10.1177/0003702820921465

Radford, F., Zapata-Restrepo, L. M., Horton, A. A., Hudson, M. D., Shaw, P. J., & Williams, I. D. (2021). Developing a systematic method for extraction of microplastics in soils. Analytical Methods, 13(14), 1695–175. 10.1039/d0ay02086a

Ramos, L., Berenstein, G., Hughes, E. A., Zalts, A., & Montserrat, J. M. (2015). Polyethylene film incorporation into the horticultural soil of small periurban production units in Argentina. Science of the Total Environment, 523, 74–81. 10.1016/j.scitotenv.2015.03.142

Rillig, M. C. (2018). Microplastic Disguising As Soil Carbon Storage. Environmental Science & Technology, 52(11), 6079–6080. 10.1021/acs.est.8b02338

Rillig, M. C. (2020). Plastic and plants. Nature Sustainability, 3(11), 887–888. 10.1038/s41893-020-0583-9

Rillig, M. C., Ziersch, L., & Hempel, S. (2017). Microplastic transport in soil by earthworms. Scientific Reports, 7(1), 1362. 10.1038/s41598-017-01594-7

Sander, M. (2019). Biodegradation of Polymeric Mulch Films in Agricultural Soils: Concepts, Knowledge Gaps, and Future Research Directions. Environmental Science & Technology, 53(5), 2304–2315. 10.1021/acs.est.8b05208

Scarascia-Mugnozza, G., Sica, C., & Russo, G. (2012). PLASTIC MATERIALS IN EUROPEAN AGRICULTURE : ACTUAL USE AND PERSPECTIVES. Journal of Agricultural Engineering, 42(3), 15–28. 10.4081/jae.2011.3.15

Scheurer, M., & Bigalke, M. (2018). Microplastics in Swiss Floodplain Soils. Environmental Science &Amp; Technology, 52(6), 3591. 10.1021/acs.est.7b06003

Schrank, I., Möller, J. N., Imhof, H. K., Hauenstein, O., Zielke, F., Agarwal, S., Löder, M. G. J., Greiner, A., & Laforsch, C. (2022). Microplastic sample purification methods - Assessing detrimental effects of purification procedures on specific plastic types. The Science of the Total Environment, 833, 154824. 10.1016/j.scitotenv.2022.154824

Seeley, M. E., Song, B., Passie, R., & Hale, R. C. (2020). Microplastics affect sedimentary microbial communities and nitrogen cycling. Nature Communications, 11(1), 2372. 10.1038/s41467-020-16235-3

Shruti, Pérez-Guevara, Roy, & Kutralam-Muniasamy. (2022). Analyzing microplastics with Nile Red : Emerging trends, challenges, and prospects. Journal of Hazardous Materials, 423(Pt B), 127171. 10.1016/j.jhazmat.2021.127171

Shu, X., Yang, M., Lin, H., Zhang, Q., Zhang, L., Liu, J., Zhang, X., Pan, F., & Xu, L. (2023). Oxalic-activated minerals enhance the stabilization of polypropylene and polyamide microplastics in soil: Crucial roles of mineral dissolution coupled surface oxygen-functional groups. Science of the Total Environment, 875, 162563. 10.1016/j.scitotenv.2023.162563

Siegfried, M., Koelmans, A. A., Besseling, E., & Kroeze, C. (2017). Export of microplastics from land to sea. A modelling approach. Water Research, 127, 249–257. 10.1016/j.watres.2017.10.011

Sobhani, Z., Fang, C., Naidu, R., & Megharaj, M. (2021). Microplastics as a vector of toxic chemicals in soil: Enhanced uptake of perfluorooctane sulfonate and perfluorooctanoic acid by earthworms through sorption and reproductive toxicity. Environmental Technology & Innovation, 22, 101476. 10.1016/j.eti.2021.101476

Su, L., Xiong, X., Zhang, Y., Wu, C., Xu, X., Sun, C., & Shi, H. (2022). Global transportation of plastics and microplastics: A critical review of pathways and influences. Science of the Total Environment, 831, 154884. 10.1016/j.scitotenv.2022.154884

Suaria, G., Achtypi, A., Perold, V., Lee, J. R., Pierucci, A., Bornman, T. G., Aliani, S., & Ryan, P. G.Microfibers in oceanic surface waters: A global characterization. Science Advances, 6(23), eaay8493. 10.1126/sciadv.aay8493

Sun, B., Hu, Y., Cheng, H., & Tao, S. (2019). Releases of brominated flame retardants (BFRs) from microplastics in aqueous medium: Kinetics and molecular-size dependence of diffusion. Water Research, 151, 215–225. 10.1016/j.watres.2018.12.017

Sun, W., Meng, Z., Li, R., Zhang, R., Jia, M., Yan, S., Tian, S., Zhou, Z., & Zhu, W. (2021). Joint effects of microplastic and dufulin on bioaccumulation, oxidative stress and metabolic profile of the earthworm (Eisenia fetida). Chemosphere, 263, 128171. 10.1016/j.chemosphere.2020.128171

Sun, Y., Li, X., Li, X., & Wang, J. (2022). Deciphering the Fingerprint of Dissolved Organic Matter in the Soil Amended with Biodegradable and Conventional Microplastics Based on Optical and Molecular Signatures. Environmental Science & Technology, 56(22), 15746–15759. 10.1021/acs.est.2c06258

Šunta, U., Prosenc, F., Trebše, P., Bulc, T. G., & Kralj, M. B. (2020). Adsorption of acetamiprid, chlorantraniliprole and flubendiamide on different type of microplastics present in alluvial soil. Chemosphere, 261, 127762. 10.1016/j.chemosphere.2020.127762

Tagg, A. S., Harrison, J. P., Ju-Nam, Y., Sapp, M., Bradley, E. L., Sinclair, C. J., & Ojeda, J. J. (2017). Fenton's reagent for the rapid and efficient isolation of microplastics from wastewater. Chemical Communications, 53(2), 372–375. 10.1039/C6CC08798A

Tarafdar, A., Choi, S., & Kwon, J. (2022). Differential staining lowers the false positive detection in a novel volumetric measurement technique of microplastics. Journal of Hazardous Materials, 432, 128755. 10.1016/j.jhazmat.2022.128755

Thomas, D., Schütze, B., Heinze, W. M., & Steinmetz, Z. (2020). Sample Preparation Techniques for the Analysis of Microplastics in Soil—A Review. Sustainability (Basel, Switzerland), 12(21), 9074. 10.3390/su12219074

Thompson, R. C., Courtene-Jones, W., Boucher, J., Pahl, S., Raubenheimer, K., & Koelmans, A. A. (2024). Twenty years of microplastic pollution research—what have we learned? Science, 386(6720)10.1126/science.adl2746

Tian, C., Lv, J., Zhang, W., Wang, H., Chao, J., Chai, L., & Lin, Z. (2022). Accelerated Degradation of Microplastics at the Liquid Interface of Ice Crystals in Frozen Aqueous Solutions. Angewandte Chemie - International Edition, 61(31)10.1002/anie.202206947

Transparency Market Research. (2013). Agricultural Films (LDPE, LLDPE, HDPE, EVA/EBA, Reclaims and Others) Market for Greenhouse, Mulching and Silage Applications-Global Industry Analysis, Size, Share, Growth, Trends and Forecast, 2013–2019. .

Tun, T. Z., Kunisue, T., Tanabe, S., Prudente, M., Subramanian, A., Sudaryanto, A., Viet, P. H., & Nakata, H. (2022). Microplastics in dumping site soils from six Asian countries as a source of plastic additives. Science of the Total Environment, 806, 150912. 10.1016/j.scitotenv.2021.150912

Uhrin, A. V., & Kershaw, P. J. (2020). GESAMP 2019 Guidelines for the monitoring & assessment of plastic litter in the ocean Reports & Studies 99 (editors Kershaw, P.J., Turra, A. and Galgani, F.)

UNEP. (2021). A GLOBAL ASSESSMENT OF MARINE LITTER AND PLASTIC POLLUTION. .United Nations Environment Programme.

Van Kleunen, M., Brumer, A., Gutbrod, L., & Zhang, Z. (2019). A microplastic used as infill material in artificial sport turfs reduces plant growth. Wiley. 10.1002/ppp3.10071

Vu, T. T. T., Nguyen, D. T., Nguyen, N. T. M., & Nguyen, M. N. (2022). Coaggregation of micro polystyrene particles and suspended minerals under concentrated salt solution: A perspective of terrestrial-to-ocean transfer of microplastics. Marine Pollution Bulletin, 185, 114317. 10.1016/j.marpolbul.2022.114317

Wan, Y., Wu, C., Xue, Q., & Hui, X. (2019). Effects of plastic contamination on water evaporation and desiccation cracking in soil. Science of the Total Environment, 654, 576–582. 10.1016/j.scitotenv.2018.11.123

Wang, C., O'Connor, D., Wang, L., Wu, W., Luo, J., & Hou, D. (2022). Microplastics in urban runoff: Global occurrence and fate. Water Research, 225, 119129. 10.1016/j.watres.2022.119129

Wang, F., Wang, X., & Song, N. (2021). Polyethylene microplastics increase cadmium uptake in lettuce (Lactuca sativa L.) by altering the soil microenvironment. Science of the Total Environment, 784, 147133. 10.1016/j.scitotenv.2021.147133

Wang, H., Yu, B., Li, B., Zhao, T., Cai, Y., Luo, Y., & Zhang, H. (2022). A contrasting alteration of sulfamethoxazole bioaccessibility in two different soils amended with polyethylene microplastic: In-situ measurement using diffusive gradients in thin films. Science of the Total Environment, 808, 152187. 10.1016/j.scitotenv.2021.152187

Wang, J., Huang, M., Wang, Q., Sun, Y., Zhao, Y., & Huang, Y. (2020a). LDPE microplastics significantly alter the temporal turnover of soil microbial communities. Science of the Total Environment, 726, 138682. 10.1016/j.scitotenv.2020.138682

Wang, J., Li, J., Wang, Q., & Sun, Y. (2020b). Microplastics as a Vector for HOC Bioaccumulation in Earthworm Eisenia fetida in Soil: Importance of Chemical Diffusion and Particle Size. Environmental Science & Technology, 54(19), 12154–12163. 10.1021/acs.est.0c03712

Wang, J., Luo, Y., Teng, Y., Ma, W., Christie, P., & Li, Z. (2013). Soil contamination by phthalate esters in Chinese intensive vegetable production systems with different modes of use of plastic film. Environmental Pollution, 180, 265–273. 10.1016/j.envpol.2013.05.036

Wang, T., Yu, C., Chu, Q., Wang, F., Lan, T., & Wang, J. (2020). Adsorption behavior and mechanism of five pesticides on microplastics from agricultural polyethylene films. Chemosphere, 244, 125491. 10.1016/j.chemosphere.2019.125491

Wang, Y., Yang, Y., Liu, X., Zhao, J., Liu, R., & Xing, B. (2021). Interaction of Microplastics with Antibiotics in Aquatic Environment: Distribution, Adsorption, and Toxicity. Environmental Science & Technology, 55(23), 15579–15595. 10.1021/acs.est.1c04509

Wang, Y., Xiang, L., Wang, F., Wang, Z., Bian, Y., Gu, C., Wen, X., Kengara, F. O., Schäffer, A., Jiang, X., & Xing, B. (2022). Positively Charged Microplastics Induce Strong Lettuce Stress Responses from Physiological, Transcriptomic, and Metabolomic Perspectives. Environmental Science & Technology, 56(23), 16907–16918. 10.1021/acs.est.2c06054

Wang, Y., Wang, X., Li, Y., Li, J., Liu, Y., Xia, S., & Zhao, J. (2021). Effects of exposure of polyethylene microplastics to air, water and soil on their adsorption behaviors for copper and tetracycline. Chemical Engineering Journal, 404, 126412. 10.1016/j.cej.2020.126412

Wu, J., Gao, J., Pei, Y., Luo, K., Yang, W., Wu, J., Yue, X., Wen, J., & Luo, Y. (2024a). Microplastics in agricultural soils: A comprehensive perspective on occurrence,

environmental behaviors and effects. Chemical Engineering Journal, 489, 151328. 10.1016/j.cej.2024.151328

Wu, S., Chen, Z., Zhou, M., Shao, Y., Jin, C., Tang, J., Fang, F., Guo, J., Stibany, F., & Schäffer, A. (2022). Freeze-thaw alternations accelerate plasticizers release and pose a risk for exposed organisms. Ecotoxicology and Environmental Safety, 241, 113742. 10.1016/j.ecoenv.2022.113742

Xu, G., Liu, Y., Song, X., Li, M., & Yu, Y. (2021). Size effects of microplastics on accumulation and elimination of phenanthrene in earthworms. Journal of Hazardous Materials, 403, 123966. 10.1016/j.jhazmat.2020.123966

Xu, Y., Zeng, L., Tao, Y., Xu, J., He, Y., & Lu, Z. (2023). Release of Additives from Agricultural Plastic Films in Water: Experiment and Modeling. Environmental Science & Technology, 57(27), 10053–10061. 10.1021/acs.est.2c09738

Yang, Y., Xu, G., & Yu, Y. (2022). Microplastics impact the accumulation of metals in earthworms by changing the gut bacterial communities. Science of the Total Environment, 831, 154848. 10.1016/j.scitotenv.2022.154848

Yousif, E., & Haddad, R. (2013). Photodegradation and photostabilization of polymers, especially polystyrene: review. SpringerPlus, 2(1), 398. 10.1186/2193-1801-2-398

Yu, H., Qi, W., Cao, X., Hu, J., Li, Y., Peng, J., Hu, C., & Qu, J. (2021). Microplastic residues in wetland ecosystems: Do they truly threaten the plant-microbe-soil system? Environment International, 156, 106708. 10.1016/j.envint.2021.106708

Yu, Y., & Flury, M. (2021). How to take representative samples to quantify microplastic particles in soil? The Science of the Total Environment, 784, 147166. 10.1016/j.scitotenv.2021.147166

Zhang, G. S., Zhang, F. X., & Li, X. T. (2019). Effects of polyester microfibers on soil physical properties: Perception from a field and a pot experiment. Science of the Total Environment, 670, 1–7. 10.1016/j.scitotenv.2019.03.149

Zhang, M., Zhao, Y., Qin, X., Jia, W., Chai, L., Huang, M., & Huang, Y. (2019). Microplastics from mulching film is a distinct habitat for bacteria in farmland soil. Science of the Total Environment, 688, 470–478. 10.1016/j.scitotenv.2019.06.108

Zhang, S., He, Z., Wu, C., Wang, Z., Mai, Y., Hu, R., Zhang, X., Huang, W., Tian, Y., Xia, D., Wang, C., Yan, Q., He, Z., & Shu, L. (2022). Complex Bilateral Interactions Determine the Fate of Polystyrene Micro- and Nanoplastics and Soil Protists: Implications from a Soil Amoeba. Environmental Science & Technology, 56(8), 4936–4949. 10.1021/acs.est.1c06178

Zhang, W., Morales, V. L., Cakmak, M. E., Salvucci, A. E., Geohring, L. D., Hay, A. G., Parlange, J., & Steenhuis, T. S. (2010). Colloid Transport and Retention in Unsaturated Porous Media: Effect of Colloid Input Concentration. Environmental Science & Technology, 44(13), 4965–4972. 10.1021/es100272f

Zhao, Y., Li, Y., Wang, J., Pang, H., & Li, Y. (2016). Buried straw layer plus plastic mulching reduces soil salinity and increases sunflower yield in saline soils. Soil and Tillage Research, 155, 363–370. 10.1016/j.still.2015.08.019

Zhou, Y., Liu, X., & Wang, J. (2019). Characterization of microplastics and the association of heavy metals with microplastics in suburban soil of central China. Science of the Total Environment, 694, 133798. 10.1016/j.scitotenv.2019.133798

Zhou, Y., Liu, X., & Wang, J. (2020). Ecotoxicological effects of microplastics and cadmium on the earthworm Eisenia foetida. Journal of Hazardous Materials, 392, 122273. 10.1016/j.jhazmat.2020.122273

Zhu, L., Zhao, S., Bittar, T. B., Stubbins, A., & Li, D. (2020). Photochemical dissolution of buoyant microplastics to dissolved organic carbon: Rates and microbial impacts. Journal of Hazardous Materials, 383, 121065. 10.1016/j.jhazmat.2019.121065

Zubris, K. A. V., & Richards, B. K. (2005). Synthetic fibers as an indicator of land application of sludge. Environmental Pollution, 138(2), 201–211. 10.1016/j.envpol.2005.04.013

# Overview to the thesis

Plastic contamination in soil is a growing environmental concern with significant implications for agricultural sustainability, ecosystem health, and long-range pollutant transport. This PhD research addresses the critical challenge of plastic contamination in soils by systematically developing, evaluating, and applying advanced analytical methodologies to detect and quantify microplastics and nanoplastics in soil, bridging methodological innovation with practical environmental assessments. The five chapters of this thesis are designed to build progressively, creating a cohesive narrative that addresses both the technical and applied dimensions of this pressing issue.

**Chapter 1** offers a broad introduction to plastic pollution, with a focus on microplastics and nanoplastics as emerging environmental contaminants. It emphasizes soil as a major sink for plastic accumulation and reviews current literature on the behavior and ecological effects of plastics in soil systems. The chapter also explores analytical methods, outlining major challenges and recent progress in detection and quantification. It concludes by presenting the aims and objectives of the thesis, framing the research within the wider context of soil plastic contamination, methodological developments, and environmental relevance.

**Chapter 2** focuses on the development, optimization, and validation of fluorescence microscopy as a rapid, user-friendly, and high-throughput approach for detecting microplastic across diverse soil and plastic types. This foundational work enhances the method's accuracy and broadens its applicability to complex environmental matrices. Building on this groundwork, **Chapter 3** expands the scope by comparing six microplastic detection methods—fluorescence microscopy, digital microscopy, Fourier transform infrared and Raman micro-spectroscopy, quantitative nuclear magnetic resonance and pyrolysis-gas chromatography coupled with mass spectrometry. These techniques are applied to the same soil and plastic materials as in Chapter 1, with extraction protocols tailored to the requirements of each analytical endpoint. This comparative study rigorously evaluates the strengths and limitations of each method, ensuring robust and reliable assessments of their effectiveness.

**Chapter 4** transitions from method development to applied research, using validated Fourier transform infrared techniques to investigate microplastic contamination in agricultural soils following sewage sludge application. The study begins by identifying and quantifying plastics in sewage sludge, then examines fields where the sludge has been applied, comparing them to untreated background fields to evaluate its impact on soil plastic contamination.

**Chapter 5** extents this investigation by exploring the long-term presence of microplastic in soils that were historically treated with sewage sludge and later amended with anaerobic digestate derived from animal manure—an emerging agricultural practice in the UK. This chapter assesses how these amendments influence plastic accumulation and

persistence over time. By applying Raman spectroscopy, Fourier transformed infrared micro-spectroscopy, and fluorescence microscopy to the same samples, it provides a comprehensive analysis while critically examining the strengths and limitations of these techniques for detecting MPs in complex soil environments.

**Chapter 6** focuses on nanoplastic, pioneering a novel approach for their detection and quantification in soils from remote environments. The findings provide critical insights into nanoplastic presence in one of Earth's most pristine regions, Antarctica, serving as a proxy for assessing baseline contamination levels in global soils. Potential sources of plastics, particularly those associated with long-range atmospheric transport, are explored using backward trajectory models.

In addition to these chapters, the author also collaborated on two other projects: one investigating plastic inputs and dynamics in industrial composting processes (**Appendix 1**), and the other exploring the microbial associations of plastic mulching in soil (**Appendix 2**). These complementary studies broaden the understanding of plastic behaviour and impacts across different environmental contexts.

Together, these chapters form a cohesive narrative that begins with method development, advances through validation and comparative analysis, and culminates in applied research addressing real-world contamination scenarios. By integrating laboratory advancements with environmental applications, this thesis significantly enhances the ability to detect MPs and NPs with precision while providing crucial data on their sources, persistence, and transport. The findings contribute to a deeper understanding of plastic contamination in soils, offering valuable insights for developing mitigation strategies and supporting global monitoring efforts.

# 2 Toward quality-assured measurements of microplastics in soil using fluorescence microscopy

*This chapter develops and validates a fluorescence microscopy method using Nile red staining for microplastic detection in soil. It integrates a streamlined extraction protocol with automated image analysis to improve accuracy and throughput. The study evaluates its robustness across various microplastic types, sizes, and soil textures, while also examining the fluorescence behaviour of Nile red in different polymers. The method's applicability is demonstrated on real environmental soil samples, with results compared to Fourier-transformed infrared micro-spectroscopy, contributing to fast, reliable, and high-throughput MPs analysis in soils.*

# Towards quality-assured measurements of microplastics in soil using fluorescence microscopy

Quynh Nhu Phan Le[1], Crispin Halsall[1], Stoyana Peneva[2,3], Olivia Wrigley[3], Melanie Braun[3], Wulf Amelung[3], Lorna Ashton[4], Ben W.J. Surridge[1], John Quinton[1]

[1]Lancaster Environment Centre, Lancaster University, Lancaster, LA1 4YQ, UK

[2] Wessling GmbH, Am Umweltpark 1, Bochum, 44793, Germany

[3] Institute of Crop Science and Resource Conservation, University of Bonn, Bonn, 53115 Germany

[4]Department of Chemistry, Lancaster University, Lancaster, LA1 4YQ, UK

Corresponding author:Crispin Halsall (c.halsall@lancaster.ac.uk)

# Abstract

Fluorescence microscopy is increasingly seen as a fast, user-friendly, and high-throughput method for detecting microplastics (MPs) in soil; however, its effectiveness across diverse MP types and soil properties remains underexplored. This study tested a fluorescence microscopy–Nile red (NR) staining approach on eight MP types, covering both biodegradable and non-biodegradable plastics, in three size ranges (≤150 µm, 100–250 µm, 500–1000 µm) across loamy, clayey, and sandy soils. Each sample, processed in triplicate, underwent a relatively quick and straightforward extraction procedure involving density separation, organic digestion, and NR staining, followed by fluorescence microscopy and bright-field microscopy. A new digital image analysis pipeline using Image J was developed to expedite and automate MPs quantification. Recoveries ranged 80-90% for MPs with Feret diameter of 500-1000 µm, regardless of soil type. In contrast, the recovery of smaller MPs (Feret dia. ≤ 250 µm) varied depending on the soils and plastic types: recoveries for low-density polyethylene (LDPE) reached 85% in sandy soil and 90% in loamy soil, whereas those for biodegradable polybutylene adipate terephthalate/polylactic acid (PBAT/PLA) were only 60% and 10%, respectively. The lowest recovery rate was observed in clayey soil and for biodegradable plastics. The method was tested on non-agricultural soil samples, yielding a MPs mean number concentration of 20.7 ± 9.0 MPs/g for MPs sized from dia. ≥25 µm; comparable to Fourier Transform Infrared (FPA-µ-FTIR) results of 13.1 ± 7.3 MPs/g ($p > 0.05$). We conclude that fluorescence microscopy with NR staining and automated particle quantification offers a time-efficient, reproducible, and accurate method for MPs detection in light-textured soils, whereas limitations remain for reliable MPs analysis in clay dominated soils.


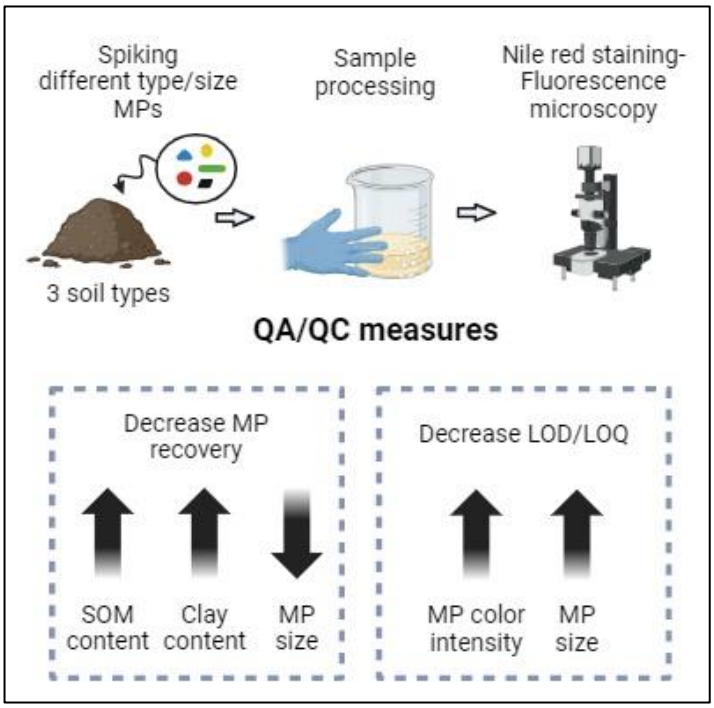


**Keywords**: polymers, soil organic matter, fluorescence microscopy, Nile red staining.

## 2.1 Introduction

Plastic debris is of increasing concern due to enormous levels of plastic production coupled with inefficient recovery and recycling of used plastic products. Plastic pollution has emerged as a major global environmental challenge in recent decades (GESAME, 2015; Werner & O'Brien, 2017). In the environment, plastic debris disintegrates into smaller pieces through chemical, physiochemical, and biological processes. Those with dimensions ranging from 1 µm to 5 mm are defined as microplastics (MPs), accumulating readily in terrestrial and aquatic ecosystems, including freshwaters, sediments, and soils, as well as within the atmosphere and in foodstuffs (Hartmann et al., 2019; Mariano et al., 2021). While MPs pollution in aquatic ecosystems has been widely studied, less research has focused on understanding the occurrence and fate of MPs in terrestrial ecosystems, particularly agricultural soils where plastics are frequently used (e.g., as mulching films or inadvertently applied through biosolid amendments) (Corradini et al., 2019; Crossman et al., 2020a; Huang et al., 2020). Reliable methods for detecting, characterising, and quantifying MPs in soil are essential for understanding their environmental fate and ecological impacts.

Fluorescence microscopy using Nile Red (NR) staining has emerged as a low-cost, relatively simple-to-use approach for analysing a broad spectrum of MPs in complex environmental matrices like soils (Maes et al., 2017a; Shim et al., 2016a; Stanton et al., 2019; Thomas et al., 2020b). The fluorescent tag NR (9-(diethylamino)-5H-benzo[a]phenoxazin-5-one) is the most commonly applied fluorescent dye in MPs research due to its strong fluorescence in a hydrophobic environment (GREENSPAN, P. et al., 1985)(Andrady, 2011). However, the presence of lipophilic natural organic debris in soils can lead to false positives (Michelaraki et al., Oct 05, 2020; Prata et al., 2021; Shim et al., 2016a), and is an example of a potential source of error that needs to be examined further in tests soils with varying natural organic matter (OM) content.

The effectiveness of fluorescence microscopy-NR staining for detecting MPs is strongly influenced by the physiochemical properties of the plastics, including the presence of additives, which can vary widely, particularly in commercial plastics (Maes et al., 2017a). However, most research has concentrated on pristine MPs (Erni-Cassola et al., 2017; Gao, Z. et al., 2022; Shim et al., 2016a) resulting in a limited understanding of NR fluorescence in MPs derived from commercial sources. Moreover, larger-sized MPs fragments (>300 µm) are frequently utilized for method assessment due to their availability and ease of identification (Pérez-Guevara et al., 2022). However, these larger MPs constitute only a minor proportion of the MPs present in the environment and are less relevant to ecotoxicological studies (Pérez-Guevara et al., 2022). The behaviour of smaller MPs, especially in terms of their interaction with soil matrices, can affect the efficiency of MPs extraction and identification from soil, yet our understanding of these processes remains limited.

Given the increasing interest in using fluorescence microscopy for measuring MPs in complex environmental matrices, this study aimed to establish an accurate, reproducible fluorescent-based methodology for analysing MPs in soil, which discriminates plastic size and type across different soil types. Here, a comprehensive appraisal of the method – based on spiking three different soil types with a variety of plastics of varying size categories (dia. ≤150 µm, 100-250 µm and 500-1000 µm) – was undertaken. The method was then applied to non-spiked background soil samples (rural, non-agricultural soil) and compared to an infrared spectroscopy-based methodology. Our hypothesis is that a fluorescent microscopy-NR staining approach is suitable for analysing MPs in soil,

although the efficiency of this technique is influenced by polymer type and size, as well as by the soil characteristics.

# 2.2 Materials and methods

## 2.2.1 Preparation of soil and microplastic standards

### 2.2.1.1 Soil

Sandy and clayey soils (Cambisol and Stagnosol, respectively) were collected near Bonn, Germany, with sandy soil from an agricultural topsoil and clay soil from a forest subsoil (Stoyana Peneva et al.), air-dried and passed through a 2-mm sieve. Standard agricultural loamy soil (air-dried, 2 mm sieved, LUFA 2.4, LUFA Speyer, Germany) was also included for systematic method validation. The physiochemical properties of the LUFA soil were determined and provided according to good laboratory practices, whereas those for sand and clay soils were measured according to reference methods at Bonn University (**Table** S1). In addition, pasture-land soil (with no known recent agricultural amendments) was sampled from Lancaster University, Hazelrigg meteorological field station and used as a non-spiked test soil.

### 2.2.1.2 Reference MPs materials

A mixed MPs standard was created for the recovery experiment, comprising various polymers across size ranges of dia. ≤ 150 µm (low-density polyethene, LDPE), dia. 100-250 µm (polybutylene adipate-co-terephthalate/polylactic acid blend (PBAT/PLA), and dia. 500-1000 µm. For small microplastics (SMPs, ≤ 250 µm), LDPE and PBAT/PLA were used to represent conventional and biodegradable MPs. LDPE particles (≤ 150 µm) were sourced from Goonvean Fibres Ltd, UK, while PBAT/PLA particles (100–250 µm) were cryo-milled and sieved from biodegradable mulching films (Bionov Black, Barbier Group, France).

The larger microplastics (LMPs, dia. 500-1000 µm) are selected from polymer materials that represent the most commonly encountered synthetic polymers in the environment, including low-density and high-density polyethene (LDPE and HDPE), polypropylene (PP), polystyrene (PS), polyethene terephthalate (PET), polyamide (PA), polyvinyl chloride (PVC) (Andrady, 2011) and the biodegradable plastic PBAT/PLA. These LMPs were prepared using a razor blade from consumer items like milk bottle caps and food packaging, as listed in **Table** S2. They were distinguishable for separation from non-spiked MPs and external contaminants, with polymer types confirmed by attenuated total reflectance Fourier transformed infrared spectroscopy ATR FTIR (Lumos II, Bruker) and Raman micro-spectroscopy (WITec alpha 300R, Oxford) (**Figure** S1).

Each 10 g of soil was spiked with MPs to achieve a MPs concentration below 0.1% (w/w). Forty LMPs (five of each polymer type) were counted, photographed, and fixed to a gelatin plate (1 × 1 cm, Dr Oetker Blatt Gelatine) using a needle and fine-point high-precision forceps. Further, 3 mg each of PBAT/PLA (dia. 100-250 µm) and LDPE (dia. ≤150 µm) particles were encapsulated in gelatin "dumplings" for loss-free soil incorporation (**Figure** S2 and S3). (Möller et al., 2022) The gelatin plate and “dumplings” were added to soil, shaken in water and zinc chloride ($ZnCl_2$) solution for 2 hours at room temperature to dissolve the gelatin and release the MPs for subsequent extraction.

## 2.2.2 Extraction of microplastics from soils

MPs were extracted from the soil, starting with a density separation step (**Figure** 2.1.) using a 1.5 g $cm^{-3}$ $ZnCl_2$ solution (≥ 97%, APC Pure, UK) in a Sediment Microplastic Isolation (SMI) unit (**Figure** S4). (Coppock et al., 2017; Vermeiren, P. et al., 2020) The pre-cleaned unit was filled with 10 g of soil and 50 mL of $ZnCl_2$, shaken for 2 hours, and settled overnight after an additional 200 mL of $ZnCl_2$. The supernatant was filtered on a stainless-steel mesh (pore dia. 6 µm, 47-mm Ø, GKD industrial, Germany), rinsed with HPLC-grade water ($H_2O$, Fisher Scientific, UK), and Zn precipitates dissolved with 10% sulfuric acid ($H_2SO_4$, Fisher Scientific, UK). The filter was placed in a beaker containing 0.05M iron (II) sulphate heptahydrate solution ($FeSO_4.7H_2O$, ≥ 99%, Acros Organics, UK), sonicated, rinsed with HPLC-grade water to collect the extracted particles from the filter. This was followed by addition of 20 mL of 30% hydrogen peroxide ($H_2O_2$, Fisher Scientific, UK) to initiate a Fenton reaction. After 24 hours, samples were filtered onto a glass fibre filter (GFF, pore dia. 0.7 µm, 47-mm Ø, Cytiva Whatman GF/F, Fisher Scientific, UK), stained with 5 mg $L^{-1}$ NR ($C_{20}H_{18}N_2O_2$, 99%, Acros Organics, UK), rinsed with hexane ($C_6H_6$, ≥ 95%, Fisher Scientific, UK), and dried in the dark. Further details of this extraction procedure are provided in the supporting information.

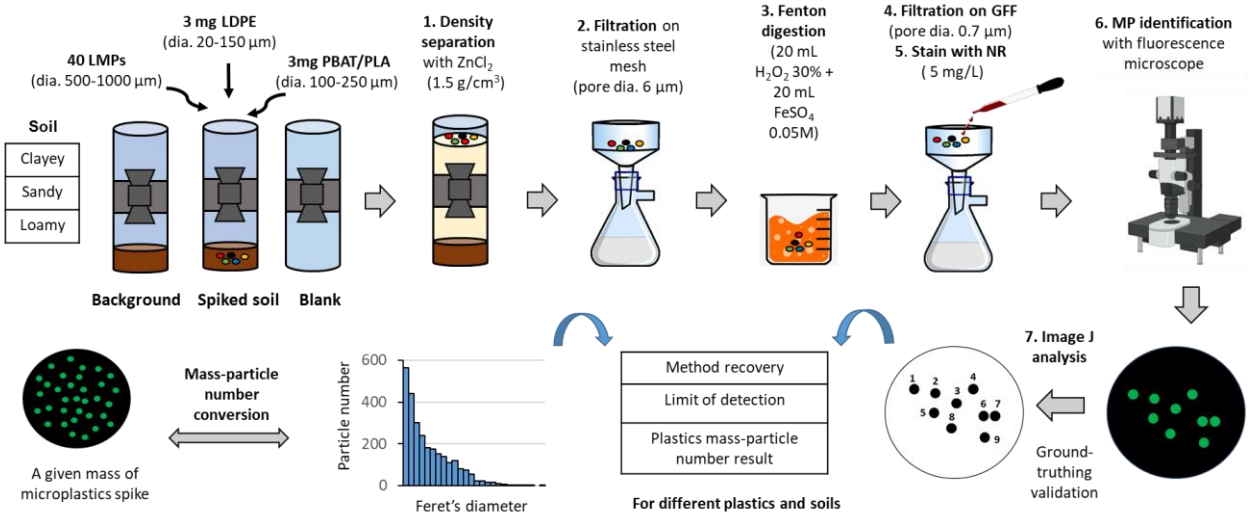


**Figure 2.1.** A schematic showing the extraction and separation steps of the MPs-soil measurement procedure

## 2.2.3 Fluorescence microscopy and image analysis

Fluorescence microscopy imaging was performed using a Zeiss Axio Zoom.V16 microscope equipped with a macro lens, 12MP camera, and automated stage. In a darkroom, samples stained with NR were illuminated at 470 nm and observed through the green filter set (emission 524/50 nm). Images were captured in green fluorescence and BF modes at 50× magnification using Zen Pro software's stitching function and surface focusing.

Particle recognition and quantification were performed in Fiji-ImageJ 1.53t (https:// imagej. nih. gov/ ij/, accessed 21 October 2022), as described in **Figure** S5. Images were imported in Carl Zeiss format (czi) and processed in Tag Image File (tif) format. A Gaussian blur filter was applied to smooth the image, followed by subtraction from the original to minimise noise and reduce detection runtime. Global thresholding segmented particles from the background, with specific grey values set for different experiments. A

fill-hole operation compensated for particle penetration, and watershed segmentation split agglomerated fluorescent particles. For BF images of PBAT/PLA, watershed segmentation was avoided to prevent overcounting caused by irregular shapes. Particles were quantified and classified based on Feret's diameter. LMPs (500-1000 μm) were manually counted due to their varying fluorescence, diverse shapes, and low abundance. Further details of the detection protocols are provided in the supporting information.

*Evaluation of the image segmentation algorithm*

*Accuracy* or *validity* was assessed by comparing manual counts of particles by a human expert with algorithmic counts from Image J. For both fluorescence and BF images, the accuracy—indicating the correct identification rate of particles and background—and sensitivity—reflecting the true positive rate of particle detection—were determined using the following equations (Haibo He & Garcia, 2009):

$$Accuracy\ (\%) = \frac{N_{true\ possitive} + N_{true\ negative}}{N_{true\ positive} + N_{true\ negative} + N_{false\ positive} + N_{false\ negative}} \times 100 \quad (1)$$

$$Sensitivity\ (Recall, \%) = \frac{N_{true\ possitive}}{N_{true\ positive} + N_{false\ negative}} \times 100 \quad (2)$$

where $N_{\text{true positive}}$ and $N_{\text{false positive}}$ are the number of correctly or incorrectly identified particles, respectively, and $N_{\text{true negative}}$ and $N_{\text{false negative}}$ are the number of particles identified correctly or falsely as background pixels, respectively. *Precision (or reliability),* which is the ability of the algorithm to yield the same results from repeat scans of the same image, was assessed by rotating the filter image by 90° counterclockwise, vertically flipping the original image, and comparing the results to the initial scan.

## 2.2.4 Quality assurance and quality control

### 2.2.4.1 Plastic mass versus particle number relationship

Small microplastic particles (SMPs) were spiked at a specific mass instead of particle number, due to the difficulty in handling particles with dia. ≤ 250 μm. SMP particle concentration was determined by introducing 5.0 mg of each reference material (LDPE and PBAT/PLA) to a 100 mL volumetric flask filled with ethanol (five replicates). Samples were sonicated for 15 minutes at room temperature to ensure particle dispersion. Next, 10 mL aliquots were vacuum filtered onto GFFs. LDPE particles were subsequently stained with NR, while PBAT/PLA particles were not stained due to the absence of a detectable fluorescence signal in previous experiments (**Figure** S6) and were instead analysed in BF mode. Both types of SMPs were examined under a fluorescence microscope, followed by ImageJ analysis as previously described, to assess their particle concentration relative to mass and size distribution.

Additionally, particle size distributions of SMPs in ethanol suspension were measured using a Syringe particle counter equipped with a laser diode sensor LDS 30/30 and SW-PE evaluation software (Markus Klotz GmbH, Germany). Each 1.5 mL suspension sample was mixed with a magnetic stirrer to ensure even particle distribution. Measurements were conducted on five replicates per sample, and results were reported as mean values.

#### 2.2.4.2 Quality control

Strict quality control measures were implemented to prevent potential sample contamination with MPs. Non-plastic laboratory equipment was used, when possible, cleaned several times with HPLC gradient grade water and acetone ($(CH_3)_2CO$, ≥ 99.5%, Acros Organics, UK), and covered with clean aluminium foil. All GFFs, stainless-steel meshes and non-volumetric glassware were baked at 500°C for 4 hours before use. 100% cotton pink-dyed lab coats and nitrile gloves were worn during sample handling. Procedures were conducted in a fume hood thoroughly cleaned with HPLC water and acetone. All reagents, including $ZnCl_2$, $H_2O_2$, and $FeSO_4$ solutions, were filtered through GFFs before use. Routinely, laboratory blanks (triplicate) were processed with each batch of samples, undergoing the same procedures as the spiked and background samples in order to monitor potential contamination.

The limit of detection (LOD) was determined for different MPs sizes as the mean of blanks (n=3) plus three standard deviations (SD), and the limit of quantification (LOQ) was calculated as LOD + 3SD (Brander et al 2020). To assess the method's precision, triplicate spiked soil samples were analysed, and the relative standard deviation (%RSD) was calculated for each soil type

#### 2.2.4.3 Validation of the fluorescent staining protocol on rural soil samples

Six soil samples were randomly taken from the Hazelrigg field station (54.01° N, 2.77° W) near to Lancaster University campus in northwest England. The site has been free from tillage farming practices for decades. A 4 m margin along the field borders was avoided to prevent contamination from adjacent areas or dirt roads. Each sample was collected from a depth of 0–20 cm within a 50 x 50 cm quadrat and thoroughly mixed with a stainless-steel shovel. Subsamples (1–2 kg) from each site were stored in 100% cotton bags and kept at 4°C. Soil physicochemical properties are detailed in **Table** S3. For MPs extraction, 50 g of each soil sample was dried at 40°C and sieved through a 2 mm mesh. The sieved soil was then subjected to the described MPs extraction process, samples analysed using fluorescence microscopy, as well as Fourier Transform Infrared (FTIR) microscopy coupled with a focal plane array (FPA) detector in the transmission mode. Detailed procedures for soil sampling and FPA-μ-FTIR analysis are provided in the supporting information.

## 2.3 Results and discussion

### 2.3.1 Recovery of various large microplastic particles

#### 2.3.1.1 Fluorescence of test polymers stained with Nile red

The NR fluorescence strength varied for different LMPs under the green filter, with variations in intensity based on each polymer's physiochemical properties (**Figure** S6). Black PBAT/PLA from the mulching film did not fluoresce with NR and brown PA fragments from the fishing line showed a weak fluorescence signal before the extraction. This is consistent with the observations of Stanton et al. (Stanton et al., 2019), where brown HDPE and black PP were stained only around their edges, whereas red PA, black polyester, and blue acrylic fibres were not stained by NR. The authors suggested that the presence of plastic dyes affected the affinity for NR.

Interestingly, our research didn't find a direct link between polymer hydrophobicity and fluorescence intensity. This differs from previous reports suggesting that plastics with greater hydrophobicity, such as PE, PP and PS, generally exhibit stronger fluorescence than less hydrophobic surfaces, like PET, PU, and PVC (Erni-Cassola et al., 2017; Gao, Z. et al., 2022; Nel et al., 2021). In our research, plasticised PVC from insulated cables displayed the most intense fluorescence, outperforming PS, LDPE, PET, PP, HDPE, and PA.

Understanding NR's fluorescence mechanism is crucial for elucidating its varying behaviour in different polymers. Upon excitation, NR can adopt either the twisted intramolecular charge transfer (TICT) state or the planar intramolecular charge transfer (PICT) state, influenced by the rotation or electron movement leading to cross conjugation within its diethylamino group (Cser et al.; Greenspan, Phillip & Fowler; Guido et al., 2010; Martinez & Henary, 2016; Sasaki et al., 2016). This results in distinct fluorescence behaviours due to molecular interactions with NR's π electron system. Moreover, interactions such as π-π, electrostatic interactions, hydrogen bonding, van der Waals forces, and pore-filling affect NR's sorption on MPs, which vary based on carrier solvents, polymer crystallinity, and functional groups (Ho et al., 2023).

The strong fluorescence of NR in PVC can be attributed to the polymer's increased flexibility due to the presence of plasticisers, which reduce the intermolecular forces between polymer chains and increase chain mobility (free volume of polymer) (Rahman & Brazel, 2004). This allows the plasticised PVC to absorb NR into its bulk polymer due to the potential for segmental chain movements and allows for TICT conformation of excited NR, as the diethylamino groups of NR have more freedom to rotate. Nel et al. (Nel et al., 2021) also found stronger fluorescence of NR in plasticised PVC compared with rigid PVC, although the reason for this difference was not discussed. Polystyrene also showed strong fluorescence of NR, not only due to its porous structure but also its aromatic groups allowing for π–π interactions with NR, leading to increased NR sorption capacity.

In contrast, highly rigid MPs such as HDPE and PET exhibit weaker fluorescence with NR due to limited chain flexibility, as NR absorbs more on the surface than in the bulk polymer. Heating polymers to their glass transition temperature ($T_g$) enhances NR fluorescence by reducing cohesive forces and cross-linkages, thus increasing chain mobility and free volume for NR sorption (Konde et al., 2020; Lv et al., 2019; Maxwell S et al., 2020; Shim et al., 2016a; Wang, Chun et al., 2021). However, determining precise $T_g$ values is complex due to factors like molecular weight, polar groups, side group immobility, chemical structure crosslinking, and the presence of moisture and plasticisers (Ho et al., 2023). Heat treatment can also lead to physiochemical changes, such as PE blackening at 100°C (Lv et al., 2019). In our study, staining was performed at room temperature to avoid potential adverse effects on PBAT/PLA. Additionally, treatments like Fenton's reagent and possibly acidic $ZnCl_2$ might increase NR absorption capacity, likely through minor surface modifications, additive leaching, etc. (see section 3.1.2).

Indeed, caution is crucial when classifying and identifying MPs based solely on their NR fluorescence intensity. This is because NR fluorescence in MPs is affected by various factors, including the chemical characteristics of the plastics, such as polarity, crystallinity, functional groups, presence of additives, and staining conditions like NR concentration, carrying solvents, and heating conditions (when applied). This complexity also underscores the need for careful evaluation, especially when considering weathered or contaminated MPs.

NR fluorescence variability among plastics also complicates MPs segmentation followed by (semi)-automatic quantification using digital colour data. Setting appropriate pixel brightness thresholds is challenging, as it must distinguish polymer fluorescence from interfering substances like organic residues while ensuring accuracy and reproducibility. In our study, HDPE fragments showed lower fluorescence, and PP and LDPE films fluoresced strongly only at the edges, making threshold settings difficult. Erni-Cassola et al. (Erni-Cassola et al., 2017) found that lower thresholds increased the recovery of polymers like PS, PE, PP, and Nylon-6 but also caused false positives from natural OMs like wood and chitin, and errors from halo effects and particle merging. Nel et al. (Nel et al., 2021) recommended a minimum brightness threshold of 100 arbitrary units to include polymers like expanded polystyrene (EPS), HDPE, PP, and Nylon-6 while excluding natural fluorescing matter. However, this threshold excludes highly crystalline plastics like PVC and PET and may miss dimly fluorescing plastics and small particles. Longer exposure times for enhanced fluorescence can also lead to oversaturation and data loss (Ho et al., 2023). Therefore, manual counting was applied for LMP fractions to ensure accurate method validation and circumvent digital analysis errors for a wide range of plastic types. However, future advancements in machine learning and artificial intelligence might offer potential solutions for these issues (Ho et al., 2023).

#### 2.3.1.2 Recoveries of LMPs (dia. 500-1000 µm) from soils

Approximately 90% of the LMPs were successfully recovered across all soil types (**Figure** 2.2 and 2.4), demonstrating the effectiveness of the MPs extraction method coupled with NR staining for most polymers, except for PBAT/PLA and highly rigid HDPE. The use of a $ZnCl_2$ solution with a density of 1.5 g.cm³ was sufficient for extracting most plastic types tested within this size ranges. Our results also indicate negligible interference from soil-MPs interactions for MPs in this size category under the tested conditions. However, this observation is specific to the interaction duration and conditions used in this research. Longer MPs-soil interaction periods or multiple wet-dry cycles, which enhance soil-MPs contact, could lead to different outcomes in terms of extraction efficiency and NR detection.

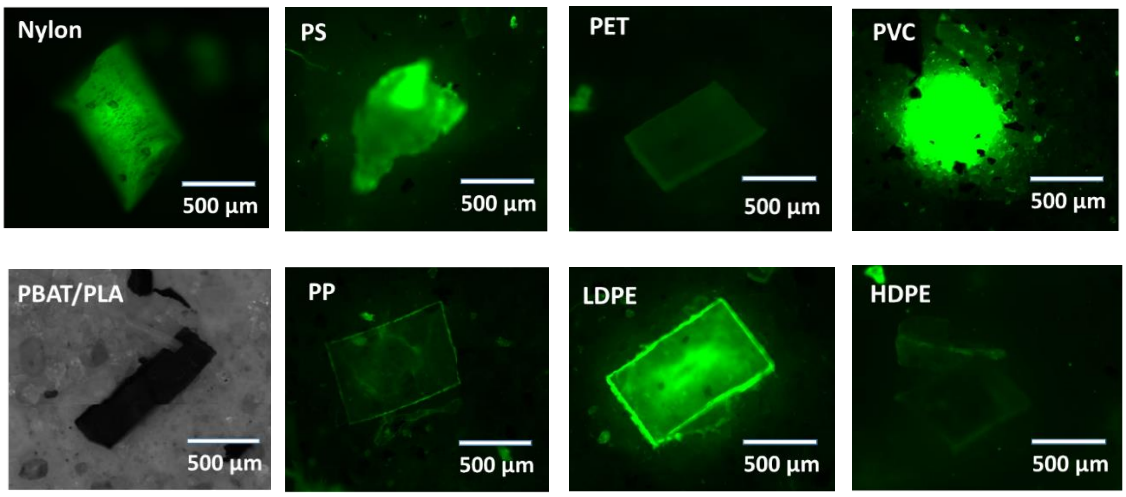


**Figure 2.2.** Fluorescence image of different polymer types (from left to right: nylon, PS, PET, PVC, PBAT/PLA, PP, LDPE, HDPE) with dia. 500-1000 µm after being extracted from the soil matrix. The MPs were stained with NR, illuminated under 470 nm, and

observed through a green filter set. Black PBAT/PLA, which exhibited no fluorescence signal, was captured and analysed in brightfield mode.

After extraction from the soil matrices, nylon fibres from the fishing line showed noticeable surface damage characterised by hole formation and increased fluorescence intensity (**Figure** 2.3.), phenomena not distinctly observed for other spiked polymer types. This enhanced fluorescence could result from changes in the polymer structure, such as splitting of the polymer backbone at the C-N linkages leading to alterations in the chemical structure of the polymer, changes in molecular orientation or local order, and/or from the loss of associated materials or additives (Achhammer et al., 1951). PA degradation might be caused by acidic $ZnCl_2$ and/or the oxidative Fenton reaction. Although previous studies have not observed PA degradation due to $ZnCl_2$, some research has noted fragmentation and degradation of PA under specific acidic and alkaline conditions (Hurley et al.2018, Cole et al.2014).

Importantly, our research emphasises the sensitivity of NR toward changes in polymer hydrophobicity, rigidity, free volume, associated materials, etc., which could be utilised for plastic degradation in future studies.

Previous studies reported the shrinking of PE, PET, and biodegradable polymers, particularly PLA-based MPs, upon Fenton digestion, similar to the effects of $H_2O_2$ (Noaa & Program, 2015; Pfohl et al., 2021; Tagg et al., 2016). However, in our research, no noticeable changes were observed for LMPs except for LDPE, which had enhanced fluorescence of NR after extraction. Indeed, the Fenton reagent has been reported to remove SOM efficiently and to have a milder impact on MPs than other treatments, such as alkaline and acidic methods (Hurley, R. R. et al., 2018; Pfohl et al., 2021; Tagg et al., 2016). While combining oxidative and enzymatic digestion is considered the most effective SOM removal method, it is expensive, time-consuming, and can degrade some biodegradable MPs. (Catarino et al., 2016).

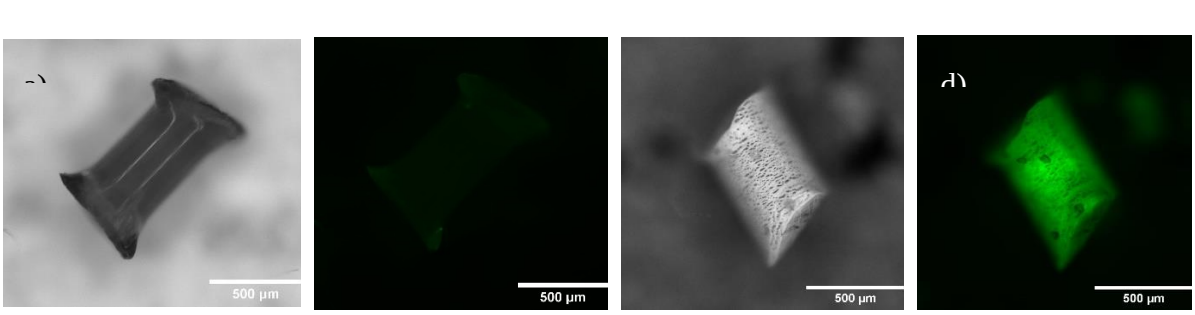


**Figure 2.3**. Bright-field (a, c) and fluorescence images (b, d) of nylon before and after extraction from soil, respectively

## 2.3.2 Recovery of small microplastics

### 2.3.2.1 Particle concentration of spiked material

For LDPE (dia. 20-150 µm), the particle concentration determined by the microscopic method was 4,900 ± 1,100 particles/mg, while for the PBAT/PLA (dia. 100-250 µm), it was found to be 2,300 ± 140 particles/mg. These particle numbers were utilised to establish SMP recoveries from different soil types. To this end, introducing 3 mg of LDPE

dia. 20-150 µm or PBAT/PLA dia. 100-250 µm into the soils corresponds to approximately 14,700 ± 4,500 particles and 6,900 ± 420 particles, respectively.

Notably, the results from the image analysis of fluorescence microscopy align well with those from the particle counter in the liquid phase, demonstrating the effectiveness of NR staining for small LDPE particles followed by subsequent image analysis. The average particle numbers found using the particle counter were 15,730 ± 140 particles in 3 mg for LDPE in a size range of 20-150 µm, and for PBAT/PLA, 3,200 ± 30 particles in 3 mg in the size range of 100-250 µm (**Figure** S8). For PBAT/PLA, a higher particle count was observed with the microscopic method compared to the particle counter. This may be due to difficulties in particle segmentation caused by irregular film fragment shapes and background contrast. Additionally, the discrepancy between the two methods could be influenced by substantial variations in PBAT/PLA particle size, as the particles become more fragile after cryo-milling.

The size distribution of the spiked LDPE (dia. ≤150 µm) and PBAT/PLA (dia. 100-250 µm) showed inconsistencies between the theoretical sieve mesh size and the actual particle sizes on the filter, with most particles being smaller than expected, regardless of plastic type. (**Figure** S7) This is possibly due to the spontaneous self-assembly of SMPs into crystal superstructures upon solvent evaporation (Deng et al., 2020; Lee, Y. H. et al., 2018), a phenomenon that becomes less frequent when the polymer powder is diluted and sonicated during size characterisation. These very small particles contribute negligibly to the MPs mass but are significant in contributing to the overall particle number for any given plastic type. (Gardon et al., 2022) In the research reported here, for consistency, we only considered the sieved size ranges when assessing the recovery of SMPs.

Validation of the microscopic method combined with Image J analysis for automated particle segmentation and quantification of SMPs was established for comprehensive quality assurance. A comparison with manual counting for a section of the whole filter of only spiked SMP gave an agreement of 88% for LDPE and 78% for PBAT/PLA. The reliability or precision, based on repeated scans of the same image but at different angles (see section 2.4 above), revealed no differences in particle count. Under 50X magnification, the smallest detected particle for spiked fluorescent LDPE and black PBAT/PLA particles (in BF mode) had a Feret's diameter of 3.5 µm. However, a 20 µm size threshold was set for assessment of method recovery of LDPE particles (dia. ≤ 150 µm) due to large uncertainty in measuring smaller fluorescence particles (**Figure** S7) and increased soil matrix interference below this threshold (**Figure** S11).

#### 2.3.2.2 Recovery of SMPs from different soil types

The recovery of SMPs was determined by calculating the number of particles in spiked soil samples (both fluorescence and BF modes) after subtracting the number of particles found in non-spiked (background) soil, expressed as a percentage of the initial number of spiked SMP particles in 3 mg (**Figure** S9). The number of fluorescence particles (dia. 20-150 µm) found in background soils after blank correction was 880 ± 800, with clayey soils having the highest count, followed by loamy (LUFA 2.4) and sandy soils (**Table** S4). These fluorescence particles might represent the 'native MPs' but could also be the residual SOM particles being co-stained, as they were positively correlated with the soil OM content ($R^2$ = 0.998, **Figure** S10). The size distribution of fluorescent particles in the background soils (clayey, sandy, and loamy soils) shows an increasing number of MPs in the size range ~20-60 µm (**Figure** S9).

The number of black particles detected in background soils was relatively low, totalling 26 ± 30, with clayey soil having the highest count, followed by loamy and sandy soil. These black particles could be plastics (e.g., tyre rubber), or black carbon (i.e., soot and char formed during incomplete combustion of fossil and biomass fuels). The fluorescence image shows that these black materials were not labelled with NR, thus interfering only with the detection of black PBAT/PLA in the BF mode.

Although Fenton treatment was applied, incomplete SOM removal led to a high level of fluorescent particles in the background soil, potentially causing false positives if no background subtraction had been applied. This underscores the need for improvement of SOM removal, possibly by employing more effective oxidative digestion, multiple Fenton treatments, or the addition of enzymatic treatments. However, caution is necessary as more aggressive removal of SOM can adversely affect the MPs particles. Advanced image analysis using machine learning has shown promise in distinguishing plastics from SOM (Lorenzo-Navarro et al., 2020a, 2020b; Meyers et al., 2022). Additionally, incorporating hydrophilic water-based dyes such as Methylene Blue, Calcofluor White, Evans Blue, and DAPI alongside NR can help distinguish SOM from NR-stained MPs, improving differentiation (Maxwell S et al., 2020; Michelaraki et al., Oct 05, 2020; Tarafdar et al., 2022). Ongoing research and the refinement of color thresholding techniques also hold promise for more effectively distinguishing MPs from SOM (Ho et al., 2023).

MPs recovery for different polymers and MPs size classes across the three soil types. Percent recoveries are reported as a mean of three replicates with standard deviation error bars

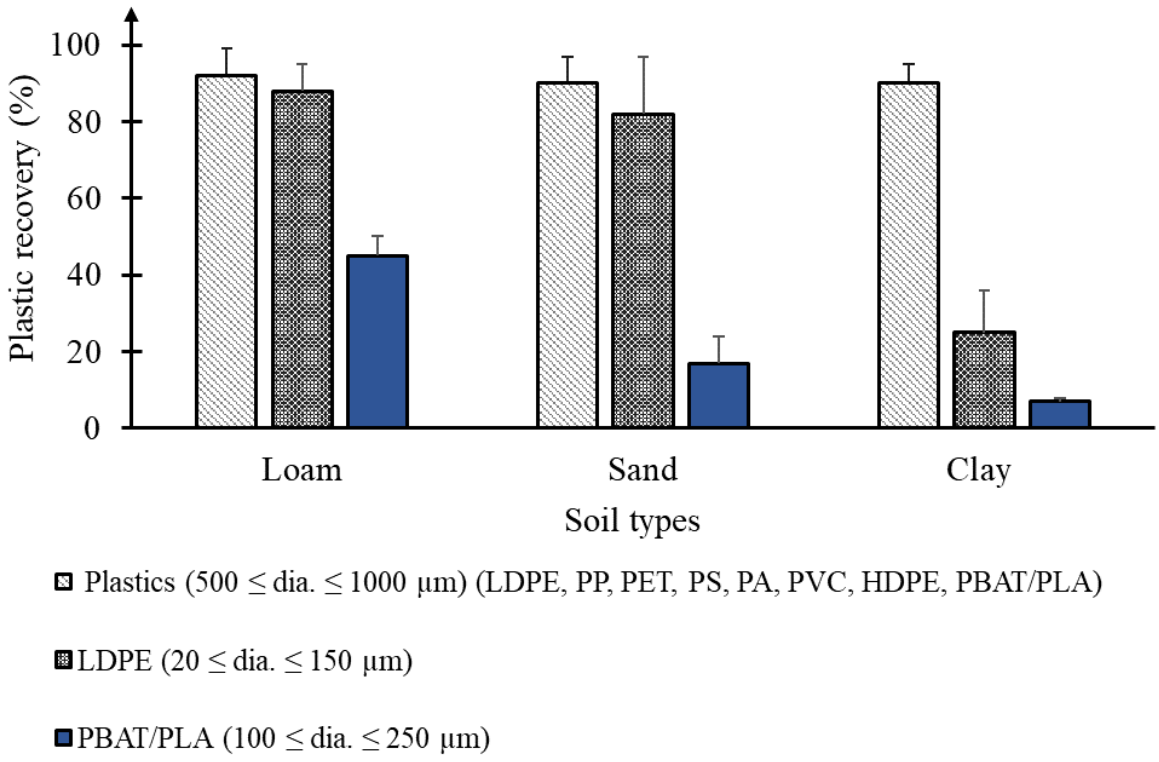


**Figure 2.4.** MPs recovery for different polymers and MPs size classes across the three soil types. Percent recoveries are reported as a mean of three replicates with standard deviation error bars.

The recovery rates for SMPs are strongly dependent on soil type (**Figure** 2.4.), polymer type and size range. LDPE (dia. 20-150 µm) achieved a relatively high recovery rate of approximately 82 ± 15% in sandy soil and 88 ± 7% in loamy soil (standard LUFA 2.4). In contrast, PBAT/PLA (dia.100-250 µm) had lower recovery rates for all soil types, measuring 17±7% in sandy soil and 45±20% in loamy soil. For both polymer types, the recovery of SMP particles was notably lower in clayey soil, with LDPE at 25±11% and PBAT/PLA at 7±1%.

The results show that compared to SMPs, LMPs were more efficiently extracted from soils, as evidenced by their higher recovery rates, which consistently exceeded 90%. Several factors contribute to the potential loss of SMPs during sample processing, such as particles sticking to glass beakers or glass filtration holders since these small particles are invisible to the naked eye. Additionally, SMPs may adhere to the surface of LMPs or plant debris after being concentrated on a filter, making their detection and quantification challenging through image analysis. These potential issues could be addressed by applying finer soil sieving before processing and by improving the organic digestion step. Furthermore, it is highly recommended to use lower MPs concentrations per filter, either by subsampling or using larger filter diameters, to prevent particle agglomeration.

The recovery of SMPs also appears to be influenced by MPs type. For instance, while small LDPE (dia. 20-150 µm) exhibited relatively high recovery rates in sand and loamy soil, lower recoveries were observed for the biodegradable PBAT/PLA MPs. This difference can likely be attributed to the increased degradation of biodegradable plastics relative to non-biodegradable plastics during Fenton's digestion step, and during the subsequent ultrasonication after filtration on the stainless steel meshes which could lead to mechanical degradation and the loss of PBAT/PLA into smaller fraction. Notably, PBAT/PLA MPs were cryo-milled from thin mulching films and wet-sieved with acetone, and thus were easily fragmented to much smaller sizes.

Soil characteristics play a crucial role in the extraction and quantification of SMPs. Among all soil types, clayey soil was associated with the lowest recovery, likely due to its higher SOM (5.9%) and clay content (52%). Incompletely digested SOM, particularly large plant debris, can obscure SMPs on filters, hindering microscopic detection and leading to lower recovery rates. (Radford et al., 2021) Furthermore, clay minerals consist of silica and aluminium layers. These are often negatively charged, either due to isomorphic replacement within the mineral structure or from the dissociation and protonation of chemical groups along their edges (Ashman & Puri, 2002). This characteristic results in the hetero aggregation between MPs and clay particles, as previously observed (Wang, Yi et al., 2023). The hetero-aggregation process of MPs, influenced by factors like hydrochemical conditions and mineral types, is primarily driven by electrostatic interactions. High cation concentrations, particularly divalent ones ($Ca^{2+}$, $Mg^{2+}$, $Zn^{2+}$), promote MPs aggregation by neutralising their negative charge, as per DLVO theory (Liu, Yanjun et al., 2019; Singh et al., 2019; Wang, Yi et al., 2023). Therefore, we propose that using $ZnCl_2$ as a density separation medium could enhance MPs-clay aggregation, especially in clay-rich soils, raising concerns about potential MPs loss. However, further studies are needed to explore the specific impacts of $ZnCl_2$ on MPs-clay mineral aggregation in such soils, as it is currently one of the most used salts in MPs separation (Coppock et al., 2017; Crutchett & Bornt, 2024b; Debraj & Lavanya, 2023; Mintenig et al., 2016; Vermeiren, Peter et al., 2021).

The relative standard deviation (%RSD), a method repeatability (precision) measure, varied with soil types and MPs characteristics. For small LDPE (dia. 20-150 µm), %RSDs

were 5% in loamy, 18% in sandy, and 60% in clayey soil. Biodegradable PBAT/PLA showed higher %RSDs: 10% in loam LUFA 2.4, 50% in sandy, and 60% in clayey soil. These values are substantially higher than those in conventional chemical testing and for LMPs (dia. 500-1000 µm), which range from 5-10% depending on soil type. This is attributed to soil sample heterogeneity, which affects the level of interference associated with factors such as SOM and clay content. Uniformly spiking and effectively separating MPs from complex matrices is also challenging. In experiment 3.2.1, inconsistencies were observed in delivering a uniform number of particles (%RSD for LDPE and PBAT/PLA was 25% and 10%, respectively) when pipetting from a stock suspension. Image analysis presents additional difficulties, particularly with smaller particles. Watershed segmentation helps resolve particle clumps but can also lead to the over-segmentation of LMPs, especially co-stained plant material and natural fibres with uneven fluorescence intensity. Therefore, obtaining a robust automatic image analysis becomes very challenging when a wide range of plastic sizes and types occur in organic-rich matrices.

The blanks for the entire protocol revealed an average of 130 fluorescence particles (dia. ≥ 20 µm) and none for black particles (dia. 100-250 µm), suggesting possible contamination of MPs from PVC density separation kits or airborne sources during processing. Notably, the number of particles in the blank is substantially lower than in the background and spiked soil samples. The method LOD varied with the MPs' cut size and color intensity. For instance, the LODs for small LDPE particles were 570, 190, 130, and 50, and the LOQs were 1000, 330, 220, and 80 for cut sizes of 20 µm, 40 µm, 50 µm, and 100 µm, respectively. The LOD for PBAT/PLA with a 100 µm cut size was much lower than for small transparent LDPE particles, likely due to the enhanced detectability of its black color during sample processing, which warranted greater caution.

The selectivity of fluorescence techniques for different polymer types is clearly limited, unlike spectroscopic methods such as FTIR and Raman, which can determine polymer types with reasonable accuracy for individual MPs particles. The data we report here highlight that some plastics, such as PET and HDPE, have reduced selectivity because they exhibit low fluorescence intensity when stained with NR, making it challenging to distinguish them from other matrix interferences (e.g., co-stained SOM). To assess method selectivity more precisely, other techniques for chemical identification of MPs particles can be employed and compared with fluorescence microscopy results. While relatively few studies have conducted such comparisons between NR-fluorescence microscopy and FTIR/Raman spectroscopy, there is generally good agreement between the two methods (Shim et al., 2016a; Vermeiren, P. et al., 2020).

The complete microplastic (MPs) analysis protocol described in this study took approximately two days per sample, excluding pre-processing steps such as soil sieving, drying, and MPs spiking. A batch of six samples, including procedural blanks, can be processed simultaneously. This included 12 hours for density separation, 24 hours for Fenton digestion (for a batch of 6 samples), and about an hour for staining and capturing images for one sample filter. This is much faster than most existing procedures, e.g., where enzymatic digestion is applied (Löder et al., 2017) (Möller et al., 2022). The complexity of these procedures, however, is justified for better organic matter removal, particularly when using spectroscopy methods like FTIR and Raman, where higher particle counts on a filter can significantly increase the analysis time.

### 2.3.3 Comparison of fluorescence microscopy with FTIR microspectroscopy

The mean concentration of MPs detected in soil samples from the research station fields using NR staining with fluorescent microscopy was 20.7 ± 9.0 MPs/g. In comparison, the FPA-μ-FTIR method, after blank subtraction, showed a concentration of 13.1 ± 7.3 MPs/g (**Figure** 2.5.). A detailed comparison of each sample is provided in **Figure** S12. Both methods detected MPs levels above the limit of detection (LOD) in all samples. FTIR analysis identified several types of MPs, including polyethylene (8.6 MPs/g), polyester (0.31 MPs/g), polypropylene (1.25 MPs/g), polystyrene (0.80 MPs/g), styrene-butadiene rubber (3.1 MPs/g), polyvinyl chloride (2.4 MPs/g), and polyamide (0.1 MPs/g).

To the best of our knowledge, previous studies have not reported MPs concentrations for non-agricultural soils with particles as small as 25 μm using fluorescence microscopy methods. However, the results of this study are consistent with those reported by Tagg et al., who found 6.39 MPs/g in a background (non-amended) soil from a research station in Germany using a similar FPA-μ-FTIR method, comparable to our FTIR approach (Tagg et al., 2022).

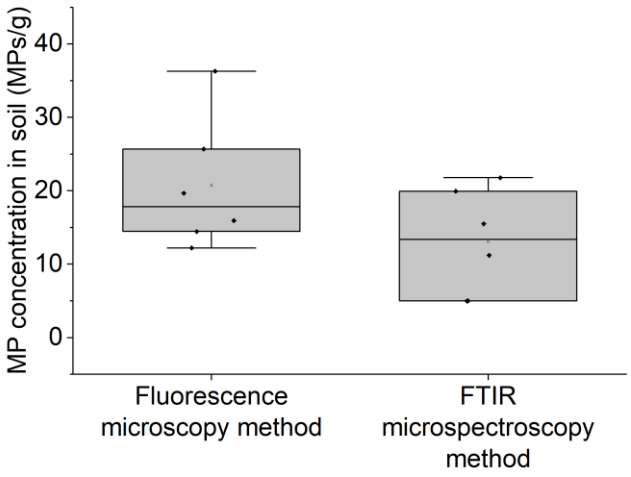


**Figure 2.5.** Box and whisker plot displaying the MPs number concentrations in soil samples (n=6) collected from the Hazelrigg field station, as measured by fluorescence microscopy and FTIR spectroscopy methods.

Although the MPs concentration detected by fluorescence microscopy was slightly higher than that by FTIR, a paired t-test showed no significant difference between the two methods ($p = 0.153$, two-tailed test). Slightly higher counts for the fluorescence method could be due to false positives arising from NR co-staining with soil organic matter. Similarly, FTIR spectroscopy may experience matrix interferences, leading to false positives from polymers like polyethylene, ethylene vinyl acetate, acrylics, and polyurethane (Ivleva, 2021; Moses et al., 2023; Witzig et al., 2020). Regarding true negatives, fluorescence microscopy struggles to detect black or dark-coloured MPs or those with physicochemical properties that weaken NR fluorescence as discussed above. FTIR can miss particles below the infrared diffraction limit or particles that are too thick, especially in transmission mode. FTIR also has challenges in detecting weathered MPs because weathering can alter their spectra, making them unrecognizable in spectral

libraries. However, weathering increases surface sorption and decreases polymer crystallinity, which can enhance NR staining's ability to detect these particles, as shown in our study.

## 2.4 Conclusions

Fluorescence microscopy with NR staining and a semi-automatic particle recognition pipeline provides a reproducible and accurate method for counting MPs in heterogeneous matrices like soil. This method is suitable for routine soil analysis, accommodating a wide range of plastics (excluding black/dark-coloured plastics and less ideal for highly rigid plastics) with dia. ≥ 20 µm. Although the method has limitations in terms of polymer selectivity, enhancing the removal of SOM can help reduce false positives. This study also underscores the impact of soil properties and MPs characteristics, especially size and polymer type, on MPs extraction efficiency. Biodegradable plastics (dia. 100-250 µm) had lower recovery rates from soil compared to non-biodegradable plastics (dia. 20-150 µm), possibly due to degradation during sample preparation. Soils with a higher OM content and very small and negatively charged mineral particles are complex matrices from which to extract MPs.

While no significant differences in MPs concentrations were detected between fluorescence microscopy and FTIR spectroscopy, fluorescence microscopy offers a more cost-effective and time-efficient approach compared to existing spectroscopic methods. Fluorescence microscopy requires just 15 minutes to scan a 47mm diameter filter disk in both fluorescence and brightfield modes using a x50 objective, enabling high sample throughput, which makes it particularly well-suited for environmental monitoring. In contrast, spectroscopic methods like FTIR and Raman micro-spectroscopy, despite technological advancements, remain slow and expensive. For example, Bergmann et al. needed 4.5 hours to analyse a small portion (14.1 mm x 14.1 mm) of a filter using µFT-IR imaging, making these methods impractical for high throughput environmental monitoring (Bergmann et al., 2017). In this study, an FTIR protocol was developed to analyse a full 25mm diameter Anodisc filter in about 3-4 hours; however, data processing and analysis for each sample still required a minimum of an additional 4 hours.

Optical and fluorescence microscopy offer faster analysis compared to FTIR or Raman; however, these methods cannot chemically identify MPs or provide insights into their physical-chemical properties, which can be achieved using FTIR or Raman (Ivleva, 2021). While advanced FTIR techniques, such as quantum cascade laser (QCL)-based setups, can significantly enhance the speed of FTIR analysis (Tian, X. et al., 2022), integrating fluorescence microscopy with spectroscopic methods serves as a complementary approach to improve both sample throughput and polymer identification. For example, Prata et al. demonstrated the effectiveness of fluorescent NR tagging as a preparatory step for Raman spectroscopy, resulting in a more efficient and systematic workflow for comprehensive microplastic analysis (Prata et al., 2021).

Enhancing NR-stained fluorescence imaging for environmental monitoring still requires a number of important challenges to be addressed. These include minimising potential matrix interferences, understanding plastic properties and weathering, standardising staining procedures (NR concentration, staining duration, solvent, and heating conditions) and microscopic setup (excitation source, camera configuration, and image

analysis parameters). Rigorous quality assurance and control are also essential for method harmonisation and standardisation, with criteria such as method recovery using universal MPs standards, detection limits, and reproducibility needed to be incorporated. Implementing these recommendations will enhance research compatibility, advance fluorescence imaging, and improve the reliability of this method for monitoring environmental plastic pollution.

**Acknowledgements**

This work was supported by the European Union's Horizon 2020, ITN SOPLAS, with grant agreement No. 55334. The authors thank Elisabeth Shaw and Alexandre Benedetto (Lancaster University) for their help with the fluorescence microscope. We also thank Andrew Mayes for his helpful advice on the technical and theoretical aspects of the fluorescence microscopy–Nile red staining approach.

**Credit authorship contribution statement** Q.N. Phan Le: conceptualisation, methodology, samples analysis, data evaluation, writing, review and editing of the manuscript; C. Halsall: funding acquisition, conceptualisation, supervision, review and editing of the manuscript; S. Peneva and O. Wrigley: sample analysis, review and editing of the manuscript; M. Braun and W. Amelung: review and editing of the manuscript; L. Ashton and B. Surridge: supervision, review and editing of the manuscript; J. Quinton: funding acquisition, supervision, review and editing of the manuscript.

**Data availability** Data will be made available on request.

**Declaration**

**Ethical approval** This research did not involve human or animal samples.

**Competing interest;** The authors declare no competing interests.

# References

Achhammer, B. G., Reinhart, F. W., & Kline, G. M. (1951). Mechanism of the degradation of polyamides. *Journal of Applied Chemistry*, *1*(7), 301–320. doi:10.1002/jctb.5010010704

Andrady. (2011). Microplastics in the marine environment. *Marine Pollution Bulletin*, *62*(8), 1596–1605. doi:10.1016/j.marpolbul.2011.05.030

Ashman, M., & Puri, G. (2002). *Essential soil science a clear and concise introduction to soil science*. Oxford; Malden, MA: Blackwell Science.

Brander, S.M., Renick, V.C., Foley, M.M., Steele, C., Woo, M., Lusher, A., Carr, S., Helm, P., Box, C., Cherniak, S., Andrews, R.C., Rochman, C.M. *Sampling and Quality Assurance and Quality Control: A Guide for Scientists Investigating the Occurrence of Microplastics Across Matrices.* Applied Spectroscopy. 2020 Sep;74(9):1099-1125. doi:10.1177/0003702820945713.

Catarino, A. I., Thompson, R., Sanderson, W., & Henry, T. B. (2016). *Development and optimization of a standard method for extraction of microplastics in mussels by enzyme digestion of soft tissues* Wiley. doi:10.1002/etc.3608

Cole, M., Webb, H., Lindeque, P. *et al. Isolation of microplastics in biota-rich seawater samples and marine organisms. Sci Rep* **4**, 4528 (2014). https://doi.org/10.1038/srep04528

Coppock, R. L., Cole, M., Lindeque, P. K., Queirós, A. M., & Galloway, T. S. (2017). A small-scale, portable method for extracting microplastics from marine sediments. *Environmental Pollution (1987), 230*, 829–837. doi:10.1016/j.envpol.2017.07.017

Corradini, F., Meza, P., Eguiluz, R., Casado, F., Huerta-Lwanga, E., & Geissen, V. (2019). Evidence of microplastic accumulation in agricultural soils from sewage sludge disposal. *Science of the Total Environment, 671*, 411–420. doi:10.1016/j.scitotenv.2019.03.368

Crossman, J., Hurley, R. R., Futter, M., & Nizzetto, L. (2020). Transfer and transport of microplastics from biosolids to agricultural soils and the wider environment. *The Science of the Total Environment, 724*, 138334. doi:10.1016/j.scitotenv.2020.138334

Crutchett, T. W., & Bornt, K. R. (2024). *A simple overflow density separation method that recovers >95% of dense microplastics from sediment* Elsevier BV. doi:10.1016/j.mex.2024.102638

Cser, A., Nagy, K., Bicz, & Ok. *Fluorescence lifetime of nile red as a probe for the hydrogen bonding strength with its microenvironment*

Debraj, D., & Lavanya, M. (2023). *Microplastics everywhere: A review on existing methods of extraction* Elsevier BV. doi:10.1016/j.scitotenv.2023.164878

Deng, K., Luo, Z., Tan, L., & Quan, Z. (2020). Self-assembly of anisotropic nanoparticles into functional superstructures. *Chemical Society Reviews, 49*(16), 62–638. doi:10.1039/d0cs00541j

Erni-Cassola, G., Gibson, M. I., Thompson, R. C., & Christie-Oleza, J. A. (2017). *Lost, but found with nile red: A novel method for detecting and quantifying small microplastics (1 mm to 20 μm) in environmental samples* American Chemical Society (ACS). doi:10.1021/acs.est.7b04512

Gao, Z., Wontor, K., & Cizdziel, J. V. (2022). Labeling microplastics with fluorescent dyes for detection, recovery, and degradation experiments. *Molecules (Basel, Switzerland), 27*(21), 7415. doi:10.3390/molecules27217415

Gardon, Paul-Pont, Le Moullac, Soyez, Lagarde, & Huvet. (2022). Cryogrinding and sieving techniques as challenges towards producing controlled size range microplastics for relevant ecotoxicological tests. *Environmental Pollution (1987), 315*, 120383. doi:10.1016/j.envpol.2022.120383

GESAME. (2015). *Sources, fate and effects of microplastics in the marine environment: A global assessment*. London: International Maritime organization.

GREENSPAN, P., MAYER, E. P., & FOWLER, S. D. (1985). Nile red: A selective fluorescent stain for intracellular lipid droplets. *The Journal of Cell Biology, 100*(3), 965–973. doi:10.1083/jcb.100.3.965

Greenspan, P., & Fowler, S. D. *Spectrofluorometric studies of the lipid probe, nile red*

Guido, C. A., Mennucci, B., Jacquemin, D., & Adamo, C. (2010). *Planar vs. twisted intramolecular charge transfer mechanism in nile red: New hints from theory* Royal Society of Chemistry (RSC). doi:10.1039/b927489h

Haibo He, & Garcia, E. A. (2009). Learning from imbalanced data. *IEEE Transactions on Knowledge and Data Engineering, 21*(9), 1263–1284. doi:10.1109/TKDE.2008.239

Hartmann, Hüffer, Thompson, Hassellöv, Verschoor, Daugaard, et al. (2019). *Are we speaking the same language? recommendations for a definition and categorization framework for plastic debris* American Chemical Society (ACS). doi:10.1021/acs.est.8b05297

Ho, D., Liu, S., Wei, H., & Karthikeyan, K. G. (2023). *The glowing potential of nile red for microplastics identification: Science and mechanism of fluorescence staining* Elsevier BV. doi:10.1016/j.microc.2023.109708

Huang, Y., Liu, Q., Jia, W. Q., Yan, C. R., & Wang, J. (2020). Agricultural plastic mulching as a source of microplastics in the terrestrial environment. *Environmental Pollution, 260* doi:10.1016/j.envpol.2020.114096

Hurley, R. R., Lusher, A. L., Olsen, M., & Nizzetto, L. (2018). Validation of a method for extracting microplastics from complex, organic-rich, environmental matrices. *Environmental Science & Technology, 52*(13), 7409–7417. doi:10.1021/acs.est.8b01517

Ivleva, N. P. (2021). *Chemical analysis of microplastics and nanoplastics: Challenges, advanced methods, and perspectives* American Chemical Society (ACS). doi:10.1021/acs.chemrev.1c00178

Konde, S., Ornik, J., Prume, J. A., Taiber, J., & Koch, M. (2020). *Exploring the potential of photoluminescence spectroscopy in combination with nile red staining for microplastic detection* Elsevier BV. doi:10.1016/j.marpolbul.2020.111475

Lee, Y. H., Lay, C. L., Shi, W., Lee, H. K., Yang, Y., Li, S., et al. (2018). *Creating two self-assembly micro-environments to achieve supercrystals with dual structures using polyhedral nanoparticles* Springer Science and Business Media LLC. doi:10.1038/s41467-018-05102-x

Liu, Y., Hu, Y., Yang, C., Chen, C., Huang, W., & Dang, Z. (2019). Aggregation kinetics of UV irradiated nanoplastics in aquatic environments. *Water Research (Oxford), 163*, 114870. doi:10.1016/j.watres.2019.114870

Löder, Imhof, Ladehoff, Löschel, Lorenz, Mintenig, et al. (2017). Enzymatic purification of microplastics in environmental samples. *Environmental Science &Amp; Technology, 51*(24), 14283–14292. doi:10.1021/acs.est.7b03055

Lorenzo-Navarro, J., Castrillón-Santana, M., Sánchez-Nielsen, E., Zarco, B., Herrera, A., Martínez, I., et al. (2020a). *Deep learning approach for automatic microplastics counting and classification* Elsevier BV. doi:10.1016/j.scitotenv.2020.142728

Lorenzo-Navarro, J., Castrillon-Santana, M., Santesarti, E., De Marsico, M., Martinez, I., Raymond, E., et al. (2020b). *SMACC: A system for microplastics automatic counting and classification* Institute of Electrical and Electronics Engineers (IEEE). doi:10.1109/access.2020.2970498

Lv, L., Qu, J., Yu, Z., Chen, D., Zhou, C., Hong, P., et al. (2019). *A simple method for detecting and quantifying microplastics utilizing fluorescent dyes - safranine T, fluorescein isophosphate, nile red based on thermal expansion and contraction property* Elsevier BV. doi:10.1016/j.envpol.2019.113283

Maes, Jessop, Wellner, Haupt, & Mayes. (2017). A rapid-screening approach to detect and quantify microplastics based on fluorescent tagging with nile red. *Scientific Reports, 7*(1), 44501. doi:10.1038/srep44501

Mariano, S., Tacconi, S., Fidaleo, M., Rossi, M., & Dini, L. (2021). *Micro and nanoplastics identification: Classic methods and innovative detection techniques* Frontiers Media SA. doi:10.3389/ftox.2021.636640

Martinez, V., & Henary, M. (2016). *Nile red and nile blue: Applications and syntheses of structural analogues* Wiley. doi:10.1002/chem.201601570

Maxwell S, H., Melinda K, F., & Matthew, G. (2020). *Counterstaining to separate nile red-stained microplastic particles from terrestrial invertebrate biomass* American Chemical Society (ACS). doi:10.1021/acs.est.0c00711

Meyers, N., Catarino, A. I., Declercq, A. M., Brenan, A., Devriese, L., Vandegehuchte, M., et al. (2022). *Microplastic detection and identification by nile red staining: Towards a semi-automated, cost- and time-effective technique* Elsevier BV. doi:10.1016/j.scitotenv.2022.153441

Michelaraki, M., Joseph, O., Karnik, S., Devalla, S., Madanan, K., & Prabhu, R. (Oct 05, 2020). Potential for nile red dye-based analysis of microplastics from oceanic samples. Paper presented at the pp. 1–4. doi:10.1109/IEEECONF38699.2020.9389207

Mintenig, S. M., Int-Veen, I., Löder, M. G. J., Primpke, S., & Gerdts, G. (2016). *Identification of microplastic in effluents of waste water treatment plants using focal*

*plane array-based micro-fourier-transform infrared imaging* Elsevier BV. doi:10.1016/j.watres.2016.11.015

Möller, J. N., Heisel, I., Satzger, A., Vizsolyi, E. C., Oster, S. D. J., Agarwal, S., et al. (2022). Tackling the challenge of extracting microplastics from soils: A protocol to purify soil samples for spectroscopic analysis. *Environmental Toxicology and Chemistry, 41*(4), 844–857. doi:10.1002/etc.5024

Moses, S. R., Roscher, L., Primpke, S., Hufnagl, B., Löder, M. G. J., Gerdts, G., et al. (2023). *Comparison of two rapid automated analysis tools for large FTIR microplastic datasets* Springer Science and Business Media LLC. doi:10.1007/s00216-023-04630-w

Nel, H. A., Chetwynd, A. J., Kelleher, L., Lynch, I., Mansfield, I., Margenat, H., et al. (2021). Detection limits are central to improve reporting standards when using nile red for microplastic quantification. *Chemosphere (Oxford), 263*, 127953. doi:10.1016/j.chemosphere.2020.127953

Noaa, M. D., & Program. (2015). NOAA–USGS debris-flow warning System—Final report. doi:10.3133/cir1283

Pérez-Guevara, F., Roy, P. D., Kutralam-Muniasamy, G., & Shruti, V. C. (2022). Coverage of microplastic data underreporting and progress toward standardization. *Science of the Total Environment, 829* doi:10.1016/j.scitotenv.2022.154727

Pfohl, P., Roth, C., Meyer, L., Heinemeyer, U., Gruendling, T., Lang, C., et al. (2021). Microplastic extraction protocols can impact the polymer structure. *Microplastics and Nanoplastics, 1*(1) doi:10.1186/s43591-021-00009-9

Prata, J. C., da Costa, J. P., Fernandes, A. J. S., da Costa, F. M., Duarte, A. C., & Rocha-Santos, T. (2021). Selection of microplastics by nile red staining increases environmental sample throughput by micro-raman spectroscopy. *The Science of the Total Environment, 783*, 146979. doi:10.1016/j.scitotenv.2021.146979

Radford, F., Zapata-Restrepo, L. M., Horton, A. A., Hudson, M. D., Shaw, P. J., & Williams, I. D. (2021). Developing a systematic method for extraction of microplastics in soils. *Analytical Methods, 13*(14), 1695–175. doi:10.1039/d0ay02086a

Rahman, & Brazel. (2004). The plasticizer market: An assessment of traditional plasticizers and research trends to meet new challenges. *Progress in Polymer Science, 29*(12), 1223–1248. doi:10.1016/j.progpolymsci.2004.10.001

Sasaki, S., Drummen, G. P. C., & Konishi, G. (2016). *Recent advances in twisted intramolecular charge transfer (TICT) fluorescence and related phenomena in materials chemistry* Royal Society of Chemistry (RSC). doi:10.1039/c5tc03933a

Shim, W. J., Song, Y. K., Hong, S. H., & Jang, M. (2016). Identification and quantification of microplastics using nile red staining. *Marine Pollution Bulletin, 113*(1-2), 469–476. doi:10.1016/j.marpolbul.2016.10.049

Singh, N., Tiwari, E., Khandelwal, N., & Darbha, G. K. (2019). Understanding the stability of nanoplastics in aqueous environments: Effect of ionic strength, temperature, dissolved organic matter, clay, and heavy metals. *Environmental Science. Nano, 6*(1), 2968–2976. doi:10.1039/c9en00557a

Stanton, Johnson, Nathanail, Gomes, Needham, & Burson. (2019). *Exploring the efficacy of nile red in microplastic quantification: A costaining approach* American Chemical Society (ACS). doi:10.1021/acs.estlett.9b00499

Stoyana Peneva, Quynh Nhu Phan Le, Davi Munhoz, Olivia Wrigley, Flora Wille, Heidi Doose, et al. *Microplastic analysis in soils: A comparative assessment.* Unpublished manuscript.

Tagg, A. S., Harrison, J. P., Ju-Nam, Y., Sapp, M., Bradley, E. L., Sinclair, C. J., et al. (2016). *Fenton's reagent for the rapid and efficient isolation of microplastics from wastewater* Royal Society of Chemistry (RSC). doi:10.1039/c6cc08798a

Tagg, A. S., Brandes, E., Fischer, F., Fischer, D., Brandt, J., & Labrenz, M. (2022). Agricultural application of microplastic-rich sewage sludge leads to further uncontrolled contamination. *Science of the Total Environment, 806* doi:10.1016/j.scitotenv.2021.150611

Tarafdar, A., Choi, S., & Kwon, J. (2022). Differential staining lowers the false positive detection in a novel volumetric measurement technique of microplastics. *Journal of Hazardous Materials, 432*, 128755. doi:10.1016/j.jhazmat.2022.128755

Thomas, D., Schütze, B., Heinze, W. M., & Steinmetz, Z. (2020). Sample preparation techniques for the analysis of microplastics in Soil—A review. *Sustainability (Basel, Switzerland), 12*(21), 9074. doi:10.3390/su12219074

Tian, X., Beén, F., & Bäuerlein, P. S. (2022). Quantum cascade laser imaging (LDIR) and machine learning for the identification of environmentally exposed microplastics and polymers. *Environmental Research, 212*, 113569. doi:10.1016/j.envres.2022.113569

Vermeiren, P., Muñoz, C., & Ikejima, K. (2020). Microplastic identification and quantification from organic rich sediments: A validated laboratory protocol. *Environmental Pollution (1987), 262*, 114298. doi:10.1016/j.envpol.2020.114298

Vermeiren, P., Lercari, D., Muñoz, C. C., Ikejima, K., Celentano, E., Jorge-Romero, G., et al. (2021). *Sediment grain size determines microplastic exposure landscapes for sandy beach macroinfauna* Elsevier BV. doi:10.1016/j.envpol.2021.117308

Wang, C., Jiang, L., Liu, R., He, M., Cui, X., & Wang, C. (2021). *Comprehensive assessment of factors influencing nile red staining: Eliciting solutions for efficient microplastics analysis* Elsevier BV. doi:10.1016/j.marpolbul.2021.112698

Wang, Y., Chen, X., Wang, F., & Cheng, N. (2023). Influence of typical clay minerals on aggregation and settling of pristine and aged polyethylene microplastics. *Environmental Pollution (1987), 316*, 120649. doi:10.1016/j.envpol.2022.120649

Werner, & O'Brien. (2017). Marine litter. *Handbook on marine environment protection* (pp. 447–461). Cham: Springer International Publishing. doi:10.1007/978-3-319-60156-4_23

Witzig, C. S., Földi, C., Wörle, K., Habermehl, P., Pittroff, M., Müller, Y. K., et al. (2020). *When good intentions go Bad—False positive microplastic detection caused by disposable gloves* American Chemical Society (ACS). doi:10.1021/acs.est.0c03742

# Supporting information

## Towards quality-assured measurements of microplastics in soil using fluorescence microscopy

Nhu Phan[1], Crispin Halsall[1], Stoyana Peneva[2], Olivia Wrigley[3], Melanie Braun[3], Wulf Amelung[3], Lorna Ashton[4], Ben W.J. Surridge[1], John Quinton[1]

[1]Lancaster Environment Centre, Lancaster University, Lancaster, LA1 4YQ, UK

[2] Wessling GmbH, Am Umweltpark 1, Bochum, 44793, Germany

[3] Institute of Crop Science and Resource Conservation, University of Bonn, Bonn, 53115 Germany

[4]Department of Chemistry, Lancaster University, Lancaster, LA1 4YQ, UK

Email contact: c.halsall@lancaster.ac.uk, q.phanle@lancaster.ac.uk

---

1. **Microplastic extraction from soil**

The extraction of microplastics from soil comprised of a density separation step and the removal of soil natural organic matter using a Fenton reagent. The microplastic content in non-spiked soil was screened using the same protocol (three background samples for three soil types). Microplastic content from spiked samples was subtracted with the number of particles found in the non-spiked soils to avoid false-positive results, as previous studies pointed out that natural organic matter causes false positives when staining with Nile red.

A density separation step was first applied to isolate MPs from soils, which exploits the buoyancy of MPs particles in a higher-density solution of $ZnCl_2$. The Sediment Microplastic Isolation (SMI) unit was utilized as a simple-to-use kit for density separation, with outstanding performance proven in previous studies. (Coppock et al., 2017; Vermeiren, P. et al., 2020) The SMI unit was assembled (with smaller dimensions, **Figure** S4), cleaned, and purged before the introduction of 10 g of soil and 50 mL of $ZnCl_2$. After that, the ball valve was tightly locked, and the SMI was shaken vigorously under an orbital shaker for 2 hours to ensure full contact between the sample and $ZnCl_2$ and to dissolve the gelatine. The valve was then set in the open position, and an additional 200 mL $ZnCl_2$ was added, which was then allowed to settle overnight to allow dense particles to settle out. Once the $ZnCl_2$ solution became apparent, the valve was carefully closed. The supernatant in the headspace was vacuum filtered through a stainless-steel mesh, retaining the zinc chloride for further recycling. The SMI headspace was rinsed thoroughly with HPLC-grade water to recover any remaining particles and remove $ZnCl_2$. Stainless steel meshes were then transferred to a 500 mL beaker containing 20 mL of 0.05M $FeSO_4$, followed by 10-minute sonication at room temperature to wash off any particles attached closely. The meshes were then rinsed with HPLC water, removed, and washed carefully for further use. To start the Fenton reaction, 20mL of $H_2O_2$ was added to the beaker. After 24h, the samples were filtered on glass fibre filters (GFFs) and submerged with 5-7 drops of 5 µm /mL Nile red solution using a glass pipette while filters were still laid on the filter head. After 10 min, filters were thoroughly rinsed with hexane and vacuum-filtered to discard any accumulated liquid. Finally, filters were carefully transferred onto and stored inside covered glass Petri dishes and left air-dried in the dark before being observed under a fluorescence microscope. Samples were analysed within one week after staining to avoid precipitation and quenching of Nile red.

2. **Fluorescence microscopy and automated digital image analysis**

Microscopic imaging was performed using a stereo zoom microscope (Zeiss Axio Zoom.V16) equipped with a long working distance high-aperture macro lens (Plan NeoFluar Z 1.0x/0.25, FWD 56mm) and a fast, sensitive 12Mpixel camera (Zeiss AxioCam 512mono). The microscope had an automated stage and image stitching function to capture the entire filter surface (Zen Blue 2.6 and Zen-pro software). Sample filters stained with Nile Red were directly illuminated with the 470 nm light (CoolLED) and observed through the green filter (GFP filter, emission 524/50 nm) in the darkroom. Green fluorescence was chosen over the red counterpart due to the better fluorescence of synthetic polymers, less fluorescent interference from natural organic matter, and lower background signal intensity in green compared to red fluorescence mode. (Erni-Cassola et al., 2017; Shim et al., 2016a). As almost no fluorescence signal was detected from black and dark-coloured microplastics, the bright field mode was added to quantify black microplastic particles, e.g., PBAT/PLA and potentially the brownish nylon fibres.

Therefore, the whole filter images were obtained for both green fluorescence and bright field, all at a magnification of 50× and a sensitivity of 1 without pixel binning, using the stitching function and surface focusing with several local support points.

Automated particle recognition and quantification based on the fluorescent images were performed in Fiji-ImageJ. The stitched images of the whole filter area in the Carl Zeiss CZI Format (.czi) were converted into a TIFF file (Tag Image File Format) and processed according to the workflow displayed in **Figure** 2. Firstly, a smoothing operation approximating a Gaussian distribution (Gaussian blur filter, **Figure** 2b) was applied. The original image was then subtracted with the Gaussian blurred image to reduce the particle detection runtime and prevent random noise from being falsely detected as particles (**Figure** 2c). This step is beneficial when fluorescence background/noise is present, possibly due to the uncompleted wash of Nile red and the signal from strongly fluoresced materials. Gaussian blur windows (sigma/radius) were set between 100-500 pixels depending on the level of background interference. Afterwards, a global thresholding method was applied to segment the images into particles of interest and background, with colour and intensity parameters adjusted individually to each image to avoid selecting the background as much as possible. Normally, the grey value was set from 400-800 to 65535 (maximal grey value for the 16-bit images of 65535) for the detection of LDPE (dia. 20-150 µm) in the fluorescence mode and from 0 to 1200 (dia. 100-250 µm) for black PBAT/PLA in the bright field mode. The pixel intensity threshold was chosen based on experiment 2.5.1 so that the threshold value can pick as much of all the particles of interest. Fill Hole operation was then applied to compensate for particle penetration resulting from a large Gaussian window and global thresholding. After that, watershed segmentation was used to separate fluorescence particles that lay in proximity to each other and were agglomerated. Watershed segmentation, however, was not applied for bright-field images for the quantification of PBAT/PLA particles due to the potential overestimation of PBAT/PLA particles caused by cracking and the spike shape of cryo-milled particles. Finally, particles were quantified based on Feret's diameter, which is defined as the mean of all diameters over all angles. The lowest size limit of 20 µm was chosen due to the high uncertainty in quantifying particles smaller than that (result from experiment 2.5.1, **Figure** 6) and the use of 6-µm stainless steel mesh during sample preparation. Larger size microplastics prepared from consumer materials (dia. 500-1000 µm) were counted manually instead of Image J due to a variety of shapes and fluorescence intensities induced by different polymers.

## 3. Validation of the Fluorescent Staining Protocol with Environmental Samples

### 3.1. Sampling soil

The study area includes Field 1 (54°00′52″ – 54°00′48″N, 002°46′47″ – 002°46′43″W) and Field 2 (54°00′52″ – 54°00′47″N, 002°46′34″ – 002°46′25″W), both located southeast of Lancaster, United Kingdom. The annual mean temperature is 10.5°C, with daily and annual precipitation recorded at 34.5 mm and 414.2 mm, respectively (Time and Date, 2023). Both fields serve as field stations for Lancaster University and have not been used for agriculture for decades. Additionally, the fields are enclosed by barriers to protect against potential contamination from animals and humans.

For each field, five sampling sites were randomly selected within a 4-meter margin from the field's edge. At each site, a 50 cm x 50 cm quadrat was used to define the sampling area. Soil was dug to a depth of 20-25 cm using a stainless-steel shovel to reach the

ploughing depth, though deeper soil could not be obtained due to high soil compaction. The soil within the quadrat was thoroughly mixed to a 20 cm depth, and a subsample of 1-2 kg of wet soil was collected, stored in 100% cotton bags, and kept at 4°C until further analysis, including pH, conductivity, organic matter content, and particle size distribution.

### 3.2. Microplastic extraction and Fourier transformed infrared micro-spectroscopy measurement

For MPs extraction, 50 g of each soil sample was dried at 40°C, homogenised and sieved through a 2 mm mesh. The sieved soil was then subjected to the previously described MPs extraction process. However, after Fenton digestion, the extracted MPs were filtered through a stainless-steel filter. The particles deposited on the filter were sonicated, rinsed into a clean beaker, and transferred to a 100 mL volumetric flask with HPLC-grade water. From this, 15 mL subsamples were taken using a glass pipette under magnetic stirring for fluorescence microscope analysis. Additionally, 0.5–1.8 mL aliquots were used for FPA-µ-FTIR analysis.

For FTIR analysis, aliquots of samples were filtered on 25 mm Anodiscs™ (Whatman™, PP-supported, 0.2 µm pore size) and analysed via focal plane array micro-Fourier-transform infrared spectroscopy (FPA-µ-FTIR). A Bruker Hyperion 3000 FTIR microscope with a 64×64-pixel FPA detector and Bruker Tensor 27 FTIR spectrometer was used for imaging in transmission mode. Filters were placed on $CaF_2$ windows (25 mm diameter, 2 mm thickness, Korth Kristalle, Germany). The entire surface of the filter was scanned using a 3.5× IR objective. Spectra were collected with a coaddition of 32 scans at an 8 $cm^{-1}$ resolution and a measuring range between 1250 and 3600 $cm^{-1}$. Pixel sizes of the measured data were about 11 µm. Imaging data were then compared against a reference database using siMPle (v. 1.0.1).

**Table S1.** Selected Physicochemical Properties of Agricultural Soils Used for Extractions

| Soil | Sand[(a)] | Silt[(b)] | Clay[(c)] | organic-C (%) |
|---|---|---|---|---|
| | Mass (%) | | | |
| Sand | 73.3 | 16.5 | 8.5 | 0.9 |
| Clay | 9.9 | 36.3 | 50.3 | 5.9 |
| LUFA 2.4 | 22.4 | 42.2 | 2.7 | 2.83a |

(a)Sand refers to soil particles with a diameter of 0.05-2.0 mm. [(b)] Silt refers to soil particles with diameters 0.002-0.05 mm. [(c)] Clay refers to soil particles with a diameter < 0.002 mm.

**Table S2**. Details of MPs used in the recovery experiments, including polymer type, form/shape, size, colour, and original product. Density data correspond to those of pure polymers. (Radford et al., 2021)

| Size range | Plastics | Form shape | Colour | Source | Density (g $cm^{-3}$) |
|---|---|---|---|---|---|
| Consumer material plastics 500-1000 µm | LDPE | film | transparent | food packaging | 0.91–0.92 |
| | PP | film | transparent | food packaging | 0.90–0.91 |
| | PS | fragment | white | insulation board | 0.015-0.03 |
| | Nylon | fibre | brown | carp fishing line | 1.13-1.41 |
| | PET | fragment | transparent | food packaging | 1.37-1.45 |
| | PBAT/PLA | film | black | agricultural mulching film | 1.23-1.29 |
| | HDPE | fragment | white | milk bottle cap | 0.93-0.97 |
| | PVC | fragment | transparent | insulated cable | 1.16-1.58 |
| 100-250 µm | PBAT/PLA | film | black | agricultural mulching film | 1.23-1.29 |
| ≤ 150 µm | LDPE | particle | white | Goonvean Fibre Ltd. | 0.91-0.92 |

**Table S3**. Characterization of soil samples collected from Hazelrigg field for the validation of the fluorescent staining methods.

| Sampling date | Field Area (ha) | Sample code | Latitude | Longitude | Soil physiochemical characterization | | | | | | | |
|---|---|---|---|---|---|---|---|---|---|---|---|---|
| | | | | | Moisture | Temperature | % C | pH | Conductivity (uS/cm) | Particle size analysis | | |
| | | | | | | | | | | % clay | % silt | % sand |
| 08/06/2023 | 0.59 | HF1-S1 | 54.01365 | -2.779300 | 16.4 | 21.0 | 14.2 | 5.9 | 166 | 28.5 | 45.2 | 26.3 |
| | | HF1-S2 | 54.01408 | -2.779208 | 15.4 | 22.9 | 12.8 | 5.7 | 191 | 19.4 | 27.5 | 53.1 |
| | | HF1-S5 | 54.01376 | -2.778979 | 30.9 | 24.7 | 13.3 | 5.5 | 222 | 21.7 | 33.3 | 45 |
| | | HF2-S3 | 54.01322 | -2.775445 | 9.1 | 30.4 | 10.6 | 5.1 | 117 | 20.9 | 40.7 | 38.4 |
| | | HF2-S4 | 54.01314 | -2.775675 | 10.6 | 31.0 | 10.7 | 5.2 | 137 | 17.4 | 32.5 | 50.1 |
| | | HF2-S5 | 54.01371 | -2.775629 | 7.0 | 28.7 | 10.6 | 5.2 | 125 | 15.8 | 27 | 57.2 |

**Table S4**. Number of SMP particles recovered from three soil types (including spiked soil, background, and blanks).

| | **LUFA 2.4** | | | **Sandy** | | | **Clayey** | | | **Blank** |
|---|---|---|---|---|---|---|---|---|---|---|
| Number of particles | spiked | Back-ground | recovered | Spiked | Back-ground | Recovered | Spiked | Back-ground | Recovered | |
| LDPE<br>dia. 10-150 µm | 14010 ± 2130 | 2230 | 11780 | 10830 ±1780 | 540 | 10290 | 5300 ±1760 | 2620 | 2680 | 130 |
| PBAT/PLA<br>dia. 100-250 µm | 4800 ± 480 | 82 | 4718 | 1820 ± 820 | 222 | 1598 | 715±30 | 22 | 693 | 0 |
| Plastics<br>dia. 500-1000 µm | 39 ±3 | 0 | 39 | 35 | 4 | 31 | 38±2 | 2 | 36 | 1 |

**Figure S1** ATR-FTIR (a) and Raman (b) spectra of LMP prepared from consumer products using in the recovery experiment. All the spectra were normalised with the highest peak using Spectragryph software and plotted in Matlab**.** Spectra were compared with OpenSpecy library and confirmed with their own labels.

**a.**

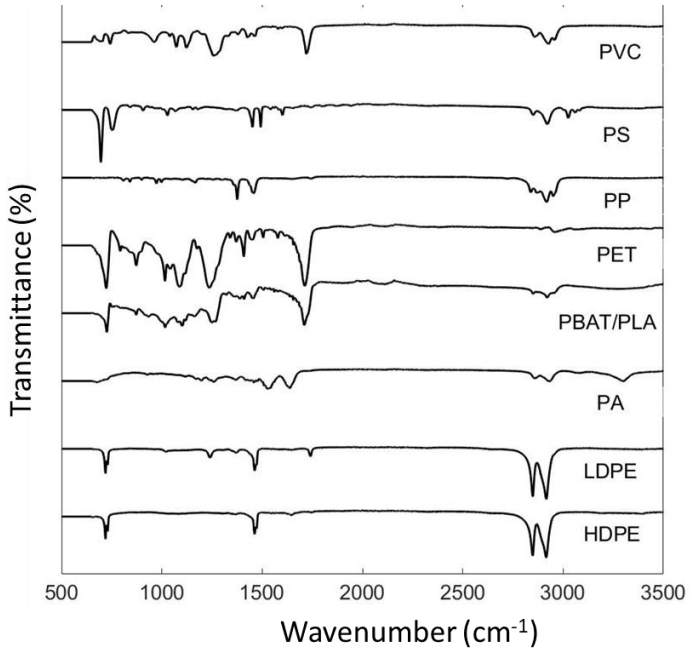


b.

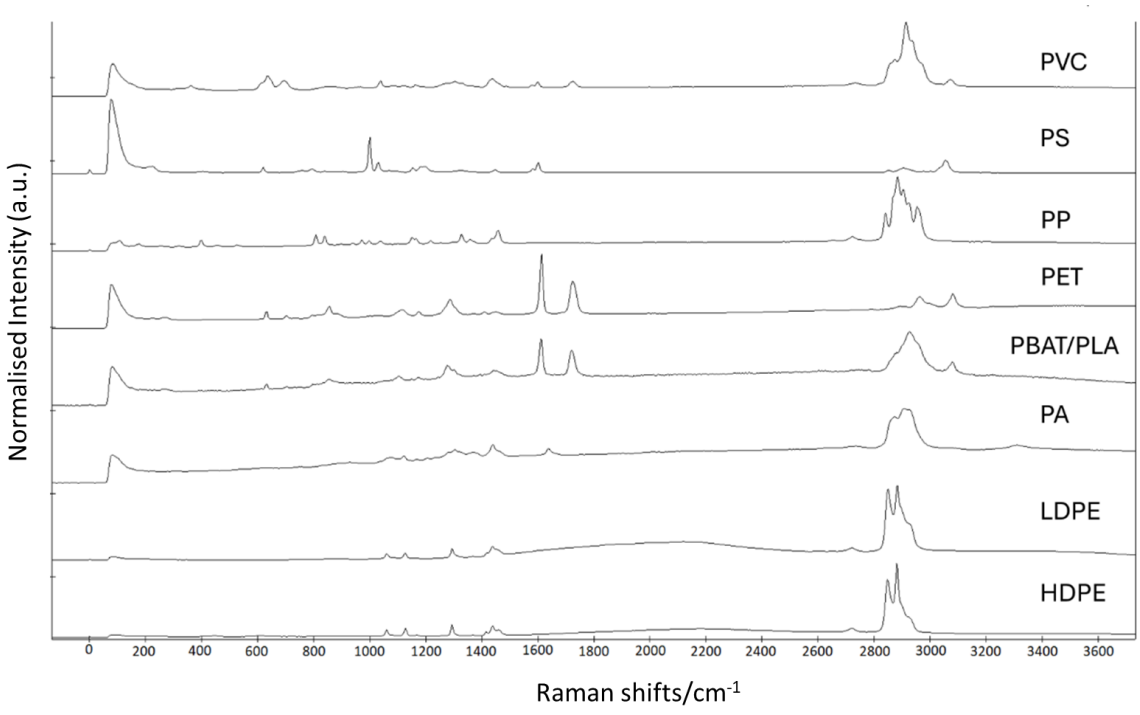

**Figure S2** Microplastic spikes prepared in gelatin sheets: a) larger-sized microplastics (500-1000 µm) including eight type of plastics low-density and high-density polyethylene (LDPE and HDPE), polypropylene (PP), polystyrene (PS), polyethylene terephthalate (PET), poly (PA), polyvinyl chloride (PVC) and the biodegradable plastic polybutylene adipate-co-terephthalate/polylactide blend (PBAT/PLA). B) smaller-sized microplastics including black PBAT/PLA particles (dia. 100-250 µm) and white LDPE particles (dia. ≤ 150 µm)

**a)** **b)**

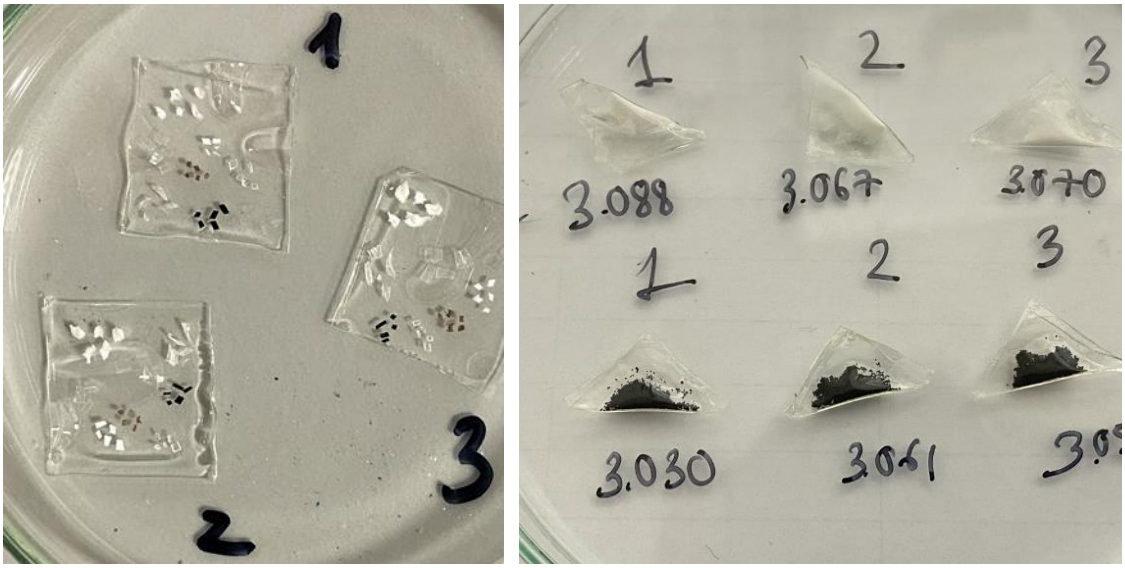

**Figure S3**. Microscopic images of the eight large MPs used for the soil spiking. As it follows, A. polypropylene (PP); B. low density polyethylene (LDPE); C. high density polyethylene (HDPE); D. polystyrene (PS); E. polybutylene adipate terephthalate/polylactic acid (PBAT/PLA); F. polyamide – nylon 6,6 (PA); G. polyethylene terephthalate (PET) and H. polyvinyl chloride (PVC).

**A.**

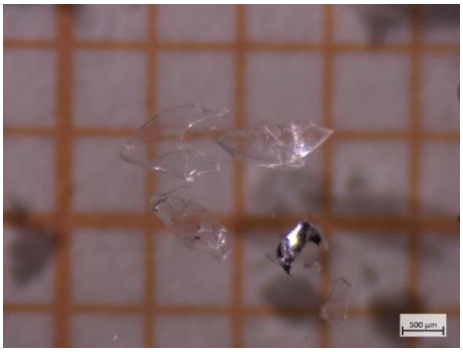

**B.**

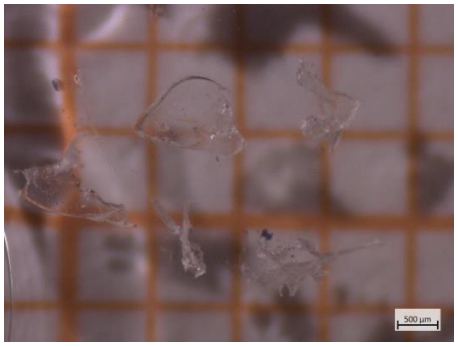

**C.**

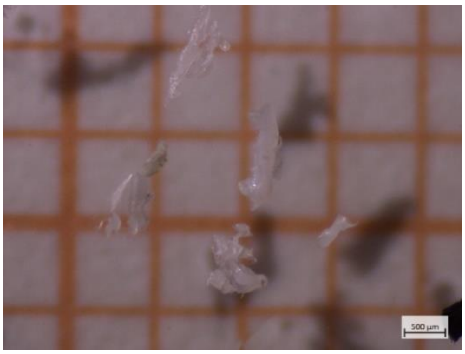

**D.**

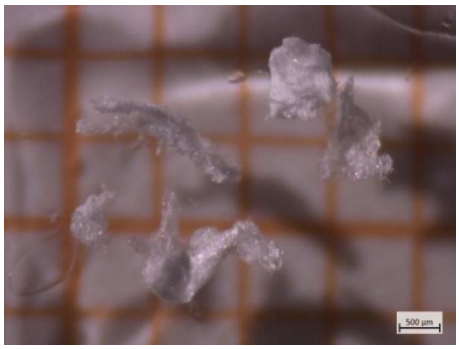

**E.**

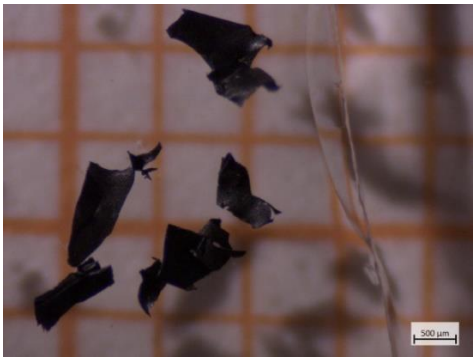

**F.**

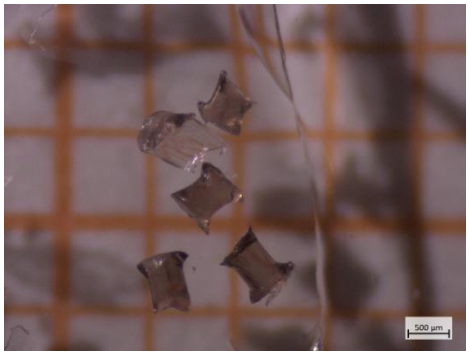

**G.**

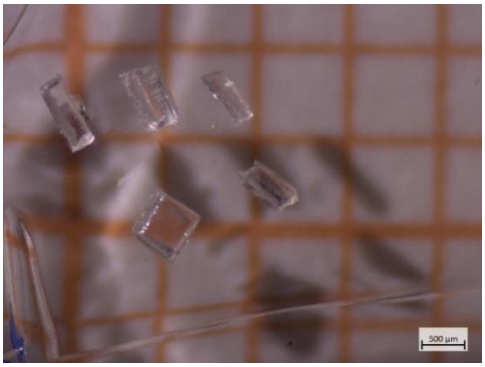

**H.**

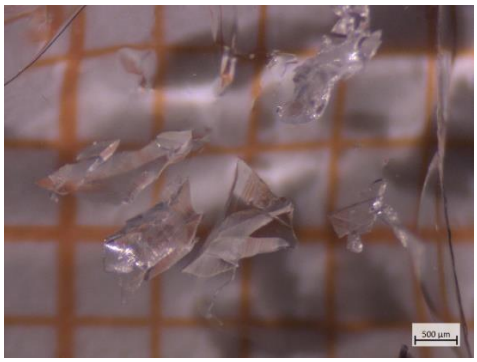

**Figure S4:** Dimensions for the Sediment Microplastic Isolation (SMI) unit using in density separation step.

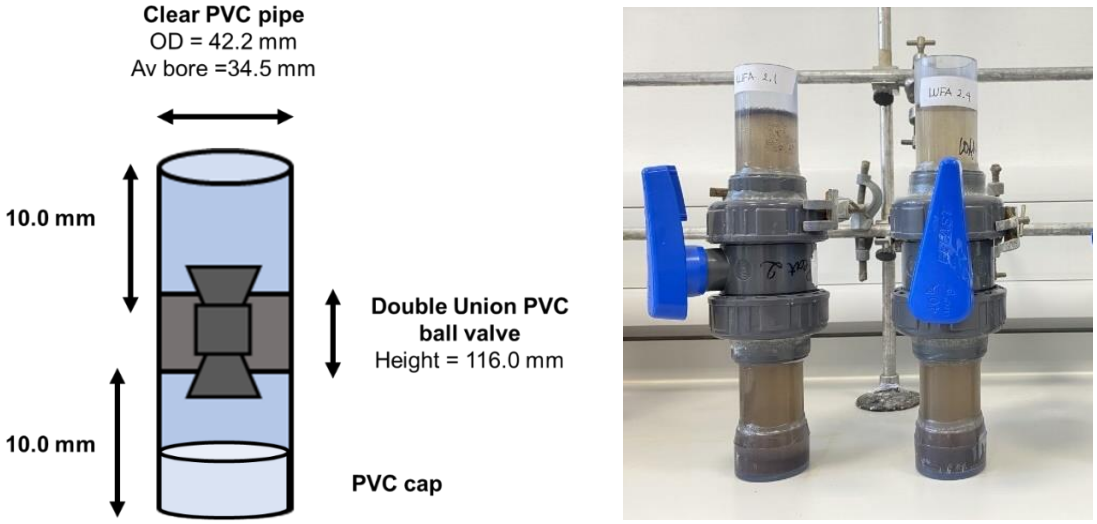


**Figure S5**: Image processing scheme: a) cropped section of the original image; b) Gaussian blur image; c) Gaussian subtracted image; d) threshold image; e) filled hole image; f) Watershed segmentation image.

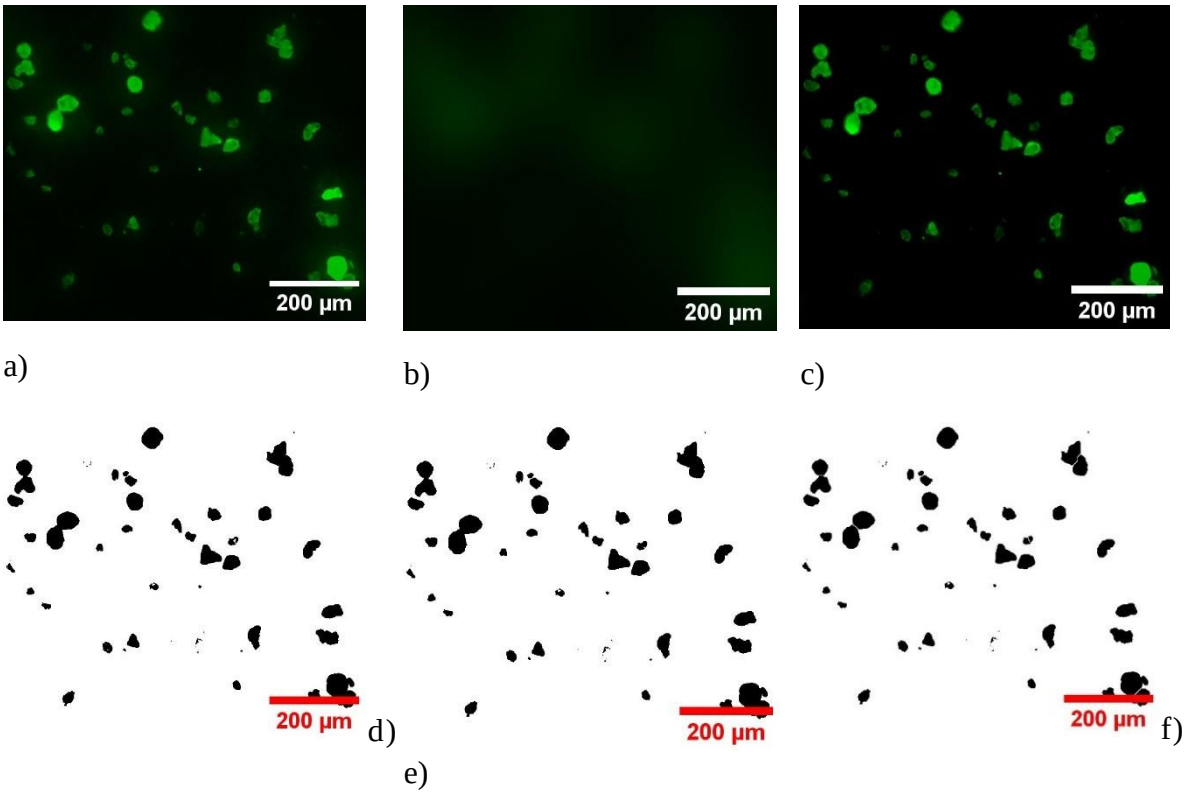

**Figure S6**: Bright-field (top) and Fluorescence images (bottom) of large MPs (dia. 500-1000 µm) prior to being spiked into soil.

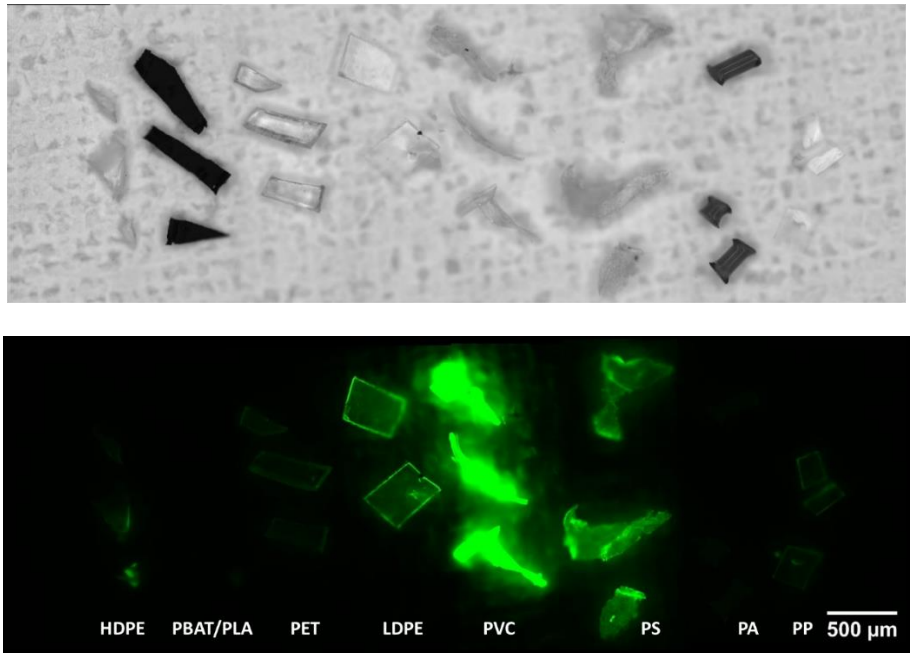


**Figure S7:** Particle size distribution of PBAT/PLA SMPs (1) and LDPE SMPs (2) as assessed by optical and fluorescence microscopies coupled with ImageJ, respectively. The number of particles in each size category is reported as a mean (n=5) with their standard deviation. The light grey area corresponds to the sieving ranges used in the microplastic production method.

1)

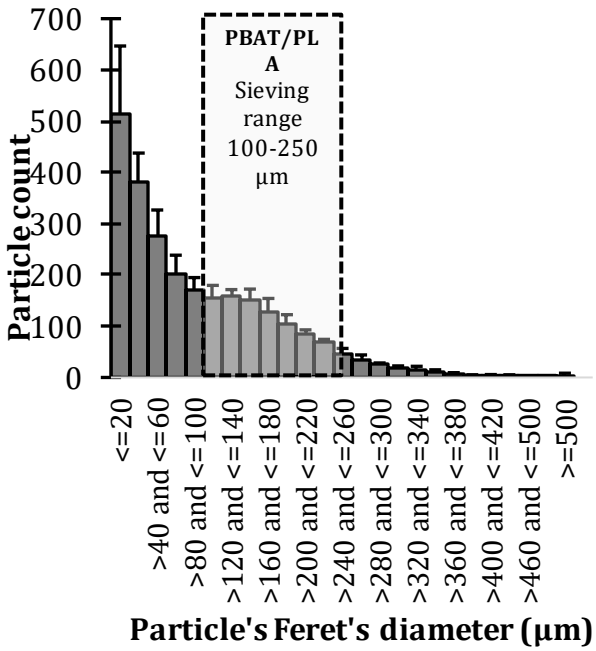


2)

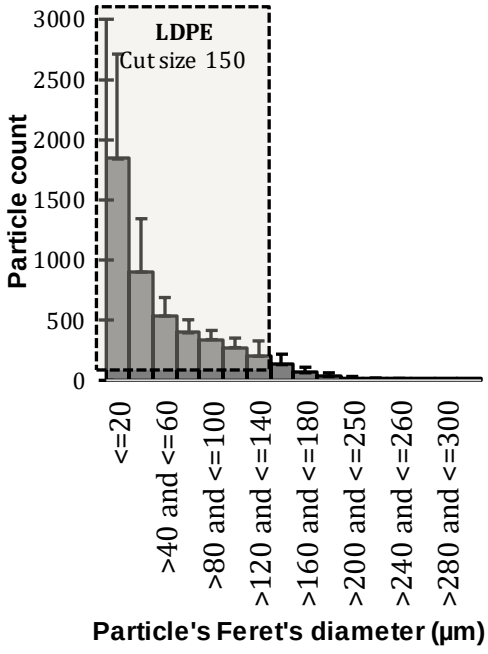

**Figure S8.** Particle size distribution of small MPs from (1) LDPE and (2) PBAT/PLA. Visualized on the x-axis - number of particles in 3 mg and on the y-axis – size of particles in µm. Average particle numbers found were 15733 +/- 138 particles in 3g for LDPE in a size range of 20-150 µm, and for PBAT/PLA we received 3200 +/- 30 particles in 3g in the size range of 100-250µm. These numbers served as a reference for the calculation of recovery rates.

1.

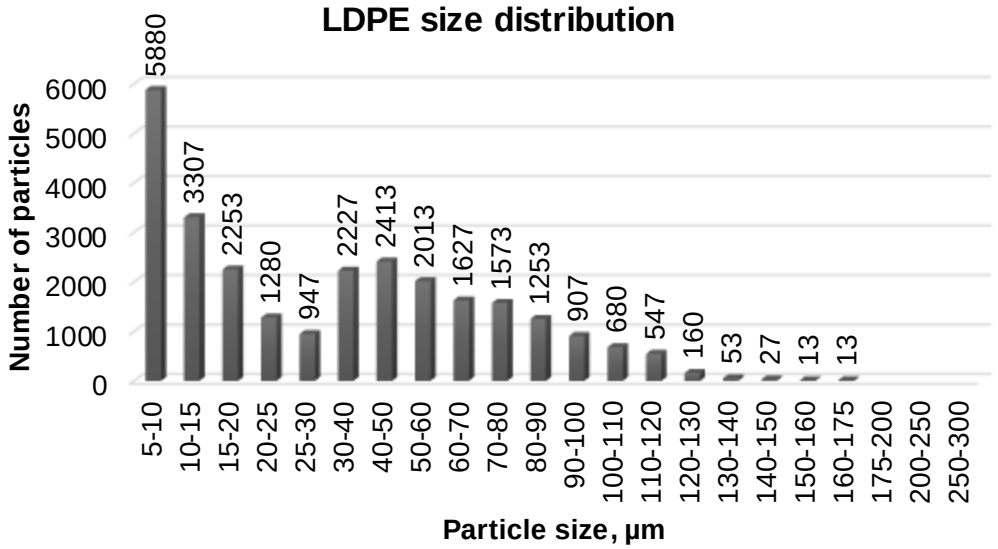


2.

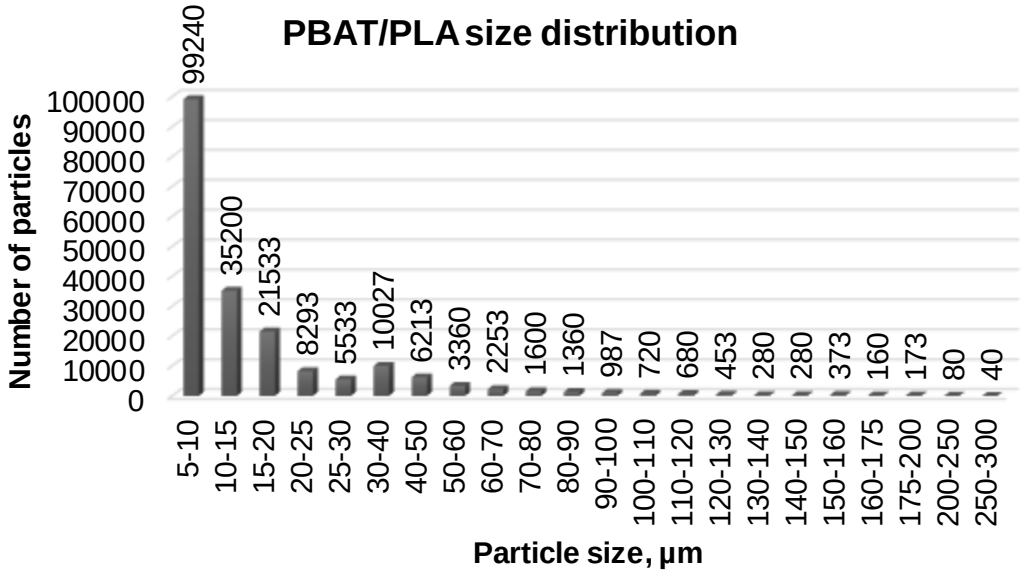

**Figure** S9. Images of filters Comparison images of fluorescence images A: procedural lab blank, B: non-spiked background soil, and C: Plastic-spiked soil sample and bright-field images: C: procedural lab blank, D: non-spiked background soil, and E: Plastic-spiked soil sample and bright-field images. All samples were treated using the same workflow described previously.

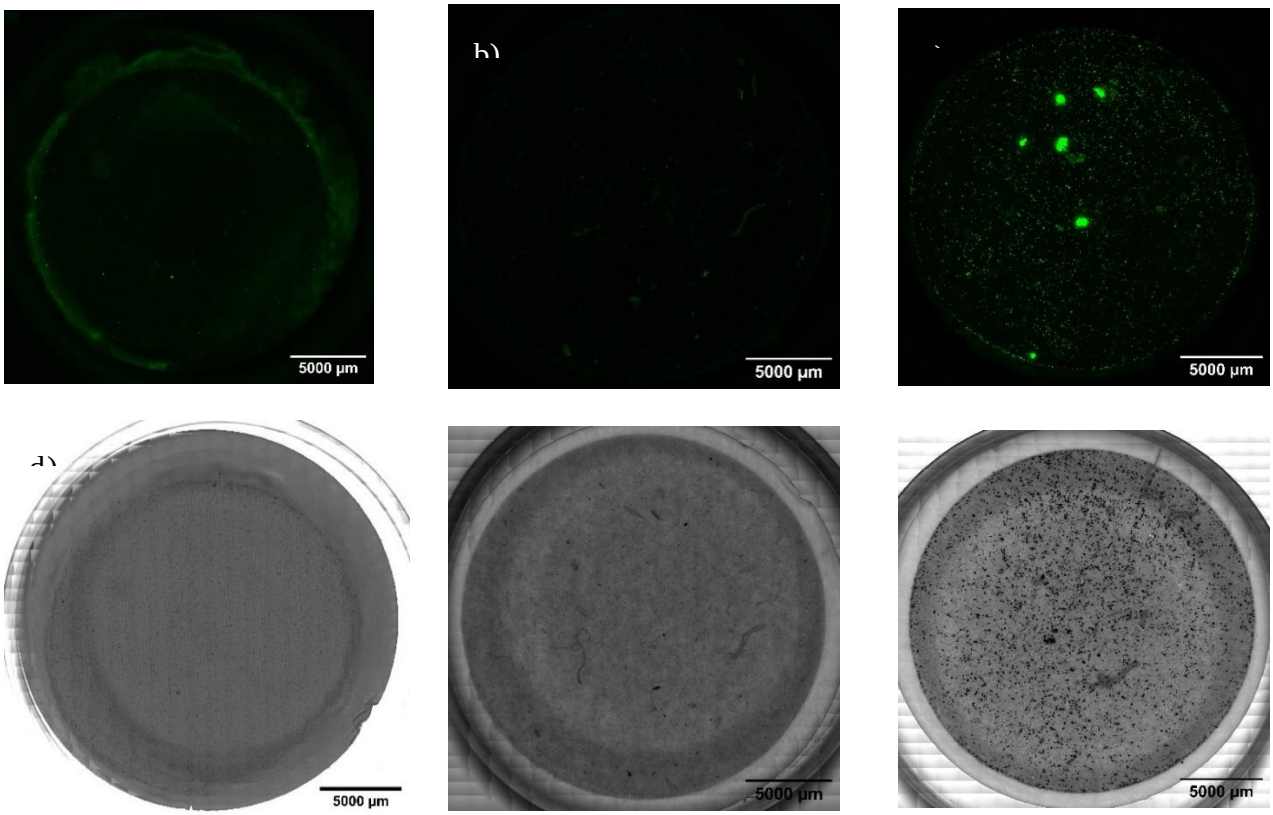


**Figure S10**: Correlation between fluorescence particles (left **Figure**) and black particles (right **Figure**) with natural organic matter content for non-spiked background soils. Organic matter content was 5.90%, 1.83% and 0.83%, respectively, for clay, LUFA 2.4 and sandy soils.

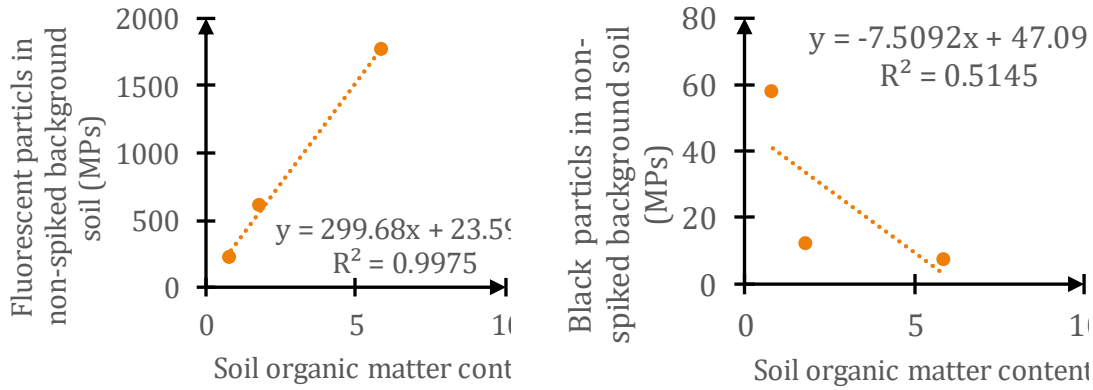


**Figure S11**: Size distribution of fluorescence particles detected soil backgrounds.

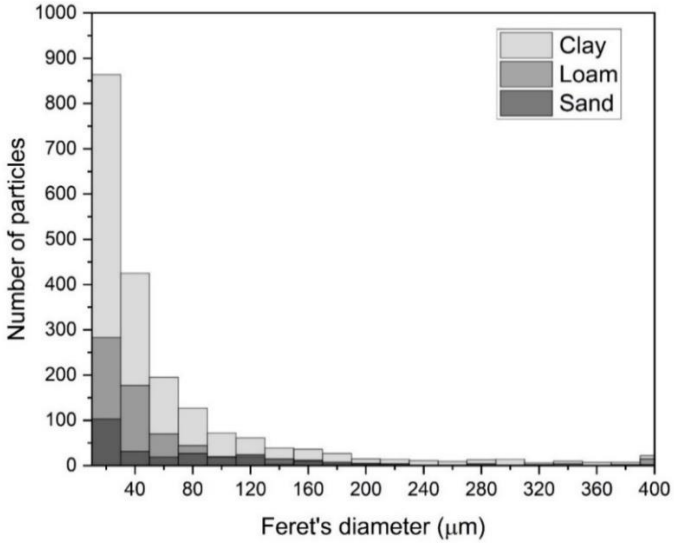


**Figure S12:** Microplastic number concentrations of soil samples collected from the Hazelrigg field station measured by Nile-red staining- fluorescence microscopy and by FTIR micro-spectroscopy method.

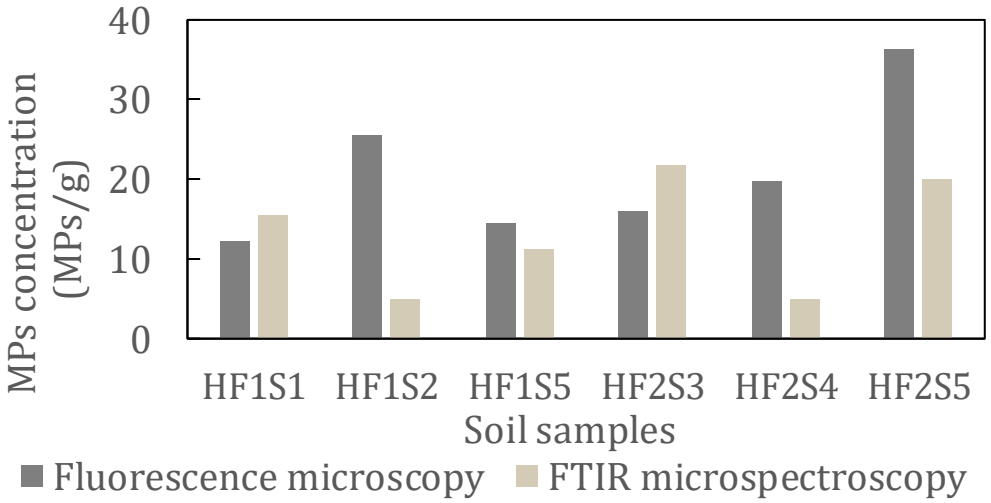

# 3 Microplastic analysis in soil: A comparative assessment

*Accurate quantification of microplastics (MPs) in soil remains a significant challenge due to variations in analytical techniques and sample matrices. This chapter evaluates and compares multiple MPs detection methods, including Digital, Fluorescence, Fourier-transform infrared (FTIR), and Raman microscopy, as well as quantitative Pyrolysis-Gas Chromatography-Mass Spectrometry (Py-GC-MS) and Proton Nuclear Magnetic Resonance ($^1$H-NMR) spectroscopy. Each method was tested with tailored extraction protocols across different soil types and a range of plastic polymers, including conventional and biodegradable MPs of varying sizes. The findings highlight the strengths and limitations of each approach, emphasizing the influence of soil texture and organic content on method performance.*

# Microplastic analysis in soils: a comparative assessment

Stoyana Peneva[1,4], Quynh Nhu Phan Le[2*], Davi R. Munhoz[3*], Olivia Wrigley[4], Flora Wille[5], Heidi Doose[6], Crispin Halsall[2], Paula Harkes[3], Michael Sander[5], Melanie Braun[4], Wulf Amelung[4, 7]

[1]*Wessling GmbH, AM Umweltpark 1, Bochum, 44793, Germany*

[2]*Lancaster Environment Centre, Lancaster University, Lancaster LA1 4YQ, UK*

[3]*Soil Physics and Land Management Group, Wageningen University & Research, P.O. Box 47, 6700 AA Wageningen, the Netherlands*

[4]*Institute of Crop Science and Resource Conservation (INRES), Soil Science and Soil Ecology, University of Bonn, Nussallee 13, 53115 Bonn, Germany*

[5]*Insitute of Biogeochemistry and Pollutant Dynamics, ETH Zurich, 8092 Zurich, Switzerland*

[6] *Wessling Consulting Engineering GmbH & Co.KG, Feodor-Lynen Straße 23, Hannover, 30625, Germany*

[7]*Agrosphere Institute (IBG-3), Forschungszentrum Jülich GmbH, Wilhelm-Johnen-Str. 52425 Jülich, Germany*

**Shared first authorship*

E-mail contact: Melanie Braun (melanie.braun@uni-bonn.de)

# Abstract

Microplastic (MPs) contamination poses environmental risks but harmonizing data from different quantification methods and sample matrices remains challenging. We compared analytical protocols for MPs quantification in soil, consisting of Digital, Fluorescence, Fourier-transform infrared (FTIR), and Raman Microscopy as well as quantitative Pyrolysis-Gas Chromatography-Mass Spectroscopy (Py-GC-MS) and 1-proton nuclear magnetic resonance ($^1$H-NMR) spectroscopy as detection techniques. Each technique was coupled with a specific extraction procedure and evaluated for three soils with different textures and organic carbon contents, amended with eight types of large MPs (0.5 - 1mm) – high- and low-density polyethylene (HDPE and LDPE), polypropylene (PP), polystyrene (PS), polyamide (PA), polyethylene terephthalate (PET), polyvinyl chloride (PVC), and a biodegradable mulch film product composed of polybutylene adipate-co-terephthalate/ polylactic acid (PBAT/ PLA). In addition, we included two types of small MPs (20 - 250 µm) composed of either LDPE or PBAT/ PLA in the tests. The results showed that protocols for Digital, Fluorescence, and ATR-FTIR microscopy recovered 74% to 98% of the large MPs, with fluorescence yielding the highest recoveries. Raman spectroscopy was most sensitive to soil organic matter residues, requiring more sophisticated sample pretreatment. Fluorescence staining with subsequent Fluorescence microscopy detection effectively recovered most small-sized LDPE-MPs but missed 56 - 93% of small PBAT/ PLA particles. For the latter, reliable quantification was achieved only using Soxhlet extraction combined with $^1$H-NMR spectroscopic quantification. Pyrolysis-GC-MS showed intermediate results, displaying low sensitivity to plastic type and lower recoveries as soil clay content increased. We conclude that different methods have different sensitivities for different MPs materials in different soils, i.e., comparisons of MPs loads and threshold settings for MPs loads across methodologies require careful consideration. Yet, our data indicates that adding stained large MPs as an internal standard could enhance extraction control, while Soxhlet-extraction with subsequent $^1$H-NMR analysis is most powerful for controlling future thresholds of small MPs from biodegradable materials.



Keywords: Spectroscopy, soil pollution, conventional synthetic and biodegradable polymers

# 3.1 Introduction

Since the first fully synthetic polymer material was discovered in the early 20$^{th}$ century, plastic materials have found widespread use due to their outstanding chemical and physical properties such as their inertness, lightweight, and flexible usability, as well as their fast production at low cost. In the meantime, consumption of plastics has quadrupled over the past 30 years, resulting in a total global plastic production of 400.3 Mio t in 2022 (OECD, Global Plastic Outlook Database, 2023; PlasticsEurope, 2023). Because of mismanaged waste, a significant fraction of plastics ends up in the environment (OECD, Global Plastic Outlook Database, 2022). Consequently, macroplastics (MaPs, > 2.5 cm), mesoplastics (5 mm - 2.5 cm), and microplastics (MPs, 1 µm – 5 mm) have been found in both aquatic and terrestrial ecosystems (Lebreton et al., 2017; Sajjad et al., 2022). Yet, reliable extraction and accurate quantification in various environments, especially in soils, remains challenging (Astner et al., 2023; Wang et al., 2023). Current reports point to highly variable MPs loads, which could reflect different plastic exposure and input pathways (e.g., plastic mulching, application of compost or sewage sludge) as well as more diffuse sources (such as flooding of rivers, lakes, and seawater, littering or atmospheric deposition; Büks & Kaupenjohan, 2020; Zhou et al., 2020; Braun et al., 2023). However, variations in the reported MPs concentrations in soil could also reflect differences in analytical protocols used for MPs isolation and detection, with different sensitivities to plastic types, sizes and masses, and limits of detection (Bläsing & Amelung, 2018; Büks & Kaupenjohan, 2020; Primpke et al., 2020).

Most extraction methods for analyzing MPs in soil contain two removal steps, one for the mineral phase and one for soil organic matter (SOM; Möller et al., 2020). The removal of the mineral phase is mostly accomplished by density separation: a salt solution with a specific density higher than the one of the plastics is used to separate minerals from plastics which float on the solution surface and can be collected (Coppock et al., 2017; Ribeiro et al., 2017). Sodium chloride (NaCl) is the preferred salt by most scientists, due to its low price and lack of toxicity (Han et al., 2019). However, using NaCl achieves a maximum density of only 1.2 g $mL^{-1}$, insufficient for extracting high-density plastics like polyvinyl chloride (PVC) or polyethylene terephthalate (PET), both of which have a density of appr. 1.37 g $mL^{-1}$. Hence, other solutions, such as zinc chloride ($ZnCl_2$), adjustable to a density of up to 2.1 g $mL^{-1}$, have been recommended for isolating plastic particles with higher densities (Mintenig et al., 2016; Löder et al., 2017; El Hayani et al., 2020). However, caution is required when working and disposing of $ZnCl_2$ or sodium iodide (NaI), which are suitable for extracting of high-density plastics, but are considered hazardous (Perez et al., 2022). Besides, $ZnCl_2$ is a rather strong Lewis acid, thus potentially altering biodegradable plastics upon use.

The extracted plastic fraction, however, also contains SOM, which may interfere with MPs identification. Therefore, several studies use an acid, alkaline, enzymatic, or oxidative pretreatment for SOM removal, e.g., using oxidative agents like hydrogen peroxide ($H_2O_2$) or Fenton's reagent ($H_2O_2$ with iron (II) sulfate, $FeSO_4$ as a catalyst; Zhou et al., 2020; Junhao et al., 2021). While methods such as Fenton's reaction or strong or alkaline acidic digestion pose the risk of degrading some polymer types (Nuelle et al., 2014; Radford et al., 2021), enzymes can be considered as more gentle reagents (Löder et al., 2017; He et al., 2018; Zhang et al., 2018), and may not completely eliminate SOM.

These mineral phase and SOM removal steps have advantages and limitations, requiring careful consideration in protocols for MPs analysis.

The extent to which SOM needs to be removed also depends on the microscopic and spectroscopic technology subsequently used for MPs detection. While larger particles (>0.5 mm) can be identified by eye and removed by hand, for smaller particles, optical microscopy can be used (Mani et al., 2019; Möller et al., 2021; Perez et al., 2022; Braun et al., 2023). Fluorescent staining, using Nile red (NR) as an example fluorophore, combined with automated detection of the stained particles, accelerates MPs detection (Shim et al., 2016). However, there is a risk of false positive results due to the co-staining of SOM with NR, and not all plastics uniformly interact with fluorophores. Moreover, this approach, akin to digital microscopy, cannot differentiate between plastic types (Sturm et al., 2021). For the identification of plastics, techniques like Fourier-transform infrared (FTIR) (Primpke et al., 2020) or Raman spectroscopy (Ribeiro, 2017) have been recommended. When operating as an Imaging spectrometer, µ-FTIR can be used for particles of sizes down to 20 µm (Primpke et al., 2018), whereas µ-Raman possesses a better spatial resolution down to 1 µm (Imhof et al., 2013), but also needs exhaustive sample clean-up to prevent SOM auto-fluorescence from distorting the Raman-signal (Löder et al., 2015; Anger et al., 2018). Additionally, the high-resolution mode and accuracy in particle counting makes these techniques very time-consuming (Araujo et al., 2018); sometimes only 1-2 samples can be processed per day. Also, the techniques have specific analytical window for MPs sizes, leading to method inherent challenges particle counting. Yet, a systematic study evaluating the potential of these techniques together for known MPs contaminations in different soils, is still lacking.

In contrast to the above-mentioned particle-based techniques, there are also methods that quantify absolute MPs concentrations without determining MPs sizes. Thermo-extraction desorption (TED-) Gas Chromatography–Mass Spectroscopy (GC-MS) and Pyrolysis (Py-) GC-MS have been proposed for this purpose (Dümichen et al., 2017; Kittner et al., 2023). The limit of detection (LOD) for TED- as well as Py-GC-MS, depends on several factors, including the MPs type, the applied method for sample preparation, the analytical instrument used, and the expertise of the analyst (El Hayany et al., 2018; Ivleva et al., 2021). Comparing the particle-based and total mass of microplastics (MPs) remains challenging (Caputo et al., 2021). Primpke et al. (2020) explored the detection and identification of microplastics in wastewater, water, and marine sediments using FTIR and Py-GC-MS. While both techniques showed similar trends overall, FTIR often indicated higher concentrations of specific polymer types like PMMA/PUR, whereas Py-GC-MS detected higher shares of PE and PVC. Also, the calculated masses were primarily driven by particles larger than 100 µm. That led to an overestimation of mass, especially for PP, where a few large-sized particles could significantly inflate the calculated masses. Furthermore, TED- and Py-GC-MS are typically conducted on extracted materials due to the specificity of the analysis and the potential overlap of pyrolyzed products from plastic with organic compounds and minerals in uncleaned soil samples.

The presence of SOM and contaminants from other soil components can additionally hinder MPs quantification (Primpke et al., 2020). One approach to address this challenge involves dissolving MPs in solvents before, e.g., Py-GC-MS and $^{1}$H-NMR analyses. Here the solubility of the polymers in the chosen solvent and the heterogeneous nature of the soil matrix has to be considered (Nelson et al., 2019; Steinmetz et al., 2020). Using only one solvent, the application of this method will be limited to polymer types

that dissolve in the chosen solvent. Nonetheless, the varying solubility of polymers can allow for the separation and individual analysis of different polymer types. Such logic is also used in a method to quantify polymers using $^{1}$H-NMR. Recently, $^{1}$H-NMR has gained attraction for monitoring PBAT/ PLA biodegradation in soils, given its precision and low LOD/ limit of quantification (LOQ) values (1.3 and 4.4 µg mL$^{-1}$ respectively for PBAT in deuterated chloroform ($CDCl_3$; Nelson et al, 2019). Hence, this study tested this method against other potential mass-based (e.g., Py-GC-MS) and particle-based methods for PBAT/ PLA quantification, such as µ-Raman and µ-FTIR. Since these standard analytical techniques are not yet routinely used for biodegradable plastics, we aimed to assess them alongside the established protocol based on solvent extraction and $^{1}$H-NMR.

In summary, several extraction protocols with subsequent detection techniques for MPs in soil are available, with their unique strengths and limitations. However, comparative analysis is missing, which hinders a direct comparison of results from different studies. Hence, our goal was to evaluate the efficiency of commonly used methods to recover MPs particles from soils by adding these particles to different soils in known amounts and particle numbers. We focused on two MPs size ranges: visible pieces in the size range of 500 - 1000 µm, which provide robust quality control as they are easy to spike and identify, and small MPs in the size range of ~100 µm diameter, not clearly visible by the naked eye as individual particles. In addition, we selected different polymer types (biodegradable versus non-biodegradable, low-density versus high-density plastics), and performed our analyses with different soil types (sandy, loamy, and clayey mineral soils). The application of all common methods for plastic analyses to the same samples set allows us to provide clearer insights into possible bias of common plastic detection methods towards material origins and soil interferences.

# 3.2 Materials and methods

## 3.2.1 Soil used for spike-recovery experiments.

To assess the potential effects of texture and soil organic carbon content on the extraction of MPs, we chose three mineral soils with different textures: we used sandy and clayey soils (Cambisol and Stagnosol, respectively) from sampling campaigns near Bonn, Germany, and supplemented it with certified loamy topsoil to allow standardized comparisons in future studies (LUFA soil SP 2.4.; Speyer, Germany). All soils were air-dried and sieved to 2 mm (**Table** 3.1.). Measured background contaminations were negligibly small for all analytical techniques (**Table** S1), but for fluorescence microscopy up to 3590 fluorescent particles were detected in loamy soil. However, this count may include false positive results attributed to SOM. Thus, background subtraction is highly important for accurate analyses, especially for fluorescence techniques. (See Results and Discussion section).

**Table 3.1.** Physicochemical properties of soils used for comparative method assessment.

| **Texture** | **Sandy** | **Loamy (LUFA 2.4)** | **Clayey** |
|---|---|---|---|
| **Organic carbon, g kg $^{-1}$** | 9 ± 2 | 18 ± 2 | 59 ± 1 |
| **Particle size distribution (mm) (g kg $^{-1}$)** | | | |
| < 0.002 | 85 ± 0.5 | 238 ± 1.5 | 503 ± 0.5 |

| | | | |
|---|---|---|---|
| 0.002 - 0.006 | 37 ± 7.5 | 76 ± 6 | 82 ± 3.7 |
| 0.006 - 0.02 | 38 ± 2.5 | 146 ± 10 | 140 ± 0.3 |
| 0.02 - 0.063 | 89 ± 6 | 264 ± 14 | 141 ± 13.5 |
| 0.063 - 0.2 | 169 ± 2.5 | 208 ± 12 | 58 ± 0.6 |
| 0.2 - 0.63 | 515 ± 29 | 55 ± 19 | 23 ± 2 |
| 0.63 - 2 | 49 ± 8.5 | 13 ± 4 | 1.7±0.4 |

### 3.2.2 Plastic materials used for recovery experiments.

To cover a range of potential polymer types of plastic found as MPs in soil, we used two different MPs size groups, (500 - 1000 µm and 5 - 250 µm) and different plastic types as examples for conventional and biodegradable plastics. For larger MPs (500 - 1000 µm), we used eight plastic types derived from household products (**Table** 3.2.); MPs were produced using a standard razor blade and ensured to be the desired size with a digital microscope (Zeiss STEMi 305). For small MPs (5 - 250 µm), we obtained LDPE microparticles from Goonvean Fibers Ltd (Cullompton, England) and cryo-milled a PBAT/ PLA blend film (BIONOV B, Barbier, France). While LDPE was specified to be 10 - 150 µm, the PBAT/ PLA was sieved to 100 to 250 µm. Quality assurance using fluorescence and Raman microscopes, and a particle measuring system (model Syringe, Markus Klotz GmbH) in ethanol suspension revealed actual sizes between 5 to 250 µm for both plastics (Phan Le et al., see Chapter 2).

### 3.2.3 Spiking of soil samples

To determine the recovery of MPs from the soils by each of the different methodologies, 10 g of each soil (in 3-fold replication) was spiked with large and small MPs (**Table** 3.2.): for large MPs, five particles of each of the eight plastic types were added to the soil, and for small MPs, 3 mg of each LDPE and PBAT/ PLA was added (**Table** S2). To minimize particle loss during spiking, MPs were placed on pre-wetted gelatin sheet, 1 cm x 1 cm (one sheet for large particles and two sheets for each LDPE and PBAT/ PLA; Hurley et al., 2018; Zhang et al., 2018), which can be re-dissolved and homogenized in a mixture of soil and water (Möller et al., 2020). Large MPs were placed onto the gelatin sheet using either non-static tweezers or a needle, while small MPs were directly weighted on the gelatin sheet. Three gelatin sheets (one with large and two with small MPs) were added to each soil in a beaker and left overnight, covered with a small amount of water to ensure their dissolution. For the Soxhlet – extraction coupled to $^{1}$H-NMR analysis, 3mg of PBAT/ PLA (**Table** S2) was directly added to the tested soils. For each analytical test, the whole 10 g of spiked soil was processed in replicates.

**Table 3.2.** Characteristics of plastics used for method testing (UF: uniform fragment, NUF: non-uniform fragment, NUFF: non-uniform film fragment)

| Type | Source | Color | Shape | Size | Density, g/cm$^3$ | Chemical Structure |
|---|---|---|---|---|---|---|
| PP | Milk bottle lids | Transparent | NUF | 0.5 – 1 mm | 0.91 | 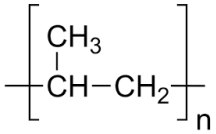 |
| LDPE | Packaging bags | Transparent, with black writing | NUFF | 0.5 – 1mm, 10 – 150 µm powder | 0.91-0.93 | 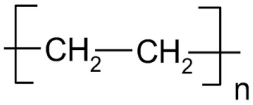 |
| HDPE | Packaging bags | White | NUF | 0.5 – 1 mm | 0.93 - 0.97 | |
| PS | Foam - styropor | White | NUF | 0.5 – 1 mm | 1.02 | 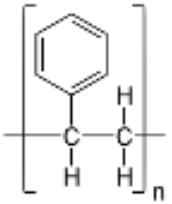 |

| | | | | | | |
|---|---|---|---|---|---|---|
| Biodegradable mulch film PBAT/ PLA | Novamont | Black | NUFF | 0.5 – 1 mm, 10 - 250 µm powder | 1.23 - 1.29 | (a) PLA 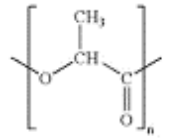 (b) PBAT 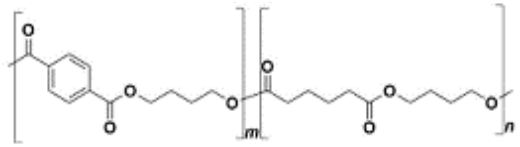 |
| PA - Nylon 6,6 | Fishing net | Light brown | UF | 0.5 – 1 mm | 1.14 | 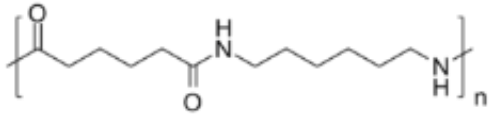 |
| PET | Restaurant boxes | Transparent | UF | 0.5 – 1 mm | 1.38 | 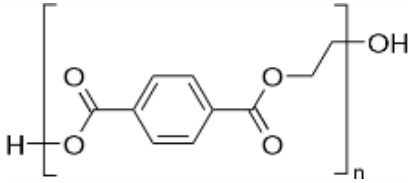 |
| PVC | Isolating cable | Transparent | NUF | 0.5 – 1 mm | 1.38 | 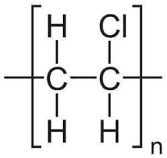 |

For each detection technique specific sample preparation is required and was subsequently tested (**Figure** 3.1. and description in Supplementary Materials, **Figure** S2, and **Table** S3 and S4 for details):

- Method A – Density separation followed by Digital Microscopy analysis (Braun et al., 2021, 2023).
- Method B – Density separation, Fenton's digestion, followed by fluorescence staining and Fluorescence Microscopy (Coppock et al., 2017; Shim et al., 2016).
- Method C – Density separation, Enzymatic, and Fenton's digestion and followed by ATR- and focal plane array (FPA-) µ-FTIR (method C1 and C2), µ-Raman spectro-microscopy (method C3), and Py-GC-MS analysis (method C4; Löder et al., 2017; Mintenig et al., 2017; Primpke et al., 2018; Mbachu et al., 2021).
- Method D - Soxhlet extraction coupled to quantitative $^{1}$H-NMR spectroscopy (Nelson et al., 2020).

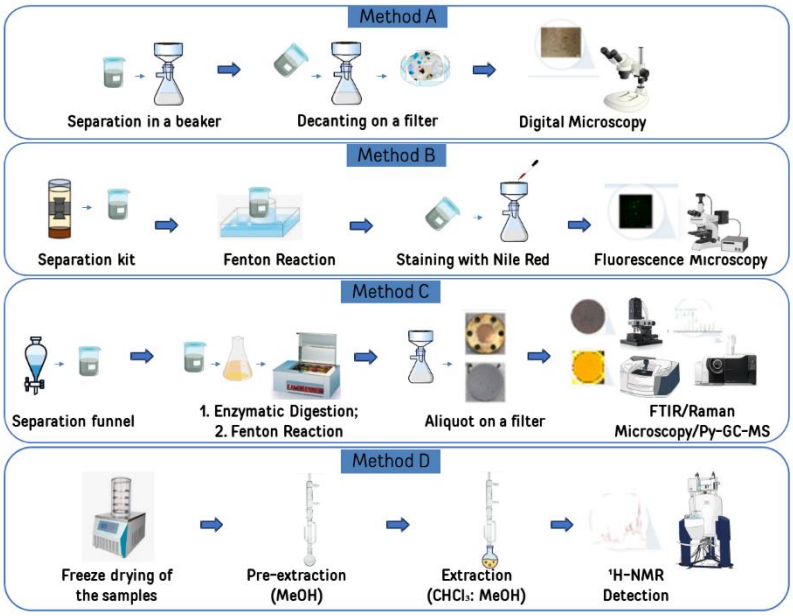


**Figure 3.1.** Illustration of main approaches used for microplastic extraction (SOM = soil organic matter; for additional information on the methods, see also **Table** S3, Supplementary Materials).

Methods C with excessive SOM removal treatments involved four different detection techniques, equated with C1, C2, C3 and C4, respectively. In line with common reports in the literature, Methods A - Digital Microscope and method C1 – ATR-FTIR were applied for large MPs only (Perez et al., 2022). In contrast, methods B - Fluorescence Spectroscopy and method C3 - µ-Raman Microscope were used for both small and large MPs, while methods C2 – FPA - µ-FTIR, C4 – Py-GC-MS and D – $^{1}$H-NMR were used for small MPs only. It's worth noting that each extraction protocol and subsequent purification protocol is considered to be optimal for matching the respective detection method. For each of the seven analytic techniques included (procedure in Supplementary Materials), one of four extraction methods was selected to match the requirements of the technique. We used $ZnCl_2$ as this salt is the most commonly used salt for extraction when high-density plastics are also included in the analysis (Mintenig et al., 2016; Löder et al., 2017; Prosenc et al., 2021; Way et al., 2022). For the small-sized MPs, aliquots of samples

prepared for µ-FTIR, and µ-Raman were used for the Py-GC-MS measurements as well. Additionally, to the comparison of spectral libraries and matching indexes we used to evaluate the potential effects of sample pre-treatment on the MPs, we inspected the large MPs for visual changes (via digital microscope), as these changes might also disturb IR or Raman signals or interfere with the staining efficiency for the Fluorescence Microscope.

Each analytical protocol, except for $^{1}$H-NMR spectroscopy, begins with a density separation step (**Figure** 3.1.). We used a prefiltered $ZnCl_2$ solution with a density of 1.5 g mL $^{1}$, which was added in a soil: solution ratio of 1:20 (m/v).

The recovery of small particles for methods C2 - FPA-µ-FTIR and C3 - µ-Raman was calculated as a percentage of the expected number in the aliquot taken. In the case of method B - Fluorescence Microscopy the entire sample was considered when calculating recovery. Specific care to prevent sample contaminations from airborne dust or clothes during setup and spiking was taken in each lab as described in Supplementary Materials.

### 3.2.4 Data Analysis

Statistical analysis was completed using R (V 4.1.2; (R Core Team 2018), with the packages ggplot, tidyverse, and dplyr (Wickham, 2016), car (Fox and Weisberg, 2019), and FSA (Ogle *et al.*, 2023). Data were first tested for normality and homoscedasticity by applying a Shapiro-Wilk and Levene's tests, respectively. Although the Shapiro-Wilk test is typically used for larger datasets, we could not perform the more typical Kolmogorov-Smirnov test due to the factor variables involved. For normally distributed and homoscedastic data, a one-way ANOVA, and post-hoc Tukey test where necessary, were applied to complete pairwise analysis of means. Where data were determined to be either not from a normally distributed sample or heteroscedastic, a non-parametric alternative was performed (Kruskal-Wallis and a post-hoc Dunn's test, where necessary). In all cases, a significance level of 0.05 was applied. When means are expressed, deviations (±) are given as standard error.

## 3.3 Results

Changes in the physical appearance of the large MPs were uncommon. However, nylon underwent bleaching when a $ZnCl_2$ density separation solution was used (**Figure** S1). Upon microscopic examination (method B and method C3), the surface of the large PBAT/PLA particles appeared altered, exhibiting signs of thinning. Furthermore, PP and PS resulted in diminished recoveries when subjected to method C3, possibly due to fragmentation.

### 3.3.1 Recovery of large microplastics

The mean recovery of large MPs across all soils was highest for method B - Fluorescence microscopy (88 ± 4%), and method A - Digital microscopy (86 ± 3%), followed by method C1 - ATR-FTIR (80 ± 3%), and method C3 – µ-Raman (60 ± 17%) (**Table** 3.3.). The reduced recoveries observed with the latter method were primarily attributed to MPs analyses of soils with heavier textures, loamy, and clayey (**Table** 3.3.). For large MPs only the number of particles rather than their total concentration or mass are routinely

determined. Hence, we did not apply $^{1}$H-NMR and Py-GC-MS to large MPs but exclusively applied these quantification techniques to small MPs, calculating recoveries based on their absolute content.

**Table 3.3.** Mean recoveries (%) with standard error (SE) of large MPs (0.5 - 1 mm) for all types of soils; all using microscopical techniques.

| | Method A - Digital* | | | Method B - Fluorescence* | | | Method C1 - ATR-FTIR | | | Method C3 - µ-Raman ** | | | | | |
|---|---|---|---|---|---|---|---|---|---|---|---|---|---|---|---|
| | Sandy | Loamy | Clayey | Sandy | Loamy | Clayey | Sandy | Loamy | Clayey | Sandy | | Loamy | | Clayey | |
| PP | - | - | - | - | - | - | 50 ± 21 | 60 ± 14 | 50 ± 7 | 47 ± 14 | 53 ± 14 | 27 ± 5 | 27 ± 5 | 40 ± 9 | 40 ± 16 |
| LDPE | - | - | - | - | - | - | 90 ± 7 | 80 ± 14 | 80 ± 0 | 20 ± 0 | 86 ± 24 | 20 ± 16 | 47 ± 24 | 40 ± 16 | 73 ± 36 |
| HDPE | - | - | - | - | - | - | 70 ± 7 | 70 ± 7 | 80 ± 14 | 127 ± 30 | 100 ± 41 | 47 ± 20 | 47 ± 5 | 113 ± 14 | 53 ± 20 |
| PS | - | - | - | - | - | - | 60 ± 0 | 80 ± 28 | 80 ± 14 | 13 ± 5 | 60 ± 9 | 20 ± 9 | 60 ± 16 | 0 ± 0 | 33 ± 11 |
| PBAT/PLA | - | - | - | - | - | - | 80 ± 14 | 110 ± 7 | 100 ± 0 | 140 ± 25 | 86 ± 5 | 0 ± 0 | 40 ± 9 | 27 ± 22 | 7 ± 5 |
| PA | - | - | - | - | - | - | 90 ± 7 | 100 ± 0 | 100 ± 0 | 73 ± 5 | 80 ± 9 | 40 ± 25 | 47 ± 20 | 33 ± 14 | 60 ± 0 |
| PET | - | - | - | - | - | - | 90 ± 7 | 60 ± 14 | 90 ± 7 | 87 ± 5 | 80 ± 9 | 53 ± 20 | 13 ± 11 | 47 ± 20 | 67 ± 14 |
| PVC | - | - | - | - | - | - | 60 ± 0 | 110 ± 7 | 90 ± 7 | 80 ± 9 | 106 ± 5 | 40 ± 0 | 67 ± 5 | 33 ± 14 | 73 ± 14 |
| Total | 93 ± 5 | 88 ± 11 | 79 ± 3 | 80 ± 4 | 97 ± 4 | 89 ± 3 | 74 ± 4 | 84 ± 4 | 84 ± 3 | 73 ± 10 | 84 ± 5 | 31 ± 3 | 45 ± 3 | 42 ±10 | 51 ± 8 |

* No material identification can be performed for large MPs using digital microscopy and fluorescence staining, since methods are not polymer specific.

** Recoveries for µ-Raman microscopy analyses in the first column for each soil are recorded using autofocus, whereas in the second column - applying the focus manually.

Method A - Digital microscopy revealed recovery rates of 80 to 103% in sandy soil, 75 to 105% in loamy soil, and 75 to 83% in clayey soil. These findings suggest that the recoveries remained consistent across different soil textures (**Figure** S3) and were confirmed by a one-way ANOVA ($p > 0.05$). High recovery rates were accomplished by the introduction of a second decanting step, which significantly enhanced the recovery, resulting in the retrieval of an additional one-third of all plastics (see Supplementary Materials for details). Also, method B - Fluorescence microscopy stood out as highly effective in isolating and identifying large MPs regardless of the soil type (**Table** 3.3.). While this method does not offer precise identification of plastic types, the fluorescence of stained MPs particles varies depending on their characteristics (polarity, morphology, presence of additives, etc.) (Phan Le et al., 2025, see Chapter 2). PET and HDPE displayed weaker fluorescence than LDPE and PVC, occasionally complicating the detection of these MPs particles in spiked soils (Phan et al., 2025, see Chapter 2).

The average recovery for the large MPs using method C1 - ATR-FTIR ranged from 68 to 90% for the different soils, with a better recovery for the finer textured background (**Table** 3.3.). However, no significant difference between the soil types was observed. We collected up to three spectra of each spiked plastic (0.5 – 1 mm size), which was then added to a reference library. Compared with the other methods, method C3 - µ-Raman, faced challenges to identify large MPs in all three soils (see Supplementary Materials). We started by applying autofocus settings when obtaining the spectra from the particles on the filters. However, due to much lower recoveries in comparison with the previously mentioned methods, we also applied manual focus for the large MP particles on the filters, which led to increased recoveries (**Table** 3.3.). The recoveries for all three replicates were highest for the sandy soil (73 to 93%), followed by the loamy (40 to 50%) and the clayey soil (33 to 63%), with significant differences between all soil types, shown by an ANOVA and post-hoc Tukey test ($p < 0.05$). As Raman led to a frequent misidentification of PBAT/ PLA as PET, those misidentifications were included in the overall recoveries for PBAT/ PLA. Moreover, PBAT/ PLA spectra showed high noise resulting in poor identification, as already noted by Araujo et al. (2018). For less than 2% of the cases, PBAT/ PLA was not misidentified as PET but also as PVC, HDPE, and LDPE.

## 3.3.2 Recovery of small microplastics

The average recoveries for small MPs across all soil types varied among the different methods (**Figure** S4). For LDPE, the highest mean recoveries across the three soil types were achieved with method B – Fluorescence microscopy (62 ± 22%), followed by method C2 – FPA-µ-FTIR (40 ± 7%), method C3 - µ-Raman (38 ± 10%), and method C4 – Py-GC-MS (34 ± 5%), although there were no significant differences between the four ($p > 0.05$). For both PBAT and PLA, method D – $^{1}$H-NMR yielded the highest recoveries (92 ± 0% for PBAT and 98 ± 2% for PLA), followed by method C4 – Py-GC-MS (49 ± 21%), which, however, detects PBAT only not PLA due to the lack of reliable marker signals for PLA in the samples, likely reflecting the very low concentration of the PLA polymer in the biodegradable plastic mulch blend (See Supplementary Materials). Recoveries further tended to decline in the order of method C3 - µ-Raman (39 ± 13%), method C2 – FPA-µ-FTIR (34 ± 13%), and method B – Fluorescence (25 ± 15%) (refer

to **Figure** 3.3. for details). Significant differences between the microscopic methods were not observed based on the Kruskal-Wallis test; however, recovery in sandy and loamy soils was significantly higher than in clayey soil ($p < 0.05$) with post-hoc Dunns analysis. It is noteworthy, that $^{1}$H-NMR provided additional information on the PLA and PBAT content; hence, both components in the biodegradable mulch film were displayed separately in **Figure** 3.3. Across all the microscopic methods, recoveries were consistently higher for conventional LDPE than for biodegradable PBAT/ PLA, except for method D – $^{1}$H-NMR, as it was tested exclusively for PBAT/ PLA.

For the calculation of particle numbers in spiked soil, the particles found in the non-spiked background and blanks were subtracted (Supplementary Materials, **Table** S1). Overall, these numbers accounted for 23 - 98% of the spiked MPs amounts. For method B – Fluorescence microscopy about 12,500 ± 2,400 small LDPE particles were recovered from sandy soil, 13300 ± 1000 from the loamy soil, but only 3,800 ± 18,00 from the clayey soil. Considering the expected number of LDPE particles (15,300 ± 4,500), and 540 to 3,590 particles in the non-spiked, background soils, this method reached final recoveries for the LDPE of 83 to 88% for sandy and loamy soil, but only 8 ± 3% for the clayey one. For PBAT/ PLA, recovery rates across different soils were notably lower, ranging from 61 ± 3% in the loamy soil to 5 ± 1% in the clayey one (**Figure** 3.3.). The reduced recovery reflects difficulties in identifying black particles in bright field mode, given that these black PBAT/ PLA particles did not exhibit a distinct fluorescence response to NR staining.

The recoveries of added particles for the small LDPE MPs for method C2 – FPA-µ-FTIR ranged from 29 ± 0% for the loamy soil to 57 ± 13% for the sandy soil. In method C3 - µ-Raman, the recoveries ranged from 13 ± 11% for clay to 52 ± 4% for the loamy soil of spiked small MPs. These were comparatively lower than the recoveries from method B – Fluorescence microscopy, where the overall recovery in sandy and loamy soil was significantly higher than in the clayey one ($p < 0.05$). In contrast, recovery of PBAT/ PLA was similar, ranging from 2 ± 1% to 50±2% for the different soils using method C2 – FPA-µ-FTIR, and from 8 ± 6% to 58 ± 12% using method C3 - µ-Raman, respectively (**Figure** 3). Method C3 - µ-Raman produced more variable outcomes across different soil types than method C2 – FPA-µ-FTIR for small MPs. A similar pattern was observed for large MPs. Noteworthy, the identification of PBAT/ PLA was easier when using method C3 - µ-Raman than with method C2 – FPA-µ-FTIR. In all cases, recovering small MPs was more challenging from the clayey soils than from the sandy ones (**Figure** 3). The standard errors of the recoveries for the standard LUFA-loamy soil were much lower than for the other two soils, making the certified soils superior to non-standard environmental soils for such methodological tests. In summary, using FPA-µ-FTIR and µ-Raman techniques holds significant promise for even smaller MPs identification, however, the overall recovery rates across different soil types were not yet satisfactory when utilizing the extraction protocol included in Method C.

As the aliquot used for method C4 – Py-GC-MS analysis was obtained from the same final extraction suspension employed for methods C2 – FPA-µ-FTIR and C3 - µ-Raman, this enabled direct comparisons between samples, although it is relevant to acknowledge the presence of a residual mineral fraction in the suspension. The concentrations for LDPE found ranged from 73 - 139 µg $g^{-1}$ (25 ± 4% to 46 ± 9% recovery), and for PBAT from 12.5 to 283 µg $g^{-1}$ (4 ± 3% and 94 ± 17%) for the different soils, again with the highest recoveries for the sandy soil (**Figure** 3).

Finally, method D – $^{1}$H-NMR provided the most efficient and reliable protocol for the mass determination of biodegradable PBAT/ PLA particles, with recoveries reaching 91 - 92% for PBAT and 92 - 100% for PLA for the different soils, with standard errors not exceeding 4.1% in all approaches (**Figure** 3).

## 3.4 Discussion

When analyzing MPs, it's noteworthy that while digital microscopy and fluorescence dye staining are relatively simple, FPA-µ-FTIR and µ-Raman microscopy are time-consuming, requiring several hours for sample processing. Moreover, these techniques typically demand expertise, experience, and training, even though protocols for their use in analyzing MPs are relatively well established. Data interpretation is also feasible once a library is used for recognition and a satisfactory matching index is recognized. Py-GC-MS in contrast requires more careful data interpretation even though it is one of the most widely used techniques for mass determination of plastics (Steinmetz et al., 2020; Ivleva, 2021). Hence, the joint application of complementary techniques may be needed to give accurate estimates of MPs amounts, particles numbers and size – the latter requires the use of micro-spectroscopy, despite all challenges (Primpke et al., 2020).

### 3.4.1 Microplastic properties as affected by the extraction method

For plastic extraction from soils and sediments, $ZnCl_2$ is one of the most common salts used for density separation, especially when high-density plastics are analyzed (Coppock et al., 2017; Möller et al., 2020; Prosenc et al., 2021). However, former studies indicate that "harsh" extraction methods may lead to (surface) alteration and fragmentation of MPs (Hurley et al., 2018; Pfohl et al., 2021). We also observed these alterations in all used protocols for nylon, caused by the corrosive action of $ZnCl_2$ used for density fractionation (**Figure** S1). As $ZnCl_2$ can act as a Lewis acid due to its hydrolytic activity by generating HCl, $ZnCl_2$ can promote an acidic environment. While Nylon bleaching, the loss of its color, occurred, it did not impact its recovery, nor did it affect the recovery of the other conventional large MPs (Schrank et al., 2022). However, it is noteworthy that as nylon is an amide, it can undergo hydrolysis under acidic conditions, which might affect the particles size and for smaller particles presumably even the recovery (Brette et al., 2024).

In contrast, fragmentation with a potential breakdown of large to small MPs was observed for the PBAT/PLA, as also previously reported by Möller et al. (2021) for biodegradable PLA particles. These alterations may affect both the particle size as well as the spectra of biodegradable plastics, one potential reason for comparably low recoveries obtained by spectroscopic analyses coupled to microscopical identification, such as in method C. As the spectra of PBAT/PLA particles were only marginally affected by extraction (**Figure** S5), fragmentation might have mainly caused low recoveries. Consequently, to reduce the potential degradation of biodegradable and conventional plastics during density separation, a replacement of $ZnCl_2$ by other salt solutions, such as the environmentally friendly potassium formate (KCOOH) might be suitable (Jarosz et al., 2022).

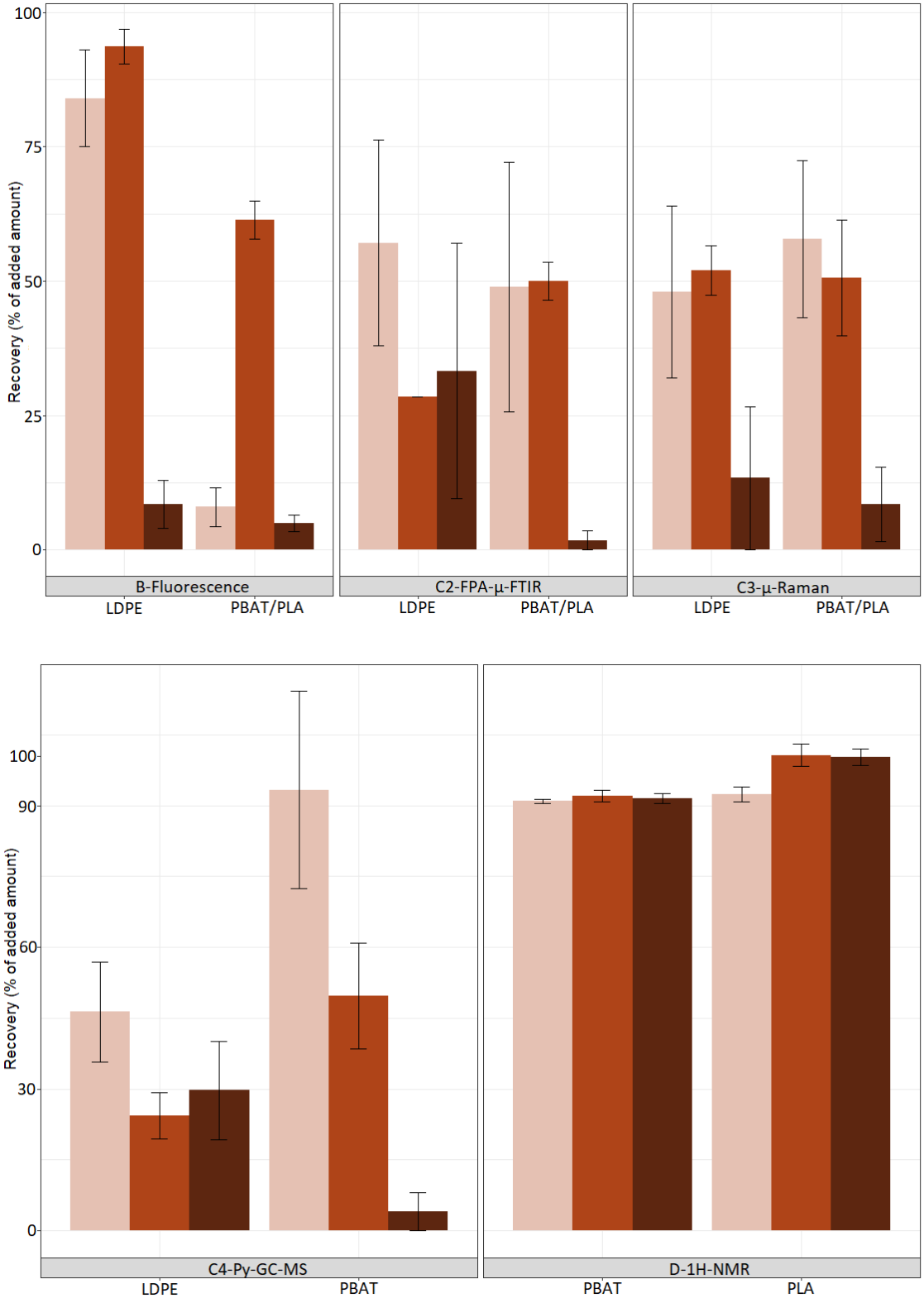


**Figure 3.2** Recoveries in percent of added number of particles on the y-axis, of small particles, for LDPE and PBAT/ PLA with methods using particle counting, i.e., method B – Fluorescence microscopy, method C2 – FPA-µ-FTIR and method C3 - µ-Raman microscopy and methods assessing bulk polymer amounts, i.e., method C4 - Py-GC-MS and method D - $^{1}$H-NMR. Note that $^{1}$H-NMR allowed a differentiation of PBAT

and PLA from the added Mulch-derived MPs; hence, both polymers are displayed separately. The solvent used for the Soxhlet-extraction was chosen exclusively for PBAT/PLA and Py-GC-MS failed to identify PLA. Error bars represent standard errors.

We explain the low recoveries for PP and PS (leading to a loss of particles that were finally not detected) as well as recoveries that exceed 100% for PVC (leading to smaller items that were then also counted) with such a fragmentation process. They were presumably caused by mechanical abrasion during the final sieving step from the extraction protocol in method C (Löder et al., 2015; Dong et al., 2020). For the other plastic materials, no secondary MPs were formed during extraction. We suggest that when digesting SOM with Fenton's reagent and especially when dealing with biodegradable plastics and enzymes like protease (Möller et al., 2021), meticulous attention should be given to these potential fragmentation effects. Conversely, when seeking to characterize surface alterations of plastic particles, as in assessments of plastic weathering in the environment, it might be advisable to refrain from using corrosive substances like $ZnCl_2$ and oxidative chemicals, particularly when subsequent surface-sensitive techniques are used such as Scanning Electron Microscopy. When analyzing biodegradable plastics, Soxhlet extraction combined with $^1$H-NMR stood out compared to other protocols when assessing the total mass of remaining PBAT or PLA.

### 3.4.2 Implications for the extraction of large microplastics

All tested methods in this study are frequently described in the literature for MPs analysis (Blasing and Amelung, 2018; Mariano et al., 2021). All methods but method C3 – µ-Raman, yielded recoveries > 75%. Therefore, we conclude that in principle all are suitable for analyzing large MPs in soils, enabling comparable results for large MPs are comparable.

Even the simplest extraction and detection method in method A – digital microscopy, which only included one density separation and no SOM digestion, recovered between 88 – 93% of particles across all soils, thus performing at least as reliably as other methods with more sophisticated sample preparation (Braun et al., 2021, 2023). In our tests, the second decanting step after density separation improved the recovery substantially and is recommended for further studies. One notable drawback of this method is the inability to identify the type of plastic. This limitation includes the risk of annotating other foreign particles as false positives as MPs or falsely annotating MPs as SOM, thus introducing errors in the assessment of the number of larger MPs in environmental samples, especially if inexperienced users mistake MPs for SOM, as reported in the case of PBAT/ PLA and black carbon by Mariano et al. (2021). Besides, very small MPs particles can be missed during detection, i.e., as with all other methods, only certain size ranges are reliably analyzed, i.e., with the lowest size limit of 200 µm, as underlined by Kotar et al. (2022).

In summary, the success of digital microscopy to identify MPs depends on plastic color and size. Hence, the method is problematic when analyzing organic soils due to uncertainties in particle identification (Primpke et al., 2020). For other soils, this is less of an issue, and because only images are taken, the methodology does not discriminate against certain plastic materials during detection. We recommend this technique as a fast

and simple method for analysis of large MPs in soil, as no complex pre-treatment besides density fractionation is needed, and many laboratories have access to such microscopes. The analyses of smaller and dark-colored MPs may demand special training of the operator and/or automatic plastic identification via machine learning (Primpke et al., 2020).

Elevated clay and thus usually also elevated SOM contents may not only interfere with detection by introducing interfering compounds on the filters but may also interfere with extraction protocols. Likely, such challenges contributed to generally lower recoveries from the clayey soil, which also contained the highest SOM content. The SOM and clay particles may adhere to MPs, thus potentially forming aggregates that reduce recovery during the density fractionation step, potentially leading to an underestimation of the total MPs content.

A very reliable method for plastic detection other than digital microscopy was the NR staining and particle counting using Fluorescence microscopy in method B (Primpke et al., 2020). Recovery rates exceeded 87%, despite single plastic types showing different staining intensities. Hence, this method is suitable for reliable detection of large MPs in mineral soils. The result refers to both the efficiency of the NR staining method (except for HDPEs, where the low recoveries occurred due to their dimmed fluorescence with NR) and the extraction efficiency towards larger MPs (Phan Le et al., 2025, see Chapter 2). Using a green fluorescent protein filter set (excitation/emission 470/525 nm) in this study was a valid approach to acquiring fluorescence signals of all plastics (Primpke et al., 2020). This is in accordance with previous studies, where green fluorescence was chosen over the red counterpart due to the better fluorescence of synthetic polymers, less fluorescent interference from natural organic matter, and lower background signal intensity in green compared to red fluorescence mode (Shim et al., 2016; Erni-Cassola et al., 2017). Organic digestion with Fenton's reagent did not affect the overall quantitative analysis, even though bleaching of dye/ additive and surface damages were observed. While the extraction process for Fluorescence microscopy takes longer due to the additional Fenton digestion step, data evaluation is faster compared to digital microscopy. This is because Fluorescence microscopy benefits from the automatic quantification of fluorescence-tagged particles through digital image analysis approaches. However, ensuring accuracy and avoiding false-positive identifications still requires expert knowledge. This enables high sample throughput, rendering this method a noteworthy candidate for large environmental monitoring programs. However, the use of automatic quantification with digital image analysis is less reliable and requires additional adjustments when fluorescence intensity varies greatly among different plastics, thus including the risk of overlooking weakly fluorescent MPs and overestimation of strong fluorescence in SOM, i.e., the analytical result might be more selective to certain plastic types.

The ATR-FTIR and µ-Raman spectroscopies included in method C entail the most sophisticated and time-consuming extraction and purification procedures, along with subsequent detection and data evaluation. In method C the combination of the chosen extraction protocol with subsequent MPs identification using ATR-FTIR and especially µ-Raman spectroscopy yielded lower recoveries than the simpler extractions of one or two steps, which were then followed by the detection via digital microscopy and fluorescence microscopy in methods A and B. When characterizing with ATR-FTIR in method C1 – ATR-FTIR some large MPs might have been lost when transferring the particles from the Petri dishes to the sampling stage due to static forces causing the

particles to “jump” which has also been observed by Möller et al. (2021) and described in a comprehensive review paper by Primpke et al., 2020. While Löder et al. (2017) documented comparable recoveries for ATR-FTIR, they employed a distinct, more rigorous extraction procedure for PE beads ranging from 180 - 212 µm, whereas our methodology is tailored for larger sizes ranging from 500 - 1000 µm.

Additional challenges were faced during the ATR-FTIR analysis. The enzymatic and oxidative steps needed to reliably recover most plastics generally include the risk of altering the plastic composition, particularly evident in our case for PS and PBAT/PLA, which had matching scores of about 60% (Radford et al., 2021). As no significant changes were observed in the spectra, we assume alterations of PS were purely physical and that the fragile physical characteristic of the foamy particles resulted in potential shrinkage, thus hindering good contact between the ATR crystal and the surface of the plastic (Prata et al., 2021). For the PBAT/ PLA blend, surface alterations and its black color led to higher absorbance of the IR light (Ribeiro, 2017), which presumably hindered a good matching score. The main difference we noticed between the spectra of the extracted PBAT/ PLA and pristine PBAT/ PLA is expressed as a loss of intensity and broadening of the peaks. Additionally, a slight increase in the shoulder of the peak around 2918 $cm^{-1}$ (-$CH_3$ stretching) and 2845 $cm^{-1}$ (-$CH_2$ stretching) was observed, while the two peaks at around 1408 and 1388 $cm^{-1}$ (O-$CH_2$ bending) almost disappeared for the extracted polymer, presumably due to partial de-esterification in the PBAT (Cai et al., 2013; **Figure** S5). For PET, PA, HDPE, LDPE, PVC, and PP a matching score > 90% was accomplished, indicating no changes in the functional groups on the surface of these plastics. Interestingly, for PP lower recoveries were obtained, an explanation for which could be that it was easy to overlook or miss due to its transparency. Overall, we can confirm that ATR-FTIR is a suitable technique for analyzing biodegradable and conventional large MPs. As the analytical procedure is more time-consuming compared to digital microscopy or fluorescence microscopy, ATR-FTIR is mainly recommended to identify the plastic type. In that case, ATR-FTIR stands out as the main method for identifying the type of meso- or macroplastics.

In method C3 - µ-Raman, PBAT/ PLA required lower laser power than conventional plastic to avoid damage and burning its surface (Ribeiro, 2017). After automatic spectra collection, we observed that most of the spectra were still very noisy. Hence, a manual spectra collection was needed (**Table** 3.2.). Due to the broad focus range used in automatic recognition, the machine took much longer to identify MPs particles compared to optimized manual settings. To capture the entire filter, approximately 40 minutes were required, and then, depending on the number of identified particles, an additional 20 to 60 minutes are needed for full identification. In manual identification, we adjusted settings for each particle individually to obtain a high-quality spectrum, rather than pre-setting a range for automatic recognition. There are multiple reasons for noise in the spectra of the automatic spectra collection, including: i) the remnants of SOM on the filter, ii) a lack of universally appropriate laser settings for all plastic and the use of a short acquisition time for rapid measurements, iii) the physical necessity of using a 10x objective, iv) surface differences between conventional and biodegradable plastic, v) the possibility that the automatically selected central position of each plastic particle, differs to the bulk of said particle (Araujo et al., 2018; Prata et al., 2021). These challenges lead to increases in the signal-to-noise ratios in the spectra as well as the need for stronger

laser power to compensate for the lower magnification (Araujo et al., 2018). Unfortunately, due to physical limitations, i.e., the working distance between the filter and the objective itself, it is unfeasible to use objectives with a higher magnification, like 50x or 100x, when analyzing comparable large particles (0.5 – 1 mm).

In summary, method C3 - µ-Raman demonstrated selectivity towards various plastic materials. The weakened resistance of PBAT/ PLA to laser strength, caused by surface degradation due to hydrolysis-prone ester linkages, made the spectra more difficult to detect compared to the virgin PBAT/ PLA blend spectra. Owing to these differences in material resistance, it is thus not feasible to establish a single, specific laser setting (Araujo et al., 2018); additionally, recommended laser energy power ranges from 3 - 4eV for PBAT/ PLA to 11 - 12eV for HDPE. To address inaccuracies resulting from property changes in MPs, current spectral libraries should be extended to surface-altered plastic types for additional benchmarking or for improving existing references (Dong et al., 2020; Cowger et al., 2021).

In contrast to PBAT/ PLA, MPs of PET and PVC were very resistant to enzymatic and oxidative steps and showed neat spectra for both automatic and manual recognition. Overall, the Raman spectra changed little, suggesting that functional group composition remained intact for the eight types of conventional plastics. LDPE, in turn, showed strong fluorescence compared with other plastics (Dong et al., 2020; Mariano et al., 2021). A possible explanation could be the presence of additives and that it had black letter writings on its surface, i.e., the remaining ink may have distorted spectral quality. Overall, Raman thus proved to be efficient for detecting PET, PVC, and PA. The protocol used here, however, was not sufficient to recover the large MPs from loamy and clayey soils. All in all, Raman still has advantages, particularly in detecting very fine, small MPs items. Nevertheless, it is less recommended for rapid screening of large MPs in the soil.

### 3.4.3 Implications for the extraction of small microplastics

In contrast to the large MPs, the recoveries for the two types of small MPs (LDPE and the biodegradable PBAT/ PLA) varied. Method B – Fluorescence microscopy was the most efficient in detecting high numbers of small LDPE MPs, at least for the non-clayey soils. Differences in the recovery of LDPE particles between methods B and C could be due to the number of sample preparation steps, which are fewer for method B – Fluorescence microscopy, or due to the quantity of sample scanned on the filters: for fluorescence microscopy the whole sample extracts (after Fenton digestion) are usually examined, resulting in 2 - 3 filters per sample, whereas for method C, only 1.5% v/v of the total extracted sample was analyzed, with higher respective risks that non-representative aliquots are processed. Considering the number of spiked soil sample replicates used, it's worth noting that although triplicates are common in many studies, as emphasized by Ramage et al. (2022), they may not provide sufficient statistical power for robust outcomes. Therefore, running a larger number of replicates is advisable.

For method B – Fluorescence, the fluorescent particles identified in non-spiked soils encompass both "naturally occurring MPs" and co-stained soil organic residues, especially within the size range of 20 to 60 µm (Phan Le et al., 2025, see Chapter 2). This presence could pose a challenge in the analysis of smaller MPs (e.g., LDPE $\leq$ 150 µm), leading to false positives, a concern also noted by other authors (e.g., Prata et al., 2021). When applying green light at 470 nm, both nonpolar LDPE and these organic parties have strong fluorescent effects (Prata et al., 2019); for other excitation wavelengths, e.g., 560

and 630 nm, interference from fluorescent SOM is expected to be even stronger (Sturm et al., 2021). As a result, background assessment is important when using fluorescence techniques, and background subtraction is needed when establishing the recovery method. Overall, the use of a small MPs isolation (SMI) unit, proposed by Coppock et al. (2016), and the chosen fluorescent microscope settings proved to be a good method for extracting and identifying LDPE particles from soils with low SOM content. Black materials did not fluoresce. Therefore, they interfere with detecting black PBAT/ PLA but not with LDPE.

Unlike LDPE, the recovery rates for PBAT/ PLA MPs were consistent across the protocols. However, in method C, the recovery rates did not exceed 60%, indicating potential PBAT/ PLA degradation, low matching indexes, and matrix interferences. These issues were less pronounced in the SOM-poor sandy soils. Consequently, the better extraction for PBAT/ PLA MPs in this sandy soil using µ-Raman spectroscopy indicated a greater degree of certainty in identifying these black particles on the filter (**Figure** 3.3.). The entrapment of particles within clay minerals, particularly when the texture becomes adhesive upon wetting, likely contributed to the loss of these particles for analysis (Primpke et al., 2020). It is pivotal, however, to state that µ-FTIR with microscope magnification of 15x is expected to achieve higher recovery rates of the small MPs since it would be testing pixel sizes of 5.5 µm instead of 20.6 µm. Nevertheless, the process is more time-consuming and may be cost-prohibitive.

The presence of organic residues affects the smallest size detectable with Raman spectroscopy. In this context, we set a limit of 40 µm due to the presence of noisy spectra for many smaller than 40 µm particles. However, it's worth noting that under different conditions, the limit of detection for Raman spectroscopy can be improved to as low as 1.3 µm, as extensively reviewed by Anger et al. (2018). After conducting the µ-FTIR and µ-Raman analyses, we found no alterations in the spectra of LDPE following the extraction protocol outlined in method C. Thus, for not LDPE surface changes but the increased complexity of steps in this method and potential particle loss may lead to reduced recoveries of small LDPE particles. For PBAT/PLA, additional surface changes (as observed for FTIR spectra, **Figure** S5) and fragmentation to sizes below the detection limits of the technique can hamper detection of small MPs. Hence, there is a need to establish optimized software settings and extraction protocol steps (Primpke et al., 2020). The advantage of using $ZnCl_2$ as heavy density liquid is then hampered by the corrosive nature of the reagent for these materials. Additionally, comprehensive investigations into structural changes in particles, especially as their surface-to-volume ratio increases, are imperative.

Method C4 - Py-GC-MS, similar to methods C2 – FPA-µ-FTIR and C3 - µ-Raman, necessitated subsampling of an aliquot before analysis due to the inability to assess the entire extracted solution. Despite this, we achieved a recovery of 94% (± 17%) for PBAT in sandy soil, suggesting that subsampling for the total mass analyses of MPs is not a problem per se. Difficulties to recover LDPE-MPs and other PBAT particles in loamy and clayey soil (**Figure** 3) are thus likely related to some SOM and soil minerals still being present (Primpke et al., 2020; Bradt et al., 2021; Bouzid et al., 2022). These minerals can affect pyrolysis yields and may adsorb pyrolysis products of the polymers before they are transmitted to the mass spectrometer (Bouzid et al., 2022). To better control samples' heterogeneity, Steinmetz et al. (2020) adopted a dissolving approach

using 1, 2, 4 – trichlorobenzene to analyze PP, PE and PS in soil samples via Py-GC-MS without any further treatment. However, this method excludes polymers like PET that do not dissolve in this solvent and requires further optimization for better matrix cleanup.

On the other hand, dissolving polymers in suitable solvents and afterwards quantifying via $^{1}$H-NMR spectroscopy analysis offers a fast and high-throughput extraction technique particularly for biodegradable plastics. Using chloroform: methanol – 9:1 as a solvent for the PBAT/ PLA mulch film extraction in method D – $^{1}$H-NMR proved to be exceptionally efficient for extracting and further analyzing these biodegradable MPs. Additionally, $^{1}$H-NMR has demonstrated its effectiveness as a method for quantifying a wide range of polymers, including LDPE, PET, PS, PVC, ABS, PA, and PBAT, within diverse and complex matrices (Ivleva et al., 2021).

In general, for smaller MPs, lower recoveries and larger errors were observed compared to large MPs. Larger particles are less efficiently absorbed and more effectively separated during density separation (Kotar et al., 2020). On the contrary, this effect is irrelevant for the small-sized MPs as their larger specific surface area makes them more prone to being lost through adsorption (Primpke et al., 2020). Therefore, if there is no need to determine the number and size of MPs particles but rather the total amount, we recommend employing method D – Soxhlet - extraction coupled with $^{1}$H-NMR spectroscopy.

## 3.5 Conclusions

Comparing different methodologies for the extraction and detection of large MPs (0.5-1 mm) showed that their analyses are reliable for samples extracted from soils, a pattem likely perceived for other environmental samples. Digital microscopy already performed well in screening MPs without excessive sample pretreatment, i.e., this respective method protocol is useful for fast comparisons of larger sampling sets. Yet, staining of the particles followed by Fluorescence microscopy stood out in terms of short protocol duration and reliability. Additional detection techniques such as ATR-FTIR or µ-Raman spectroscopy are, however, necessary for the identification of the MPs type. While µ-FTIR and µ-Raman spectroscopy can potentially identify very small MPs, it is more sensitive to sample inhomogeneity when smaller volumes are used and can be affected by organic residues, resulting in an approximate loss of roughly 50% of particles in our case. This low recovery rate is a critical concern, particularly when MPs analyses are intended for legislative monitoring. Future efforts to quantify and compensate for these losses, such as the use of appropriate surrogate standards, require immediate attention. Yet even though the analyses of small MPs are more challenging, excellent recoveries were recorded with Fluorescence microscopy for small LDPE MPs (sandy and loamy soil), and the biodegradable PBAT/ PLA blends using Soxhlet - extraction followed by quantitative $^{1}$H-NMR.

**Acknowledgements**

This work was supported by the European Union's Horizon 2020, ITN SOPLAS, with grant agreement No. 55334 to the first five authors. The authors thank Elisabeth Shaw and Alexandre Benedetto (Lancaster University) for their help with the fluorescence microscope measurement; Markus Rhode, Ulrich Meinke and Sven Simons (Wessling GmbH) for the expertise provided for the measurements with Raman Microscope and

Pyrolysis–Gas Chromatography–Mass Spectroscopy; Prof Violette Geissen for supporting and supervising the work done at Wageningen University and Research.

**Credit authorship contribution statement**: S. Peneva: writing of the manuscript, methodology, samples analysis, data evaluation, preparing figures; extraction and detection with µ-FTIR, Raman and Py-GC-MS; Q.N. Phan Le: methodology, samples analysis, data evaluation, preparing figures, review and editing of manuscript; extraction and detection with Fluorescence; D. R. Munhoz: methodology, samples analysis, data evaluation, review and editing of manuscript; extraction and detection with µ-FTIR; O. Wrigley: methodology, samples analysis, statistical analysis, review and editing of manuscript; extraction and detection with Digital Microscopy; F. Wille: methodology, samples analysis, data evaluation, review and editing of manuscript; Soxhlet – extraction and 1H-NMR quantification of biodegradable PBAT and PLA; H. Doose, C Halsall, M. Sander, P. Harkes: supervision, review and editing of manuscript; M. Braun and W. Amelung: supervision, review and editing of manuscript, conceptualization.

**Declaration of competing interest**: The authors declare that they have no known competing financial interests or personal relationships that could have appeared to influence the work reported in this paper.

# References


Anger P.m., von der Esch E., Baumann T., Elsner M., Niessner R., Ivleva N.P. 2018. Raman microspectroscopy as a tool for microplastic particle analysis, TrAC Trends in Analytical Chemistry, Volume 109, p. 214-226 https://doi.org/10.1016/j.trac.2018.10.010

Araujo CF, Nolasco MM, Ribeiro AMP, Ribeiro-Claro PJA. Identification of microplastics using Raman spectroscopy: Latest developments and future prospects. Water Res. 2018 Oct 1;142:426-440. doi: 10.1016/j.watres.2018.05.060.

Astner AF, Gillmore AB, Yu Y, Flury M, DeBruyn JM, Schaeffer SM, Hayes DG, Formation, behavior, properties and impact of micro- and nanoplastics on agricultural soil ecosystems (A Review), NanoImpact, Volume 31, 2023, 100474, ISSN 2452-0748, https://doi.org/10.1016/j.impact.2023.100474.

Bläsing M, Amelung W. Plastics in soil: Analytical methods and possible sources. Sci Total Environ. 2018 Jan 15;612:422-435. doi: 10.1016/j.scitotenv.2017.08.086.

Braun M, Mail M, Heyse R, Amelung W. Plastic in compost: Prevalence and potential input into agricultural and horticultural soils. Sci Total Environ. 2021 Mar 15;760:143335. doi: 10.1016/j.scitotenv.2020.143335. Epub 2020 Nov 4. PMID: 33199003.

Braun M, Mail M, Krupp AE, Amelung W. Microplastic contamination of soil: Are input pathways by compost overridden by littering? Sci Total Environ. 2023 Jan 10;855:158889. doi: 10.1016/j.scitotenv.2022.158889.

Brette, M.M.; Holm, A.H.; Drozdov, A.D.; Christiansen, J.d.C. Pure Hydrolysis of Polyamides: A Comparative Study. *Chemistry* 2024, *6*, 13-50. https://doi.org/10.3390/chemistry6010002

Büks, F. and Kaupenjohann, M.: Global concentrations of microplastics in soils – a review, SOIL, 6, 649–662, https://doi.org/10.5194/soil-6-649-2020, 2020.

Bouzid, N.; Anquetil, C.; Dris, R.; Gasperi, J.; Tassin, B.; Derenne, S. Quantification of Microplastics by Pyrolysis Coupled with Gas Chromatography and Mass Spectrometry in Sediments: Challenges and Implications. *Microplastics* 2022, *1*, 229-239. https://doi.org/10.3390/microplastics1020016

Cai, Y., Lv, J. & Feng, J. Spectral Characterization of Four Kinds of Biodegradable Plastics: Poly (Lactic Acid), Poly (Butylenes Adipate-Co-Terephthalate), Poly (Hydroxybutyrate-Co-Hydroxyvalerate) and Poly (Butylenes Succinate) with FTIR and Raman Spectroscopy. *J Polym Environ* 21, 108–114 (2013). https://doi.org/10.1007/s10924-012-0534-2

Caputo F., Vogel R., Savage J., Vella G., Law A., Della Camera G., Hannon G., Peacock B., Mehn D., Ponti J., Geiss O., Aubert D., Prina-Mello A., Calzolai L., Measuring particle size distribution and mass concentration of nanoplastics and microplastics: addressing some analytical challenges in the sub-micron size range, Journal of Colloid and Interface Science, Volume 588, 2021, Pages 401-417, ISSN 0021-9797, https://doi.org/10.1016/j.jcis.2020.12.039.

Coppock RL, Cole M, Lindeque PK, Queirós AM, Galloway TS. A small-scale, portable method for extracting microplastics from marine sediments. Environ Pollut. 2017 Nov;230:829-837. doi: 10.1016/j.envpol.2017.07.017.

Cowger W, Steinmetz Z, Gray A, Munno K, Lynch J, Hapich H, Primpke S, De Frond H, Rochman C, Herodotou O. Microplastic Spectra Classification Needs an Open Source Community : Open Specy to the Rescue!. Analytical Chemistry (2021) 93(21), 7543-7548. DOI: 10.1021/acs.analchem.1c00123

Dong M, Zhang Q, Xing X, et al. Raman spectra and surface changes of microplastics weathered under natural environments. The Science of the Total Environment. 2020 Oct;739:139990. DOI: 10.1016/j.scitotenv.2020.139990.

Dümichen E, Eisentraut P, Bannick CG, Barthel AK, Senz R, Braun U. Fast identification of microplastics in complex environmental samples by a thermal degradation method. Chemosphere. 2017 May;174:572-584. doi: 10.1016/j.chemosphere.2017.02.010.

El Hayany B, El Fels L, Quénéa K, Dignac MF, Rumpel C, Gupta VK, Hafidi M. Microplastics from lagooning sludge to composts as revealed by fluorescent staining-image analysis, Raman spectroscopy and pyrolysis-GC/MS. J Environ Manage. 2020 Dec 1;275:111249. doi: 10.1016/j.jenvman.2020.111249.

Fox J, Weisberg S (2019). *An R Companion to Applied Regression*, Third edition. Sage, Thousand Oaks CA. https://socialsciences.mcmaster.ca/jfox/Books/Companion/.

Han X., Lu X., Vogt R.D. 2019. An optimized density-based approach foe extracting microplastics from soil and sediment samples., Environmental Pollution https://doi.org/10.1016/j.envpol.2019.113009

Hurley RR, Lusher AL, Olsen M, Nizzetto L. Validation of a Method for Extracting Microplastics from Complex, Organic-Rich, Environmental Matrices. Environ Sci Technol. 2018 Jul 3;52(13):7409-7417. doi: 10.1021/acs.est.8b01517.

Hurley RR, Nizzetto L. Fate and Occurance of micro (nano) plastics in soils: Knowledge gaps and possible risks Current Opinion in Environmental Science & Health, Volume 1, 2018, Pages 6-11, ISSN 2468-5844, https://doi.org/10.1016/j.coesh.2017.10.006.

Imhof H.K., Schmid J., Niessner R., Ivleva N.P., Laforsch C. 2012. A novel, highly efficient method for separation and quantification of plastic particles in sediments of aquatic environments, p. 524-537 https://doi.org/10.4319/lom.2012.10.524

Ivleva N. P., Chemical Analysis of Microplastics and Nanoplastics: Challenges, Advanced Methods, and Perspectives, Chemical Reviews 2021 121(19). 11886-11936, DOI: 10.1021/acs.chemrev.1c00178

Jarosz, K.; Natkański, P.; Michalik, M. Microplastic Extraction from the Sediment Using Potassium Formate Water Solution ($H_2O$/KCOOH). *Minerals* 2022, *12*, 269. https://doi.org/10.3390/min12020269

Junhao C, Xining Z, Xiaodong G, Li Z, Qi H, Siddique H.M. K, Extraction and identification methods of microplastics and nanoplastics in agricultural soil: A review, Journal of Environmental Management, Volume 294, 2021, 112997, ISSN 0301-4797, https://doi.org/10.1016/j.jenvman.2021.112997.

Kittner M, Eisentraut P, Dittmann D, Braun U., 2023, Decomposability versus detectability: First validation of TED-GC/MS for microplastic detection in different environmental matrices, Applied Research, April 2023, DOI: 10.1002/appl.202200089

Kotar S, McNeish R, Murphy-Hagan C, Renick V, Lee CT, Steele C, Lusher A, Moore C, Minor E, Schroeder J, Helm P, Rickabaugh K, De Frond H, Gesulga K, Lao W, Munno K, Thornton Hampton LM, Weisberg SB, Wong CS, Amarpuri G, Andrews RC, Barnett SM, Christiansen S, Cowger W, Crampond K, Du F, Gray AB, Hankett J, Ho K, Jaeger J, Lilley C, Mai L, Mina O, Lee E, Primpke S, Singh S, Skovly J, Slifko T, Sukumaran S, van Bavel B, Van Brocklin J, Vollnhals F, Wu C, Rochman CM. Quantitative assessment of visual microscopy as a tool for microplastic research: Recommendations for improving methods and reporting. Chemosphere. 2022 Dec;308(Pt 3):136449. doi: 10.1016/j.chemosphere.2022.136449. Epub 2022 Sep 14. PMID: 36115477.

Lebreton, L., van der Zwet, J., Damsteeg, JW. *et al.* River plastic emissions to the world's oceans. *Nat Commun* 8, 15611 (2017). https://doi.org/10.1038/ncomms15611iSQAPER, 2018;

Löder, M.G.J., Imhof, H.K., Ladehoff, M., Löschel L.A., Lorenz, C., Mintenig, S., Piehl, S., Primpke, S., Schrank, I., Laforsch, C., Gerdts, G., (2017). Enzymatic Purification of Microplastics in Environmental Samples. Environmental Science & Technologz 2017 51(24), 14283-14292, DOI: 10.1021/acs.est.7b03055

Mani T., Frehland S., Kalberer A., Burkhardt-Holm P., Using castor oil to separate microplastics from four different environmental matrices, Anal. Methods 11 (2019) 1788–1794, https://doi.org/10.1039/C8AY02559B.

Mariano S, Tacconi S, Fidaleo M, Rossi M, Dini L. Micro and Nanoplastics Identification: Classic Methods and Innovative Detection Techniques. Front Toxicol. 2021 Feb 26;3:636640. doi: 10.3389/ftox.2021.636640.

Mbachu O, Jenkins G, Pratt C, Kaparaju P. Enzymatic purification of microplastics in soil. MethodsX. 2021 Jan 31;8:101254. doi: 10.1016/j.mex.2021.101254.

Mintenig SM, Int-Veen I, Löder MGJ, Primpke S, Gerdts G. Identification of microplastic in effluents of waste water treatment plants using focal plane array-based micro-Fourier-transform infrared imaging. Water Res. 2017 Jan 1;108:365-372. doi: 10.1016/j.watres.2016.11.015.

Möller J.N., Loder M.G.J., Laforsch C. 2020. Finding Microplastics in Soil: A review of Analytical Methods, *Environ. Sci. Technol.* 2020, 54, 4, 2078–2090, https://doi.org/10.1021/acs.est.9b04618

Möller J.N., Heisel I., Satzger A., Vizsolyi E.C., Jacob Oster S.D., Agarwal S., Laforsch C., Loder M.G.J., Tackling the challenge of extracting microplastics from soils: A protocol to purify soil samples for spectroscopic analysis, Environ Toxicology and Chemistry, 2021, https://doi.org/10.1002/etc.5024

Nuelle MT, Dekiff JH, Remy D, Fries E. A new analytical approach for monitoring microplastics in marine sediments. Environ Pollut. 2014 Jan;184:161-9. doi: 10.1016/j.envpol.2013.07.027.

OECD Policy Highlights, Global Plastic Outlook Database: Economic Drivers, Environmental Impacts and Policy Opitons, 2022, https://doi.org/10.1787/de747aef-en,

Ogle DH, Doll JC, Wheeler AP, Dinno A (2023). *FSA: Simple Fisheries Stock Assessment Methods*. R package version 0.9.5, https://CRAN.R-project.org/package=FSA.

Perez C.N., Carre F., Hoarau-Belkhiri A., Joris A., Leonardis P.E.G., Lamoree M.H., Innovations in analytical methods to assess the occurance of microplastics in soil, Journal of Environmental Chemical Engineering, Volume 10, Issue 3, 2022, 107421, ISSN 2213-3437, https://doi.org/10.1016/j.jece.2022.107421

Phan Le, Q. N., Halsall, C., Peneva, S., Wridley, O., Amelung, W., Braun, M., Quinton, J., and Surridge, B.: Towards quality-assured measurements of microplastics in soils using fluorescence microscopy, EGU General Assembly 2023, Vienna, Austria, 24–28 Apr 2023, EGU23-13873, https://doi.org/10.5194/egusphere-egu23-13873, 2023.

Pfohl, P., Roth, C., Meyer, L. *et al.* Microplastic extraction protocols can impact the polymer structure. *Micropl.&Nanopl.* 1, 8 (2021). https://doi.org/10.1186/s43591-021-00009-9

Prata, Joana & Sequeira, Inês & Monteiro, Silvia & Patricio Silva, A.L. & Da Costa, Joao & Dias-Pereira, Patrícia & Fernandes, Antonio & Costa, Florinda & Duarte, Armando & Rocha-Santos, Teresa. (2021). Preparation of biological samples for microplastic identification by Nile Red. Science of The Total Environment. 783. 147065. 10.1016/j.scitotenv.2021.147065.

Prata, Joana & Da Costa, Joao & Fernandes, Antonio & Costa, Florinda & Duarte, Armando & Rocha-Santos, Teresa. (2021). Selection of microplastics by Nile Red staining increases environmental sample throughput by micro-Raman spectroscopy. Science of The Total Environment. 783. 146979. 10.1016/j.scitotenv.2021.146979.

Primpke, S., Wirth, M., Lorenz, C. *et al.* Reference database design for the automated analysis of microplastic samples based on Fourier transform infrared (FTIR) spectroscopy. *Anal Bioanal Chem* 410, 5131–5141 (2018). https://doi.org/10.1007/s00216-018-1156-x

Primpke, S., Fischer, M., Lorenz, C. *et al.* Comparison of pyrolysis gas chromatography/mass spectrometry and hyperspectral FTIR imaging spectroscopy for the analysis of microplastics. *Anal Bioanal Chem* 412, 8283–8298 (2020). https://doi.org/10.1007/s00216-020-02979-w

Primpke S, Christiansen SH, Cowger W, et al. Critical Assessment of Analytical Methods for the Harmonized and Cost-Efficient Analysis of Microplastics. *Applied Spectroscopy*. 2020;74(9):1012-1047. doi:10.1177/0003702820921465

Prosenc, F.; Leban, P.; Šunta, U.; Bavcon Kralj, M. Extraction and Identification of a Wide Range of Microplastic Polymers in Soil and Compost. *Polymers* 2021, *13*, 4069. https://doi.org/10.3390/polym13234069

https://plasticseurope.org/knowledge-hub/plastics-the-facts-2022/

Ramage SJFF, Pagaling E, Haghi RK, Dawson LA, Yates K, Prabhu R, Hillier S, Devalla S. Rapid extraction of high- and low-density microplastics from soil using high-gradient magnetic separation. Sci Total Environ. 2022 Jul 20;831:154912. doi: 10.1016/j.scitotenv.2022.154912. Epub 2022 Mar 29. PMID: 35364148.

R Core Team (2018). R: A language and environment for statistical computing. R Foundation for Statistical Computing, Vienna, Austria. URL: https://www.R-project.org/

Radford F., Zapata-Restrepo L.M., Horton A.A., Hudson M.D., Shaw P.J., Williams, I.D. 2021. Developing a systematic method for extraction of microplastics in soils. Analytical Methods https://doi.org/10.5258/SOTON/D1455

Ribeiro-Claro, Paulo J. A. et al. "Chapter 5 - Characterization of Microplastics by Raman Spectroscopy." *Comprehensive Analytical Chemistry* 75 (2017): 119-151.

Sajjad, M., Huang Q., Kahn S., Khan M.A., Liu Yin, Wang J., Lian F., Wang Q., Guo G. 2022. Microplastics in the soil environment: A critical review. Environmental Technology & Innovation https://doi.org/10.1016/j.eti.2022.102408

Shim W.J., Song Y.K., Hong S.H., Jang M. 2016. Identification and quantification of microplastics using Nile Red staining, Marina Pollution Buletin Volume 113, Issues 1–2, 15 December 2016, Pages 469-476 https://doi.org/10.1016/j.marpolbul.2016.10.049

Schrank, I., Möller, J.N., Imhof H.K., Hauenstein O., Zielke F., Agarwal S., Löder M.G.J., Greiner A., Laforsch C., Microplastic sample purification methods - Assessing detrimental effects of purification procedures on specific plastic types, Science of The Total Environment, Volume 833, 2022, 154824, ISSN 0048-9697, https://doi.org/10.1016/j.scitotenv.2022.154824.

Steinmetz Z., Kintzi A., Munoz Katherine, Schaumann G. E., A simple method for the selective qunatification of polyethylene, polypropylene, and polystyrene plastic debris in soil by pyrolysis-gas chromatography/mass spectrometry, Journal of Analytical and Applied Pyrolysis, Volume 147, 2020, 104803, ISSN 0165-2370, https://doi.org/10.1016/j.jaap.2020.104803

Sturm, M.T., Horn, H. & Schuhen, K. The potential of fluorescent dyes—comparative study of Nile red and three derivatives for the detection of microplastics. *Anal Bioanal Chem* 413, 1059–1071 (2021). https://doi.org/10.1007/s00216-020-03066-w

Wang Y, Xiang L, Amelung W, Elsner M, Gan J, Kueppers S, Laforsch C, Jiang X, Adu-Gyamfi J, Heng, Sik Ok Y, Ivleva N P., Luo Y, Barceló D, Schäffer A, Wang F, Micro- and nanoplastics in soil ecosystems: Analytical methods, fate, and effects, TrAC Trends in Analytical Chemistry, 2023, 117309, ISSN 0165-9936, https://doi.org/10.1016/j.trac.2023.117309.

Way C, Hudson MD, Williams ID, Langley GJ. Evidence of underestimation in microplastic research: A meta-analysis of recovery rate studies. Sci Total Environ. 2022 Jan 20; 805:150227. doi: 10.1016/j.scitotenv.2021.150227. Epub 2021 Sep 9. PMID: 34537704.

Wickham, H. ggplot2: Elegant Graphics for Data Analysis. https://doi.org/10.1007/978-3-319-24277-4

# Supporting Information

## Microplastic analysis in soil: a comparative assessment

Stoyana Peneva[1,4], Quynh Nhu Phan Le[2, *], Davi R. Munhoz[3, *], Olivia Wrigley[4], Flora Wille[5], Heidi Doose[6], Paula Harkes[3], Crispin Halsall[2], Paula Harkes[3], Melanie Braun[4], Wulf Amelung[4]

[1]*Wessling GmbH, AM Umweltpark 1, Bochum, 44793, Germany*

[2]*Lancaster Environment Centre, Lancaster University, Lancaster LA1 4YQ, UK*

[3]*Soil Physics and Land Management Group, Wageningen University & Research, P.O. Box 47, 6700 AA Wageningen, the Netherlands*

[4]*Institute of Crop Science and Resource Conservation (INRES), Soil Science and Soil Ecology, University of Bonn, Nussallee 13, 53115 Bonn, Germany*

[5]*Insitute of Biogeochemistry and Pollutant Dynamics, ETH Zurich, 8092 Zurich, Switzerland*

[6] *Wessling Consulting Engineering GmbH & Co.KG, Feodor-Lynen Straße 23, Hannover, 30625, Germany*

[7]*Agrosphere Institute (IBG-3), Forschungszentrum Jülich GmbH, Wilhelm-Johnen-Str. 52425 Jülich, Germany*

**Shared first authorship*

---

**Detailed preparation of plastic materials used for spiking**

The large MPs, originated from households' products (see **Table** 1 for details) and were cut with a razor, graded on its blades. The desired size of the particles was confirmed using Digital Microscopy. They were then picked with a tweezer and placed on a wetted gelatin sheet, which was directly added to the soil and dissolved during the homogenization of 2 hours.

For small MPs, the LDPE particles were directly purchased from a manufacturer (Goonvean Fibers Ltd, Cullompton, England). As for biodegradable plastics no commercial standard material was available, small MPs were produced from larger pieces (PBAT/PLA, BIONOV B, Barbier, France). In detail, we made small balls from these pieces with a knot, around 20-25 mm in diameter, thus similar in size as the stainless-steel ball used for the cryo mill (20 mm diameter). Afterwards, two PBAT/PLA balls and 1 stainless steel ball were placed in the container and attached to the holder of a standard cryo-mill (RETSCH). We used the following program for cryo-milling: 3 min precooling (or 7.5 min for the first run) at 5Hz, with 3 cryo cycles, each of 3 min at 25Hz and 2x1.5 min of intercooling at 5Hz. After the milling was finished, the black powder was transferred onto a cascade of 100 µm and 250 µm sieves and stored in glass vials. Both LDPE and PBAT/PLA were placed onto two different wetted gelatin sheets which were closed in the shape of dumplings. These were then dried for 10-15 min, and directly added with the help of tweezers to the soil that already contained the large MPs items. Caution was required when working with the PBAT/PLA particles, since their small size made them fragile. The final size of the particles was confirmed with a particle-size counter (model Syringe, Markus Klotz GmbH, Germany).

**Analytical protocols, validation, and analysis**

The following section describes the individual extraction techniques, as well as the respective technical details on sample processing and detection:

<u>Method A – Density separation followed by Digital Microscopy analysis (Braun et al., 2021; 2023):</u>

Method A started with a simple density fractionation by shaking the soil 2 hours end over end. We then transferred the suspension to a beaker and allowed soil materials to settle for 12 hours. The next day we decanted the solution and filtered it using a quartz filter (Macherey-Nagel, MN QF 10, diameter 125 mm, particle retention: 0.3 µm). As no digestion of soil organic matter (SOM) had to be applied, two decanting steps were conducted to analyze the MPs within a matrix that also contained SOM.

Final particle counting was performed via Digital Microscopy (Keyence VHX 7000 model, VH Z20R lens). Each discovered fragment was photographed - length, thickness and width of the supposed plastic material were measured using the internal software tool of the microscope. Items were identified as plastic based on their color, shape, texture and stability.

<u>Method B – Density separation, Fenton's digestion, and Fluorescence Microscopy (Coppock et al., 2017)</u>

For fluorescence analyses, density separation was conducted using a Sediment Microplastic Isolation (SMI) unit. After cleaning and purging, we filled the SMI with soil and $ZnCl_2$, locked the ball valve tightly, and shook the SMI vigorously in an orbital shaker for 2 hours. After adding an additional 200 mL of $ZnCl_2$, the particles in the suspension were again allowed to settle overnight. After the $ZnCl_2$ solution became visible, the valve was cautiously shut. The supernatant in the headspace was vacuum filtered through a stainless-steel mesh (mesh size = 6µm). The SMI headspace was rinsed thoroughly with HPLC - grade water to recover remaining particles and remove excess $ZnCl_2$. Thereafter, Fenton's reaction was used to oxidize SOM. For this purpose, the stainless steel meshes were transferred to a 500 mL beaker containing 20 mL of 0.05M $FeSO_4$, sonicated for 10 minutes at room temperature, rinsed, removed, and re-washed carefully for further use. To start the Fenton reaction, 20 mL of $H_2O_2$ was added to the beaker. After 24 h, the samples were filtered on glass **fibres** filters (GFFs) and stained with 5 - 7 drops of Nile red solution (5 µm Nile Red/ mL). After 10 min, filters were thoroughly rinsed with n-hexane and vacuum-filtered again to discard any accumulated liquid. Finally, filters were carefully transferred onto and stored inside covered glass Petri dishes and left air-dried in the dark before analysis via a fluorescence microscope. All samples were analyzed within one week after staining to avoid precipitation and quenching of Nile red.

A fluorescence microscope (Zeiss Axio Zoom.V16), equipped with a long working distance high-aperture macro lens (Plan NeoFluar Z 1.0x/0.25, FWD 56mm) and a fast, sensitive 12 Mpixel camera (Zeiss AxioCam 512mono) was used. The microscope was set to bright mode, illuminated with the 470 nm light (CoolLED) and observed through the green filter (green fluorescent protein filter, emission 524/ 50 nm). To quantify black microplastic particles, e.g., PBAT/ PLA and potentially the brownish nylon particles dark field mode was added. The whole filter images were obtained at a magnification of 50x.

Method C – Density separation, Enzymatic and Fenton's digestion and ATR- (method C1 – for large MPs identification), µ-FTIR (method C2 – for small MPs identification), Raman Microscopy (method C3 – for both large and small MPs identification) and Py-GC-MS analysis (method C4 – for small MPs identification; Löder et al., 2017; Mintenig et al., 2017; Primpke et al., 2018; Mbachu et al., 2021).

For ATR-FTIR, µ-FTIR and Raman Microscopes analyses (methods C1, C2 and C3), the spiked soil was mixed with 150 mL $ZnCl_2$ in a beaker using a magnetic stirrer. The resulting solution, along with an additional 50 ml of $ZnCl_2$ used to rinse the beaker, was transferred to a 1 L glass density separation funnel. The funnel's outlet was sufficiently large, enabling easy removal of the mineral part without clogging. The collected mineral phase at the bottom of the funnel was released two to three times on the same day, depending on the soil, and the solution was shaken again before being left to settle overnight.

To destroy the SOM, the supernatant was filtered, and the funnel was rinsed using a 6 µm stainless steel filter. The filter was then placed in a beaker with approximately 100 mL of ultrapure water (UPW) and subjected to 5 minutes of ultrasonication using a VWR ultrasonic cleaner at 45 kHz. The resulting aqueous solution was transferred to an Erlenmeyer flask for enzymatic digestion, following methods described by Mbachu et al. (2021) and Löder et al. (2017) with a shorter exposure time. Short ultrasonication (5

minutes) was applied between most steps to ensure proper particle dispersion. The solution was filtered again over the same filter before proceeding from staying over a weekend at the cellulase/ amylase step with sodium acetate buffer, NaAc, pH = 5, to the lipase step, for one night with a change of the buffer solution with hydroxymethyl aminomethane, TRIS, pH = 9. After the step with the lipase, the last enzyme used is protease without changing the buffer (**Table** S3). All enzymes had been ordered from Spezialenzyme GmbH.

At the end of the enzymatic digestion, the final ultra-sonication of the filter was performed using a 25 ml 15% $FeSO_4.5H_2O$ (VWR Chemicals) solution. This solution was then transferred to a four-neck round bottom flask. Three of the necks were equipped with 100 ml dripping funnels, containing 100 ml 30% $H_2O_2$ solution, 8 ml $H_2SO_4$, and 100 ml $H_2O$, respectively, with the last to dilute the reaction if necessary. The flask was placed in a water bath, and 40 ml of 30% $H_2O_2$ was directly added through the fourth neck. After the reaction calmed down (approximately 5 minutes), the 100 ml of $H_2O_2$ in the dripping funnel was added drop by drop over around 30 minutes. The reaction was then stopped by slowly adding sulfuric acid.

The final solution was poured on the same 6 µm filter, subjected to another 5 minutes of ultrasonication, and sieved over a 300 µm sieve. The use of the sieve was needed to separate the large and the small MPs. The large MPs were washed away by distilled MPs-free water stored in PTFE bottles onto 47 mm PC filter (Whatman INT. LTD), and the suspension containing the smaller plastics was brought to a volume of 100 ml, and rigorously shaken, and an aliquot of 1.5 ml was taken for Raman detection on a 47 mm golden filter (Whatman INT. LTD) or for the FPA-µ-FTIR analysis on a 47 mm $Al_2O_3$ anodisc filter (Whatman INT. LTD). Previous analyses had shown that rigorous shaking had been sufficient in reproducing the analytical results from this aliquot.

For Py-GC-MS analysis (method C4), three quartz tubes were prepared from the solution, each with a volume of 45 µl. As the filters were weighed empty and full, we could estimate the mass of the particle alongside their number.

The fraction > 300 µm, containing the large MPs, was poured onto 2 - 3 polycarbonate filters (PC) filters (Whatman, 25mm, 1µm) for further µ-Raman and ATR-FTIR detection.
Large MPs were analyzed using ATR-FTIR, while small MPs were examined via FPA-µ-FTIR. Raman analysis was conducted for both size categories. Large MPs for ATR-FTIR were manually selected based on visual observation and analyzed using an Agilent Cary 630 FTIR in absorbance mode. The spectral range was 4000 - 650 $cm^{-1}$, with 8 background and sample scans, resolution of 4 $cm^{-1}$, minimum hit quality of 60, and maximum hits displayed set to 6. A diamond crystal was used.

µ-FTIR analyses were performed in transmission mode on an Agilent FTIR with focal plane array (FPA) detectors and microscope magnification of 4x. Spectra were analyzed using siMPLe software (version 1.3.2ß), considering particles of a minimum size of 1pxl (equivalent to 20.6 µm). Pre-tests with pure PBAT/PLA revealed detection as PET, so PET particles were included in the count for PBAT/PLA. Further improvements were made to enhance the library and avoid misidentification (to be published).

For µ-Raman analyses of large MPs, PC filters were placed on a holder and examined using a WITec alpha 300R Confocal Raman Microscope. The microscope operated in

bright and dark field modes with a 532 nm laser wavelength and CCD detector, covering a spectral range of 50 - 4000 $cm^{-1}$. The laser power was kept low (up to 5.5 meV) due to the fragile nature of PBAT. Large MPs were imaged with a 10x objective, and spectra were recorded.

Automatic and manual spectra of large MPs were recorded to assess potential recovery improvements after placing particles on scotch tape. For small MPs, images were obtained using 10x and 50x objectives, covering 5 to 100% of the filter area, with spectra collected using the 50x objective. The matching index for Raman measurement of small fractions was 88% for LDPE and 50 % for PBAT, with a limit of detection set at 40 µm. Multiple scans (3 - 5), exposure times (0.03 - 5 s), and laser energies (2.5 - 20 mW) were used based on measurement type. Libraries containing the plastics used in the study were created for Raman, ATR-FTIR, and µ-FTIR measurements, facilitating recognition for all fractions and filters.

Py-GC-MS measurements

The measurements were carried out in a TDU 2 – Gerstel Pyrolyser equipped with a Multipurpose samples Gerstel. The pyrolyser was mounted to an Agilent 7890B B GC system with HP-5ms Ultra Inert column. The GC system was attached to an Agilent 5977B MSD mass spectrometer with C506 Controller. Data processing and polymer identification were performed using Agilent Masshunter software and National Institute of Standards and Technology (NIST) library. The initial temperature of the oven was 40°C with a heating rate of 5°C/ min up to 180°C and 15 °C/ min heated up to the second value of 300°C. The gas carrier was He and the split 1:100. We used quartz tubes (45 µl) to carry the material mass. The minimum needed material for each tube was 0.1 mg and the LOD: 15 µg/g. Prior to the measurement, we calibrated the instrument for the type of LDPE we used and for biodegradable plastic, with 6 steps of 20, 50, 70, 100, 120 and 150 µg. For LDPE, after calibration and recording of the chromatogram and the mass spectra, the chosen m/z numbers for the LDPE were: 83 (alkene), 81 (for diene) and 85 (alkane) with retention times of respectively, 19.9, 19.8 and 20.2 min for the C14-chain compounds (summarized in Bouzed et al., 2022).

For the biodegradable plastic Barbier, BIONOV B mulch film, $^{1}$H-NMR measurements revealed that this mixture consists of 71.3 wt% PBAT and 3.2 wt% PLA. Because of the low content of PLA its GC-MS signal was too low, hence analyses focused on PBAT as main constituent with subsequent correction for PLA masses. The chosen marker for PBAT was pentanoic acid, 3-butenyl ester with a retention time of 11.37 minutes and masses of m/z 85, 54/57, 115. Other main pyrolysis products of the PBAT were 1,2 butadiene, THF, Benzol, cyclopentanone and benzoic acid, these were however not specific for PBAT and hence not used as a marker for this compound. (**Figure** S6)

Method D - Soxhlet extraction coupled to quantitative $^{1}$H-NMR spectroscopy (Nelson et al., 2020).

Spiked soils were freeze-dried to remove water traces and thereafter extracted for 30 minutes with methanol in a Soxhlet apparatus to pre-extract large parts of SOM, followed by a 75-minute Soxhlet extraction (9:1 v:v mixture of chloroform and methanol ($CHCl_3$:

MeOH) to extract the PBAT and PLA components of the mulch film. The extract was dried and reconstituted in deuterated chloroform with 1,4-dimethoxybenzene as internal standard. The soil extracts from the Soxhlet extractions were analyzed by quantitative $^{1}$H-NMR spectroscopy (Bruker Avance III 400 MHz NMR) after the method of Nelson et al. (2020).

Prevention and assessment of sample contamination

All sample preparations were carried out in a flow box to minimize contamination from airborne dust. We wore blue or pink-dyed cotton lab coats for better recognition of contamination with **fibres** steaming from clothes, and all the glassware used was heated at 500°C and thereafter rinsed with EtOH (method B) or filtered water, dried at 140°C, covered with Al foil (method C). For the $^{1}$H-NMR measurements, we worked in a laboratory never exposed to concentrations of biodegradable mulch films. All reagents were filtered with cellulose-nitrate filters (0.45 µm pore width) before use. Samples, tools, and lab ware were always covered with Al foil and rinsed with filtered water or ethanol prior to work or unless direct handling is necessary. When not working with the soil samples, they were stored in a fridge at 4°C. For each batch of samples, the soil background was detected, and blanks were analyzed. Further, those were subtracted during the final step of calculating recovery rates. For each background and blank sample analysis in each laboratory, we accounted for the presence of each reagent used. $ZnCl_2$ was filtered three times before being discharged and density was adjusted when needed.

To estimate the number of LDPE and PBAT/PLA microplastic particles of ~10-250 µm diameter prior to the measurements with spiked soil, we used Fluorescence microscopy by counting the number of particles. In detail, for fluorescence 3 x 5 ml aliquots (of 5 mg MPs 100 mL EtOH solution). For an even better understanding, 3 x 1.5 ml for the Particle Size counter Klodz Syringe (both of 3 mg MPs 100 mL EtOH solution) were analyzed. Additionally, we took aliquots for the µ-Raman, 3 x 1.5 ml (of 3 mg MPs 100 mL EtOH solution), and for the FPA-µ-FTIR, 2 x 1.5 ml.

For better visualization the main steps of each protocol are summarized in **Table** S3, S4 and **Figure** S2.

**Supplementary Figures and Tables:**

**Table** S1. Number of particles and masses, based on the respective technique, found on average in the spiked soil samples, blanks and background (bg) samples, from which recovery rates were calculated. No background correction was done for the $^{1}$H-NMR measurements, as the final concentrations and recoveries were calculated directly on narrow integrations and recoveries for both PBAT, and PLA are shown with the $^{1}$H-NMR.

| **Method B - Fluorescence Microscopy** | | | | | | | | |
|---|---|---|---|---|---|---|---|---|
| **LDPE expected – 15300 ± 4500** | | | | | **PBAT/PLA expected – 3840 ± 420** | | | |
| Number of particles, total | bg | blank | after subtraction of bg and blank | recovery LDPE, % | bg | blanks | after subtraction of bg and blank | recovery PBAT/PLA, % |
| sandy | 540 | 330 | 12500 | 84 ± 7 | 58 | 0 | 316 | 8 ± 3 |
| clayey | 2620 | 330 | 3800 | 8 ± 3 | 7 | 0 | 192 | 5 ± 1 |
| loamy (lufa 2.4.) | 3590 | 330 | 13300 | 94 ± 3 | 12 | 0 | 2354 | 61 ± 3 |
| **Method C2 - µ-FPA-FTIR Microspectroscopy** | | | | | | | | |
| **LDPE expected – 11 ± 7** | | | | | **PBAT/PLA expected – 144 ± 10** | | | |
| Number of particles, aliquot | bg | blank | after subtraction of bg and blank | recovery LDPE, % | bg | blanks | after subtraction of bg and blank | recovery PBAT/PLA, % |
| sandy | 0 | 0 | 6 | 57 ± 13 | 0 | 0 | 71 | 49 ± 16 |
| clayey | 0 | 0 | 4 | 33 ± 17 | 0 | 0 | 3 | 2 ± 1 |
| loamy (lufa 2.4.) | 0 | 0 | 3 | 29 ± 0 | 0 | 0 | 72 | 50 ± 2 |
| **Method C3 - µ-Raman Microspectroscopy** | | | | | | | | |
| **LDPE expected – 25 ± 9** | | | | | **PBAT/PLA expected – 229 ± 86** | | | |
| Number of particles, aliquot | bg | blank | after subtraction of bg and blank | recovery LDPE, % | bg | blank | after subtraction of bg and blank | recovery PBAT/PLA, % |
| sandy | 0 | 4 | 12 | 48 ± 13 | 0 | 5 | 132 | 58 ± 12 |
| clayey | 0 | 1 | 3 | 13 ± 11 | 0 | 0 | 19 | 8 ± 6 |

| | | | | | | | | |
|---|---|---|---|---|---|---|---|---|
| loamy (lufa 2.4.) | 2 | 3 | 13 | 52 ± 4 | 0 | 0 | 116 | 51 ± 8 |
| **Method C4 - Py-GC-MS, ug/g** | | | | | | | | |
| **LDPE expected – 300 ug/g** | | | | | **PBAT/PLA expected – 300 ug/g** | | | |
| | bg | blank | after subtraction of bg and blank | recovery LDPE, % | bg | blank | after subtraction of bg and blank | recovery PBAT/PLA, % |
| sandy | 0.9 | - | 139 | 46 ± 9 | 0 | - | 282 | 94 ± 17 |
| clayey | 4.8 | - | 94 | 31 ± 9 | 0 | - | 13 | 4 ± 3 |
| loamy (lufa 2.4.) | 0 | - | 74 | 25 ± 4 | 0 | - | 150 | 50 ± 9 |
| **Method D - $^{1}$H-NMR, mg** | | | | | | | | |
| **PBAT/PLA expected = 3 mg** | | | | | | | | |
| | PBAT, average, mg | | recovery PBAT, % | | PLA, average, mg | | recovery, PLA, % | |
| sandy | 1.96 | | 91 ± 1 | | 0.09 | | 92 ± 3 | |
| clayey | 1.97 | | 92 ± 2 | | 0.1 | | 100 ± 3 | |
| loamy (lufa 2.4.) | 1.99 | | 92 ± 2 | | 0.1 | | 101 ± 4 | |

**Table** S2. Masses (g) of small microplastics, LDPE and PBAT/PLA, used for all soil types and techniques.

| | **mass, g, average ± SD** | **Fluorescence** | **Raman** | **Py-GC-MS** | **FTIR** | **$^{1}$H-NMR** |
|---|---|---|---|---|---|---|
| **Sand** | LDPE | 3.09 ± 0.06 | 3.02 ± 0.07 | 3.02 ± 0.07 | 3.00 ± 0.02 | |
| | PBAT/PLA | 3.09 ± 0.05 | 3.03 ± 0.07 | 3.03 ± 0.07 | 3.03 ± 0.00 | 3.03 ± 0.04 |
| **Clay** | LDPE | 3.03 ± 0.03 | 2.99 ± 0.00 | 2.99 ± 0.00 | 2.98 ± 0.02 | |
| | PBAT/PLA | 3.02 ± 0.03 | 3.04 ± 0.03 | 3.04 ± 0.03 | 2.99 ± 0.02 | 3.02 ± 0.01 |
| **LUFA** | LDPE | 3.1 ± 0.01 | 3.07 ± 0.01 | 3.07 ± 0.01 | 2.99 ± 0.03 | |
| | PBAT/PLA | 3.13 ± 0.15 | 3.05 ± 0.02 | 3.05 ± 0.02 | 2.97 ± 0.06 | 3.02 ± 0.02 |

**Table S3: Overview of analytical techniques used for small and large microplastic (MPs) analysis.**

| **Analytical technique** | **Large MPs** | **Small MPs** | **Manufacturer** | **References** |
|---|---|---|---|---|
| Method A - Digital microscopy | X | | Keyence VHX 7000 model, Japan | Braun et al., 2021, 2023 |
| Method B - Fluorescence microscopy | X | X | Zeiss Axio Zoom.V16, Germany | Coppock et al., 2017 Shim et al., |
| Method C1 - ATR-FTIR microscopy | X | | Agilent Cary 630 FTIR, US | Loder et al.,2017, Mbachu et al.,2021 Primpke et al., 2018 Mintenig et al., 2017 |
| Method C2 - µ-FTIR microscopy | | X | Agilent Cary 620 FTIR, US | |
| Method C3 - µ-Raman microscopy | X* | X | WITec alpha 300R, Germany | |
| Method C4 - Py-GC-MS | | X | TDU 2 Gerster Pyrolyser-Agilent 7890B GC-Agilent 5977 MSD, US | |

| | | | | |
|---|---|---|---|---|
| Method D - $^{1}H$ – NMR | | X | Bruker Avance III 400 MHz, US | Nelson et al.,2020 |

*** For both manual and automatic focusing modes**

**Table S4.** Reagents and materials used for different extraction methodologies.

| | **Density Separation** | **Enzymatic digestion** | **Oxidative digestion** | **Filters** | **Total length of protocol (days)** |
|---|---|---|---|---|---|
| Method A – Digital microscopy | $ZnCl_2$, 2 h mixing and separation overnight | - | - | Quartz filter (Macherey-Nagel, MN QF 10, diameter 125 mm, particle retention: 0.3 µm); sum of two decanting steps | 2 |
| Method B – Fluorescence microscopy | $ZnCl_2$, 2 h mixing and separation overnight | - | 20 ml 0.05M $FeSO_4.5H_2O$ + 20 mL 30% $H_2O_2$, 24 h | Glass **fibres** filters (GFFs) and stained with 5-7 drops of 5 µm $mL^{-1}$ Nile red | 3 |
| Method C - ATR-FTIR (C1)/ FPA-µ-FTIR (C2)/ µ-Raman (C3)/ Py-GC-MS (C4) | $ZnCl_2$, 2 h mixing and separation overnight | 1. Over weekend – Cel/Amy – 50°C, pH = 5 (NaAc) | 25 ml 15%M $FeSO_4.5H_2O$ + 140 mL 30% $H_2O_2$, 1 h | 1. fraction >300 µm – Raman/ATR-FTIR – PC filters | 7 |
| | | 2. Overnight – Lip – 40°C, pH = 9 (TRIS) | | 2. fraction <300 µm – Raman (Au filters), µ-FTIR ($Al_2O_3$, anodisc) | |
| | | 3. Overnight – Pro - 50°C, pH = 9 (TRIS) | | | |
| **Soxhlet extraction protocol** | | | | | |
| Method D - $^{1}H$-NMR | 30 min pre-extraction in methanol | 75 min extraction 9:1 $CHCl_3$: methanol | Drying of the extract and reconstitution in 3 mL of deuterated $CHCl_3$ with 1,4-dimethoxybenzene as internal standard | | 1 |

ATR-FTIR – Attenuated total reflectance – Fourier transform infrared Spectroscopy; FPA - µ-FTIR – Focal plane array – micro – FTIR; Py – GC – MS – Pyrolysis – Gas

Chromatography – Mass Spectrometry; $^{1}H$ – NMR – 1 proton – Nuclear Magnetic Resonanse

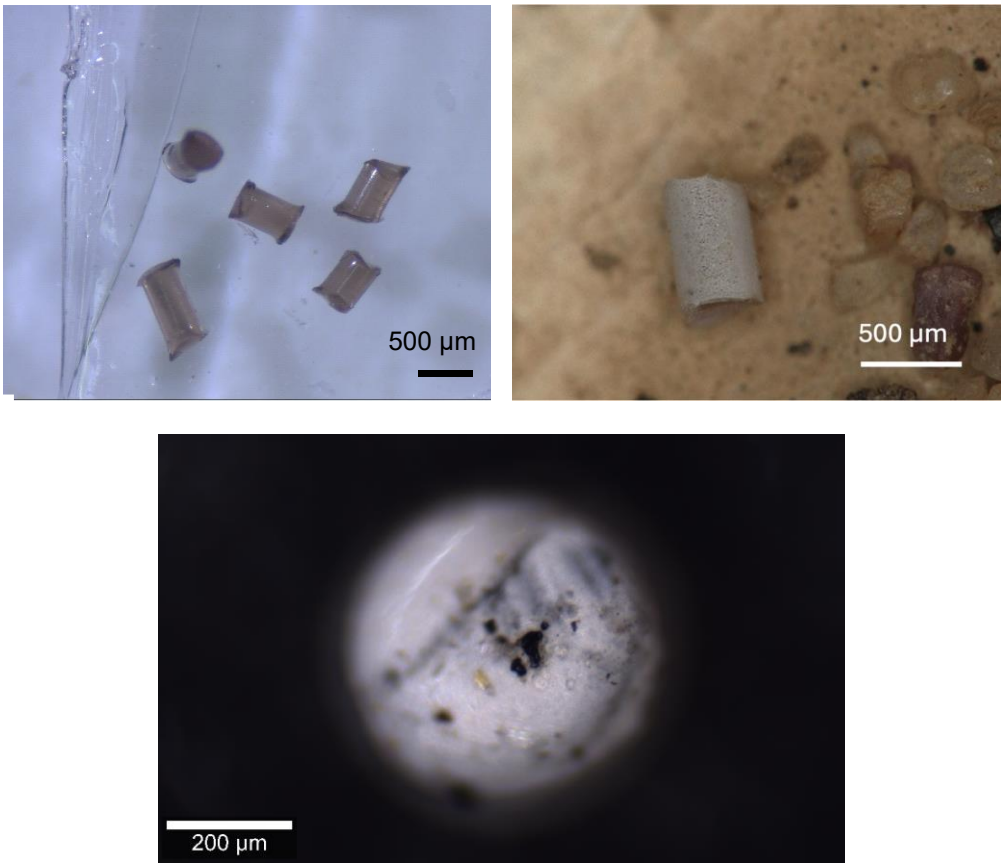


**Figure S1.** Bleaching of the initially brown-colored Nylon large particles after applying extraction with $ZnCl_2$. The upper - left image, captured with Zeiss Stemi 1000 Microscope and is representing the five large particles of Nylon (Polyamide - PA) used for spiking before the start of the extraction procedures. The image in the upper - right corresponds to a Nylon particle, extracted using method , and the bottom image shows a Nylon particle, after extraction with method C3, as obtained with a µ-Raman Microscopes.

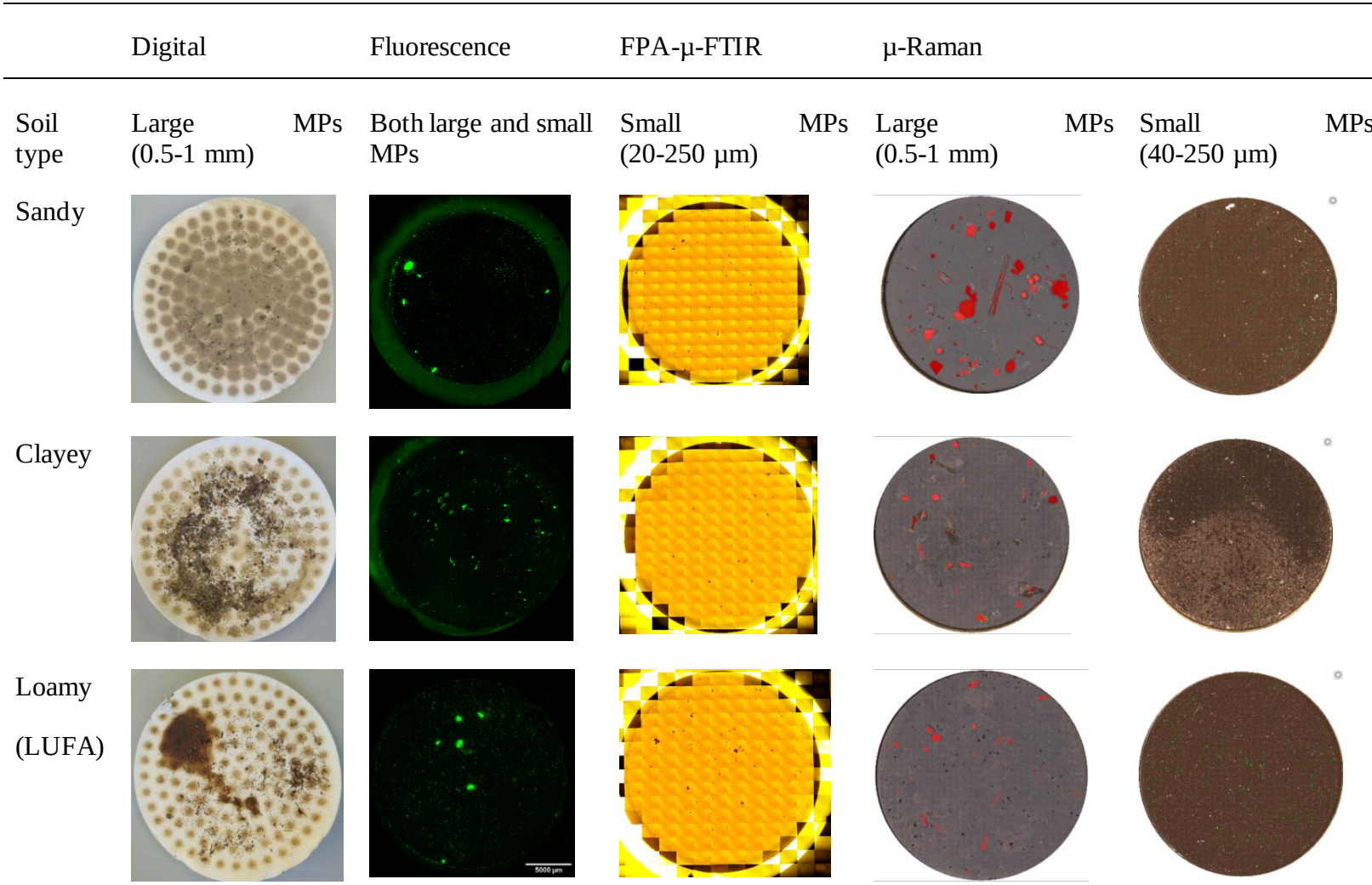


**Figure S2.** Images of the filters with small and large microplastics (MPs) for each soil type, sandy, clayey and loamy (standardized LUFA) used for the different microscopic techniques.

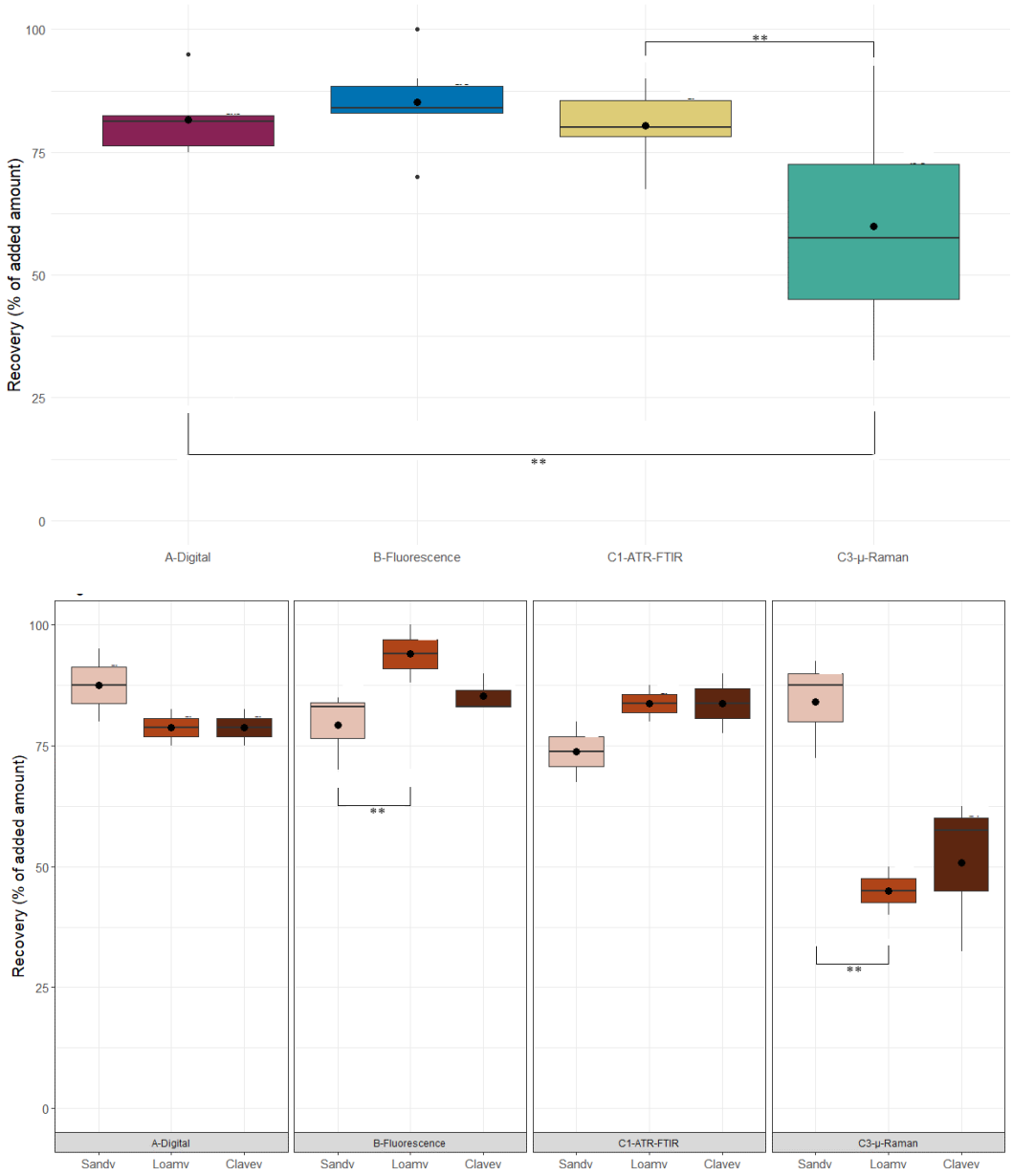


**Figure S3.** Box-Whisker plots for the recoveries of large MPs (in % of spiked amount): upper graph per method and bottom graph - between soil types within each method. Significant levels are indicated with the letters "a", "b" and "c" for upper graph, whereas more different letters are used within each method as soils within were compared. The three colors in the graph at the bottom indicate the three types of soil used during the trial – sandy, loamy and clayey, as of increase of intensity of the color. The following methods were applied: method A – Digital microscopy, B - Fluorescence microscopy, method C1 – ATR-FTIR and method C3 - µ-Raman Spectroscopy. The significant difference was observed between methods B – Fluorescence and method C3 - µ-Raman for upper graph. For bottom graph we observed significant differences between sandy and loamy in method B – Fluorescence and between sandy and loamy in method C3 - µ-Raman. Additionally, significant difference was observed between method B – Fluorescence and method C3 - µ-Raman for clay soil ($p < 0.05$) and for loamy soil ($p < 0.01$).

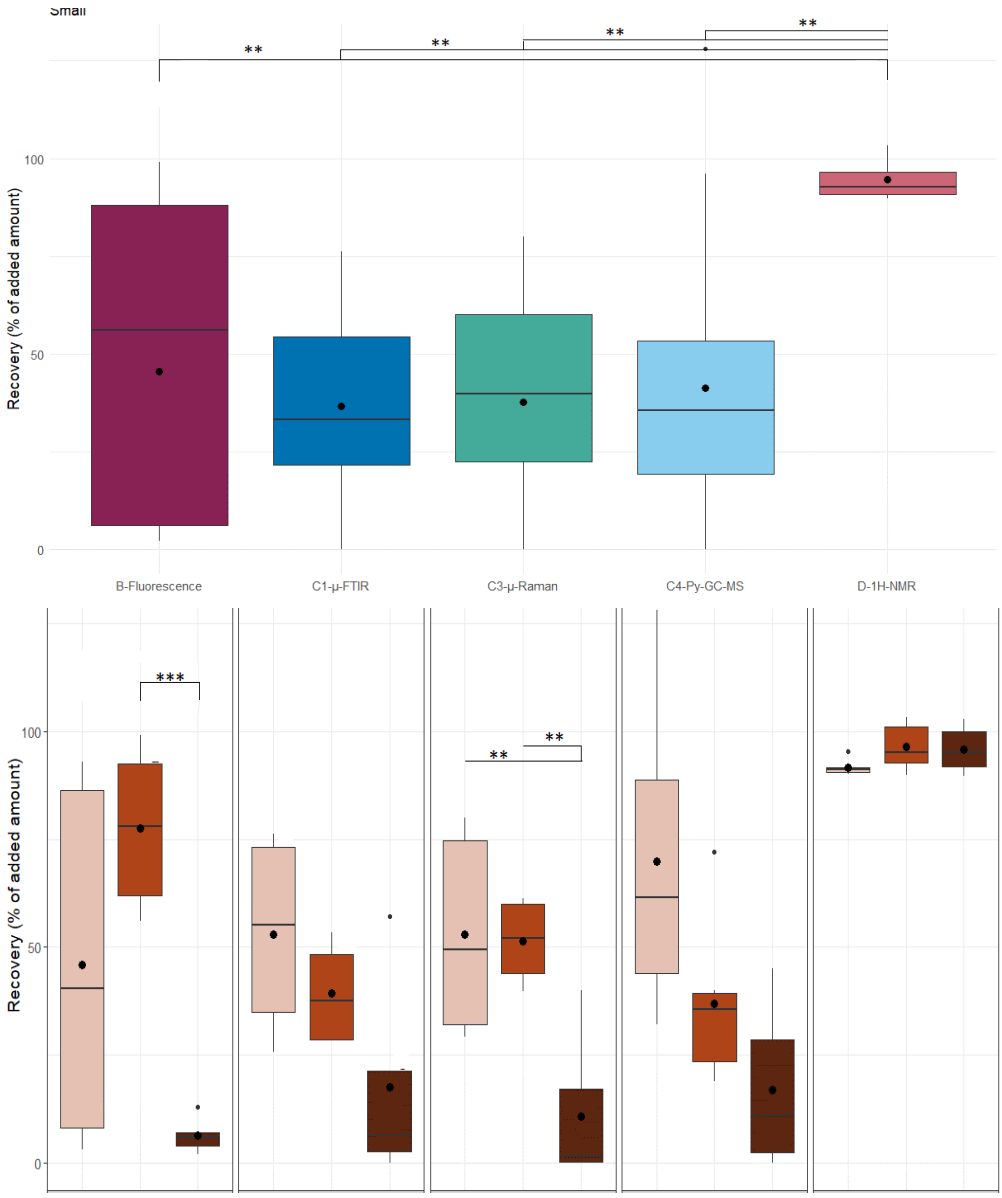


**Figure S4.** Box – Whisker plots for the recoveries of small MPs (in % of added amount): upper graph - per method and bottom graph - between soil types within method. Significant differences are indicated by the letters "a" and "b" in the upper graph, whereas different letters are used within each method as soils within are compared. The three colors in the graph at the bottom indicate the three types of soil used during the trial – sandy, loamy and clayey, as of increase of intensity of the color. The following methods were applied method B – Fluorescence microscopy, method C2 – FPA-μ-FTIR, method C3 – μ-Raman, method C4 – Py-GC-MS and method D – $^{1}$H-NMR. The line crossing the box represents the arrhythmic means. For the upper graph a significant difference was observed between method D – $^{1}$H-NMR and all of the rest of the methods. For the bottom graph – differences were observed between clayey and loamy in method B – Fluorescence ($p < 0.01$), between loamy and clayey ($p < 0.05$) and sandy and clayey ($p < 0.05$) for method C3 - μ-Raman and between sandy and clayey in method C4 – Py-GC-MS ($p < 0.01$).

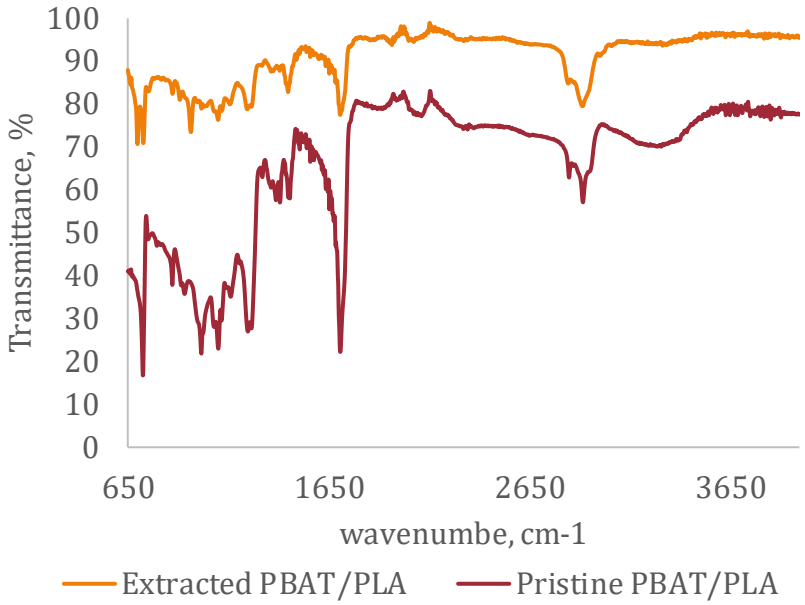


**Figure 5.** Size distribution of fluorescent particles, method B - Fluorescence microscopy, in the background soils (clayey, LUFA- loamy and sandy soils).

**Figure 61.** Exemplary photos of the extraction in method C applied to sandy soil. The extraction procedure prior to the detection method C1 – ATR-FTIR, method C2 – FPA-µ-FTIR, method C3 - µ-Raman and method C4 – Py-GC-MC was the same. Starting from left to right with first image - filtration after density separation, second – after enzymatic digestion with cellulase/amylase, third - lipase/protease enzymatic digestion and fourth – after applied Fenton reagent oxidation reaction. Note that these pretreatments usually hydrolyze PBAT and PLA.

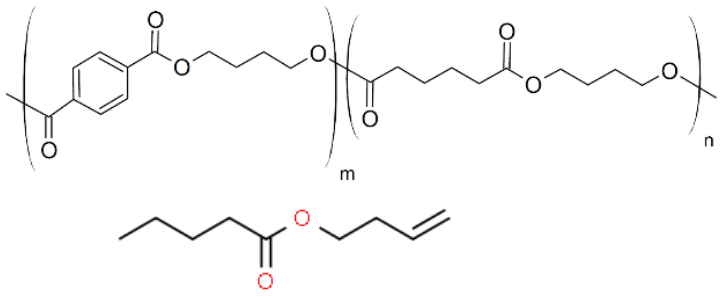


**Figure S7.** Chemical structure of PBAT (left) and the chemical structure of the chosen marker for Py-GC-MS recognition, 3-butenyl pentanoate (right).

# 4 Transfer and loading of microplastics in sewage-sludge amended agricultural soil

*Sewage sludge application is a major source of microplastics (MPs) in agricultural soils, yet its contribution to smaller MPs contamination in soil remain underexplored. This chapter quantifies and characterizes MPs in sewage sludge and sludge-amended soils using FPA-µ-FTIR, detecting particles as small as 25 µm. Findings confirm significant MPs accumulation in sludge-treated soils, with possible additional contributions from atmospheric deposition and fragmentation. The study advances analytical methods for MPs detection and underscores the need for policies to mitigate sludge-derived plastic contamination in agriculture.*

# Transfer and loading of microplastics in sewage sludge amended agricultural soil

Quynh Nhu Phan Le[1], Crispin Halsall[1*], Marco Kunaschk[2], Ben W.J. Surridge[1], Lorna Ashton[3], John Quinton[1]

[1]Lancaster Environment Centre, Lancaster University, Lancaster LA1 4YQ, UK

[2] Bavarian Environment Agency (LfU), Demollstrasse 31, Wielenbach 82407, Germany

[3]Department of Chemistry, Lancaster University, Lancaster, LA1 4YQ, UK

Corresponding author: Crispin Halsall (c.halsall@lancaster.ac.uk)

---

## Abstract

The application of sewage sludge to agricultural land may represent a significant source of microplastics (MPs) in soils. Previous studies have documented MPs accumulation in soil following sewage sludge application, but smaller-sized MPs remain underexplored due to analytical challenges. This study quantified and characterized MPs in sewage sludge and sludge-amended soils using a representative block sampling method and automated focal plane array Fourier Transform Infrared Micro-spectroscopy (FPA-µ-FTIR), detecting MPs as small as 25 µm. Our findings revealed that digested sewage sludge cake contained 3640±2100 MPs/g dry weight, with 70.2% smaller than 50 µm. Most detected MPs were fragments (83%), while the rest were fibres (17%), composed of polymers like polyethylene, polypropylene, polyester, polystyrene, and acrylic resins. Sludge-amended soil had a similar MPs profile to sewage sludge, with concentration of 39±27 MPs/g DW, significantly higher than non-sludge-amended agricultural soils (9.6±4.4 MPs/g) and non-agricultural soils (17±13 MPs/g). The elevated MPs concentration in sewage sludge-amended soils exceeded theoretical loads from sewage sludge, indicating additional sources such as atmospheric deposition and potential fragmentation of sewage sludge-derived MPs. This research provides a robust analytical framework for accurately assessing MPs concentrations in sewage sludge and soils, advancing understanding of soil MPs contamination. These results emphasize the role of sewage sludge application as a significant driver of soil MPs pollution and underline the urgent need for policies and practices to mitigate MPs input into agricultural land from sewage sludges.

## 4.1 Introduction

Microplastics (MPs, 1 µm to 5 mm) are a growing environmental concern, being found in freshwater, seawater, soil, air, and various biota. Soil acts as a major repository for MPs, with agricultural practices such as plastic mulching, wastewater irrigation, greenhouse operations, and particularly the use of sewage sludge from wastewater treatment plants (WWTPs), contributing significantly to this issue (Nizzetto et al., 2016). While sewage sludge has been shown to enhance soil fertility by enhancing levels of organic carbon, nitrogen, and phosphorus, thereby supporting crop growth (Shan et al., 2021), the environmental safety of its application in agriculture is increasingly under scrutiny. Beyond concerns about heavy metals, organic and inorganic chemicals, and microbial resistance (Lamastra et al., 2018) the potential for MPs pollution through sludge application is a pressing issue. It is estimated that each year, between 63,000 and 430,000 tonnes of MPs are spread across European farmlands via sewage sludge application.(Nizzetto et al., 2016)

The application of treated sludge, or biosolids, to agricultural land is promoted by many countries as an environmentally sustainable practice. The European Union and the UK Government consider it the most sustainable option in most circumstances. (Environment Agency, 2023) Additionally, the recycling of sewage sludge is a key component of the circular economy concept. (Collivignarelli et al., 2019b) As a result, each year, the UK recycles 87% of its sewage sludge in agriculture, compared to the European average of 50% (Collivignarelli et al., 2019a). Land application of sewage sludge is also popular in the USA, where 55 % of sludge is managed in this way. In Australia, its use in agriculture has increased from 55 % (2010) to 73 % (2021) (Kominko et al., 2024). Despite this large input, the presence and behaviour of MPs in agricultural soils following sludge application are not well understood. There is an urgent need for new research to fundamentally understand the occurrence and environmental impacts of sludge-derived MPs in agriculture, and to use this understanding in the design of appropriate mitigation strategies to ensure safe and sustainable farming practices.

Considerable uncertainty surrounds the magnitude and characteristics of MPs transfer from sewage sludge to soils. This uncertainty stems from challenges in obtaining representative samples from field sites, as well as in extracting and analysing MPs from sewage sludge and soils. As a result, to date, only 11 reported studies have quantified MPs loading in sludge-amended agricultural soil (table S1). (Adhikari et al., 2023; Corradini et al., 2019; Crossman et al., 2020b; Ragoobur et al., 2021; Schell et al., 2022; Tagg et al., 2022; van den Berg et al., 2020; Weber et al., 2022; Yang, Jie et al., 2021; Zhang, Lishan et al., 2020)Recent findings emphasize the importance of representative sampling and adequate subsampling for MPs analysis, especially from soil, as inadequate methods can cause a bias in the concentrations of MPs measured, especially in less contaminated soils. (Cowger et al., 2024; Yu & Flury, 2021) These considerations render many previous results on MPs pollution unreliable, despite their valuable insights, highlighting a pressing need for appropriate sampling and analytical approaches.

Sampling MPs in soils is particularly challenging due to their discrete and non-uniform spatial distribution. Common methods, such as using soil cores to sample small soil volumes, can result in significant errors when estimating MPs concentrations. (Yu &

Flury, 2021) Among the 11 studies reviewed that quantified MPs in sludge-amended soils, nine used soil cores for sampling. (Corradini et al., 2019; Crossman et al., 2020b; Ragoobur et al., 2021; Schell et al., 2022; Tagg et al., 2022; van den Berg, P. et al., 2020; Weber et al., 2022; Yang, Jie et al., 2021; Zhang, Lishan et al., 2020) Meanwhile, most studies (9 out of 11) relied on less reliable microscopic visual inspection for MPs analysis, with some using vibrational spectroscopy on a limited number of randomly selected particles.(Corradini et al., 2019; Ragoobur et al., 2021; van den Berg, P. et al., 2020; Weber et al., 2022; Yang, Jie et al., 2021; Zhang, Lishan et al., 2020) A study by Cowger et al. emphasizes the importance of analysing a sufficient number of particles, highlighting the limitations of past research (Cowger et al., 2024). Importantly, none of these studies adequately addressed particles smaller than 50 µm, even though finer size fractions often dominate in many environmental matrices. As these have been excluded from most previous studies, it is highly likely that the extent of MPs pollution in sewage sludge, and in soils treated with sludge, has been significantly underestimated, particularly in terms of MPs frequency, if not mass.

The research reported here aimed to investigate the transfer of MPs from sewage sludge to agricultural soils, using systems in the northwest of England, UK as exemplars of this agricultural practice. Despite the high sewage sludge recycling rate in the UK, only two studies have examined MPs in sewage sludge (Harley-Nyang et al., 2022), (Horton et al., 2020), and none have provided field data on MPs concentrations in soils resulting from this practice. Here, anaerobically digested sludge cake was sampled for MPs analysis, and soil samples were collected from farms that had applied sewage sludge over the past decade. It was hypothesized that repeated applications of sewage sludge would lead to the accumulation of MPs in agricultural soils. The study specifically aimed to (1) quantify the concentration of MPs in digested sludge cake, control soils (untreated), and sludge-amended soils (treated with sewage sludge); and (2) characterize the physical and chemical properties of MPs found in these samples.

## 4.2 Materials and methods

### 4.2.1 Sewage sludge and soil sampling

Anaerobically digested and dewatered sewage sludge cake (~5 kg) was collected from a WWTP in northwest England in May 2022. A detailed description of the WWTP is provided in supporting information SI2, with chemical analyses of the sludge reported in Table S2.

Soil samples (Brickfield 1 and 2 associations) were collected from a local forage maize farm where sludge from the referenced WWTP was applied in 2013 and 2021. These included fields RF1 (n = 5), RF2 (n = 5), and RF3 (n = 5), with a cumulative sludge application rate of 10.13 tonnes/ha dry weight (DW) and a ploughing depth of 30 cm. An adjacent grass field (RF4, n = 5), managed by the same farm but without any history of sludge application, served as a non-sludge-amended agricultural controls. Sludge-amended fields also received NPK fertilizers, while the RF4 control field received NPK, cattle slurry, or farmyard manure. None of the fields were subject to mulching, greenhouse cover, seed protection, or wastewater irrigation—common contributors to MPs pollution. Additionally, two fields with no agricultural activity for over a century (HF1, n = 5; HF2, n = 5) were sampled as non-agricultural backgrounds.

The soil sampling volume was determined based on simulations by Yu and Flury et al. (2021) (Yu & Flury, 2021), which identified the elementary volume required to minimize uncertainty while accounting for the non-uniform distribution of MPs particles. Using our analytical method, the lowest detectable MPs concentration was 0.4 MPs/g of soil, relevant for control soils with expected low MPs levels. Assuming a sampling depth of 20 cm and a typical topsoil bulk density of 1.2 g/cm³, this concentration corresponds to $9.6 \times 10^4$ particles/m². For this concentration, a representative elementary volume (REV) of 0.80 m² was estimated to achieve a 5% sampling error. This estimation was modelled by the equation $y=48286x^{-0.969}$ where $y$ represents the REV and $x$ corresponds to the MPs concentration for plastic particles arranged in random clusters of 100 particles per cluster (Yu & Flury, 2021). While theoretical, these assumptions serve as a foundation for estimating the necessary sampling volume.

Five sites were randomly selected for soil sampling within each field, ensuring a 4-meter margin from field borders to minimize the risk of contamination. Each sample was taken from a 0–20 cm depth within a 50 × 50 cm quadrat, thoroughly mixed with a stainless-steel shovel to capture spatial variability. Soil below 20 cm was excluded due to compaction which is assumed to result in minimal MPs transport beyond this level. From each site, 2–5 kg of soil was collected and stored in 100% cotton bags at 4°C. Soil physicochemical property analyses included pH, electrical conductivity (EC), soil organic matter, and soil texture. Soil samples were dried at 40°C for MPs analysis (details in SI3).

### 4.2.2 Microplastic extraction from sewage sludge and soil matrices

Sewage sludge (three subsamples of 10–15 g) and soil samples (subsample of 600–800 g per site) were homogenized and sieved through a 500 µm stainless steel sieve. Large microplastics (LMPs, 500–5000 µm) were manually collected for ATR-FTIR analysis, while small microplastics (SMPs, 25–500 µm) were extracted using tailored protocols optimized for their organic matter of parent soil or sewage sludge (Peneva et al., 2024; Phan Le et al. 2025, see Chapter 2 and 3).

The extraction of SMPs from soil began with the density separation of a 50 g subsample of 500 µm-sieved soil using a zinc chloride ($ZnCl_2$) solution with a density of 1.5 g/cm³. This process was conducted in a sediment-microplastic isolation (SMI) unit, following the method previously described (Coppock et al., 2017). The supernatant was filtered through a 25 µm stainless-steel mesh, rinsed with HPLC-grade water and ethanol, sonicated for 10 mins, and treated with Fenton's reagent (20 mL hydrogen peroxide, $H_2O_2$, and 20 mL 0.05M iron (II) sulphate, $FeSO_4$). A second density separation with $ZnCl_2$ solution followed. For samples with >15% OM, an additional digestion step using Fenton's reagent was applied. The final extract was filtered through the same stainless-steel mesh, rinsed with HPLC water and ethanol, and diluted to 100 mL with HPLC water in a volumetric flask.

Sewage sludge samples, characterized by higher OM content, required a modified extraction procedure developed and tested in this study. X for sewage sludge or 0.3–8.7% for soil, were taken using a 5 mL glass pipette from each 100 mL aqueous extract for subsequent SMP analysis. Aliquots were precisely measured to ensure particle counts did not exceed 70,000 particles larger than 2 µm or 200 particles larger than 70 µm,

preventing filter blockage. Particle counting was performed using a Syringe Particle Size Analyzer (Markus Klotz GmbH, Germany).

### 4.2.3 Identification and characterisation of microplastics

LMPs were visually inspected and manually collected using ultrafine tweezers, then analysed with an Agilent Cary 630 single-bounce ATR-FTIR. The LMPs were classified into three shape-based categories: fragments, films, and filaments. Fragments were defined as irregular particles produced by the breakdown of larger plastic materials. Films referred to soft, thin polymer fragments typically originating from items such as plastic bags or wrapping materials. Filaments were thread-like polymers derived were derived from the fragmentation of ropes or fishing lines and measured >50 µm. These classifications and definitions align with previously established standards (Tanaka & Takada, 2016).

For SMPs, prepared aliquot samples were filtered onto 25 mm Anodiscs™ (Whatman™, 0.2 µm pore size) and analysed using FPA-µ-FTIR. Imaging was performed in transmission mode with a Bruker Hyperion 3000 FTIR microscope equipped with a 3.5× IR objective, a 64×64-pixel FPA detector, and a Bruker Tensor 27 FTIR spectrometer. The entire filter surface was scanned, collecting spectra with 32 scans at a resolution of 8 $cm^{-1}$ across the range of 1,250 to 3,600 $cm^{-1}$. Spectra were processed using OPUS 8.5 software, with automatic MPs identification and quantification performed using siMPle software (Primpke, S. et al., 2017). All assigned spectra were manually inspected to confirm accurate library matches in term of matching index and signal to noise ratio. SMPs were further classified based on aspect ratio into particle-like SMPs and elongated (fibre-like) SMPs, defined as having an aspect ratio of 3:1 or higher. Detailed methods are provided in Supplementary Information (SI4).

### 4.2.4 Quality assurance and quality control

Quality control measures were strictly implemented to prevent contamination from ambient air, clothing, chemicals, or laboratory tools. Non-plastic equipment was used whenever possible, cleaned with water and acetone, and covered with clean aluminium foil. All stainless-steel filters (pore dia. 25 µm), glass fibre filters (GFFs, pore dia. 0.7 µm), and glassware were incinerated at 500°C for 4 hours prior to use. During sample handling, 100% cotton lab coats and nitrile gloves were worn, and all procedures were conducted in a thoroughly cleaned fume hood. Besides HPLC-grade water and ethanol for rinsing, other reagents, including $ZnCl_2$, 30% $H_2O_2$, and 0.05M $FeSO_4$ solution, were filtered through GFFs (nominal pore size 0.7 µm) before use. Procedural blanks (n=13) were processed alongside samples to monitor for contamination.

All data were blank corrected using a limit of detection (LOD) approach. For each polymer, LOD was calculated as the mean contamination from 13 blanks plus 3 times the standard deviation (Table S4). Values above the LOD were reported; those below were stated as < LOD. Analysis of 13 procedural blanks revealed averages of 3.8 ± 7.7 polyethylene (PE), 11.6 ± 12.1 polyester (PEST), 9.4 ± 13.0 polypropylene (PP), 3.1 ± 7.5 polystyrene (PS), and 2.3 ± 6.0 polyvinyl chloride (PVC), all above 25 µm in size, with none detected for other polymers. LODs were 26.9 particles for PE, 48.0 particles for PEST, 48.4 particles for PP, 25.6 particles for PS, and 25.3 particles for PVC. All samples from sludge-amended and non-agricultural fields had MPs concentrations above

LOD, except for non-amended agricultural fields, where some samples had PEST and PP below LOD.

The extraction and analysis method reported above has been rigorously validated across a wide range of plastics (Phan Le et al, 2025, see Chapter 2), covering various size ranges where fluorescence microscopy was also employed. Within the research reported here, a surrogate MPs standard using Cospheric polyethylene microspheres (100-125 µm in diameter) was utilized, as recommended by a previous study (Philipp et al., 2022), for 3 sludge samples and 6 soil samples. High recovery rates (93 ± 20%) were observed for these standards using the methods reported here, highlighting the accuracy of the method (for sphere-shaped MPs).

### 4.2.5 Statistical analysis

To evaluate the statistical significance of any variation in soil MPs concentrations across different fields, normality and homogeneity of variance were first assessed using Shapiro-Wilk tests and Levene's tests. For data meeting the criteria for parametric testing, ANOVA tests were used. For data that did not meet these criteria, Kruskal-Wallis tests were employed. In all cases, statistically significant differences were defined at p-value $\leq 0.05$. The Wilcoxon Signed-Rank Test was used to compare observed and expected MPs concentrations within the same fields (section 4.2). All analyses were performed using IBM SPSS version 28.0.0.0 (190) and visualized in Origin 2023b.

Principal Component Analysis (PCA) was conducted in SIMCA 17.0.2 to explore plastic concentration patterns across all sampling points, using concentrations of each plastic type (MPs/g). Data were log-transformed to reduce skewness and UV-scaled to ensure equal weighting, resulting in the best model fit. All detected plastics were initially included, but ABS and polyamide were later excluded due to low concentrations and many zero values, which lowered $Q^2$ and impaired model performance.

## 4.3 Results

### 4.3.1 Microplastics in digested sewage sludge

While no LMPs were detected through visual screening in the sewage sludge samples, the FPA-µ-FTIR analysis (Table S1) identified 3640 ± 2100 SMPs.$g^{-1}$ DW in the digested sewage sludge. This total includes 3010 ± 1900 particle-like SMPs and 630 ± 200 elongated SMPs. Twelve different polymers were detected in the sludge samples, including polyethylene (PE), polyester (PEST), polypropylene (PP), polyvinyl chloride (PVC), polystyrene (PS), polyamide (PA), acrylonitrile butadiene styrene (ABS), styrene butadiene rubber (SBR), acrylonitrile butadiene rubber (NBR), polylactic acid (PLA), polyurethane (PU), polymethyl methacrylate (PMMA), and other acrylic resins, which are commonly found in environmental samples. (Lassen et al., 2015)

Among particle-like SMPs, PE was the most abundant polymer, comprising 43.8%, followed by PP at 11.7% and PEST at 10.9% (**Figure** 4.1.). For elongated SMPs, the majority were PEST (30.6%), PE (28.9%), SBR (18.1%), and PP (15.1%). In terms of the

proportion of elongated versus particle-like shapes for each polymer, PEST (37%), SBR (49%), and PMMA (100%) were predominantly elongated. However, the low PMMA abundance (8 particles/gram) creates high uncertainty, requiring larger samples for accurate characterization.

The majority of SMPs (70.2%) were within the smallest size range (≤50 µm), with the highest concentration observed in the 31–51 µm size bin. Lower concentrations in the 0–11 µm and 11–31 µm bins likely result from approaching the FTIR detector's detection limits for particles smaller than 11 µm, compounded by the use of a 25 µm stainless steel mesh. The presence of particles smaller than the 25 µm mesh size can be explained by smaller particles adhering to larger particles or clustering together. Additionally, particle sizes reported by FTIR may not fully reflect their actual dimensions. This discrepancy arises because weak signals from certain pixels, especially at the edges of particles, can cause some plastics to go undetected, leading to an underestimation of particle size as defined by FTIR.

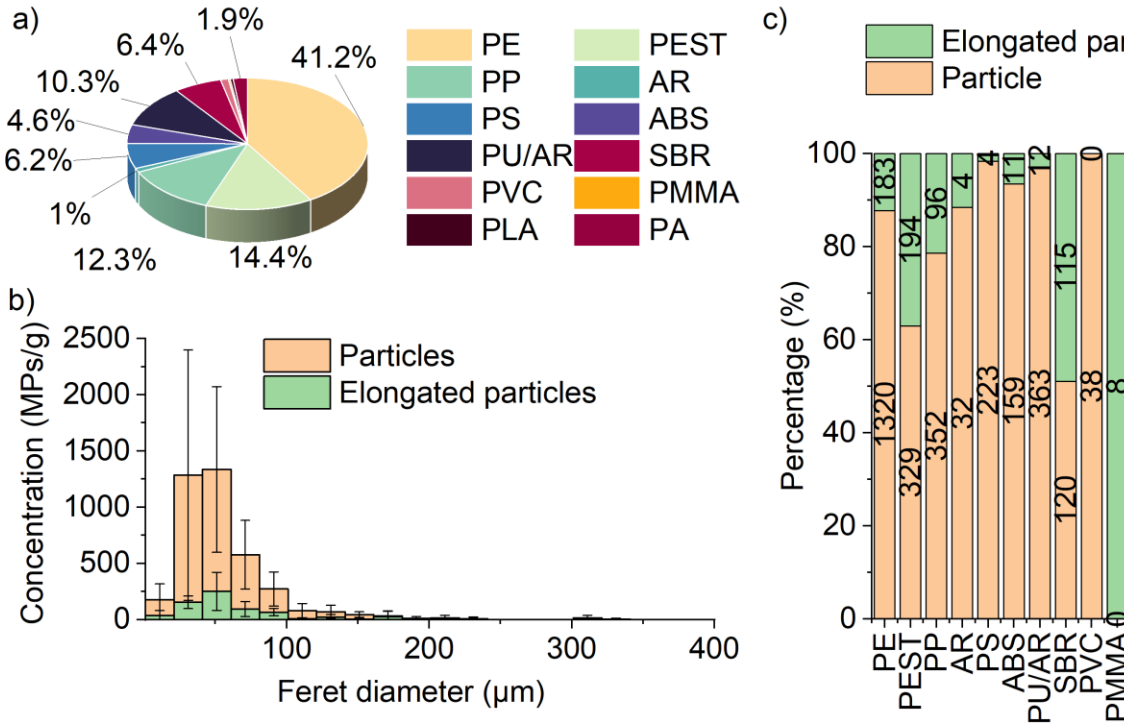


**Figure 4.1.** Characterization of SMPs in digested sludge cake, including polymer mean compositions for total SMPs (a), the size distribution for both particle like and elongated (fibre-like) SMPs, errors bars represent the standard deviation of size distribution of sewage sludge samples (n=3) (b) and the mean proportion of each shape for each polymer type (c).

### 4.3.2 Microplastics in sludge-amended and background soils

No LMPs were detected in soils collected from non-agricultural and agricultural control fields (HFs and RF4), whereas the ATR-FTIR analysis of soils from agricultural fields that had sewage sludge application (RF1, RF2 and RF3) revealed 9.5 ± 6.4 LMPs/kg (**Figure** S2). The polymers detected included PE (38.7%), PP (25.5%), PS (21.5%), and PVC (14.3%). Of these, filaments constituted 52.6% of the total MPs, fragments 30.9%,

and films 16.5%. Given the negligible presence of LMPs (0.08%) in the sewage sludge, these LMPs likely originated from other sources, such as littering, twine ropes, and packaging materials used in agricultural production and inadvertently input to soils.

**Figure** 4.2 reports SMP concentrations in soils across three field types: sewage sludge-amended, non-sewage sludge-amended agricultural control, and non-agricultural background. SMPs are categorized into total MPs, particle-like, and elongated types. Sewage sludge-amended soil exhibited significantly higher mean SMP concentrations (39 ± 27 MPs/g) compared to non-amended agricultural control (9.6 ± 4.4 MPs/g) and non-agricultural background (17 ± 13 MPs/g) ($p = 0.001$ and $p = 0.014$, respectively). No significant difference was found between non-amended and non-agricultural soils ($p = 0.688$). A similar trend was observed for the particle-like MPs concentrations, with significantly higher concentrations in sludge-amended soil (34 ± 21 MPs/g) compared to non-amended (8 ± 3 MPs/g) and non-agricultural soils (7 ± 3 MPs/g) ($p = 0.001$), with no significant difference between the latter two ($p = 0.886$). For elongated SMPs, the Kruskal-Wallis's test revealed no statistically significant differences across the fields ($p= 0.387$), indicating random variation rather than systematic differences.

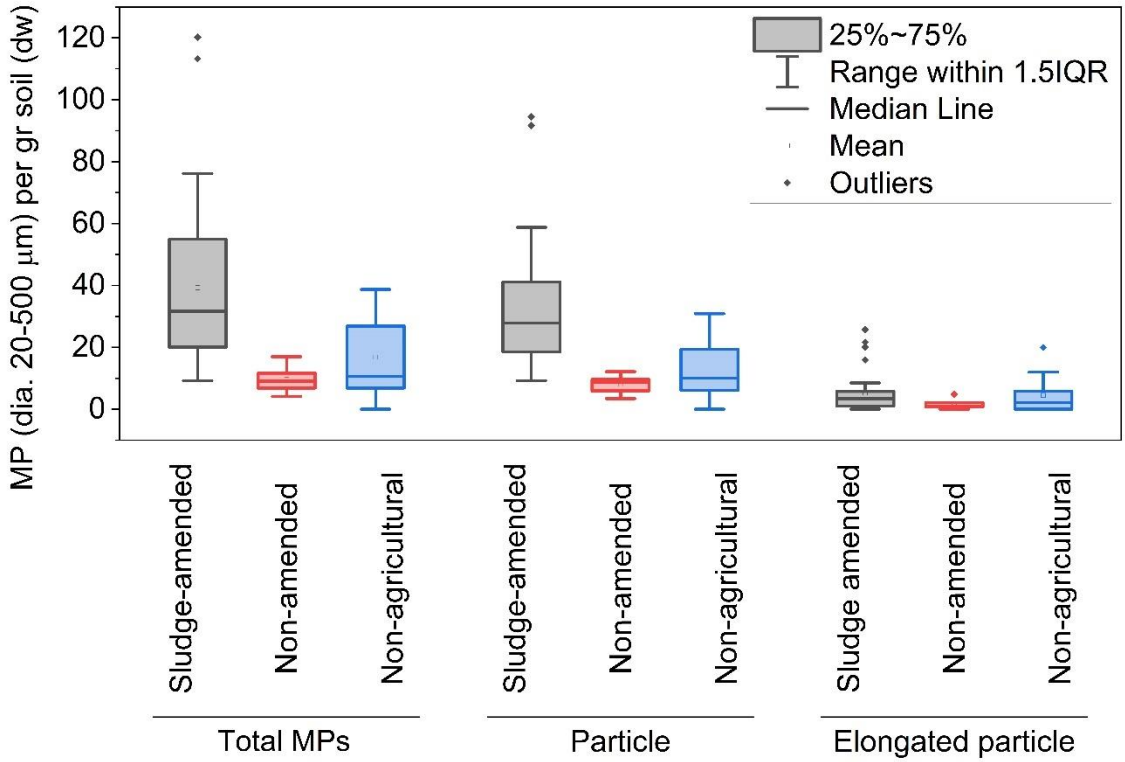


**Figure 4.2.** Mean of total SMPs, particle-like and elongated SMPs in sludge-amended agricultural soil, non-amended agricultural control and non-agricultural background soils. Each boxplot indicates the median (central mark) and 25th and 75th percentiles, with whiskers outside the box indicating the 10th and 90th percentiles. Points outside the whiskers indicate outliers.

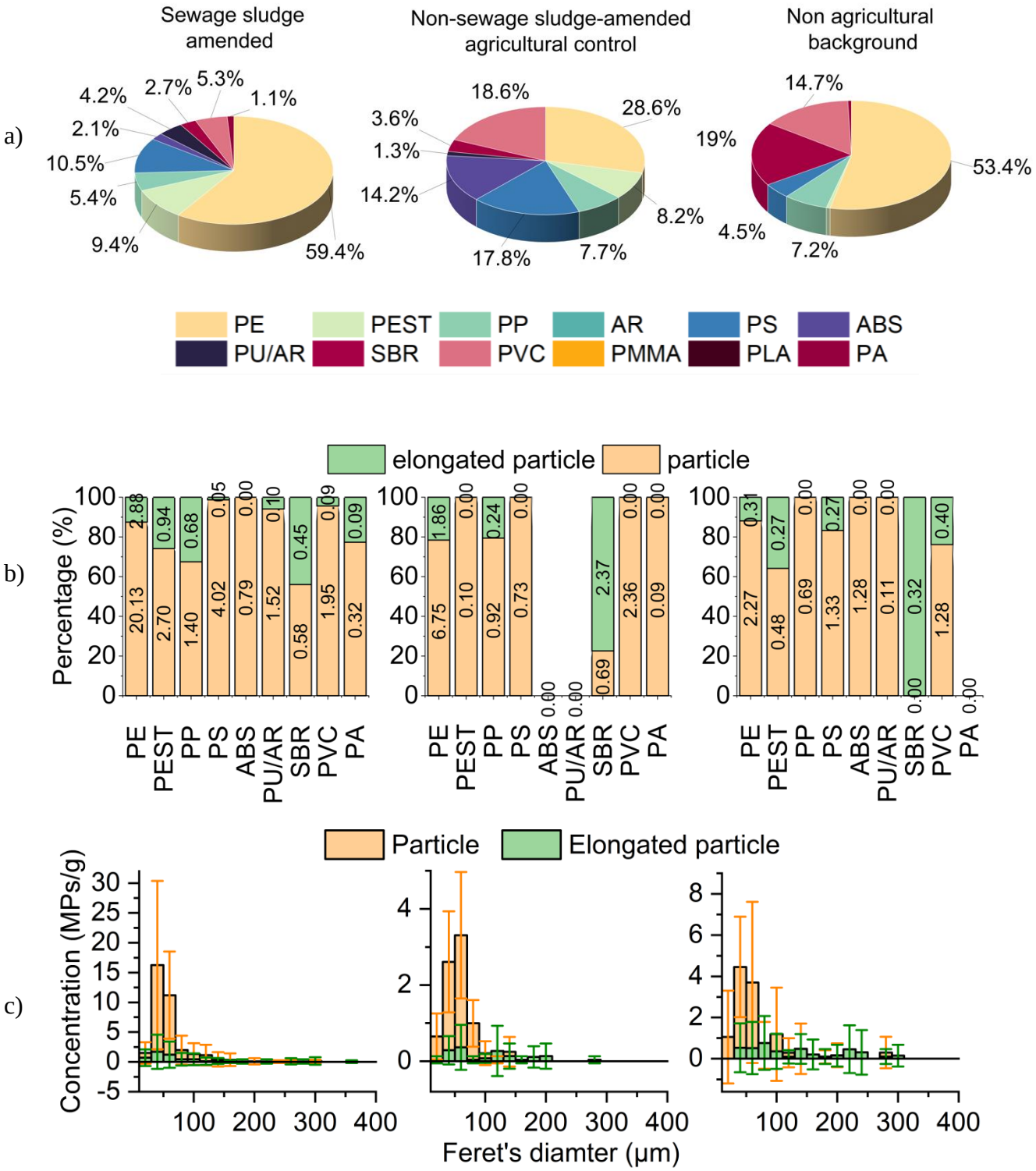


**Figure 4.3.** Polymer composition (a), proportion (%) of shape for each polymer (with number on each bar represent the actual concentration (MPs/g) (b) and size distribution for each shape for sludge-amended agricultural, non-amended agricultural and non-agricultural background soil, errors bars represent the standard deviation of size distribution of sewage sludge samples (c)

The polymer composition of MPs varied between field types. Sludge-amended soil closely mirrored the polymer profile of MPs in sewage sludge, with 9 out of 12 polymers detected in sewage sludge also detected in sludge-amended soils. Non-amended agricultural control soil contains 8 polymers (missing PMMA, PLA, acrylic resin and PA), and non-agricultural background soil has 7 polymers (missing PMMA, PLA, acrylic resin, ABS, and PU). Overall, PE was the dominant polymer in all fields, with sludge-amended agricultural fields containing 59.4% PE, along with notable amounts of acrylic resin (10.5%), PEST (9.4%), and PP (5.4%) (**Figure** 4.3.). Non-amended agricultural fields contained 28.6% PE, 18.6% PVC, 17.8% PS, and 14.2% ABS, with non-agricultural background fields containing 53.4% PE, 19% SBR, and 7.2% PP. Shape contributions for each polymer indicated that particle-shaped MPs were more prevalent than elongated particles (except for SBR) across all fields. Elongated particles were less frequent across all fields, but were more evenly distributed in size, except for the sludge-amended fields. Regarding the size distribution, sludge-amended fields contained a higher proportion of smaller plastics (peaking at 20-100 µm, similar to the size distribution of MPs in sewage sludge, **Figure** 4.1.) compared to non-sludge fields, which had a greater proportion of MPs in the 100-300 µm range. Sludge-amended fields clearly exhibited the highest concentrations of MPs, and there are significant variations in MPs composition, shape, and size distribution between field types.

The PCA conducted on the dataset of plastic type concentrations across various sampling points reveals clear compositional patterns among the samples (**Figure S3 and S4**). The first two principal components explain 68% of the total variance (PC1: 40%, PC2: 27.9%), with polyester and polystyrene contributing strongly to PC1, while polypropylene, polyethylene, and styrene butadiene rubber are positively associated with PC2 **(Figure S3**). The scores plot shows that non-agricultural background fields (HF1 and HF2) cluster in the left and lower regions, aligning with plastics such as polypropylene, polyethylene, and styrene butadiene rubber (**Figure S4**). In contrast, sewage sludge–amended soils (RF1, RF2, and RF3) are more widely dispersed and tend to occupy the right side of the plot, indicating higher concentrations of polyester, polystyrene, and polyurethane-acrylic resin. Non-amended agricultural controls (RF4) form a compact cluster near the origin, suggesting a relatively homogeneous composition with moderate contributions from both PC1- and PC2-associated plastics. However, the overall model fit remains modest ($R^2 = 0.60$; $Q^2 = 0.20$, **Figure S5**), reflecting limited explanatory and predictive power. This limitation persists despite applying log transformation and testing various variable scaling methods. A likely reason is the small number of sampling points combined with sparsity in the data, as many plastic types were not consistently detected across all sites. This led to a high proportion of zero or near-zero values, which weakens the ability of PCA to extract robust and meaningful patterns.

## 4.4 Discussion

### 4.4.1 Microplastics in sewage sludge

The average concentration of MPs in digested sewage sludge cake (3640 MPs/g (**Table** S5), is higher than many previous studies which have reported concentrations ranging from 0.193 MPs/g (Zhang, Lishan et al., 2020) to $1.69 \times 10^5$ MPs/g (Vollertsen & Hansen,

2017). Based on a systematic review of 65 studies by Harley-Nyang *et al.* (Harley-Nyang et al., 2023), mean MPs concentrations in sewage sludge of $3.12 \times 10^3$ MPs/g and 208.3 MPs/g have been reported, when including and excluding the Vollertsen & Hansen study respectively. The author claims that differences in sludge concentrations between studies can be attributed to factors such as sources of wastewater (runoff, domestic and industry), serving population size and characteristics (demographic and economic status), sewage collection system type, weather conditions, wastewater treatment processes and sludge treatment process (Harley-Nyang et al., 2023). Importantly, direct comparisons between studies are also constrained by differences in analytical methods, with variations in sampling and analytical methodologies, including minimum particle sizes analysed. For example, when analysing UK sewage sludge, Harley-Nyang et al. reported 37.7 to 286.5 MPs/g DW using µ-FTIR of manually-picked particles (Harley-Nyang et al., 2022), while Horton et al. found 301–10,380 MPs/g DW using semi-automated FPA-µFTIR of extracted MPs (Horton et al., 2020). Our data show similar MPs concentrations to those reported by Horton et al. (2020) and Simon et al. (2018) using a similar semi-automated FPA-µ FTIR method, which facilitates robust analysis of smaller particles undetectable by commonly applied manual sorting.

Among the 12 polymers detected in digested sludge cake, PE and PP were the most dominant. These polymers are among the most widely used in plastic products, for example being commonly found in plastic packaging. Additionally, 93% of microbeads in personal care products (PCCPs) are PE (EPA, 2016), suggesting that particle-like SMP contamination in sludge may at least in part originate from PCCPs, leading to a predominance of particle-like shapes of PE. Other possible sources include industrial effluents, where PE is used as 'air blasting' media to strip paint from metallic surfaces and cleaning engine parts (Lusher et al., 2012). PS and ABS were also recorded in high concentrations, and these polymers are commonly used in packaging and consumer goods. Significant amounts of polyurethane, acrylic resin, and polyurethane-acrylic resin were found, commonly associated with coatings, inks, 3D-printed parts, electronic devices, and polyurethane-foam mattresses. Road marking paint, containing 15-40% acrylic polymers, and footwear soles made of PU, synthetic rubber, and PVC also contribute to MPs contamination. (Lassen et al., 2015) Other sources of PVC include blasting, shredding, and products like pipes and agrochemical containers. (Lusher et al., 2012)

Polyester accounted for 14.4 % of total MPs detected, with approximately 40% of these being in elongated shapes. Among other fibres detected were PP, acrylic, and polyamide. Synthetic textiles are a significant source of plastic pollution in the environment, with studies showing that over 1,900 fibres can be released from a single synthetic garment per wash.(Browne et al., 2011) According to a British study from 2009, synthetic fabrics such as viscose (a semi-synthetic cellulosic material), polyester, acrylic, polyamide, polyurethane, and polypropylene account for 45% of total textile consumption. (WRAP, 2012)

Our research identified 240 ± 170 SBR particles/g DW of sewage sludge, accounting for 6.4% of the total MPs. SBR is a synthetic rubber commonly used in products such as footwear, adhesives, conveyor belts, construction materials, and medical devices, with a significant portion originating from tire industry (Dhanorkar et al., 2021). These tires fragment into tire wear particles (TWPs), which are a major source of MPs pollution and are considered the second-largest primary contributor to MPs contamination in the marine environment (Boucher & Friot, 2017). It is important to note that our findings do not

include smaller airborne TWPs, which fall below our size detection limit of 25 µm. Previous studies have reported TWP sizes ranging from 4 µm to 350 µm, with distribution peaks at 5 µm and 25 µm (Kreider et al., 2009), indicating that a significant portion of the very fine TWPs may have been undetected in our research. Additionally, the carbon black content in TWPs complicates standard FT-IR analysis, as it can absorb the IR beam. Nonetheless, we successfully identified SBR particles, with 48.9% exhibiting an elongated shape. This finding aligns with previous descriptions of TWPs as elongated, "sausage-shaped" particles, where 65% had an aspect ratio greater than 1.5 (Kovochich et al., 2020; Kreider et al., 2009)

Compared to previous research, our data show a lower proportion of fibres (elongated) relative to fragments in our sewage sludge samples, possibly due to variation in the characteristics of individual sewage sludge as described earlier, or due to analytical errors between studies. Analysis of fibres carries uncertainty as cellulose-derived fibres can survive wet peroxide oxidation, leading to possible overestimation of synthetic plastic fibres using visual inspection without chemical confirmation.(Sutton et al., 2016) A round-robin test by Hannah et al. showed that labs prioritized analysing fibre bundles (88%) over pellets (20%) and foam (30%), with larger items often selected for FTIR. (De Frond et al., 2022) These factors might explain the high reported fibre proportions in previous studies. However, with fully automated methods like FPA-µ-FTIR used in our study, challenges remain. µ-FTIR requires fibres to stay fixed during analysis, but their lightweight and small diameter complicate this. Elongated shapes are hard to fully capture in one focal plane, risking misidentification as particles. Additionally, the 11 µm pixel size (limited by mid-infrared light diffraction) can cause fibres narrower than this to go undetected, especially for typical textile fibres being 10–20 µm in diameter (up to 50 µm) (Rose Sinclair, 2014). These challenges underscore the need for improved automated micro-spectroscopy for better fibre detection.

At the same time, Sutton et al. suggested that fibres are more likely to be released in WWTP effluents, while fragments are retained in sewage sludge—an observation supported by Crossman et al (Crossman et al., 2020b; Sutton et al., 2016). Additionally, fragments or particle-like MPs may dominate due to their various sources, including both primary and secondary MPs. Primary sources include raw materials for plastic production, PCCPs, paint, sandblasting, etc. while secondary sources derive from urban dust, runoff, or fragmentation of larger plastics before or within WWTPs due to warm temperatures, mechanical processes, and biological activity. (Lassen et al., 2015) For example, nylon-6 fibres are prone to breaking under mechanical stress, forming micro-cracks that may lead to smaller fragments. (John et al., 2009), and there has also been evidence of nylon-4 biodegradation in active sewage sludge (Kazuhiko et al., 2002) These factors may explain the higher concentration of particle-like polyamide shapes compared to fibre-like shapes we observed in sewage sludge.

### 4.4.2 Microplastics in sludge-amended soil

Assuming that all sludge applied to the fields had a MPs concentration of $C_{Sludge}$ of 3640 ± 2100 MPs $g^{-1}$ dw, that the soil bulk density $D$ is 1.2 $g.cm^{-3}$, and that MPs are evenly distributed within the upper 30 cm of the soil (ploughing depth $PD$), the cumulative MPs load ($CL_{sludge}$) for a 1 ha field originating from sludge was estimated as:

$$CL_{Sludge}\,(MPs.g^{-1}) = \frac{C_{sludge}\,(MPs.g^{-1}) \times M_{sludge\ (dry\ weight)}\,(g.cm^{-2})}{D_{soil}\,(g.cm^{-3}) \times PD_{ploughing}\,(cm)}$$

where $M_{Sludge}$ is the cumulative sludge mass (DW) applied to the fields RF1, RF2 and RF3 (10.13 tonnes/ha DW, equivalent to 0.1013 g. cm$^{-2}$). $CL_{Sludge}$ resulted in just 10.3 ± 5.9 MPs g$^{-1}$ (dw), significantly less than the 38.6 ± 27.3 SMP g$^{-1}$ (dw) observed for the sludge-applied ploughing soil (Wilcoxon S-R test, p= 0.046). While our estimate carries large uncertainties, such a marked difference remains noteworthy. This discrepancy may be explained by several factors. Firstly, the SMP content in the sludge we report represents a single point in time, and MPs loads in the sludge from 2013 likely differed from more recent sludge applied in 2021. Secondly, since input to soil in 2013, sludge-derived MPs may have undergone fragmentation due to UV light, microbial and mechanical action, increasing particle numbers. This is also supported by the size distribution data we report, showing the highest frequency of MPs in sewage sludge at 40-60 µm, while in sludge-amended soil this dropped to 20-40 µm. Although these differences could be statistically insignificant due to large uncertainties in our study, there has been evidence of plastic degradation and fragmentation in soil over time. For example, under 70 days of natural summer sunlight simulated by UV irradiation, a total of 475, 163, and 147 MPs/cm², sized from 0.02 to 0.10 mm, were released from biodegradable, white, and black PE mulch films, respectively (Yang, Yang et al., 2021). However, the degradation of plastics in soil, especially sludge-derived MPs, as related to plastic types, soil properties, and weathering conditions, remained poorly understood. Another potentially important factor contributing to the apparent discrepancy between theoretical MPs load and observed data is the presence of background sources of MPs. These include fragmentation of plastics from other anthropogenic activities and atmospheric deposition, which will be discussed below.

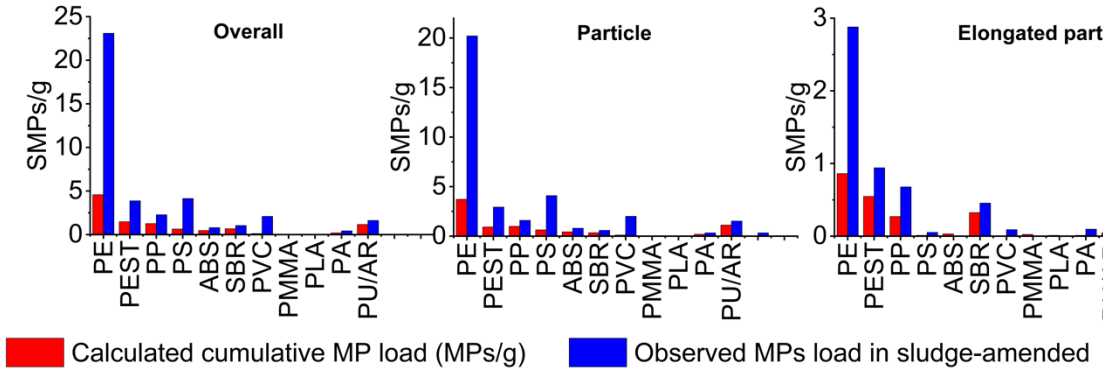


**Figure 4.4.** Comparison between expected MPs concentration for each polymer type in soil based on two sewage sludge applications, and the MPs concentration within sludge-amended soil measured in this study.

**Figure** 4.4. provides a detailed comparison between the calculated cumulative MPs load from sewage sludge and the actual observed MPs in sludge-amended fields. Interestingly, most polymers were found in higher concentrations than expected, except for a decrease in acrylic resin and the complete absence of PLA and PMMA in the observed data. The lack of PMMA and PLA may be attributed to their low concentrations in the digested sludge (8 and 16 MPs/g, respectively), which might have led to their dilution and

subsequent non-detection in the soil samples. Further, the biodegradable nature of PLA could have resulted in its degradation upon entering the soil.

Our research reveals that the ratio of particles to elongated particles for each polymer remains nearly consistent between sewage sludge and sludge amended soil (**Figure** 4.1b and 4.3b), potentially indicating no substantial difference in the retention or transport of these two MPs morphologies following input to soil. This apparent consistency may result from their complex transport mechanisms. For instance, fibres are often better retained in soil through vertical transport, due to entanglement in soil pores. (Weber et al., 2022) However, they are also more prone to loss via atmospheric/aeolian transport because of their high surface area-to-volume ratio, assuming similar densities and masses to particles (Chen et al., 2023a).

Non-sewage sludge-amended agricultural control fields and non-agricultural background fields exhibited no significant difference in MPs concentration, at 8.8 ± 4.4 and 16.7 ± 13.4 SMPs/g respectively, despite having different polymer profiles. A similar MPs concentration of 6.36 MPs/g was detected in a German agricultural test field that had never received sewage sludge, using a comparable MPs detection method and size detection limit to those reported in this study. (Tagg et al., 2022) Atmospheric deposition is likely responsible for the presence of plastics in these background fields. A spatial study of protected areas in the USA reported atmospheric MPs deposition rates of 48–435 MPs/m²/day, noting that larger MPs particles were likely sourced regionally (10–1000 km) and deposited via precipitation, while smaller particles were predominantly transported over long distances through dry deposition (Brahney et al., 2020a). Allen et al. identified fibres up to ~750 μm long and fragments ≤300 μm in atmospheric wet and dry deposition samples (Allen et al., 2019). Road areas (84%), agricultural soil (11%), and oceans (5%) were identified as key contributors to atmospherically deposited MPs in remote wilderness areas. (Brahney et al., 2020b). Additionally, the high abundances of SMPs in the background fields that we report may be attributed to other anthropogenic activities that occurred within or nearby the fields. For example, similar polymeric profiles in SMPs from non-amended fields and LMPs on the farm were observed, indicating possible fragmentation of other plastic sources like silage packaging (PE and PP), PS netting or seedling protection.

Additionally, MPs likely cross-contaminated from nearby sludge-treated fields to untreated fields. Tagg et al. reported that 44% of the MPs concentration from sludge-applied land was present in adjacent fields, indicating MPs transport via wind or water erosion. (Tagg et al., 2022) In our study, sludge-derived MPs, particularly PU, acrylic resin, and ABS, were found in adjacent non-amended fields (about 80m away) but were absent from non-agricultural fields 5.3 km away. The higher elevation of non-amended fields compared to sludge-amened fields indicates that a short-range atmospheric transport mechanism was likely responsible for the movement of MPs from sludge-amended to non-sludge-amended fields, rather than water erosion and runoff

The significantly higher concentrations of MPs in sludge-amended soil compared to non-amended and non-agricultural fields highlights the potentially substantial contribution of sludge application to MPs pollution in agricultural land, beyond sources like atmospheric deposition. This finding is consistent with earlier studies on MPs contamination in soil

post-sludge application, though results vary widely due to differences in analytical methods, size detection limits, sludge sources, and factors influencing MPs retention and transport. For instance, Corradini et al. (2019) reported 3500 MPs/kg in soil amended with 200 t $ha^{-1}$ sludge (DW) using a manual microscopy approach (smallest particle detected of 2254 $\mu m^2$ area), while Ragoobur et al. found 320.0 ± 112.2 MPs/kg sized ≥ 0.25 mm (without specifying sludge application rates). (Corradini et al., 2019; Ragoobur et al., 2021) These previously reported MPs concentration are lower than those we report here, likely due to reliance on visual inspection and microscopy which may underestimate smaller or transparent MPs. As we highlight in **Figure** 4.3c, MPs in very fine sized fractions may dominate the frequency distribution of MPs in soils receiving sewage sludge applications, limiting the potential to generate accurate estimates of MPs concentrations based solely on visual inspection and microscopy. Yang et al reported an average of 68.6 ± 21.5–149.2 ± 52.5 particles $kg^{-1}$ after nine years of sludge application (~6 t/ha/year dry sludge), using ATR-FTIR and µ-FTIR analysis on representative MPs particles with a slightly lower size detection limit of 20 µm. (Yang, Jie et al., 2021) Other studies, focusing on MPs ranging from 50 µm to 100 µm or only on light-density plastics, also reported lower MPs concentrations. (Crossman et al., 2020b; Tagg et al., 2022; van den Berg, Pim et al., 2020) Our study is the first to report the presence of small MPs (≥ 25 µm) in soil from sewage sludge application using a fully quantitative approach through a robust and automated FPA-µFTIR method. This method eliminates operator bias and reduces the likelihood of missing small particles, which are often overlooked with visual stereo-microscopy-based identification methods. We believe that the extraction and analytical protocols we report provide a robust framework for future research to generate accurate estimates of the magnitude and nature of MPs pollution in soils that receive sewage sludge inputs.

Previous studies highlight the complexity of MPs fate and transport in soil following sewage sludge applications, influenced by factors such as soil properties, faunal activity, climate, sludge application methods, and plastic characteristics. For instance, Weber et al. found that most MPs remain in the application area with minimal lateral movement over 30 years (Weber et al., 2022) Regarding vertical transport, both Weber and Tagg et al. reported the highest MPs concentrations in the topsoil (0–30 cm), with only 1.6% penetrating deeper layers (60–90 cm). (Tagg et al., 2022; Weber et al., 2022) Although we did not sample deeper soil (≥20 cm) due to high soil compaction, vertical transport of MPs is believed to be likely, especially for smaller MPs that fell below our size detection limit. In terms of erosion, Shell et al. noted that surface runoff mobilized only 0.2–0.4% of MPs from soil surface, suggesting that semi-arid agricultural soils can be long-term sinks for MPs. (Schell et al., 2022) Conversely, Crossman found that over 99% of MPs from sludge were transported from soil to aquatic environments within six months under natural heavy rainfall with high runoff volume. However, this study also faced sampling uncertainties due to small core volumes, potentially causing errors up to 100% for the lowest reported MPs concentrations, as noted by Yu et al. (Yu & Flury, 2021) Despite similar total monthly precipitation (40–140 mm/month), our findings showed no notable MPs loss years after sludge application, as indicated by the higher observed MPs concentrations compared to the theoretical load associated with sewage sludge applications. This discrepancy could be due to different soil physiochemical properties, and the predominantly flat topography of the fields used in this research which may favour retention of MPs within the upper surface of the soil. Notably, there was no significant difference in MPs concentrations among RF1, RF2, and RF3 (ANOVA, $p = 0.558$), suggesting that the slight slope in RF3 was insufficient to cause significant

differences in MPs transport or accumulation compared to the other fields. In addition, while Crossman et al. focused on MPs ≥ 50 µm, the smaller MPs in our research are more likely to penetrate into the plough horizon and integrate into soil aggregates, thereby reducing their susceptibility to lateral erosion and vertical transport.

### 4.4.3 Wider implications

Approximately 3.5 million tonnes of sewage sludge are recycled/applied to agricultural land annually in the UK. Of this, 73% is processed as digested cake, 22% as lime-treated cake, and the rest as granules and pellets. The digested cake, with an average of 23% dry solids, contributes roughly 590,000 tonnes (DW) to the soil annually. (Assured Biosolid Limited, 2024) Based on the upper and lower concentrations of MPs found in this study and assuming the wastewater treatment plant we analysed represents the national average, it is estimated that between $9.1\times10^{14}$ to $3.4\times10^{15}$ MPs are added to UK agricultural soils each year via digested cake application only. Currently, sewage sludge is applied to 1.3% of the UK's agricultural land, covering about 150,000 hectares. (Assured Biosolid Limited, 2024) This means that, on average, between 6 to 22 billion MPs could be delivered to soils from sludge applications per hectare annually. However, this estimation is based on a snapshot of plastics in sewage sludge. While we did not evaluate MPs variability over time, seasonal patterns are key factors influencing MPs levels, with higher levels often seen in warmer seasons. Winter washing and precipitation may also contribute to fibre contamination or affect particle counts. Additionally, treatment processes, population size, and other factors mentioned earlier also play a significant role in shaping this estimation.

MPs contamination has been shown to impact soil ecosystems, effects vary with MPs properties, biotic and abiotic components in soil. In terms of soil physicochemical properties, MPs may disrupt soil structure, reduce bulk density, decrease water infiltration rates, and alter levels of dissolved organic phosphorus (P), nitrogen (N), and carbon (C) (De Souza Machado et al., 2018, 2019; Kim et al., 2021; Meng et al., 2021). These changes impact enzyme activities, microbial communities, nutrient availability, collectively altering soil biochemical dynamics (Wang, Wenfeng et al., 2019). MPs, due to their small size, are readily ingested by soil organisms, leading to bioaccumulation within the soil food chain and impacts across trophic levels. Earthworm studies reveal that MPs consumption affects earthworm survival, growth, and causes intestinal damage (Cui et al., 2022). Protists, such as flagellates, amoebae, and ciliates, can absorb MPs particles smaller than a few µm (Rillig & Bonkowski, 2018). In plants, MPs delay seed germination and seedling survival, and alter biomass, elemental composition, and root morphology (Zhou, Jie et al., 2021).

Furthermore, MPs in the environment act as vectors for pollutants, including heavy metals (e.g., $Pb^{2+}$, $Cd^{2+}$, $Cu^{2+}$) and persistent organic compounds such as polycyclic aromatic hydrocarbons (PAHs), polychlorinated biphenyls (PCBs), and dichlorodiphenyltrichloroethane (DDT) (Antunes et al., 2013; Zhang, Zhenming et al., 2022). This is particularly significant in wastewater treatment plants, where some effluents have been reported to contain such pollutants at concentrations of parts per trillion (Bulloch et al., 2015; Yang, Yi et al., 2017). While the sorption and enrichment of pollutants on the surfaces of MPs remain under investigated, sewage sludge-derived

MPs can potentially impact soil ecosystems indirectly through the release of associated contaminants, in addition to the direct effects of the MPs themselves.

## 4.5 Conclusions

Sewage sludge application as part of agricultural production practices represents a potentially significant pathway for the input of MPs to soil. We demonstrate that the MPs concentration in sludge-amended soils may significantly exceed that in non-amended soils. The MPs in sludge-amended soil resemble the MPs profile (in term of polymer type, size and shape) in the sewage sludge itself and differ from MPs detected in non-amended fields. The application of sludge introduces various polymers into soil, including PE, PP, PEST, and PU acrylic resins, with fragments being the dominant morphology in the sludges and soils we analysed. Additionally, the concentration of MPs in sludge-amended soils exceeds that based on the theoretical load from sewage sludge applications, highlighting significant contributions from background sources such as atmospheric deposition and potential fragmentation of sludge-derived MPs.

While previous studies have begun to examine the influence of sewage sludge on soil microplastic concentrations, our research offers a more robust characterisation by accurately quantifying the types, sizes, and morphologies of plastics using FPA-u-FTIR. This study provides valuable insights into the retention and fate of sludge-derived microplastics in soil. However, further research is required to better understand the fate, transport, and pollution risks of microplastics in sludge-amended soils, both in terms of environmental and human health. In addition, a longer temporal study is recommended to investigate seasonal and multiyear variability in MPs loading through sludge applications. This research will help to establish a reliable evidence base to support policy changes and practical solutions that minimise the risks associated with MPs pollution within agricultural soils.

**Acknowledgements**

This work was supported by the European Union's Horizon 2020, ITN SOPLAS, with grant agreement No. 55334. The authors thank staffs at the wastewater treatment facility and the farmers for their great support with sampling.

**Credit authorship contribution statement** Q.N. Phan Le: conceptualisation, methodology, samples analysis, data evaluation, writing, review and editing of the manuscript; C. Halsall: funding acquisition, conceptualisation, supervision, review and editing of the manuscript; M. Kunask: sample analysis, review and editing of the manuscript; L. Ashton and B. Surridge: supervision, review and editing of the manuscript; C. Halsall and J. Quinton: funding acquisition, supervision, review and editing of the manuscript.

**Data availability** Data will be made available on request.

**Declaration**

**Ethical approval** This research did not involve human or animal samples.

**Competing interest** The authors declare no competing interests.

# References


Adhikari, K., Pearce, C. I., Sanguinet, K. A., Bary, A. I., Chowdhury, I., Eggleston, I., et al. (2023). Accumulation of microplastics in soil after long-term application of biosolids and atmospheric deposition. Science of the Total Environment, 912 doi:10.1016/j.scitotenv.2023.168883

Allen, S., Allen, D., Phoenix, V. R., Le Roux, G., Durántez Jiménez, P., Simonneau, A., et al. (2019). Atmospheric transport and deposition of microplastics in a remote mountain catchment. Nature Geoscience, 12(5), 339. doi:10.1038/s41561-019-0335-5

Antunes, J. C., Frias, J. G. L., Micaelo, A. C., & Sobral, P. (2013). Resin pellets from beaches of the portuguese coast and adsorbed persistent organic pollutants. Estuarine, Coastal and Shelf Science, 130, 62. doi:10.1016/j.ecss.2013.06.016

Assured Biosolid Limited. (2024). About biosolids (online)., 2024, from https://assuredbiosolids.co.uk/about-biosolids/

Boucher, J., & Friot, D. (2017). Primary microplastics in the oceans:

A global evaluation of sources IUCN, Gland, Switzerland.

Brahney, J., Hallerud, M., Heim, E., Hahnenberger, M., & Sukumaran, S. (2020). Plastic rain in protected areas of the united states.

Brahney, J., Mahowald, N., Prank, M., Cornwell, G., Klimont, Z., Matsui, H., et al. (2020). Constraining the atmospheric limb of the plastic cycle doi:10.1073/pnas.2020719118/-/DCSupplemental

Browne, M. A., Crump, P., Niven, S. J., Teuten, E., Tonkin, A., Galloway, T., et al. (2011). Accumulation of microplastic on shorelines woldwide: Sources and sinks. Environmental Science &Amp; Technology, 45(21), 9175. doi:10.1021/es201811s

Bulloch, D. N., Nelson, E. D., Carr, S. A., Wissman, C. R., Armstrong, J. L., Schlenk, D., et al. (2015). Occurrence of halogenated transformation products of selected pharmaceuticals and personal care products in secondary and tertiary treated wastewaters from southern california American Chemical Society (ACS). doi:10.1021/es504565n

Chen, Q., Shi, G., Revell, L. E., Zhang, J., Zuo, C., Wang, D., et al. (2023). Long-range atmospheric transport of microplastics across the southern hemisphere. Nature Communications, 14(1) doi:10.1038/s41467-023-43695-0

Collivignarelli, M. C., Abbà, A., Frattarola, A., Carnevale Miino, M., Padovani, S., Katsoyiannis, I., et al. (2019). Legislation for the reuse of biosolids on agricultural land in europe: Overview. Sustainability, 11(21) doi:10.3390/su11216015

Collivignarelli, M. C., Canato, M., Abbà, A., & Carnevale Miino, M. (2019). Biosolids: What are the different types of reuse? Journal of Cleaner Production, 238 doi:10.1016/j.jclepro.2019.117844

Corradini, F., Meza, P., Eguiluz, R., Casado, F., Huerta-Lwanga, E., & Geissen, V. (2019). Evidence of microplastic accumulation in agricultural soils from sewage sludge disposal. Science of the Total Environment, 671, 411–420. doi:10.1016/j.scitotenv.2019.03.368

Corradini, F., Meza, P., Eguiluz, R., Casado, F., Huerta-Lwanga, E., & Geissen, V. (2019). Evidence of microplastic accumulation in agricultural soils from sewage sludge disposal. The Science of the Total Environment, 671, 411–420. doi:10.1016/j.scitotenv.2019.03.368

Cowger, W., Markley, L. A. T., Moore, S., Gray, A. B., Upadhyay, K., & Koelmans, A. A. (2024). How many microplastics do you need to (sub)sample? Elsevier BV. doi:10.1016/j.ecoenv.2024.116243

Crossman, J., Hurley, R. R., Futter, M., & Nizzetto, L. (2020). Transfer and transport of microplastics from biosolids to agricultural soils and the wider environment. The Science of the Total Environment, 724, 138334. doi:10.1016/j.scitotenv.2020.138334

Cui, W., Gao, P., Zhang, M., Wang, L., Sun, H., & Liu, C. (2022). Adverse effects of microplastics on earthworms: A critical review. Science of the Total Environment, 850 doi:10.1016/j.scitotenv.2022.158041

De Frond, H., Cowger, W., Renick, V., Brander, S., Primpke, S., Sukumaran, S., et al. (2022). What determines accuracy of chemical identification when using microspectroscopy for the analysis of microplastics? Chemosphere, 313 doi:10.1016/j.chemosphere.2022.137300

De Souza Machado, A. A., Lau, C. W., Kloas, W., Bergmann, J., Bachelier, J. B., Faltin, E., et al. (2019). Microplastics can change soil properties and affect plant performance American Chemical Society (ACS). doi:10.1021/acs.est.9b01339

De Souza Machado, A. A., Lau, C. W., Till, J., Kloas, W., Lehmann, A., Becker, R., et al. (2018). Impacts of microplastics on the soil biophysical environment American Chemical Society (ACS). doi:10.1021/acs.est.8b02212

Dhanorkar, R. J., Mohanty, S., & Gupta, V. K. (2021). Synthesis of functionalized styrene butadiene rubber and its applications in SBR–Silica composites for high performance tire applications. Industrial &Amp; Engineering Chemistry Research, 60(12), 4517. doi:10.1021/acs.iecr.1c00013

Environment Agency. (2023). Environment agency strategy for safe and sustainable sludge use

Harley-Nyang, D., Memon, F. A., Jones, N., & Galloway, T. (2022). Investigation and analysis of microplastics in sewage sludge and biosolids: A case study from one wastewater treatment works in the UK. The Science of the Total Environment, 823, 153735. doi:10.1016/j.scitotenv.2022.153735

Harley-Nyang, D., Memon, F. A., Osorio Baquero, A., & Galloway, T. (2023). Variation in microplastic concentration, characteristics and distribution in sewage sludge & biosolids around the world. Science of the Total Environment, 891 doi:10.1016/j.scitotenv.2023.164068

Horton, A. A., Cross, R. K., Read, D. S., Jürgens, M. D., Ball, H. L., Svendsen, C., et al. (2020). Semi-automated analysis of microplastics in complex wastewater samples. Environmental Pollution, 268 doi:10.1016/j.envpol.2020.115841

John, B., Kojio, K., & Furukawa, M. (2009). High performance polyamide 6 **fibres** using polycarbonate based thermoplastic polyurethane thin film coatings- a novel method. Polymer Journal, 41(4), 319. doi:10.1295/polymj.pj2008286

Kazuhiko, H.,  , Mie, S., Kazumi, O., Takayuki, S., Hiroyuki, Y., et al. (2002). Biodegradation of Nylon4 and its blend with Nylon6. Journal of Applied Polymer Science, doi:https://doi.org/10.1002/app.11235

Kim, S. W., Jeong, S., & An, Y. (2021). Microplastics disrupt accurate soil organic carbon measurement based on chemical oxidation method. Chemosphere, 276 doi:10.1016/j.chemosphere.2021.130178

Kominko, H., Gorazda, K., & Wzorek, Z. (2024). Sewage sludge: A review of its risks and circular raw material potential. Journal of Water Process Engineering, 63 doi:10.1016/j.jwpe.2024.105522

Kovochich, M., Liong, M., Parker, J. A., Oh, S. C., Lee, J. P., Xi, L., et al. (2020). Chemical mapping of tire and road wear particles for single particle analysis. Science of the Total Environment, 757 doi:10.1016/j.scitotenv.2020.144085

Kreider, M. L., Panko, J. M., Mcatee, B. L., Sweet, L. I., & Finley, B. L. (2009). Physical and chemical characterization of tire-related particles: Comparison of particles generated using different methodologies. Science of the Total Environment, 408(3), 652. doi:10.1016/j.scitotenv.2009.10.016

Lamastra, L., Suciu, N. A., & Trevisan, M. (2018). Sewage sludge for sustainable agriculture: Contaminants' contents and potential use as fertilizer. Chemical and Biological Technologies in Agriculture, 5(1) doi:10.1186/s40538-018-0122-3

Lassen, C., Hansen, S. F., Magnusson, K., Hartmann, N. B., Rehne Jensen, P., Nielsen, T. G., et al. (2015). Microplastics occurrence, effects and sources of releases to the environment in denmarkDanish Environmental Protection Agency.

Lusher, A. L., Hurley, R., Vogelsang, C., Nizzetto, L., Olsen, M., & Hildonen, H. (2012). Mapping microplastics in sludge

Meng, F., Yang, X., Riksen, M., & Geissen, V. (2021). Effect of different polymers of microplastics on soil organic carbon and nitrogen – A mesocosm experiment. Environmental Research, 204 doi:10.1016/j.envres.2021.111938

Nizzetto, L., Futter, M., & Langaas, S. (2016). Are agricultural soils dumps for microplastics of urban origin? Environmental Science &Amp; Technology, 50(20), 10777. doi:10.1021/acs.est.6b04140

Peneva, S., Le, Q. N. P., Munhoz, D. R., Wrigley, O., Wille, F., Doose, H., et al. (2024). Microplastic analysis in soils: A comparative assessment. Ecotoxicology and Environmental Safety, 289 doi:10.1016/j.ecoenv.2024.117428

Philipp, M., Bucheli, T. D., & Kaegi, R. (2022). The use of surrogate standards as a QA/QC tool for routine analysis of microplastics in sewage sludge. Science of the Total Environment, 835 doi:10.1016/j.scitotenv.2022.155485

Quynh Nhu Phan Le, Crispin Halsall, Stoyana Peneva, Olivia Wrigley, Melanie Braun, Wulf Amelung, et al. Towards quality-assured measurements of microplastics in soil using fluorescence microscopy. Unpublished manuscript.

Ragoobur, D., Huerta-Lwanga, E., & Somaroo, G. D. (2021). Microplastics in agricultural soils, wastewater effluents and sewage sludge in mauritius. Science of the Total Environment, 798 doi:10.1016/j.scitotenv.2021.149326

Rillig, M. C., & Bonkowski, M. (2018). Microplastic and soil protists: A call for research. Environmental Pollution, 241, 1128. doi:10.1016/j.envpol.2018.04.147

Rose Sinclair. (2014). Textiles and fashion materials, design and technology

Schell, T., Hurley, R., Buenaventura, N. T., Mauri, P. V., Nizzetto, L., Rico, A., et al. (2022). Fate of microplastics in agricultural soils amended with sewage sludge: Is surface water runoff a relevant environmental pathway?*. Environmental Pollution, 293 doi:10.1016/j.envpol.2021.118520

Shan, Y., Lv, M., Zuo, W., Tang, Z., Ding, C., Yu, Z., et al. (2021). Sewage sludge application enhances soil properties and rice growth in a salt-affected mudflat soil Springer Science and Business Media LLC. doi:10.1038/s41598-020-80358-2

Sutton, R., Mason, S. A., Stanek, S. K., Willis-Norton, E., Wren, I. F., & Box, C. (2016). Microplastic contamination in the san francisco bay, california, USA. Marine Pollution Bulletin, 109(1), 230. doi:10.1016/j.marpolbul.2016.05.077

Tagg, A. S., Brandes, E., Fischer, F., Fischer, D., Brandt, J., & Labrenz, M. (2022). Agricultural application of microplastic-rich sewage sludge leads to further uncontrolled contamination. Science of the Total Environment, 806 doi:10.1016/j.scitotenv.2021.150611

van den Berg, P., Huerta-Lwanga, E., Corradini, F., & Geissen, V. (2020). Sewage sludge application as a vehicle for microplastics in eastern spanish agricultural soils. Environmental Pollution, 261 doi:10.1016/j.envpol.2020.114198

van den Berg, P., Huerta-Lwanga, E., Corradini, F., & Geissen, V. (2020). Sewage sludge application as a vehicle for microplastics in eastern spanish agricultural soils. Environmental Pollution (1987), 261, 114198. doi:10.1016/j.envpol.2020.114198

Vollertsen, J., & Hansen, A. (2017). Microplastic in danish wastewater sources, occurrences and fateThe Danish Environmental Protection Agency.

Wang, W., Ge, J., Yu, X., & Li, H. (2019). Environmental fate and impacts of microplastics in soil ecosystems: Progress and perspective. Science of the Total Environment, 708 doi:10.1016/j.scitotenv.2019.134841

Weber, C. J., Santowski, A., & Chifflard, P. (2022). Investigating the dispersal of macro- and microplastics on agricultural fields 30 years after sewage sludge application. Scientific Reports, 12(1) doi:10.1038/s41598-022-10294-w

Weber, C. J., Santowski, A., & Chifflard, P. (2022). Investigating the dispersal of macro- and microplastics on agricultural fields 30 years after sewage sludge application. Scientific Reports, 12(1), 6401. doi:10.1038/s41598-022-10294-w

WRAP. (2012). Valuing our clothes: The evidence base

Yang, J., Li, L., Li, R., Xu, L., Shen, Y., Li, S., et al. (2021). Microplastics in an agricultural soil following repeated application of three types of sewage sludge: A field study Elsevier BV. doi:10.1016/j.envpol.2021.117943

Yang, Y., Li, Z., Yan, C., Chadwick, D., Jones, D. L., Liu, E., et al. (2021). Kinetics of microplastic generation from different types of mulch films in agricultural soil. Science of the Total Environment, 814 doi:10.1016/j.scitotenv.2021.152572

Yang, Y., Ok, Y. S., Kim, K., Kwon, E. E., & Tsang, Y. F. (2017). Occurrences and removal of pharmaceuticals and personal care products (PPCPs) in drinking water and water/sewage treatment plants: A review. Science of the Total Environment, 596-597, 303. doi:10.1016/j.scitotenv.2017.04.102

Yu, Y., & Flury, M. (2021). How to take representative samples to quantify microplastic particles in soil? The Science of the Total Environment, 784, 147166. doi:10.1016/j.scitotenv.2021.147166

Zhang, L., Xie, Y., Liu, J., Zhong, S., Qian, Y., & Gao, P. (2020). An overlooked entry pathway of microplastics into agricultural soils from application of sludge-based fertilizers American Chemical Society (ACS). doi:10.1021/acs.est.9b07905

Zhang, Z., Wu, X., Liu, H., Huang, X., Chen, Q., Guo, X., et al. (2022). A systematic review of microplastics in the environment: Sampling, separation, characterization and coexistence mechanisms with pollutants. Science of the Total Environment, 859 doi:10.1016/j.scitotenv.2022.160151

Zhou, J., Wen, Y., Marshall, M. R., Zhao, J., Gui, H., Yang, Y., et al. (2021). Microplastics as an emerging threat to plant and soil health in agroecosystems. Science of the Total Environment, 787 doi:10.1016/j.scitotenv.2021.147444

# Supporting information

## Transfer and loading of microplastics in sewage sludge amended agricultural soil

Nhu Phan[1], Crispin Halsall[1*], Marco Kunaschk[2], Ben Surridge[1], Lorna Ashton[3], John Quinton[1]

[1]Lancaster Environment Centre, Lancaster University, Lancaster LA1 4YQ, UK

[2] Bavarian Environment Agency (LfU), Demollstrasse 31, Wielenbach 82407, Germany

[3]Department of Chemistry, Lancaster University, Lancaster, LA1 4YQ, UK

**SI1. Literature review on transfer of MPs from sewage sludge to soil**

| | **Countries** | **Soil sampling** | **Extraction method** | **Analytical method** | **Size range** | **MPs conc. in sludge** | **MPs conc. in soil** |
|---|---|---|---|---|---|---|---|
| (Yang, Jie et al., 2021) | China. Three experiment plots inc. control | Multipoint mixed method (2 samples each field, sampling with auger, depth 20cm | Soil (200g aliquot): Air-flow flotation and separation with NaCl (1.2 $g.cm^{-3}$) and organic digestion w $H_2O_2$ 30%.<br><br>Sewage sludge (5g): digestion with Fenton reagents | Stereomicroscope, representative MPs were selected for ATR-FTIR and u-FTIR analysis. | 0.021-4.996 mm | 108.2 ± 51.3 to 441.9 ± 126.0 MPs $g^{-1}$ | 68.6 ± 21.5 to 149.2 ± 52.5 MPs $g^{-1}$ |
| (Tagg et al., 2022) | Germany, two experiment plots inc. control | 8 cores (90cm, 3 portions) per field, combined to total mass of 1kg. | Soil; Sieved to 100um (remove clay), density separation with SPT (1.8 $g.cm^{-3}$) and organic digestion w $H_2O_2$ 30%.<br><br>Sewage sludge: repeated digestion with Fenton reagents, died at 40C, density separation. | Large MPs (> 500 µm) analysis with ATR-FTIR.<br><br>Small MPs analysis with Raman | ≥ 100 µm | 99.7 MPs $g^{-1}$ | 14.6 MPs $g^{-1}$ |
| (Crossman | Canada, four agricultural | Each field ,14-15 core (5x8 corer, sampling to 15cm depth) | Soil (10 $cm^3$) was first subjected to Fenton digestion, followed by 4- | Large MPs (> 300 µm) analysis with ATR-FTIR. | ≥ 50 µm | 8.7-14 MPs $g^{-1}$ | 4 to 541 MPs $kg^{-1}$ |

| | | | | | | | |
|---|---|---|---|---|---|---|---|
| et al., 2020a) | fields inc. control | | time density separation with water and NaI (1.8 $g.cm^{-3}$) | Small MPs analysis with µ-FTIR | | | |
| (van den Berg, P. et al., 2020) | Spain, 16 agricultural fields inc. 5 controls | 4 randomised points at a depth of 0-10 cm and 10-30 cm using a soil auger | Soil (3g) was treated with water and NaI (1.7 g. $cm^{-3}$) for density separation. | Inspection with microscope with heating. 5 frequently found MPs measure with µ-FTIR. | ≥ 50 µm | 50.7 MPs $g^{-1}$ | 2030 ± 1310 to 5190 ± 2630 MPs $kg^{-1}$ |
| (Zhang, Lishan et al., 2020) | China, 3 agricultural fields inc. controls | 5 sampling sites at a depth of 0-5 cm, 5-10 and 15-25 cm | Density separation with saturated $ZnCl_2$ and NaCl, followed by 30% $H_2O_2$ digestion | Optical microscope and µ-FTIR for 114 (from sludge) and 240 (from soil) randomly selected MPs. | | 250 ± 66 MPs $kg^{-1}$ to 5160 ± 305 MPs $kg^{-1}$ | 5 ± 0.4 MPs $kg^{-1}$ to 545.9 ± 45.7 MPs $kg^{-1}$ |
| (Corradini, F. et al., 2019) | Chile, 31 agricultural fields inc. controls | 3 randomised points at a depth of 0-25 cm using a soil auger | Soil (5g) subjected to density separation with NaCl (1.20 g $cm^{-3}$)and $ZnCl_2$ (1.55 g $cm^{-3}$), centrifugation. | Visual inspection with microscope | | 18 to 41 MPs $g^{-1}$ | 1.1 to 3.5 MPs $g^{-1}$ |
| (Schell et al., 2022) | Spain, 3 agricultural plots ($2m^2$) | 5 samples (~ 500g) was taken using 4-cm core (0-5, 5-10 and 10-15cm) | Soil (75g) subjected to two density separation with NaI (1.75 g $cm^{-3}$) followed by digestion with 30% $H_2O_2$<br><br>Sludge (10g) was treated with Fenton, followed by | Visual inspection with stereomicroscope and ATR-FTIR (MPs > 300 µm) and µ-FTIR (50-300 µm) | ≥ 50 µm | 5972 to 7771 MPs $kg^{-1}$ | 138 to 412 MPs $kg^{-1}$ |

| | | | | | | | |
|---|---|---|---|---|---|---|---|
| | | | density separation with water (twice, 1.00 g $cm^{-3}$) and NaI (twice, 1.75 g $cm^{-3}$) | | | | |
| (Weber, Collin J. et al., 2022) | Germany, 2 agricultural fields applied sludge 30 year ago | 2 drilled core (diameter 2cm) from each session. | | Nile-red staining-fluorescence microscopy. | ≥ 300um | | |
| (Ragoobur et al., 2021) | Mauritius, 3 agricultural fields | Random sampling, using 20 × 20 m grids and collecting 40 samples per grid. Sampling (0-10 cm) and (10-20 cm), composite samples for each depth. | Soil (150g) or sludge 20g (wet weight) subjected to two density separation with water & NaCl (1.19 g $cm^{-3}$) followed by digestion with 30% $H_2O_2$ for 7 days | dissecting microscope, 10% of the MPs ≥ 0.5 mm were chosen randomly for ATR-FTIR | ≥ 250um | 276.3 ± 137.3 particles. $L^{-1}$ | 320.0 ± 112.2 and 420.0 ± 244.0 particles.kg- in shallow and deep soils |
| (Yi et al., 2023) | China, experiment plots | Multi-point mixing method, collected topsoil (0–20 cm) and subsoil (20–40 cm) using metal drill | Soil (100g) subjected to $H_2O_2$ 30% digestion followed by density separation with $CaCl_2$ | Fluorescence microscope, Suspicious particles were randomly selected for ATR-FTIR | Study reported particles > 0 µm however 0.45 µm were used for filtration | 200,450 ± 48,874 p kg-1 | 4067 ± 404 p kg-1 MPs in control topsoil and in 2633 ± 161 p kg-1 control subsoil.<br><br>From 4933 ± 620 to 7216 ± 976 |

| | | | | | | | |
|---|---|---|---|---|---|---|---|
| | | | | | | | p kg-1 in sludge-amened topsoil |
| (Adhikari et al., 2023) | US, experiment plot (15 m × 213 m) | Soil was sampled from a 1 m × 1 m area defined by the wooden frame Soil was removed from two different depths (0–5 cm and 5–10 cm), and placed into stainless steel buckets for initial mixing followed by quartering method to take subsamples. | Soil subjected to Fenton digestion followed by density separation with $ZnCl_2$. | A digital microscope was used, followed by particle removal from filters with tweezers. The particles were placed in 2 mL centrifuge tubes with ethanol, then the ethanol was evaporated for LDIR analysis. | . | | 383, 500, and 361 particles/kg dry soil in the 0–10 cm depth of sludge amended soil and 117 particles/kg dry soil in control soil |

**SI2. Waste-water treatment facility description (United Utilities Water Limited 2019)**

The facility can treat up to 412,044 $m^3$ of sludge per year (equating to approximately 412,044 tonnes). There are three operational digesters, with a total storage capacity of 7,900 $m^3$. The sludge treatment facility has a total maximum treatment capacity of 1,128 $m^3$ per day (equating to approximately 1,128 tonnes per day).

The treatment of indigenous sewage sludge arising from the wastewater treatment process comprises:

- Sludge screening (solids separation)
- Sludge thickening
- Enzymic hydrolysis.
- Anaerobic digestion
- Reliquification of imported sludge.
- Disposal of process liquors.
- Odour abatement.
- Sludge dewatering.
- Storage of digestate cake.

From the strain press, the screened sludge is pumped into four enclosed mixing and balancing tanks. The tanks are mainly underground and are lidded. These tanks are extracted to an odour control unit. From the final mixing and balancing tank, the sludge is piped to a wet well and then to two Gravity Belt Thickeners, where the sludge is thickened prior to digestion. The Gravity Belt Thickeners are housed in a dedicated building. Polyelectrolyte is added to the feed tank, it is dosed at a controlled rate and mixes with sludge as it enters onto the belt, the belt moving causes flocculation, the sludge gets thicker as it moves along, and the filtrate drains off via gravity. The thickened sludge passes into a wet well in the GBT building and from there into the thickened sludge tank. This tank is equipped with two mixers and level control. Liquors from the GBT are piped into a combined liquor tank and from here pumped to the head of the works to enter the WwTW flow to full treatment, with no pre-treatment required.

Sludge cake from other WwTW's is imported for further processing. It is temporarily stored (a maximum of one week) on a concrete pad before being fed through a re-liquification unit. Final effluent is used for reliquification. Following this, it joins the thickened sludge from the GBT in the thickened sludge tank.

The thickened sludge can be pre-treated by the Enhanced Enzymic Hydrolysis (EEH) plant prior to anaerobic digestion or treated just by the primary digesters. The EEH Plant is designed to improve pathogen reduction and gas production. There are two potential process routes A or B as described below; process B has been included as a contingency in the event of problems with the primary digestors.

A) The thickened sludge is pumped to the EEH plant. This comprises six reaction tanks, although only five are used. The EEH is a staged process to produce an enhanced treated sludge before passing into three digesters. It is a batch process that increases the

temperature of the sludge initially to 42°C and subsequently to 55°C. The maximum daily throughput is 400 $m^3$/day. The treated sludge passes into a wet well before being pumped into six digested sludge tanks.

B) The thickened sludge is pumped directly to the three digesters. The digested sludge passes into a wet well before being pumped to six digested sludge tanks; all tanks are used if the sludge is not pre-treated by the EEH process.

The digested sludge is pumped to the digested sludge belt press feed tank, where polyelectrolyte is added. It then passes through three belt presses to de-water the sludge and the dry cake is collected on an open outdoor cake pad. The belt presses are housed in a dedicated building. Liquor from the belt press is transferred back into the combined liquor storage tank. Final effluent is used to continually wash the underside of the belts during operation to keep them clean.

The cake pad is impermeable surfaced. Collection vehicles pass through a wheel wash after leaving the cake bay. The cake is spread to land for agricultural benefit

**Table S2:** Biosolid analysis (report from water company)

| **Criteria** | **Unit** | **Concentration** | **Update date** |
|---|---|---|---|
| PH | pH units | 8.46 | 01/12/2020 |
| SOLIDS PER DRY | % | 26.00 | 01/12/2020 |
| NITROGEN TOTAL | g/kg | 46.942 | 01/12/2020 |
| PHOSPHORUS as P | g/kg | 27.714 | 01/12/2020 |
| SULPHUR TOTAL DW | mg/kg | 10692.86 | 01/12/2020 |
| CADMIUM | mg/kg | 0.99 | 01/12/2020 |
| CHROMIUM | mg/kg | 47.31 | 01/12/2020 |
| COPPER | mg/kg | 150.85 | 01/12/2020 |
| LEAD | mg/kg | 91.63 | 01/12/2020 |
| MERCURY | mg/kg | 0.60 | 01/12/2020 |
| MOLYBDENUM | mg/kg | 7.12 | 01/12/2020 |
| NICKEL | mg/kg | 36.87 | 01/12/2020 |
| ZINC | mg/kg | 571.29 | 01/12/2020 |

**SI3. Sampling description**

Four agricultural fields in Lancaster, UK were studied. Three maize fields (Field RF1, Field RF2, and Field RF3) acted as sludge-amended fields, having received biosolids in 2013 and 2021. A fourth control field (grass for animal use) with no biosolids history was selected. Proximity was important to minimize variability in airborne MPs contamination exposure. All sites had loam and sandy loam soils and a clear ridge and furrow pattern. Two non-agricultural fields with no agricultural history for a century were also sampled. All fields were within 1 km of the M6 highway and had flat topography, except Field RF3, which had a slight slope. Fields RF1, RF2, and RF4 are relatively flat, while RF3 has a slight slope. The non-amended field RF4 is at a higher elevation (~75 m) compared to the sludge-amended fields (~50 m on average).


**Figure S1**: Map of sampling sites

For each field, five sampling sites were randomly selected within a 4-meter margin from the edge. At each site, a 50 cm x 50 cm stainless-steel quadrat was used to define the sampling area. Plant residues and stones were then removed manually by using a metal rake. A stainless-steel shovel was used to dig soil down to 20-25 cm to ensure reaching the ploughing depth. Deeper soil was not obtained due to high soil compaction. The soil in the quadrat was thoroughly mixed to a 20 cm depth using the shovel and scoops, from which a subsample of 1-2 kg soil wet weight was taken and stored in 100% cotton bags and kept at 4°C until further soil characterization, including pH, conductivity, organic matter, and particle size analysis. Fields RF2 and RF3 had relatively steep slopes and a clear ridge and furrow pattern. Detailed soil characteristics are described in **Table**S3.

**Table S3: Sampling site description and soil physio-chemical characteristics.**

| Sampling date | Field Area (ha) | Sample code | Latitude | Longitude | Moisture | Temperature | % C | pH | Conductivity (µS/cm) | Particle size analysis | | |
|---|---|---|---|---|---|---|---|---|---|---|---|---|
| | | | | | | | | | | % clay | % silt | % sand |
| 08/06/2023 | 0.59 | HF1-S1 | 54.01365 | -2.779300 | 16.4 | 21.0 | 14.2 | 5.9 | 166 | 28.5 | 45.2 | 26.3 |
| | | HF1-S2 | 54.01408 | -2.779208 | 15.4 | 22.9 | 12.8 | 5.7 | 191 | 19.4 | 27.5 | 53.1 |
| | | HF1-S3 | 54.01400 | -2.779024 | 13.5 | 23.9 | 12.6 | 5.4 | 126 | 18.9 | 35.2 | 45.9 |
| | | HF1-S4 | 54.01400 | -2.779024 | 23.4 | 25.1 | 10.8 | 5.5 | 150 | 23.2 | 39 | 37.8 |
| | | HF1-S5 | 54.01376 | -2.778979 | 30.9 | 24.7 | 13.3 | 5.5 | 222 | 21.7 | 33.3 | 45 |
| 08/06/2023 | 0.19 | HF2-S1 | 54.01325 | -2.774940 | 10.5 | 25.1 | 9.6 | 6.7 | 173 | 18.5 | 31.4 | 50.1 |
| | | HF2-S2 | 54.01333 | -2.774849 | 6.3 | 30.6 | 11.0 | 5.2 | 136 | 17 | 29.6 | 53.4 |
| | | HF2-S3 | 54.01322 | -2.775445 | 9.1 | 30.4 | 10.6 | 5.1 | 117 | 20.9 | 40.7 | 38.4 |
| | | HF2-S4 | 54.01314 | -2.775675 | 10.6 | 31.0 | 10.7 | 5.2 | 137 | 17.4 | 32.5 | 50.1 |
| | | HF2-S5 | 54.01371 | -2.775629 | 7.0 | 28.7 | 10.6 | 5.2 | 125 | 15.8 | 27 | 57.2 |
| 09/08/2023 | 4.31 | RF1-S1 | | | | NA | 8.2 | 7.0 | 147 | 18.9 | 31.8 | 49.3 |

| | | | | | | | | | | | | |
|---|---|---|---|---|---|---|---|---|---|---|---|---|
| | | RF1-S2 | | | | NA | 7.3 | 6.2 | 110 | 14.8 | 17.9 | 67.3 |
| | | RF1-S3 | 54.06444 | -2.774574 | 21.1 | 21.9 | 8.7 | 7.8 | 226 | 12.8 | 26.7 | 60.5 |
| | | RF1-S4 | | | 22.5 | 22.9 | 12.5 | 7.2 | 256 | 20.1 | 35.6 | 44.3 |
| | | RF1-S5 | 54.06518 | -2.774121 | 25.5 | 22.9 | 8.5 | 6.6 | 201 | 20.9 | 39.2 | 39.9 |
| 09/08/2023 | 4.73 | RF2-S1 | | | | NA | 7.4 | 7.1 | 244 | 14.7 | 27.9 | 57.4 |
| | | RF2-S2 | | | | NA | 8.2 | 7.6 | 283 | 19 | 40.8 | 40.2 |
| | | RF2-S3 | 54.06535 | -2.780885 | 13.7 | 25.1 | 7.4 | 7.8 | 168 | 18.4 | 30.4 | 51.2 |
| | | RF2-S4 | 54.06534 | -2.779868 | 17.7 | 25.1 | 7.4 | 7.6 | 190 | 9.79 | 15.61 | 74.6 |
| | | RF2-S5 | 54.06526 | -2.778921 | 25.5 | 22.9 | 7.1 | 6.9 | 219 | 18.1 | 30 | 51.9 |
| 09/08/2023 | 5.56 | RF3-S1 | | | | NA | 9.1 | 7.8 | 272 | 14.7 | 25.6 | 59.7 |
| | | RF3-S2 | | | | NA | 10.9 | 7.3 | 209 | 19.4 | 33.5 | 47.1 |
| | | RF3-S3 | 54.05981 | -2.772535 | 13.0 | 22.7 | 8.7 | 6.9 | 145 | 16.8 | 32.6 | 50.6 |
| | | RF3-S4 | 54.05926 | -2.771941 | 8.6 | 20.9 | 7.9 | 7.0 | 219 | 17.5 | 21.4 | 61.1 |
| | | RF3-S5 | 54.05812 | -2.770844 | 15.5 | 20.0 | 6.4 | 7.7 | 232 | 14.7 | 45.2 | 40.1 |
| 12/10/2023 | | RF4S1 | 54.06019 | -2.766705 | | | | | | | | |
| | | RF4S2 | 54.06077 | -2.767645 | | | | | | | | |
| | | RF4S3 | 54.06126 | -2.766441 | | | | | | | | |

## SI4. Detail of MPs analytical methods

### Sample processing

Soil samples were dried at 40 °C until no more weight loss occurs. Each sample (500-800g, dry weight) was thoroughly mixed and grind using mortar and pestle to break soil aggregates. The soils were then passed onto 500 µm stainless steel mesh. Fractions larger than 500 µm were then manually examined for larger size microplastics. Following homogenization, 50 g subsamples were taken from the soil section smaller than 500 µm.

### Small microplastic extraction from soil

A density separation step was first applied to isolate MPs from soils, which exploits the buoyancy of MPs particles in a higher-density solution of $ZnCl_2$. The Sediment Microplastic Isolation (SMI) unit was utilized as a simple-to-use kit for density separation, with outstanding performance proven in previous studies. (Coppock et al., 2017; Vermeiren, P. et al., 2020) The SMI unit was assembled (with smaller dimensions, **Figure** S4), cleaned, and purged before the introduction of 50 g of soil and 50 mL of $ZnCl_2$. After that, the ball valve was tightly locked, and the SMI was shaken vigorously under an orbital shaker for 2 hours to ensure full contact between the sample and $ZnCl_2$. The valve was then set in the open position, and an additional 200 mL $ZnCl_2$ was added, which was then allowed to settle overnight to allow dense particles to settle out. Once the $ZnCl_2$ solution became apparent, the valve was carefully closed. The supernatant in the headspace was vacuum filtered through a stainless-steel mesh (pore width 25 µm), retaining the zinc chloride for further recycling. The SMI headspace was rinsed thoroughly with HPLC-grade water and ethanol to recover any remaining particles and remove $ZnCl_2$. Stainless steel meshes were then transferred to a 500 mL beaker containing 20 mL of 0.05M $FeSO_4$, followed by 10-minute sonication at room temperature to wash off any particles attached closely. The meshes were then rinsed, removed, and washed carefully for further use. To start the Fenton reaction, 20 mL of $H_2O_2$ was added to the beaker. After 24 hours, the samples were filtered using the same stainless steel meshes. A second digestion was performed if there was residual organic matter on the filter (i.e., soil with OM more than 15%). The filtered fraction was then transferred into the same beaker used for organic digestion and subsequently into a clean 100 mL volumetric flask. A subsample was taken for FPA-µ-FTIR analysis using a glass pipette under magnetic stirring.

### Microplastics extraction from sewage sludge

The sludge sample was freeze-dried prior to analysis. Three subsamples (10-15g each) were taken, weighed, and passed through a 500 µm stainless steel mesh. The fraction larger than 500 µm was screened for large microplastics. Each 1 g portion of the smaller fraction was transferred to a beaker containing 40 mL of 0.05M $FeSO_4$, followed by 40 mL of $H_2O_2$ for overnight Fenton digestion. The solution was then filtered through stainless steel mesh, rinsed with filtered HPLC water and ethanol. The samples settled overnight in a 1.5 g/cm³ $ZnCl_2$ solution in a 200 mL glass separation funnel. The settled part was removed, and the supernatant was vacuum filtered onto 25 µm stainless steel mesh filters and retained for a second Fenton digestion similar to the first Fenton digestion

step. The samples were then filtered on the same stainless-steel mesh, transferred to a 100 mL volumetric flask, and a subsample was taken for FPA-µ-FTIR analysis using a glass pipette under magnetic stirring, similar to the soil processing method.

**Visual and chemical characterization of MPs**

All suspected LMP particles (>500 µm) were further chemically characterized to confirm their plastic composition, using an Agilent Cary 630 ATR-FTIR equipped with a diamond crystal. A total of 32 co-scans were taken for each measurement, at a spectral resolution of 4 $cm^{-1}$. A new background measurement was taken prior to each particle measurement. ATR-FTIR spectra were compared to Specy open-source community spectral library.

For smaller microplastics (25-500 µm), the volume of each subsample was defined based on the microplastic count per ml to ensure particle count did not exceed 70,000 particles larger than 2 µm or 200 particles larger than 70 µm, preventing filter blockage. Particle count was measured using a Syringe Particle Size Analyzer equipped with a laser diode sensor (LDS 30/30) and evaluation software (SW-PE). The system measures particle sizes between 2 and 600 µm. Samples were stirred magnetically at a medium speed during measurement, with 1 mL for rinsing followed by three 1 mL measurements, averaging less than 1 minute per sample. Mean values of three replicates were used.

Afterward, prepared samples were filtered on 25 mm Anodiscs™ (Whatman™, PP-supported, 0.2 µm pore size) and analyzed via focal plane array (FPA-) micro-Fourier-transform infrared spectroscopy (µ-FTIR). A Bruker Hyperion 3000 FTIR microscope with a 64×64-pixel FPA detector and Bruker Tensor 27 FTIR spectrometer was used for imaging in transmission mode. Filters were placed on $CaF_2$ windows (25 mm diameter, 2 mm thickness, Korth Kristalle, Germany). The entire surface of the filter was scanned using a 3.5× IR objective. Spectra were collected with a coaddition of 32 scans at an 8 $cm^{-1}$ resolution and a measuring range between 1250 and 3600 $cm^{-1}$. Pixel sizes of the measured data were about 11 µm. Imaging data were then compared against a reference database using siMPle (v. 1.0.1).

**Table** S4: MPs in 13 Procedural Blanks. Blank sub-volumes were 9.5-10 mL, and the values below have been extrapolated to a 100 mL volumetric flask, corresponding to the whole procedures used for the extraction of ~50 g soil samples.

| Blank ID | Extrapolated MPs in 100mL | | | | | | | | | | | |
|---|---|---|---|---|---|---|---|---|---|---|---|---|
| | PE | PEST | PP | acrylic resin | PS | ABS | Polyurethane-acrylic resin | SBR | PVC | PMMA | PLA | PA |
| CF1 BLANK | 20 | 0 | 0 | 0 | 0 | 0 | 0 | 0 | 0 | 0 | 0 | 0 |
| CF1 BLANK 2 | 0 | 10 | 0 | 0 | 20 | 0 | 0 | 0 | 10 | 0 | 0 | 0 |
| CF2 BLANK | 0 | 0 | 10 | 0 | 0 | 0 | 0 | 0 | 0 | 0 | 0 | 0 |
| CF3 BLANK | 0 | 10 | 0 | 0 | 0 | 0 | 0 | 0 | 0 | 0 | 0 | 0 |
| HF1 BLANK | 20 | 40 | 30 | 0 | 0 | 0 | 0 | 0 | 0 | 0 | 0 | 0 |
| RF1 BLANK | 0 | 10 | 0 | 0 | 20 | 0 | 0 | 0 | 0 | 0 | 0 | 0 |
| RF1 BLK 2 | 10 | 0 | 0 | 0 | 0 | 0 | 0 | 0 | 20 | 0 | 0 | 0 |
| RF2 BLANK | 0 | 10 | 10 | 0 | 0 | 0 | 0 | 0 | 0 | 0 | 0 | 0 |
| RF2-BLK2 | 0 | 20 | 10 | 0 | 0 | 0 | 0 | 0 | 0 | 0 | 0 | 0 |
| RF3 BLANK | 0 | 10 | 42 | 0 | 0 | 0 | 0 | 0 | 0 | 0 | 0 | 0 |
| RF3-BLK 2 | 0 | 0 | 10 | 0 | 0 | 0 | 0 | 0 | 0 | 0 | 0 | 0 |
| RF4 BLANK 1 | 0 | 10 | 0 | 0 | 0 | 0 | 0 | 0 | 0 | 0 | 0 | 0 |
| RF4 BLK 2 | 0 | 30. | 10 | 0 | 0 | 0 | 0 | 0 | 0 | 0 | 0 | 0 |

| | | | | | | | | | | | | |
|---|---|---|---|---|---|---|---|---|---|---|---|---|
| average | 3.8 | 11.6 | 9.4 | 0 | 3.1 | 0 | 0 | 0 | 2.3 | 0 | 0 | 0 |
| stdev | 7.7 | 12.1 | 13.0 | 0 | 7.5 | 0 | 0 | 0 | 6.0 | 0 | 0 | 0 |
| LOD | 26.9 | 48.0 | 48.4 | 0 | 25.6 | 0 | 0 | 0 | 20.3 | 0 | 0 | 0 |

**Table S5: Overall microplastics concentrations in sewage sludge, sludge amended agricultural soil, non-amended agricultiural soil and non-agricultural soils.**

| | Anaerobically digested sewage sludge | | Sludge-amended soil | | Non-amended agricultural soil | | Non-agricultural soil | | Cumulated load | | Cumulated load | |
|---|---|---|---|---|---|---|---|---|---|---|---|---|
| | MPs.g$^{-1}$ | µg.g$^{-1}$ | MPs.g$^{-1}$ | µg.g$^{-1}$ | MPs.g$^{-1}$ | µg.g$^{-1}$ | MPs.g$^{-1}$ | µg.g$^{-1}$ | MPs. g$^{-1}$ | µg.g$^{-1}$ | MPs.ha$^{-1}$ | kg.ha$^{-1}$ |
| Total | 3650±2100 | 560±310 | 39±27 | 5.4±9.3 | 9.6±4.4 | 1.3±1.4 | 17±13 | 5.3±9.4 | 11.0 | 1.57 | 3.65E+10 | 5.67 |
| Particle | 3010±1900 | 300±140 | 34±21 | 2.4±2.6 | 8.0±3.0 | 0.4±0.2 | 12±9 | 1.9±2.2 | 9.2 | 0.84 | 3.05E+10 | 3.04 |
| Elongated particle | 630±200 | 250±280 | 5±7 | 3.0±8.8 | 1.6±1.7 | 0.9±1.3 | 4±6 | 3.5±7.8 | 1.9 | 0.70 | 6.38E+09 | 2.53 |

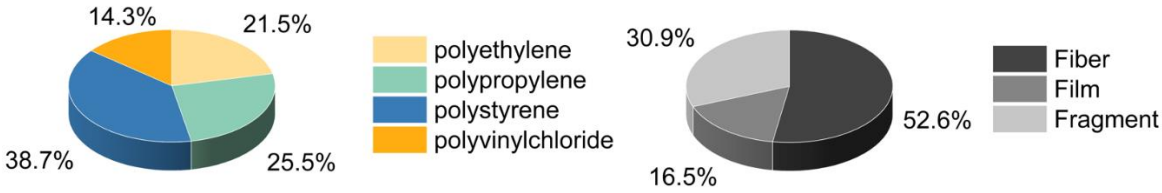


**FigureS2**: (a) Polymer composition of LMPs in sludge-amended agricultural fields from ATR-FTIR data, and (b) the proportion of plastics classified by shape (fibre, film, and fragment).

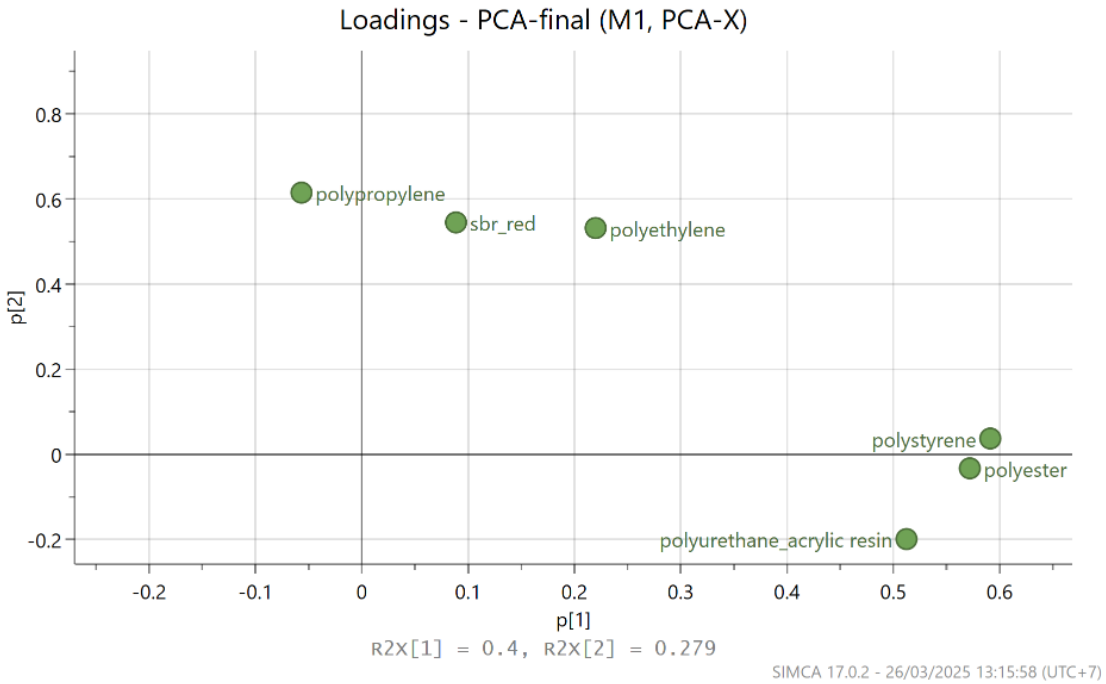


**Figure S3:** Loadings plot from principal component analysis (PCA) based on plastic type concentrations, generated using SIMCA software 17.0.2.

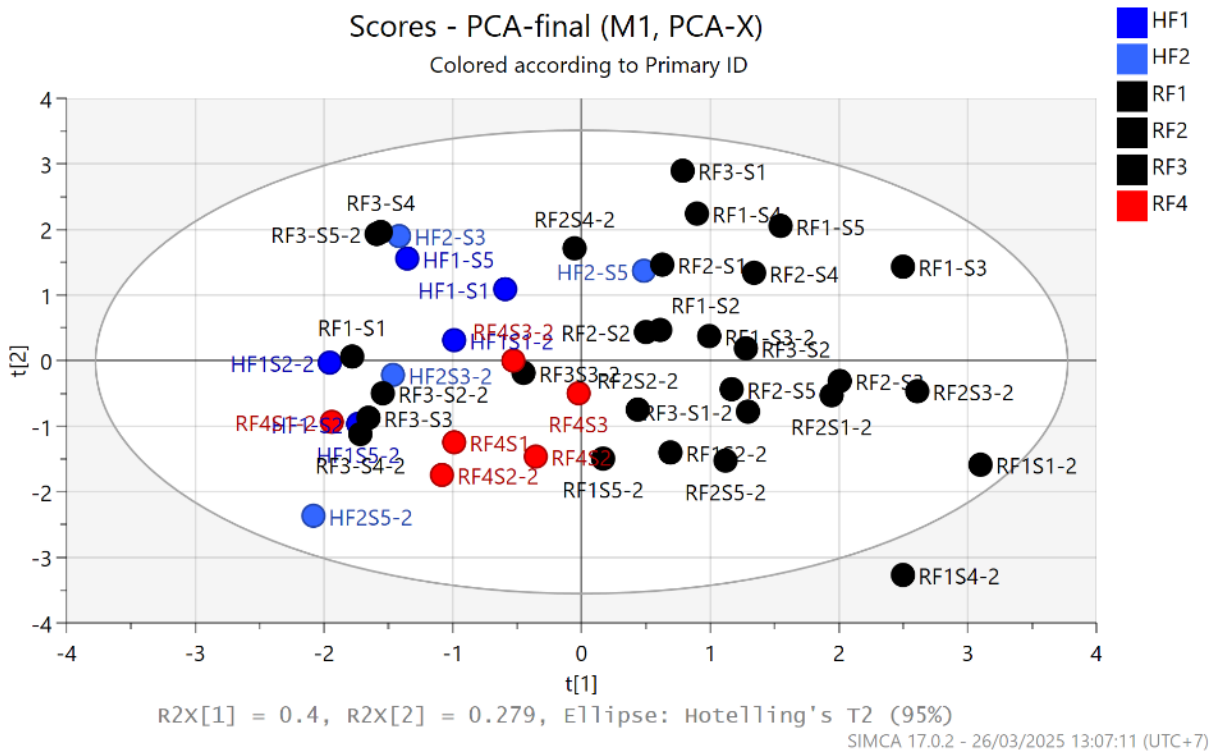


**Figure S4:** Loadings plot from principal component analysis (PCA) based on plastic type concentrations, generated using SIMCA 17.0.2 software.

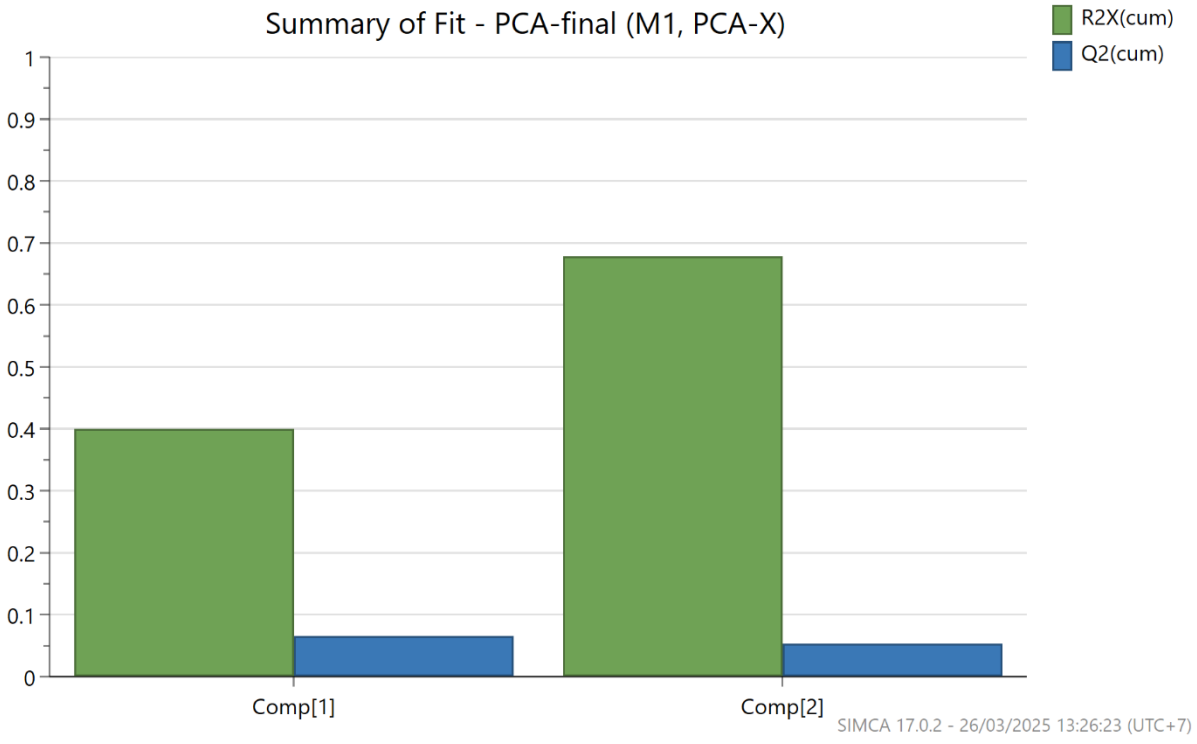


**Figure S5:** Summary of model fit from principal component analysis (PCA) based on plastic type concentrations, generated using SIMCA 17.0.2 software.

# 5 Biosolid amendments as drivers for microplastic pollution in soils: Measurements and insight from multiple analytical methods in an agricultural field study

*Anaerobic digestate (AD), increasingly used as a sustainable fertilizer, has been identified as a potential source of microplastics (MPs) in agricultural soils. This chapter provides the first comprehensive quantification of MPs as small as 25 µm in AD and soils historically amended with sewage sludge and currently treated with AD. It examines MPs concentrations, polymer composition, and particle morphology, revealing contributions from both past and present biosolid applications. Additionally, fluorescence microscopy (FM), µ-FTIR, and µ-Raman spectroscopy are compared for MPs detection, highlighting differences in their sensitivity to particle sizes and types.*

# Biosolid Amendments as Drivers for Microplastic Pollution in Soils: Measurements and Insights from Multiple Analytical Methods in an agricultural field study

Quynh Nhu Phan Le[1], Crispin Halsall[1*], Marco Kunaschk[2], Ben W.J. Surridge[1], Lorna Ashton[3], John Quinton[1]

[1]Lancaster Environment Centre, Lancaster University, Lancaster LA1 4YQ, UK

[2] Bavarian Environment Agency (LfU), Demollstrasse 31, Wielenbach 82407, Germany

[3]Department of Chemistry, Lancaster University, Lancaster, LA1 4YQ, UK

Corresponding author:Crispin Halsall (c.halsall@lancaster.ac.uk)

## Abstract

Microplastic (MPs) pollution in agricultural soils is a growing environmental concern. Anaerobic digestate (AD), derived from agricultural waste such as animal manure and increasingly used as a sustainable fertilizer, has been identified as a potential MPs source. This study provides the first comprehensive quantification of MPs as small as 25 µm in AD and soils treated with AD and historically applied sewage sludge—practices that reflect current agricultural trends. Average MPs in AD were measured at 1030 ± 390 MPs/g and comprised predominantly of polyethylene (47.1%) and styrene-butadiene rubber (32.3%). Most MPs were particle-like (64.7%), with nearly half (47%) measuring 25–50 µm (dia.). Amended soils showed significantly higher MPs concentrations (50.8 ± 36.4 MPs/g) than non-agricultural control soils (15.5 ± 13.1 MPs/g, $p<0.001$), with their MPs profile reflecting contamination from both historical sludge and current AD applications. To evaluate detection methods, fluorescence microscopy (FM), Fourier-transformed infrared micro-spectroscopy (µ-FTIR), and manual Raman micro-spectroscopy (µ-Raman) were compared. While FM and µ-FTIR yielded similar overall MPs concentrations, FM detected significantly more fibres, followed by µ-FTIR, while µ-Raman identified the lowest fibre concentrations. These findings highlight the dual contribution of past and present biosolid applications to soil MPs pollution and emphasize the importance of selecting appropriate analytical detection methods based on study objectives and sample characteristics.

# 5.1 Introduction

Microplastic pollution in agricultural soils has emerged as a growing environmental concern. Microplastics (MPs), defined as plastic particles measuring between 1 µm and 5 mm, enter soils through various pathways, including the application of biosolids as fertilizer, the use of plastic mulch, and irrigation with MPs-contaminated water sources as part of agricultural practices (Bläsing & Amelung, 2017b). Once present in the soil, MPs can alter soil structure, reduce water retention capacity, and impede root development and nutrient uptake in plants, ultimately leading to potential incorporation into the food chain (De Souza Machado et al., 2018, 2019; Kim et al., 2021; Meng et al., 2021; Wang, Wenfeng et al., 2019). Additionally, MPs can adsorb and transport other environmental contaminants, such as pesticides and heavy metals, thereby exacerbating their negative impacts on soil health and crop quality (Antunes et al., 2013; Zhou, Y. F. et al., 2019). As the accumulation of MPs in agricultural soils continues, better understanding of their source and fate is essential to preserving soil fertility and ensuring sustainable food production.

The use of anaerobic digestate (AD) from animal manure, produced by biogas and green gas plants, is gaining attraction as a sustainable alternative or supplement to inorganic fertilizers in agriculture. This trend is driven by rising demand for meat and dairy, resulting in significant manure production, with nitrogen levels reaching 128 million tonnes in 2019 (FAO, 2022).(FAO, 2022).

MPs have been detected in AD from biogas plants processing agricultural waste, including animal manure and energy crops, with concentrations ranging from 0 to 22.79 MPs/kg, predominantly in the larger size range of 1–5 mm (Porterfield et al., 2023; Steiner et al., 2022; Weithmann et al., 2018). Animal manure often contains plastic fragments from farming operations, which may not fully degrade during the digestion process ((Wu, R. et al., 2021). Consequently, the application of AD as fertilizer can systematically introduce MPs into agricultural soils ((Yang, Jie et al., 2020a). Moreover, before the widespread use of AD in recent decades, agricultural fields often received other amendments, such as sewage sludge from wastewater treatment plants, further contributing to plastic pollution. Despite this, the transfer and occurrence of plastics from these agricultural practices to soil remain poorly understood. The scarcity of data on MPs transfers from digestate and other soil amendments, particularly for smaller plastics (<500 µm), is partly due to the analytical challenges of analysing complex media like soil and organic fertilisers (Möller et al., 2022). Addressing these challenges required extensive adaptations to analytical methods, enabling the processing of large sample sizes while maintaining accuracy in MPs detection at smaller size range, e.g., down to 25 µm.

Analysing MPs pollution in soils remains challenging due to the complex nature of soils, which contain various interfering materials, and the diverse characteristics of plastics, such as variations in size, shape, and polymer type (Thomas et al., 2020b). Additionally, the wide range of analytical techniques employed across studies complicates comparisons and prevents consistent conclusions (Peneva et al., 2024). Among particle-based methods, Fourier-transform infrared (FTIR) and Raman micro-spectroscopies, as well as

fluorescence microscopy (FM), are the most commonly used, each with distinct advantages and limitations (Ivleva, 2021). Discrepancies between these methods have been observed, often attributed to false positives, while some remain unexplained. For instance, inconsistencies between Nile Red (NR) staining-FM and FTIR analyses can largely be attributed to the limited specificity of NR and the lower sensitivity of FTIR (Ivleva, 2021). Moreover, results can vary even within a single method, as demonstrated by Moses et al., who reported differences in FTIR outcomes when using different library-matching software (Moses et al., 2023).

Direct comparisons between these methods, particularly using identical sample sets, remain rare. When such comparisons occur, most studies validate fluorescence-detected particles with FTIR or Raman but seldom perform the reverse, limiting a full understanding of each method's strengths and weaknesses (Erni-Cassola et al., 2017; Shim et al., 2016b). Additionally, many comparison studies rely on tailored extraction protocols in interlaboratory settings, prioritizing broader method recovery over accuracy of analytical technique (Peneva et al., 2024). Moreover, while spiked samples are commonly used for comparisons, applying these methods to environmental samples introduces greater variability in plastic detection and more complex matrix interferences. This study addresses this gap by systematically comparing different methods on identical environmental samples, overlaying the results to provide a more comprehensive understanding of each method's strengths and weaknesses.

In this study, we provide the first assessment of MPs content in the smaller size fraction (down to 25 µm) within AD derived from agricultural waste, primarily animal manure, used in a biogas energy production plant. Additionally, we analysed MPs in agricultural soils treated with this AD. The transition from historical reliance on sewage sludge to farm-produced AD offers a unique case study. It highlights MPs pollution stemming from both past and current biosolid applications, enhancing our understanding of plastic contamination in agricultural soils from this shift. We hypothesize that (1) MPs are present in animal manure-derived AD and contribute to soil microplastic pollution and (2) historical applications of sewage sludge have caused long-term plastic accumulation in agricultural soils, further exacerbating soil pollution. Simultaneously, we compare the performance of FTIR micro-spectroscopy, fluorescence microscopy and Raman micro-spectroscopy (only for fibre analysis) in measuring MPs in environmental samples using a subset of biosolid-amended soils. The aim of utilizing these different instrumental methods is to fully capture the array of MPs present in digestate and soils, and to reduce limitations and hence bias associated with using only one measurement technique. These findings underscore the critical need for careful method selection and a deeper understanding of the analytical challenges associated with complex matrices like soil.

# 5.2 Materials and methods

## 5.2.1 Anaerobic digestate and soil sampling

In July 2023, approximately 2 kg of solid anaerobic digestate was collected from a local biogas plant in northwest England, UK. The digestate was produced in a mesophilic, single-stage digester with a retention time of 50 days. The feedstock includes livestock and poultry manure co-digested with food waste such as cereal flour, potatoes, bird feed, wet grain, rice bran, and whey. After digestion, the AD was separated into liquid and solid

fractions using a screw press. The liquid fraction is stored in covered lagoons, while the solid fraction is stored in an uncovered open area. The solid digestate samples, containing 24.4% dry matter, were collected in PET bottles, homogenized, freeze-dried, and subdivided into three 1 g subsamples for microplastic analysis. Further details on the characteristics of the AD are provided in the supplementary information (SI).

Soil samples were collected from grass fields owned by the same business/farm as the biogas production plant. Three of these fields had a history of liquid sewage sludge application spanning over a decade, from 2004 to 2014, with an average total application rate of 488.7 $m^3$/ha (3.12% dry matter). Since 2014, these fields have been treated with self-produced liquid digestate. These soils are referred to as biosolid-amended soils. For comparison, two additional grass fields (HF1 and HF2) with no history of agricultural activity for over a century were sampled to serve as non-agricultural background soils.

Three to five soil samples (2–5 kg each) were randomly collected from each field, avoiding a 4-meter margin along field borders, and stored in cotton bags (**Figure** S1). The sampling volume was determined based on simulations by Yu and Flury et al. (2021), which estimated the elementary volume required to obtain representative sampling, considering expected MPs concentrations and the method's limit of detection (LOD), as discussed in detail elsewhere (Phan Le et al., in preparation, see **Chapter 4**). Samples were collected from a depth of 0–20 cm within 50 × 50 cm quadrats, and thoroughly mixed using a stainless-steel shovel and dried at 40°C for subsequent microplastic analysis (see SI3). Laboratory analyses included measurements of pH, electrical conductivity, soil organic matter (SOM) content, and soil texture. Details on soil physiochemical characteristics are described in table S1.

## 5.2.2 Microplastic extraction

Each anaerobic digestate (10–15 g) and soil (600–800 g) sample was homogenized and sieved through 500 µm stainless steel sieve. Large microplastics (LMPs, 500–5000 µm) were manually collected using tweezers and analysed via Agilent Cary 630 ATR-FTIR. LMPs were classified as fragments (irregular particles from material breakdown), films (soft, thin polymers from items like bags and wrapping materials), and filaments (>50 µm, thread-like plastics from fragmentation of ropes or fishing lines).

The extraction of SMPs from soil followed the method in Phan Le et al. (in preparation, **see chapter 4**) (**Figure** 5.1.). Briefly, 50 g of 500 µm-sieved soil underwent overnight density separation using a $ZnCl_2$ solution ($\rho$=1.5 g/$cm^3$) in a sediment-microplastic isolation (SMI) unit (Coppock et al., 2017). The supernatant was filtered through a 25 µm stainless-steel mesh, rinsed with HPLC-grade water and ethanol, sonicated for 10 minutes, and treated with Fenton's reagent (20 mL $H_2O_2$ and 20 mL 0.05M $FeSO_4$). A second density separation with $ZnCl_2$ solution was performed, and for samples with >15% OM, an additional Fenton's reagent digestion was included. The final extract was filtered, rinsed, and diluted to 100 mL with HPLC water in a volumetric flask.

To address the higher OM content in AD samples, a modified extraction method was developed in this study. Freeze-dried AD samples (1 g, sieved to 500 µm, n = 3) were initially treated with Fenton's reagent and subjected to density separation using $ZnCl_2$

solution in a 250 mL glass separation funnel. The process included a second Fenton digestion, filtration, rinsing, and final dilution with HPLC water, with aliquots prepared for further analysis. Full procedural details are provided in SI.

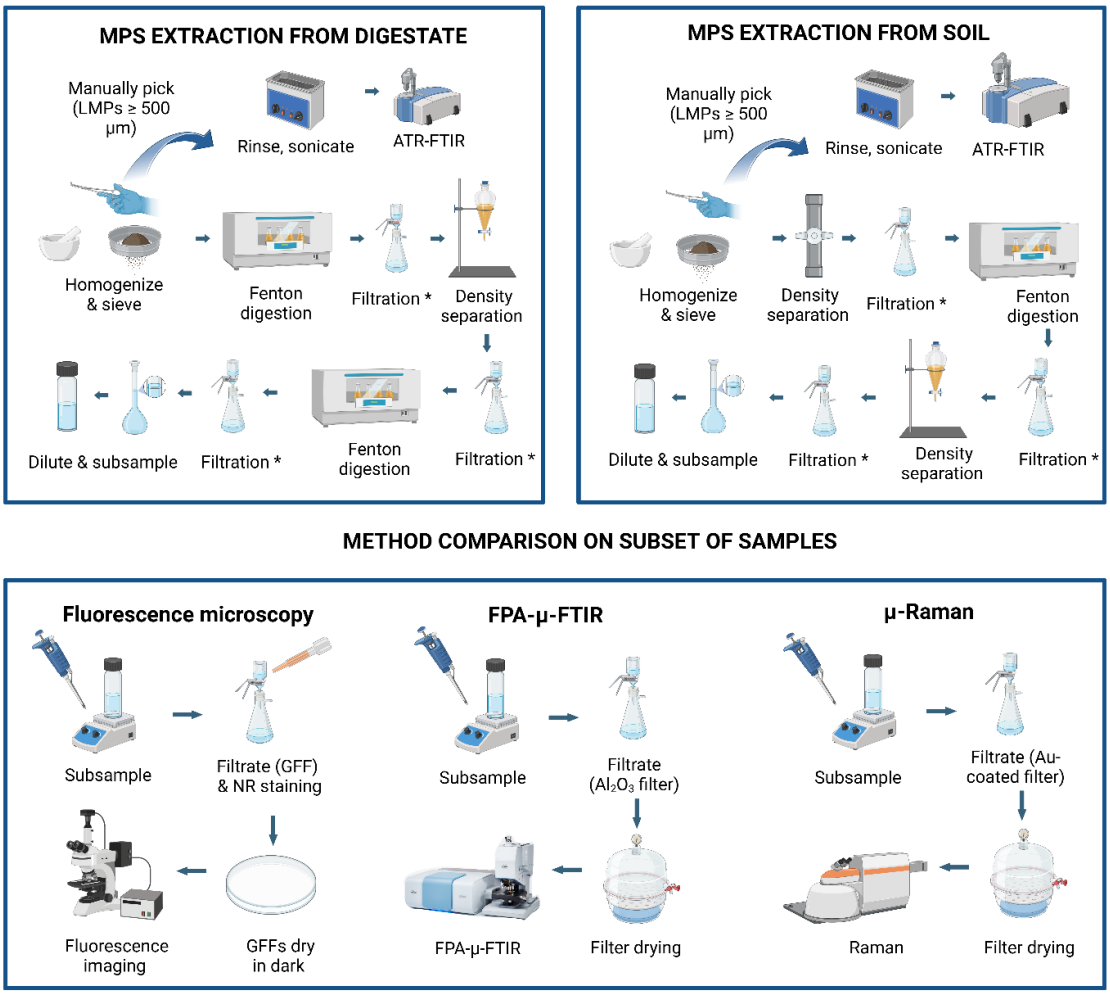


**Figure 5.1.** A schematic of the extraction protocol for MPs from digestate and soil samples, along with the analytical methods used for comparison. The bottom panel showcases images obtained using different techniques—colour, fluorescence, and u-FTIR—along with an overlay of these images for the same sample filter.

For all AD and soil samples, duplicate subsamples (0.3–0.4% of the total extract volume for AD or 0.3–8.7% for soil) were taken from each 100 mL aqueous extract using a 5 mL glass pipette for SMP analysis via FPA-µ-FTIR (Section 2.3.1). Subsample volumes were determined based on particle counts to ensure they remained below 70,000 particles >2 µm or 200 particles >70 µm, avoiding filter blockage. Particle counting was performed using a Syringe Particle Size Analyzer (Markus Klotz GmbH, Germany).

For method comparison, subsamples from a subset of samples were analysed using fluorescence microscopy (FM) and Raman micro-spectroscopy. For FM, 15–20% of the extract volume (100 mL) was filtered onto glass fibre filters (GFF, 0.7 µm pore size, 47-mm Ø, Cytiva Whatman GF/F, Fisher Scientific, UK), stained with 5 mg $L^{-1}$ Nile Red (NR, $C_{20}H_{18}N_2O_2$, 99%, Acros Organics, UK), rinsed with hexane (≥95%, Fisher Scientific, UK), and dried in the dark (Phan Le et al., 2025, see Chapter 2). For Raman analysis, 1.5–3.5% of the extract volume was filtered onto gold-coated polycarbonate filters (0.2 µm pore size, 25-mm Ø, APC GmbH, Germany).

## 5.2.3 Identification and characterisation of microplastics

### 5.2.3.1 Fourier transformed infrared spectroscopy

For SMPs, prepared aliquot samples were filtered onto 25 mm Anodisc™ (Whatman™, 0.2 µm pore size) and analysed using FPA-µ-FTIR. Imaging was performed in transmission mode with a Bruker Hyperion 3000 FTIR microscope equipped with a 3.5× IR objective, a 64×64-pixel FPA detector, and a Bruker Tensor 27 FTIR spectrometer. The entire filter surface was scanned, collecting spectra with 32 scans at a resolution of 8 $cm^{-1}$ across the wave number range of 1,250 to 3,600 $cm^{-1}$. Spectra were processed using OPUS 8.5 software, with automatic MPs identification and quantification performed using siMPle software. All assigned spectra were manually inspected to confirm accurate library matches in terms of a matching index and signal to noise ratio. SMPs were further classified based on aspect ratio into particle-like SMPs and elongated (fibre-like) SMPs, defined as having an aspect ratio of 3:1 or higher. Further details of this method are provided in SI.

### 5.2.3.2 Fluorescence microscopy for SMP analysis

Fluorescence microscopy was performed with a Zeiss Axio Zoom.V16 microscope equipped with a macro lens, 12 MPs camera, and automated stage. NR-stained samples were illuminated at 470 nm and observed through a green filter set (emission 524/50 nm) in a darkroom. Images were captured in green fluorescence at 50× magnification using Zen Pro software for stitching and surface focusing. Particle recognition and quantification followed the method of Phan Le et al. (Phan Le et al, 2025, see Chapter 2) using Fiji-ImageJ 1.53t. Briefly, background noise was reduced with a Gaussian blur filter, particles were segmented via global thresholding and classified by Feret's diameter.

An overlay of FM image, colour (RBB) images, and FTIR results, with pixels identified as plastics by siMPs software, was created using Zen Pro software.

#### 5.2.3.3 Raman microscopy for fibre analysis

Raman analysis was performed using a Renishaw InVia micro-spectrometer (Renishaw plc, UK) equipped with a 532 nm laser (15 mW at the sample) and a 50x objective lens (numerical aperture NA 0.50). Raman spectra of suspected fibres were manually collected in the 100-3500 $cm^{-1}$ range using a 2400 lines per millimetre grating, resulting in a spectral resolution of approximately 1 $cm^{-1}$. All measurements were conducted with 5 accumulations at 5% laser power. After collection, each spectrum was processed for cosmic ray removal using Wire 4.2 and baseline correction with Spectragryph version 1.2.15. Raman spectra were subsequently analysed with Open Specy for spectral library matching (Cowger et al., 2021).

### 5.2.4 Quality assurance and quality control

Strict quality control measures were implemented to prevent contamination from ambient air, clothing, chemicals, or laboratory tools. Non-plastic equipment was used whenever possible, cleaned with HPLC water and acetone, and covered with clean aluminium foil. Stainless steel filters, GFFs, and glassware were baked at 500°C for 4 hours before use. Sample handling was conducted in a cleaned fume hood, with researchers wearing 100% cotton lab coats and nitrile gloves. Reagents including $ZnCl_2$, 30% $H_2O_2$, 0.05M $FeSO_4$ solution were filtered through GFFs prior to use. Procedural blanks (n=13) underwent all extraction steps to monitor contamination.

The extraction method has been tested in terms of LOD and MPs extraction recovery and detailed elsewhere (Phan Le et al, in preparation, see Chapter 4). LODs were 26.9 particles for PE, 48.0 particles for PEST, 48.4 particles for PP, 25.6 particles for PS, and 25.3 particles for PVC. High recovery rates (93 ± 20%) were observed for Cospheric polyethylene microspheres (100-125 µm in diameter) standards using the methods reported here.

### 5.2.5 Statistical analysis

To evaluate the statistical significance of variations in soil MPs concentrations, normality and homogeneity of variance were assessed using the Shapiro-Wilk and Levene's tests, respectively. For independent data meeting the criteria for parametric testing, ANOVA was performed. For data not meeting these criteria, the Mann-Whitney U test was employed. The Wilcoxon Signed-Rank Test was used to compare MPs concentrations obtained using different methods for the same sample set when the data were normally distributed; otherwise, repeated-measures ANOVA was applied. In all cases, statistically significant differences were defined at p-value $\leq 0.05$.

## 5.3 Results

### 5.3.1 Microplastics in anaerobic digestate

The average concentration of MPs (dia. >= 25um) in AD was 1030 ± 390 MPs/g. Among the polymers detected, the majority were polyethylene (PE, 47.1%) and styrene-butadiene rubber (SBR, 32.3%), with smaller amounts of polypropylene (PP), acrylonitrile butadiene styrene (ABS), and polyamide (PA) (**Figure** 5.2.). Of these, 64.7% were

particles, while 35.3% were fibres. Fibres were found in PA, SBR, and PE. In terms of size distribution, most of the MPs detected fall within the 25-50 µm range (47%), followed by those in the 50-100 µm range (36.8%), and a smaller proportion between 100-200 µm. No MPs larger than 200 µm (in Feret diameter) were detected in the AD samples.

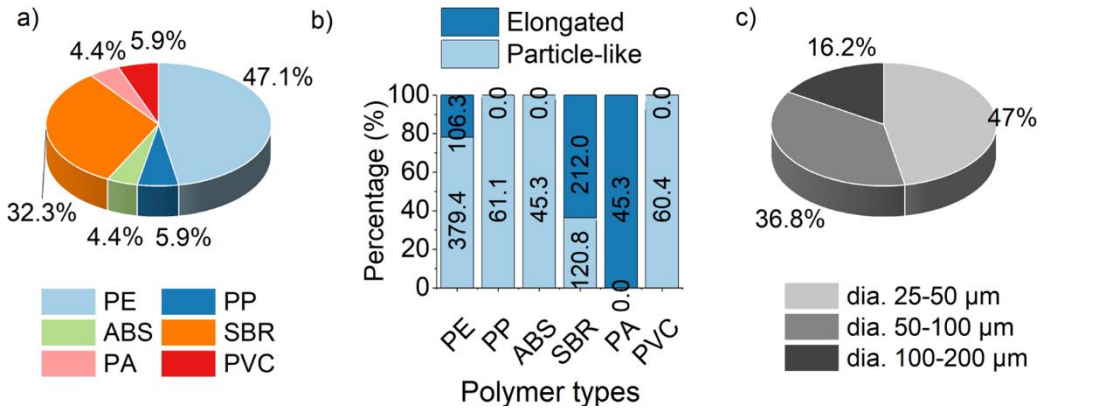


**Figure 5.2.** MPs characteristics of AD measured by FPA-µ-FTIR. **Figure** 5.2a presents the proportion of each polymer detected. **Figure** 5.2b illustrates the distribution of particle shapes for each polymer type, with the numbers on the columns representing the concentration (MPs/g) for each shape. **Figure** 5.2c shows the proportion of each size class based on the Feret diameter of the detected MPs.

## 5.3.2 Microplastics in digestate-amended soil

The biosolid-amended soil had an average MPs concentration of 50.8 ± 36.4 MPs/g, significantly higher than the non-agricultural background soil with an average concentration of 15.5 ± 13.1 MPs/g (Mann-Whitney U test, $p < 0.001$) (**Figure** 5.3.). The comparison between the two reveals differences in polymer composition, particle shapes, and size distributions. In background soil, PE dominates at 51.2%, followed by SBR at 18.6%, with smaller contributions from other polymers. In contrast, biosolid-amended soil shows a higher proportion of PE (68.5%), with reduced levels of SBR (3.5%) and other polymers like PP, PA, polyester (PEST), etc. Regarding particle shape, the background soil had a higher proportion of elongated particles, especially for PE (26.8%), while the biosolid-amended soil exhibited fewer elongated particles (19% for PE), with particle-like shapes predominating in both soils. In terms of particle size distribution, the background soil contained more MPs in the 25-50 µm range (45.6%), with smaller proportions in the 50-100 µm (35.9%) and 100-200 µm (14.3%) ranges, and very few particles >200 µm (4.2%). In biosolid-amended soil, larger-sized MPs were more prevalent, with the 50-100 µm range accounting for 54.3%, followed by 25-50 µm (24.5%), 100-200 µm (12.9%), and >200 µm (8.3%).

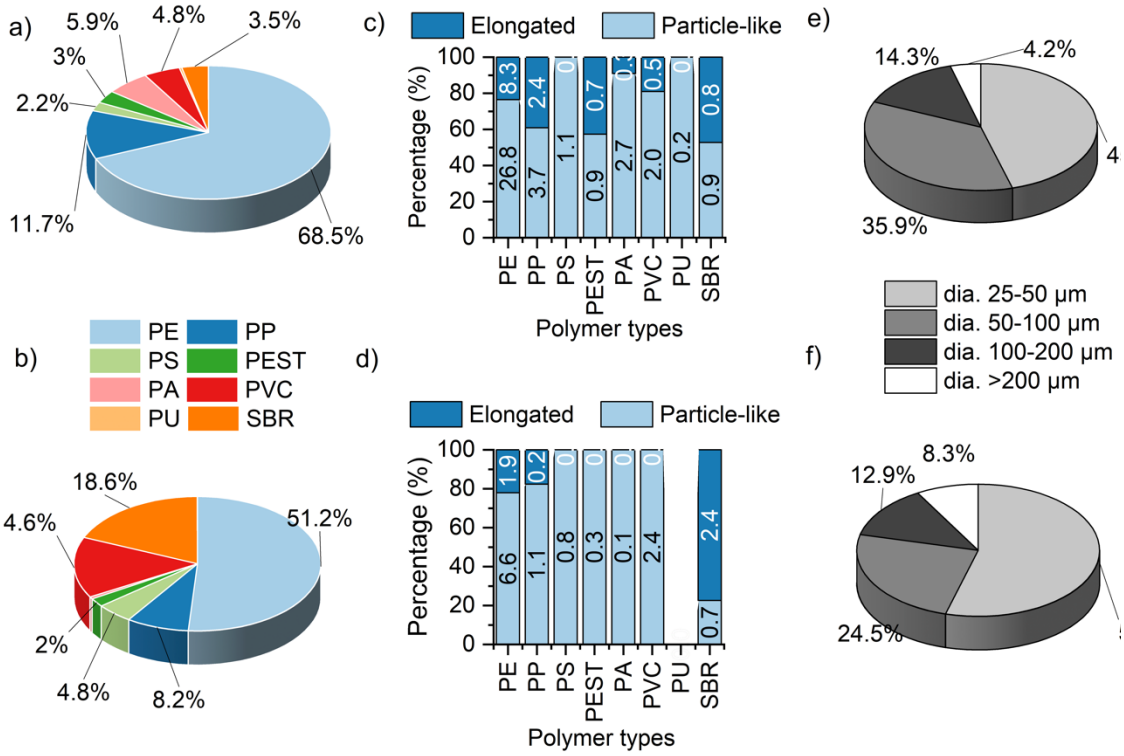


**Figure 5.3.** Polymer composition, shape, and size distribution of microplastics in biosolid-amended soil (a, c, e) and background soil (b, d, f). Pie charts (a, b) show the proportion of polymers detected. Bar charts (c, d) illustrate the proportion of elongated versus particle-like microplastics across polymer types, with the numbers on the columns representing the concentration (MPs/g) for each shape. Pie charts (e, f) represent the size distribution of the detected MPs based on their Feret diameters.

### 5.3.3 Comparison between fluorescence microscopy and FTIR

All samples were analysed using µ-FTIR, while a randomly selected subset was also analyzed using FM to facilitate method comparison. Overlaying FM and FTIR images of the same sample revealed discrepancies in particle detection between the two techniques. µ-FTIR identified 83 particles larger than 25 µm, whereas FM detected 101 particles above this size threshold. However, only 18 particles were detected by both methods, representing 22% of the particles identified by FTIR and 18% of those detected by FM. These findings highlight the methodological limitations of both techniques, including the potential for false positives and false negatives in particle identification (**Figure** 5.4.).

While some MPs were identified by both FTIR and FM (**Figure** 5.4a), discrepancies arose where MPs were detected by only one method or missed entirely. For instance, spiked fluorescent 'Cospheric' micro spheres serving as the surrogate standard (dia. 100–125 µm) were not detected by FPA-µ-FTIR. Similarly, certain synthetic fibres were identified using FM and later confirmed by Raman spectroscopy but were not detected by FTIR (**Figure** 5.4b). On the other hand, some MPs identified by FTIR as PE, PS and PEST failed to fluoresce under Nile Red staining or fluoresced too weakly to stand out from the background or SOM interferences. As a result, these MPs were missed by FM when specific image analysis pipelines were applied (**Figure** 5.4d). In addition, some fibres

detected by µ-FTIR appeared to have fragmented into multiple smaller fibres or particles, leading to potential over-quantification of MPs. µ-FTIR also failed to fully detect MPs, resulting in inaccurate size and shape estimations when only partial particles were identified (**Figure** 5.4d).

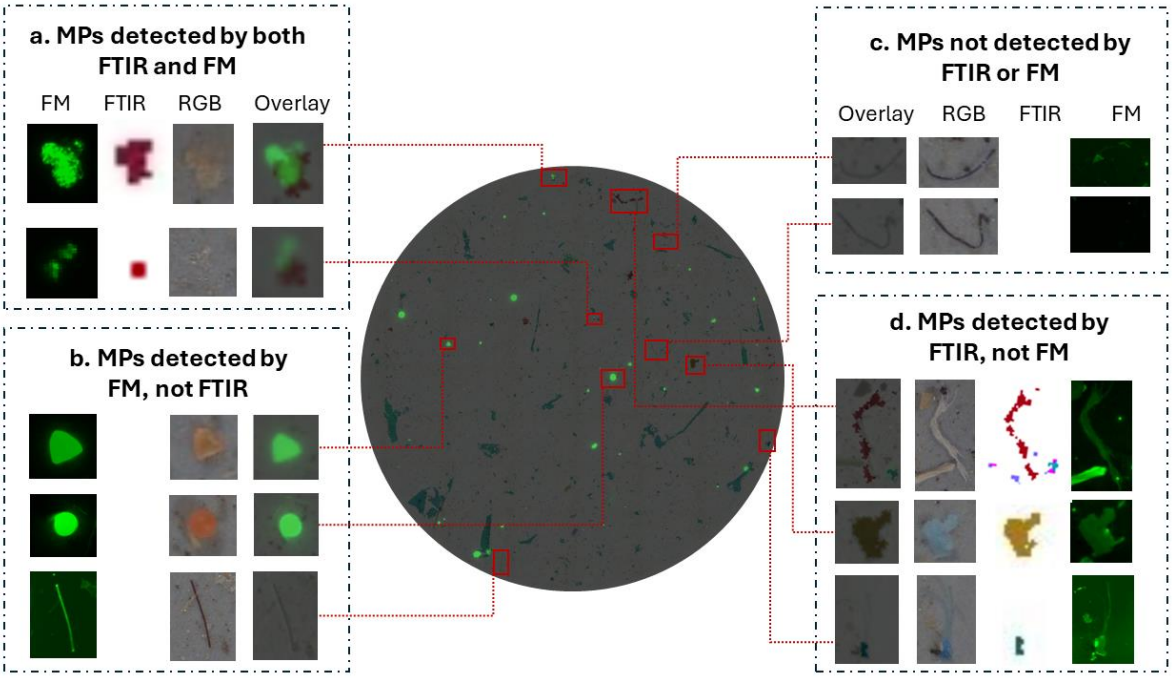


**Figure 5.4.** Comparison of MPs detection results using FM and FTIR spectroscopy on a single Anodisc filter (25 mm diameter). The central image shows an overlay of RGB, fluorescence, and FTIR images of the sample filter with highlighted regions. Insets illustrate: (a) MPs detected by both FTIR and FM, (b) MPs detected by FM but not FTIR, (c) MPs not detected by either method, and (d) MPs detected by FTIR but not FM. Individual panels display FM, FTIR, RGB, and overlay images to compare detection performance across methods.

In FM, some SOM fluoresces strongly with Nile Red, leading to misidentification and hence false positives. Similarly, in µ-FTIR analysis, certain SOM can give similar spectra to polymers such as polyurethane, acrylic/varnish, polyvinyl acetate, or polyethylene leading to misidentification of particles However, careful validation of µ-FTIR results—through detailed review of spectra, matching indices, and signal-to-noise ratios, as achieved in this study—helps mitigate these errors.

Some synthetic fibres were entirely missed by both µ-FTIR and FM but were later identified as polyester fibres using manual µ-Raman analysis, highlighting the potential for false negatives in both µ-FTIR and FM analyses. Most of these fibres had a nominal width of 10–50 µm and were predominantly black in colour. It is noteworthy that the two methods also differ significantly in their size detection limits: µ-FTIR can detect particles down to 11 µm, while FM can identify particles as small as 3 µm under the settings used in this study. However, a size threshold of 20 µm was applied for FM to ensure comparability between methods and improve reliability, as smaller particles are more susceptible to matrix interference from SOM when using fluorescence microscopy.

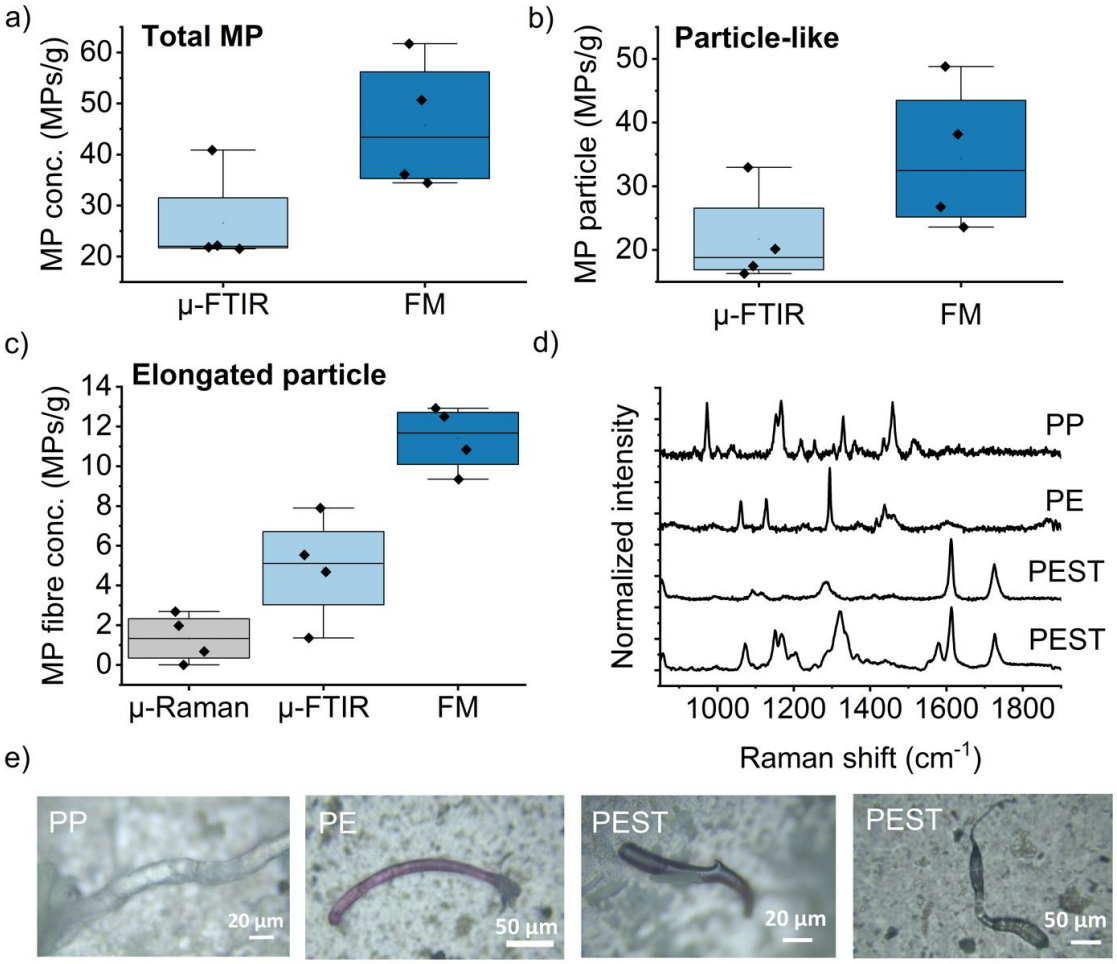


**Figure 5.5.** Comparison of MPs concentrations obtained by different methods on a subset of biosolid amended samples. Total MPs concentrations (a) and particle-like MPs (b) were measured using µ-FTIR and FM, while elongated MPs (c) were quantified using µ-Raman, µ-FTIR, and FM. Raman spectra (d) confirm the identification of PP, PE, and PEST. Microscopic images (e) show representative PP, PE, and PEST fibres with scale bars.

### 5.3.4 Comparison between Raman and FTIR for fibre analysis

A comparison of five biosolid-amended soil samples analysed using FM, µ-FTIR, and manual µ-Raman for fibre detection revealed similarity and discrepancies between the methods (**Figure** 5). Overall, there was no significant difference between total MPs concentration detected by FM (45.7 ± 12.9 MPs/g) compared to µ-FTIR (26.6 ±9.5 MPs/g) (Wilcoxon Signed Rank Test, $p > 0.05$), with a similar trend for particle-like MPs, where FM (34.3 ± 11.5 MPs/g) was not significantly different to µ-FTIR (21.7 ± 7.7 MPs/g) (Wilcoxon Signed Rank Test, $p > 0.05$) (**Figure** 5.4a, b). For elongated particles (fibres), FM showed the highest concentrations (11.4 ±1.6 MPs/g), followed by µ-FTIR (6.2 ± 3.8 MPs/g), while manual µ-Raman detected the lowest concentrations (1.4 ± 1.1 MPs/g). The repeated-measures ANOVA revealed a significant overall difference among

the methods ($p < 0.001$). Tukey's HSD revealed significant pairwise differences: Raman vs. FTIR ($p$=0.007), Raman vs. FM ($p$=0.001), and FTIR vs. FM ($p$=0.028).

In these test samples, fibres identified by manual µ-Raman included PET, PP, PE with representative microscopic images showing clear variations in size and morphology, ranging from 20–50 µm (**Figure** 5.4e). Interestingly, µ-FTIR detected higher concentrations of PE (3.01 MPs/g) and PP (1.75 MPs/g), while Raman identified more PET (1.16 MPs/g). Polyamide (PA, 0.10 MPs/g) and SBR (0.80 MPs/g) were detected only by µ-FTIR (**Figure** S1).

# 5.4 Discussion

## 5.4.1 Microplastics in anaerobic digestate

This study reported high MPs concentrations of 1030 ± 390 MPs/g DW (size ≥25 µm). Yet, comparisons with previous findings are challenging due to the limited number of quantitative studies focusing on smaller MPs (<0.5 mm) in AD. Additionally, previously reported MPs concentrations in digestate do vary significantly, influenced by factors such as feedstock composition (e.g., animal manure, food waste, green waste), treatment processes, and storage conditions. For instance, Weithman et al. (2018) detected 0–11 MPs/kg (size 1–5 mm) in digestate from biogas plants utilizing feedstocks like dung, manure, sunflowers, and fruit processing waste without biowaste inputs while digestate from biowaste inputs contained 14–895 particles/kg (Weithmann et al., 2018)

The higher concentrations reported in this study compared to previous ones may result from differences in AD processes and contamination with waste plastics as well as down to differences in analytical methods, which for this study, included MPs down to 25 µm. Many previous studies have focused on MPs ≥500 µm, likely underestimating smaller particles. In anaerobic digestion, mechanical stress during press filtration can cause fragmentation, forming smaller MPs as materials become brittle due to the loss of plasticizers (Boll et al., 2019). Large plastic fragments present in organic wastes/composts can break into numerous smaller ones. For example, PE and PS macroparticles (>25 mm) can release ~4–63 MPs during composting (Gui et al., 2021), suggesting smaller MPs form a significant but underreported fraction within digestate for those studies with larger particle size detection limits. In addition, MPs may degrade or shear during contact with Fenton's reagent, potentially increasing the proportion of smaller MPs (Peneva et al., 2024). The high organic content of AD (84.3%) may further contribute to false positives, particularly in the identification of SBR and PE, as discussed later in Section 4.3.1.

Plastic contamination in anaerobic digestate from the biogas plant in this study likely originates from the feedstock, which includes livestock and poultry manure co-digested with food waste, as well as the anaerobic digestion process and post-treatment handling. Food waste contributes MPs through contamination associated with plastic packaging, processing, and storage materials. In the United States, contamination rates in food waste streams collected for composting and anaerobic digestion range from 0.1% to 2.8% by weight (EPA, 2021). Livestock and poultry may also ingest MPs from polluted soil,

water, or feed, which are subsequently egested and present in manure. For example, MPs concentrations in feed samples have been reported as $1.39 \times 10^2 \pm 1.15 \times 10^2$ items/kg for pigs, $9.60 \times 10 \pm 1.09 \times 10^2$ items/kg for egg layers, and $3.60 \times 10^1 \pm 6.30 \times 10^1$ items/kg for cows (wet weight, mean ± standard deviation), with packaging and engineered polymers being the primary sources (Wu, R. et al., 2021). As a result, MPs are widely detected in animal manure, though concentrations vary significantly depending on species, geography, and farming practices. For instance, pig manure in China contained 1250 ± 640 particles/kg (Yang, Jie et al., 2020b), while chicken manure in Mexico showed 129.3 ± 82.3 particles/g (Huerta Lwanga et al., 2017). Additionally, MPs abundances in manure were reported as $9.02 \times 10^2 \pm 1.29 \times 10^3$ items/kg for pigs, $6.67 \times 10^2 \pm 9.90 \times 10^2$ items/kg for layers??, and $7.40 \times 10^1 \pm 1.29 \times 10^2$ items/kg for cows (wet weight, mean ± standard deviation) (Wu, R. et al., 2021).

### 5.4.2 Microplastics in biosolid-amended soils

Microplastic concentrations in the biosolid-amended soil were measured at 52 ± 14 MPs/g DW. Agricultural soils have often been reported to contain high plastic concentrations, and this aligns with the history of organic amendments applied to the field; that is10 years of sewage sludge application followed by 9 years of anaerobic digestate applications. These findings are comparable to other studies. For example, Zhang and Liu et al. (2018) reported much higher MPs concentrations ranging from 7100 to 42,960 particles/kg in arable fields in China amended with sewage sludge, inorganic fertilizers, and wastewater irrigation, with particle sizes between 50 μm and 10 mm(Zhang, G. S. & Liu, 2018).However , Tag et al. reported MPs concentrations of 14.6 MPs/g (dry weight, size ≥ 100 μm) in an experimental field that received a total of 190 t/ha of sludge since 1981, approximately 10 t every 3 years (Tagg et al., 2022).

It is evident that the microplastic (MPs) profile of biosolids-amended soil differs significantly from that of animal manure digestate in terms of polymer types, shapes, and sizes. This distinction highlights the complexity of the farm's agricultural history and the environmental processes at play. Polymers such as acrylic resin, polyurethane, and polyester, which were not detected in animal manure digestate, were identified in the amended soil. These plastics are commonly associated with sewage sludge, originating from sources like laundry wastewater, personal care products, and road materials. Detailed analysis of microplastic content in sewage sludge from the same wastewater treatment plant revealed a high concentration of MPs (3650 ± 2100 MPs/g), with detected plastics including PE, PEST, PP, PS, ABS, and PU. While this may not precisely reflect the MPs profile applied to the farm in the past (2004–2014), it provides strong evidence that sewage sludge-derived plastics persist in the soil, despite the transition to animal manure digestate. The long-term application of sewage sludge, followed by digestate, has likely contributed to the high MPs concentrations observed in the soil. Previous studies have similarly documented the persistence of plastics in soil for several decades following application. For example, polymers such as PE, PP, and PS have been detected years after sewage sludge amendments (Weber et al., 2022). These findings underscore the persistent nature of microplastics in agricultural soils and their tendency to accumulate over time.

Although non-agricultural fields have significantly lower MPs concentrations (15.5 ± 13.1 MPs/g) compared to biosolid-amended fields, the presence of plastics remains notable. For instance, a similar MPs load of 6.36 MPs/g was reported in German soil that had never received sewage sludge, using comparable detection methods and size limits

(Tagg et al., 2022). Atmospheric deposition likely explains this contamination in background soils as well as in biosolid-amended soils. A spatial study in the USA reported MPs deposition rates of 48–435 MPs/m²/day, with larger particles deposited regionally (10–1000 km) via precipitation and smaller particles transported longer distances through dry deposition (Brahney et al., 2020a). Similarly, Allen et al. detected fibres (~750 µm) and fragments (≤300 µm) in atmospheric wet and dry deposition samples (Allen et al., 2019). Major sources of atmospheric MPs include road areas (84%), agricultural soil (11%), and oceans (5%) (Brahney et al., 2020c)

## 5.4.3 Variation in microplastic concentrations based on analytical methods

The efficacy of NR staining-FM and FPA-µ-FTIR spectroscopy in detecting MPs, using a subset of biosolid-amended soil revealed significant discrepancies between the two techniques, with only 18–22% particle overlap **(Figure 5.4a).** These observations underscore the need for caution when relying solely on a single detection method for microplastic analysis, as it may compromise precision and reliability.

### 5.4.3.1 Nile red staining-fluorescence microscopy

Nile Red staining, which selectively binds to hydrophobic substances (like synthetic polymers) and has thus been used to detect a wide range of plastic particles. However, this technique does not exclusively detect MPs, as it can also stain other hydrophobic materials, such as SOM, biological detritus, or non-plastic anthropogenic contaminants. (Maes et al., 2017b). This issue may explain why FM yielded slightly higher MPs concentrations than FTIR for the subset of samples (though not statistically different). Previous studies have reported similar challenges in distinguishing MPs from naturally occurring organic matter that also fluoresce under Nile Red staining, particularly in complex environmental matrices like soil etc (Ho et al., 2023; Maes et al., 2017b; Nel et al., 2021).

Plastics with lower hydrophobicity, greater rigidity, or dark colours (e.g., black plastics) do not fluoresce effectively with Nile Red, leading to their underestimation when using fluorescence microscopy despite being identified by Raman or FTIR. Additionally, image analysis settings are crucial; for instance, increasing the colour threshold when segmenting fluorescent particles can help reduce false positives from organic matter co-stained with Nile Red but may also increase false negatives, particularly for weakly fluorescent plastic particles (Phan Le et al., in preparation, see Chapter 2).

### 5.4.3.2 FTIR micro-spectroscopy

Compared with FM, FPA-µ-FTIR, which provides molecular identification based on infrared absorption patterns, was found to be more selective for plastics. MPs particle number counts and hence concentrations obtained from FTIR were slightly lower than those obtained through FM even not significant using t pair wise test, possibly due to less false positive of these methods. However, this method is also limited by certain factors, such as the particle size detection threshold and possible spectral overlap with non-plastic materials (Ivleva, 2021).

Previous studies have highlighted the challenges of spectral overlap in complex matrices, where non-plastic materials can exhibit similar infrared absorption features, potentially leading to misclassification (Moses et al., 2023). In this study, µ-FTIR is likely prone to false positives, particularly in identifying materials such as acrylic/varnish/polyurethane, ethylene vinyl acetate (EVA), SBR, and PE. Although manual inspection of library match results was conducted, the spectral quality—compromised by the need to balance accuracy with analysis time—was insufficient to reliably distinguish false positives. Due to the inability to reliably distinguish false positives for acrylic/varnish/polyurethane and EVA, these materials are not reported here.

As discussed earlier, false positives in FTIR can be minimized through careful validation of spectral matches, increasing the matching index threshold (though this may underestimate weathered plastics due to spectral changes upon weathering), evaluating signal-to-noise ratios, and optimizing spectral acquisition conditions, such as increasing acquisition time and accumulation. While the latter adjustments improve spectral quality and enhance the ability to distinguish plastics from SOM, they also increase analysis time. This presents a trade-off between measurement quality and efficiency, particularly in environmental monitoring, where large sample volumes often require analysis.

False negatives by µ-FTIR were also observed in this study, a finding often overlooked in previous research. The inability of µ-FTIR to detect fluorescent Cospheric surrogate particles may result from their thickness and the strong fluorescence of Cospheric PE particles, which can interfere with their transmission behaviour. Additionally, smaller particles that fluoresce under Nile Red staining might fall below FTIR's detection limits or fail to generate sufficient signal for accurate spectral matching (Rocha-Santos & Duarte, 2015). FTIR's accuracy can also be affected by biofilms or surface contamination on microplastics, which may obscure their characteristic spectra and lead to misidentification (Mintenig et al., 2018).

Some fibres, later identified as polyesters, were not detected by µ-FTIR. This could be due to their small diameters (e.g., close to the lower detection limit of ~11 µm), which challenge detection because of the infrared diffraction limit (Ivleva, 2021). Additionally, fibres not positioned within a single focal plane were misinterpreted as discrete particles instead of fibres. Black fibres and other dark particles were also frequently missed by both µ-FTIR and FM as black materials absorb incoming radiation, resulting in weak transmission signals and minimal fluorescence emission (Tagg et al., 2022). The issue of under-detection, particularly for PET fibres, has also been reported in previous studies (Elert et al., 2017), highlighting the challenges of accurately analysing such fibres in environmental samples.

#### 5.4.3.3 Raman micro-spectroscopy for fibre analysis

The challenges of FTIR in fibre analysis can be mitigated using manual Raman micro-spectroscopy. This method employs a laser in the visible light range with a shorter wavelength than infrared, enabling the identification of plastics as small as ~0.5 µm. Manual identification also avoids the over-segmentation of fibres caused by their elongated shapes in FTIR and FM. Additionally, carefully tailored spectral acquisition parameters based on the shape, type, and size of plastics enhances spectral quality, improving their distinguishability from soil organic matter and reducing false positives. This likely explains the lower false positive rate observed with Raman, which detected the fewest plastic fibres compared to FTIR and fluorescence microscopy.

However, some synthetic fibres were particularly challenging to analyse with Raman due to the presence of pigments or fluorescence signals from surrounding particles, which interfered with the detection of Raman peaks. Additionally, we observed that certain black or weathered plastics with deteriorated surfaces were prone to laser-induced burning, making them undetectable with Raman.

## 5.5 Conclusions

This study comprehensively characterizes and quantifies microplastics (down to 25 µm diameter size) in anaerobic digestate derived primarily from animal manure produced at an agricultural biogas plant, as well as in agricultural soil amended with this digestate. Additionally, the soil's history of past sewage sludge applications has also contributed to microplastic contamination. The presence of microplastics from these historical applications provides valuable insights into plastic particle retention and long-term accumulation in agricultural soils. The findings clearly demonstrate that the use of digestate as an organic amendment, combined with historical sewage sludge applications, has significantly increased microplastic contamination in the agricultural soil compared to nearby background soil. This underscores the urgent need for improved agricultural practices, better waste management strategies, and measures to reduce plastic contamination in biosolid amendments applied to soil. The evidence here indicates that past sewage sludge applications accounts for the majority of MPs present in the agricultural soil, although the type of MPs will vary depending on the source material (sewage sludge vs AD).

The application of an array of different analytical instrumental methods including FTIR, FM, and Raman spectroscopy (for fibre detection only), provides a strong assurance for the MPs data, the type of plastic polymer encountered and the morphology of the particles (particularly elongated or fibre type particles). While discrepancies in microplastic concentrations between methods were not statistically significant, fibre analysis showed greater variability, with FM detecting the most fibres, followed by FTIR and Raman. Overlaying results revealed that all methods suffer from false positives and negatives, highlighting the limitations of relying on a single technique aimed at particle characterisation and counting. However, other methods that measure plastic polymer type and mass (not particle count) such as pyrolysis-GC-MS, were not employed in this study.

Nonetheless, the combination of fluorescence microscopy, FTIR, and Raman micro-spectroscopy provided valuable insights into the complexities of accurately detecting microplastics, in complex matrices like soil and bio-solid/compost material, where high organic matter content provides notable challenges to precise and accurate plastic particle characterisation and counts, particularly for particles sized <50 mm in diameter.It is clear that no single microscopy/spectroscopy method provides a comprehensive view of all plastic particles and selection of the analytical method will depend on the objectives of any given study e.g. total plastic particle count, size ranges to be identified and whether to include a full assessment of fibre-type MPs. Addressing these challenges will require future research incorporating comprehensive plastic spiking experiments and matrix interference studies.

**Acknowledgements**

This work was supported by the European Union's Horizon 2020, ITN SOPLAS, with grant agreement No. 55334. The authors thank staffs at the wastewater treatment facility and the farmers for their great support with sampling.

**Credit authorship contribution statement** Q.N. Phan Le: conceptualisation, methodology, samples analysis, data evaluation, writing, review and editing of the manuscript; C. Halsall: funding acquisition, conceptualisation, supervision, review and editing of the manuscript; M. Kunask: sample analysis, review and editing of the manuscript; L. Ashton and B. Surridge: supervision, review and editing of the manuscript; C. Halsall and J. Quinton: funding acquisition, supervision, review and editing of the manuscript.

**Data availability** Data will be made available on request.

**Ethical approval** This research did not involve human or animal samples.

**Competing interest** The authors declare no competing interests.

# References

Allen, S., Allen, D., Phoenix, V. R., Le Roux, G., Durántez Jiménez, P., Simonneau, A., Binet, S., & Galop, D. (2019). Atmospheric transport and deposition of microplastics in a remote mountain catchment. Nature Geoscience, 12(5), 339. 10.1038/s41561-019-0335-5

Antunes, J. C., Frias, J. G. L., Micaelo, A. C., & Sobral, P. (2013). Resin pellets from beaches of the Portuguese coast and adsorbed persistent organic pollutants. Estuarine, Coastal and Shelf Science, 130, 62. 10.1016/j.ecss.2013.06.016

Bläsing, M., & Amelung, W. (2017). Plastics in soil: Analytical methods and possible sources. Science of the Total Environment, 612, 422. 10.1016/j.scitotenv.2017.08.086

Boll, M., Geiger, R., Junghare, M., & Schink, B. (2019). Microbial degradation of phthalates: biochemistry and environmental implications. Environmental Microbiology Reports, 12(1), 3. 10.1111/1758-2229.12787

Brahney, J., Hallerud, M., Heim, E., Hahnenberger, M., & Sukumaran, S. (2020a). Plastic rain in protected areas of the United States.

Brahney, J., Mahowald, N., Prank, M., Cornwell, G., Klimont, Z., Matsui, H., & Prather, K. A. (2020b). Constraining the atmospheric limb of the plastic cycle10.1073/pnas.2020719118/-/DCSupplemental

Coppock, R. L., Cole, M., Lindeque, P. K., Queirós, A. M., & Galloway, T. S. (2017). A small-scale, portable method for extracting microplastics from marine sediments. Environmental Pollution (1987), 230, 829–837. 10.1016/j.envpol.2017.07.017

Cowger, W., Steinmetz, Z., Gray, A., Munno, K., Lynch, J., Hapich, H., Primpke, S., De Frond, H., Rochman, C., & Herodotou, O. (2021). Microplastic Spectral Classification Needs an Open Source Community: Open Specy to the Rescue!. American Chemical Society (ACS). 10.1021/acs.analchem.1c00123

De Souza Machado, A. A., Lau, C. W., Kloas, W., Bergmann, J., Bachelier, J. B., Faltin, E., Becker, R., Görlich, A. S., & Rillig, M. C. (2019). Microplastics Can Change Soil Properties and Affect Plant Performance. American Chemical Society (ACS). 10.1021/acs.est.9b01339

De Souza Machado, A. A., Lau, C. W., Till, J., Kloas, W., Lehmann, A., Becker, R., & Rillig, M. C. (2018). Impacts of Microplastics on the Soil Biophysical Environment. American Chemical Society (ACS). 10.1021/acs.est.8b02212

Elert, A. M., Becker, R., Duemichen, E., Eisentraut, P., Falkenhagen, J., Sturm, H., & Braun, U. (2017). Comparison of different methods for MPs detection: What can we learn from them, and why asking the right question before measurements matters? Environmental Pollution, 231, 1256. 10.1016/j.envpol.2017.08.074

EPA. (2021). EMERGING ISSUES IN FOOD WASTE MANAGEMENT Plastic Contamination. .

Erni-Cassola, G., Gibson, M. I., Thompson, R. C., & Christie-Oleza, J. A. (2017). Lost, but Found with Nile Red: A Novel Method for Detecting and Quantifying Small Microplastics (1 mm to 20 μm) in Environmental Samples. American Chemical Society (ACS). 10.1021/acs.est.7b04512

FAO. (2022). Food and Agriculture Organization of the United Nations. http://www.fao.org/home/en/. Retrieved 5 May 2022, from

Gui, J., Sun, Y., Wang, J., Chen, X., Zhang, S., & Wu, D. (2021). Microplastics in composting of rural domestic waste: abundance, characteristics, and release from the surface of macroplastics. Environmental Pollution, 27410.1016/j.envpol.2021.116553

Ho, D., Liu, S., Wei, H., & Karthikeyan, K. G. (2023). The glowing potential of Nile red for microplastics Identification: Science and mechanism of fluorescence staining. Elsevier BV. 10.1016/j.microc.2023.109708

Huerta Lwanga, E., Mendoza Vega, J., Ku Quej, V., Chi, J. D. L. A., Sanchez Del Cid, L., Chi, C., Escalona Segura, G., Gertsen, H., Salánki, T., Van Der Ploeg, M., Koelmans, A. A., & Geissen, V. (2017). Field evidence for transfer of plastic debris along a terrestrial food chain. Scientific Reports, 7(1)10.1038/s41598-017-14588-2

Ivleva, N. P. (2021). Chemical Analysis of Microplastics and Nanoplastics: Challenges, Advanced Methods, and Perspectives. American Chemical Society (ACS). 10.1021/acs.chemrev.1c00178

Kim, S. W., Jeong, S., & An, Y. (2021). Microplastics disrupt accurate soil organic carbon measurement based on chemical oxidation method. Chemosphere, 27610.1016/j.chemosphere.2021.130178

Maes, Jessop, Wellner, Haupt, & Mayes. (2017). A rapid-screening approach to detect and quantify microplastics based on fluorescent tagging with Nile Red. Scientific Reports, 7(1), 44501. 10.1038/srep44501

Meng, F., Yang, X., Riksen, M., & Geissen, V. (2021). Effect of different polymers of microplastics on soil organic carbon and nitrogen – A mesocosm experiment. Environmental Research, 20410.1016/j.envres.2021.111938

Mintenig, S. M., Löder, M. G. J., Primpke, S., & Gerdts, G. (2018). Low numbers of microplastics detected in drinking water from ground water sources. Science of the Total Environment, 648, 631. 10.1016/j.scitotenv.2018.08.178

Möller, J. N., Heisel, I., Satzger, A., Vizsolyi, E. C., Oster, S. D. J., Agarwal, S., Laforsch, C., & Löder, M. G. J. (2022). Tackling the Challenge of Extracting Microplastics from Soils: A Protocol to Purify Soil Samples for Spectroscopic Analysis. Environmental Toxicology and Chemistry, 41(4), 844–857. 10.1002/etc.5024

Moses, S. R., Roscher, L., Primpke, S., Hufnagl, B., Löder, M. G. J., Gerdts, G., & Laforsch, C. (2023). Comparison of two rapid automated analysis tools for large FTIR microplastic datasets. Springer Science and Business Media LLC. 10.1007/s00216-023-04630-w

Nel, H. A., Chetwynd, A. J., Kelleher, L., Lynch, I., Mansfield, I., Margenat, H., Onoja, S., Goldberg Oppenheimer, P., Sambrook Smith, G. H., & Krause, S. (2021). Detection limits are central to improve reporting standards when using Nile red for microplastic

quantification. Chemosphere (Oxford), 263, 127953. 10.1016/j.chemosphere.2020.127953

Peneva, S., Le, Q. N. P., Munhoz, D. R., Wrigley, O., Wille, F., Doose, H., Halsall, C., Harkes, P., Sander, M., Braun, M., & Amelung, W. (2024). Microplastic analysis in soils: A comparative assessment. Ecotoxicology and Environmental Safety, 28910.1016/j.ecoenv.2024.117428

Porterfield, K. K., Hobson, S. A., Neher, D. A., Niles, M. T., & Roy, E. D. (2023). Microplastics in composts, digestates, and food wastes: A review. Journal of Environmental Quality, 52(2), 225. 10.1002/jeq2.20450

Quynh Nhu Phan Le, Crispin Halsall, Stoyana Peneva, Olivia Wrigley, Melanie Braun, Wulf Amelung, Lorna Ashton, Ben, W.J. Surridge, & John Quinton.Towards quality-assured measurements of microplastics in soil using fluorescence microscopy. Unpublished manuscript.

Rocha-Santos, T., & Duarte, A. C. (2015). A critical overview of the analytical approaches to the occurrence, the fate and the behavior of microplastics in the environment. TrAC Trends in Analytical Chemistry, 65, 47. 10.1016/j.trac.2014.10.011

Shim, W. J., Song, Y. K., Hong, S. H., & Jang, M. (2016). Identification and quantification of microplastics using Nile Red staining. Marine Pollution Bulletin, 113(1-2), 469–476. 10.1016/j.marpolbul.2016.10.049

Steiner, T., Möller, J. N., Löder, M. G. J., Hilbrig, F., Laforsch, C., & Freitag, R. (2022). Microplastic Contamination of Composts and Liquid Fertilizers from Municipal Biowaste Treatment Plants: Effects of the Operating Conditions. Waste and Biomass Valorization, 10.1007/s12649-022-01870-2

Tagg, A. S., Brandes, E., Fischer, F., Fischer, D., Brandt, J., & Labrenz, M. (2022). Agricultural application of microplastic-rich sewage sludge leads to further uncontrolled contamination. Science of the Total Environment, 80610.1016/j.scitotenv.2021.150611

Thomas, D., Schütze, B., Heinze, W. M., & Steinmetz, Z. (2020). Sample Preparation Techniques for the Analysis of Microplastics in Soil—A Review. Sustainability (Basel, Switzerland), 12(21), 9074. 10.3390/su12219074

Wang, W., Ge, J., Yu, X., & Li, H. (2019). Environmental fate and impacts of microplastics in soil ecosystems: Progress and perspective. Science of the Total Environment, 70810.1016/j.scitotenv.2019.134841

Weber, C. J., Santowski, A., & Chifflard, P. (2022). Investigating the dispersal of macro- and microplastics on agricultural fields 30 years after sewage sludge application. Scientific Reports, 12(1), 6401. 10.1038/s41598-022-10294-w

Weithmann, N., Möller, J. N., Löder, M. G. J., Piehl, S., Laforsch, C., & Freitag, R (2018). Organic fertilizer as a vehicle for the entry of microplastic into the environment.

Wu, R., Cai, Y., Chen, Y., Yang, Y., Xing, S., & Liao, X. (2021). Occurrence of microplastic in livestock and poultry manure in South China. Environmental Pollution, 27710.1016/j.envpol.2021.116790

Yang, J., Li, R., Zhou, Q., Li, L., Li, Y., Tu, C., Zhao, X., Xiong, K., Christie, P., & Luo, Y. (2020a). Abundance and morphology of microplastics in an agricultural soil following long-term repeated application of pig manure. Environmental Pollution, 27210.1016/j.envpol.2020.116028

Yang, J., Li, R., Zhou, Q., Li, L., Li, Y., Tu, C., Zhao, X., Xiong, K., Christie, P., & Luo, Y. (2020b). Abundance and morphology of microplastics in an agricultural soil following long-term repeated application of pig manure. Environmental Pollution, 27210.1016/j.envpol.2020.116028

Zhang, G. S., & Liu, Y. F. (2018). The distribution of microplastics in soil aggregate fractions in southwestern China. The Science of the Total Environment, 642, 12–20. 10.1016/j.scitotenv.2018.06.004

Zhou, Y. F., Liu, X. N., & Wang, J. (2019). Characterization of microplastics and the association of heavy metals with microplastics in suburban soil of central China. Science of the Total Environment, 69410.1016/j.scitotenv.2019.133798

# Supporting information

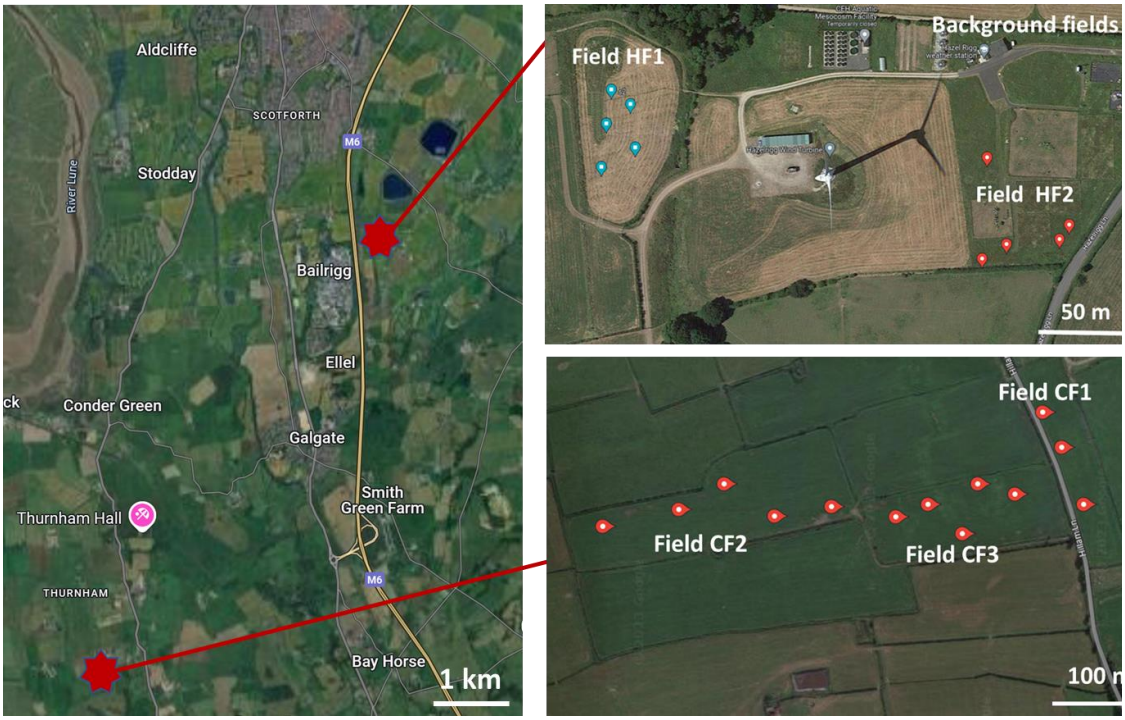


**Figure S1**: Map of sampling sites.

**Table S1: Soil physiochemical characteristics of sample across sampling site.**

| Field | Sampling date | Field Area | Sample code | Latitude | Longitude | Characterization at sampling point | | Soil physiochemical characterization | | | | | |
|---|---|---|---|---|---|---|---|---|---|---|---|---|---|
| | | | | | | Moisture | Temp. | % C | pH | Conductivity (µS/cm) | Particle size analysis | | |
| | | | | | | | | | | | % clay (< 2µm) | % silt (2≤ x ≤63 µm) | % sand (63 µm ≤ x ≤ 2mm) |
| Cockerham field 1 | 08/07/2023 | 1.62 ha | CF1-S1 | 53.97129 | -2.828795 | 27.4 | 24.8 | 8.3 | 6.9 | 163 | 10.3 | 18.5 | 71.2 |
| | | | CF1-S2 | 53.97098 | -2.829505 | 38.4 | 25.0 | 17.7 | 5.4 | 1840 | 28.3 | 59.7 | 12 |
| | | | CF1-S3 | 53.97066 | -2.830727 | 42.1 | 25.9 | 27.6 | 5.3 | 1890 | 28 | 57.3 | 14.7 |
| Cockerham field 2 | 08/07/2023 | 3.92 ha | CF2-S1 | 53.97366 | -2.830815 | 35.2 | 27.0 | 17.4 | 6.3 | 1646 | 21.2 | 51.3 | 27.5 |
| | | | CF2-S2 | 53.97450 | -2.830946 | 32.5 | 27.9 | 13.0 | 5.1 | 1417 | 27.5 | 59.5 | 13 |
| | | | CF2-S3 | 53.97505 | -2.830291 | 30.6 | 27.9 | | | | | | |
| | | | CF2-S4 | 53.97554 | -2.830852 | 32.7 | 27.9 | 15.2 | 5.2 | 891 | 28.6 | 55.6 | 15.8 |
| | | | CF2-S5 | 53.97649 | -2.831235 | 22.3 | 27.1 | 20.8 | 5.4 | 1841 | 32.7 | 59.77 | 7.53 |
| Cockerham field 3 | 08/07/2023 | 2.59 ha | CF3-S1 | 53.97296 | -2.831032 | 32.1 | 28.4 | 13.8 | 6.1 | 1836 | 24.6 | 54.1 | 21.3 |
| | | | CF3-S2 | 53.97253 | -2.830803 | 31.2 | 29.6 | 10.8 | 6.9 | 2090 | 28.6 | 56.3 | 15.1 |
| | | | CF3-S3 | 53.97199 | -2.830380 | 41.7 | 30.0 | 14.6 | 6.2 | 1097 | 24.3 | 58.6 | 17.1 |
| | | | CF3-S4 | 53.97208 | -2.831353 | 24.5 | 29.2 | 19.0 | 5.5 | 924 | 27.9 | 57.4 | 14.7 |
| | | | CF3-S5 | 53.97154 | -2.830598 | 31.0 | 28.2 | 15.6 | 6.0 | 1221 | 22.6 | 56.7 | 20.7 |
| Hazelrigg field 1 | 08/06/2023 | 0.59 ha | HF1-S1 | 54.01365 | -2.779300 | 16.4 | 21.0 | 14.2 | 5.9 | 166 | 28.5 | 45.2 | 26.3 |
| | | | HF1-S2 | 54.01408 | -2.779208 | 15.4 | 22.9 | 12.8 | 5.7 | 191 | 19.4 | 27.5 | 53.1 |
| | | | HF1-S3 | 54.01400 | -2.779024 | 13.5 | 23.9 | 12.6 | 5.4 | 126 | 18.9 | 35.2 | 45.9 |
| | | | HF1-S4 | 54.01400 | -2.779024 | 23.4 | 25.1 | 10.8 | 5.5 | 150 | 23.2 | 39 | 37.8 |

| | | | | | | | | | | | | | |
|---|---|---|---|---|---|---|---|---|---|---|---|---|---|
| | | | HF1-S5 | 54.01376 | -2.778979 | 30.9 | 24.7 | 13.3 | 5.5 | 222 | 21.7 | 33.3 | 45 |
| Hazelrigg field 2 | 08/06/ 2023 | 0.19 ha | HF2-S1 | 54.01325 | -2.774940 | 10.5 | 25.1 | 9.6 | 6.7 | 173 | 18.5 | 31.4 | 50.1 |
| | | | HF2-S2 | 54.01333 | -2.774849 | 6.3 | 30.6 | 11.0 | 5.2 | 136 | 17 | 29.6 | 53.4 |
| | | | HF2-S3 | 54.01322 | -2.775445 | 9.1 | 30.4 | 10.6 | 5.1 | 117 | 20.9 | 40.7 | 38.4 |
| | | | HF2-S4 | 54.01314 | -2.775675 | 10.6 | 31.0 | 10.7 | 5.2 | 137 | 17.4 | 32.5 | 50.1 |
| | | | HF2-S5 | 54.01371 | -2.775629 | 7.0 | 28.7 | 10.6 | 5.2 | 125 | 15.8 | 27 | 57.2 |

# 6 First evidence of nanoplastic in Antarctica soil

*Plastic contamination has reached even the most remote regions, including Antarctica, yet micro- and nanoplastic contamination in Antarctic soils remains poorly studied. This chapter investigates plastic occurrence in soils from the McMurdo Dry Valleys, analysing microplastics (≥10 µm) using fluorescence microscopy and detecting nanoplastics (20 nm–1 µm) for the first time with thermal desorption-proton transfer reaction-mass spectrometry (TD-PTR-MS). This study fills a critical knowledge gap in plastics presence, especially nanoplastic in remote soil, positioning Antarctica as a reference point for assessing global background plastic contamination.*

# First evidence of nanoplastic in Antarctica soil

Quynh Nhu Phan Le[a], Nikolaos Evangeliou[b], Crispin Halsall[a], John Quinton[a], Ben W.J. Surridge[a], Lorna Ashton[c], Sabine Eckhardt[b], Livio Ruggiero[d], Alessandra Sciarra[e], Fabio Florindo[e], Claudio Zaccone[f,e,*], Dušan Materić[g*]

[a] Lancaster Environment Centre, Lancaster University, Lancaster LA1 4YQ, United Kingdom
[b] Stiftelsen NILU (former Norwegian Institute for Air Research), Instituttveien 18, 2007 Kjeller, Norway
[c] Department of Chemistry, Lancaster University, Lancaster, LA1 4YQ, United Kingdom
[d] Italian Institute for Environmental Protection and Research, Roma, Italy
[e] Istituto Nazionale di Geofisica e Vulcanologia, Via Vigna Murata 605, 00143 Roma, Italy
[f] Department of Biotechnology, University of Verona, Strada Le Grazie 15, 37134 Verona, Italy
[g] Department of Environmental Analytical Chemistry, Helmoltz Centre for Environmental Research – UFZ, Permoserstraße 15, 04318 Leipzig, Germany

***Corresponding authors:**

For plastic analysis: Dušan Materić (dusan.materic@ufz.de)
For Antarctica soils: Claudio Zaccone (claudio.zaccone@univr.it)

# Abstract

Plastic contamination is now prevalent across the globe, including remote regions like the Arctic and Antarctica. In Antarctica, macro- and microplastic have been detected in various ecosystems, particularly in marine systems. However, the presence of plastics in Antarctic soils—particularly of micro- and nanoplastic—remains poorly studied. This study analyses soil samples collected from the Wright and Taylor Valleys in the McMurdo Dry Valleys, one of the largest ice-free areas in Antarctica, to investigate micro- and nanoplastic contamination. Nanoplastic (20 nm – 1 µm) were detected for the first time using a newly developed extraction protocol and subsequent analysis with thermal desorption-proton transfer reaction-mass spectrometry (TD-PTR-MS while microplastics (≥10 µm in diameter) were extracted and identified using Nile Red staining and fluorescence microscopy. Careful consideration was given to background contamination and detection limits. Microplastics were observed above the detection limits in only one sample from the Taylor Valley. In contrast, nanoplastic—including polypropylene (PP), polyethylene (PE), polyethylene terephthalate (PET), polystyrene (PS), polyvinyl chloride (PVC), and tyre wear particles (TWP) —were detected in surface soil at multiple sites in both Wright and Taylor Valleys, with total concentrations up to ~300 ng/g of soil. Nanoplastic were also identified in somewhat deeper soil layers (>20 cm depth), albeit at a much lower concentrations than in topsoil, providing evidence of their movement into deeper soil layers. To investigate potential sources, Lagrangian dispersion modelling was employed, revealing distinct seasonal dispersion patterns of plastic deposition in Antarctica, with direct contributions from local sources and indirect from long-range transport. This study addresses critical knowledge gaps regarding the occurrence of micro- and nanoplastic in soil from this polar region, highlighting the role of local sources (e.g. scientific bases) versus input through long-range atmospheric transport and the use of remote locations in Antarctica as a proxy for global background contamination.

## 6.1 Introduction

Plastic contamination is now widespread in Antarctica, a region considered one of the planet's last pristine environments (Barnes, D. K. A. et al., 2018; Horton & Barnes, 2020). Plastics originating from land at low latitudes and sea vessels can reach Antarctica due to their durability and transport via circumpolar currents (Barnes, David K. A. et al., 2009; Waller et al., 2017b). Local activities, such as those at scientific stations and tourism, also contribute to plastic contamination in the region (González-Pleiter et al., 2020, 2021). Additionally, there has been growing concern about plastics being carried to Antarctica through air masses, highlighting the issue of transboundary transport (Allen et al., 2021; Brahney et al., 2020c; Chen et al., 2023b; Liu et al., 2019). Consequently, plastic debris, including macro- (> 5 mm) and microplastic (MPs, 1 µm - 5 mm), has been detected in various Antarctic environments. These include the surface waters of the Southern Ocean (Cincinelli et al., 2017a; David K.A. Barnes et al.; Isobe et al., 2016a), areas off the Antarctic Peninsula (Lacerda et al., 2019), shallow waters (Munari et al., 2017; Reed et al., 2018; Waller et al., 2017b), deep-sea sediments (Cunningham et al., 2020) and island coastlines (Anfuso et al., 2020; Convey et al., 2002; Sander, Martin et al., 2009). Plastics have also been identified in snow (Aves et al., 2022), glaciers (González-Pleiter et al., 2021), sea ice (Kelly, A. et al., 2020) and freshwater systems (González-Pleiter et al., 2020) of Antarctica. This plastic contamination poses significant threat to Antarctica biodiversity and ecosystem functions. MPs ingestion has been observed across trophic levels, from benthic invertebrates (Sfriso et al., 2020) to gentoo penguins (Bessa et al., 2019), with laboratory studies showing harmful effects on marine species (Au et al., 2015; Cole et al., 2013; Wright et al., 2013). Plastic particles can also transport other pollutants (e.g., persistent organic pollutants) (Rodrigues et al., 2018), causing adverse effects through trophic transfer and bioaccumulation in top predators (Durante et al., 2016).

Although plastic contamination in Antarctica has been extensively studied, most research has focused on macroplastic and larger microplastics (≥ 20 µm) (Anfuso et al., 2020; Aves et al., 2022; Cincinelli et al., 2017a; Convey et al., 2002; González-Pleiter et al., 2020, 2021; Isobe et al., 2016a, 2016b; Lacerda et al., 2019; Reed et al., 2018; Sander, Martin et al., 2009; Waller et al., 2017b, 2017c). These larger particles are less environmentally relevant; for example, atmospheric deposition—a key source of plastics in Antarctica—primarily involves particles with smaller aerodynamic diameters (Allen et al., 2021; Aves et al., 2022; Chen et al., 2023b). Moreover, smaller plastics, especially nanoplastics (NPs, <1 µm), have a higher surface area-to-volume ratio, greater colloidal mobility than MPs, and stronger adsorption affinity for pollutants (da Costa et al., 2016b). Consequently, they are not only more prone to biological uptake but also pose greater hazards to humans and ecosystems through chemical leaching and pollutant transport. Yet, smaller MPs and NPs remain largely underexplored, with only one study documenting NPs in sea ice of Antarctica (Materić et al., 2022). This gap stems from challenges such as matrix interference, particle aggregation, and the limited sensitivity of current detection methods. Sensitivity is especially important when investigating remote regions like Antarctica, where plastic concentrations, particularly for NPs, are expected to be extremely low. Recently, thermal desorption-proton transfer reaction-mass spectrometry (TD-PTR-MS) has emerged as a highly sensitive technique capable of detecting NPs at ng levels (Materić et al., 2020), making it a promising tool for advancing research in this field.

This study investigates microplastics and, for the first time, nanoplastics in mainland Antarctic soils, addressing the knowledge gap regarding their occurrence in this polar region. The McMurdo Dry Valleys were chosen as the study area due to their inland location, far from oceanic influences, making them ideal for examining atmospheric deposition as a primary source of plastic contamination. Furthermore, their isolation and minimal human activity make the McMurdo Dry Valleys a prime location for establishing baseline MPs and NPs data, essential for future comparisons and evaluating global pollution impacts in one of Earth's most pristine environments. We hypothesize that plastics in this remote region originate predominantly from atmospheric transport, with additional contributions from human activities such as scientific expeditions and tourism. This study also introduces a novel extraction protocol for isolating NPs from soil, applied for the first time in combination with thermal desorption-proton transfer reaction time-of-flight mass spectrometry (TD-PTR-TOF-MS).

# 6.2 Materials and methods

## 6.2.1 Site description

The McMurdo Dry Valleys, located in the Trans-Antarctic Mountains near McMurdo Sound in southern Victoria Land, are the largest ice-free region in Antarctica (Levy, 2012). These east-west running valleys host some of the coldest and driest ecosystems on Earth, with annual temperatures between −18 and −28 °C (Goordial et al., 2025) and minimal precipitation (3–50 mm water-equivalent snowfall annually), most of which sublimates before melting (Fountain et al., 2009; Levy, 2012). Glacial melt, active for just 3 to 12 weeks a year, supplies ephemeral streams, the main water source in this polar desert (Peter A. Conovitz et al., 1998). Soils aways from stream, lakes, or areas with wind-blown snow depend on rare snowfall and are among the driest and most nutrient poor (oligotrophic) on Earth (Barrett et al., 2007; Goordial et al., 2025; Zeglin et al., 2009). These soils, formed on tills of diorites, granites, and sandstones (Campbell & Claridge, 1987), show a sand content commonly >85 %, an extremely low soil organic carbon (SOM) content (<0.2 %), an alkaline pH (average values ranging from 7.6 in the Wright Valley to 8.9 in the Taylor Valley (Consoli et al., in preparation), are weakly weathered, and classified as Gelisols due to their high solute content and permafrost dynamics (Bockheim, 1997).

## 6.2.2 Soil sampling

From January 8th to 28th, 2023, soil samples were collected across Wright and Taylor Dry Valleys in the McMurdo Dry Valleys region. A total of 9 topsoil samples (0–10 cm) and 4 subsurface and deep soil samples (≥20 cm to ≥40 cm) were collected from Taylor Valley, along with 4 topsoil samples (0–10 cm) from Wright Valley (**Figure** 6.1,). Samples were collected using a stainless-steel scoop, cleaned with alcohol before each sampling, and stored into new polypropylene (PP) zip-lock bags. Previous studies have demonstrated that new plastic materials, such as PP, pose minimal risk of cross-contamination (Jones et al., 2024). The samples were stored in a −25 °C freezer and kept chilled with dry ice during transit to Italy and then stored at the same temperature. Before

MPs and NPs extraction and analysis, the soil samples were oven-dried at 40 °C. Details of the sampling methods, site descriptions, and soil characteristics are provided elsewhere (Consoli et al., in preparation).

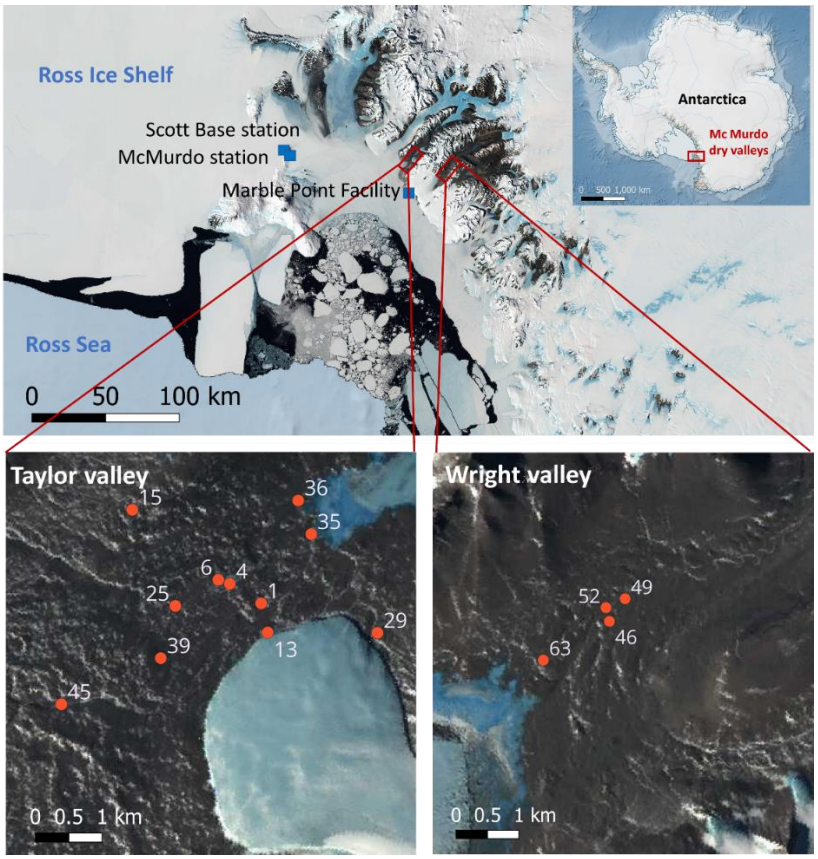


**Figure 6.1.** Sampling locations in the McMurdo Dry Valleys, Antarctica. The main map shows the proximity of Taylor Valley and Wright Valley to the Ross Ice Shelf, Ross Sea and some research stations, with detailed views of sampling points (red dots) in both valleys. The inset map provides the broader geographical context of the McMurdo Dry Valleys within Antarctica.

## 6.2.3 Microplastic analysis

### 6.2.3.1 Microplastics extraction

40 g of soil were mixed with 40 mL of 1.5 g/cm³ zinc chloride solution ($ZnCl_2$, ≥97%, APC pure, UK) in a 100 mL Erlenmeyer flask and stirred for 2 hours to disperse MPs. The flask was placed in a 400 mL beaker for overnight density separation (**Figure** 6.2.). To isolate MPs, 60 mL of $ZnCl_2$ was added in five 12 mL increments, with ~2 cm of overflow collected in a beaker after each addition (Crutchett & Bornt, 2024c) and filtered using a Nuclepore polycarbonate filter (Θ = 0.2 µm, dia. 25mm, Cytiva Whatman, Germany). The filter mesh was sonicated for 10 minutes, and particles were rinsed into the same beaker with 20 mL of 0.05 M iron sulphate ($FeSO_4$, ≥ 99%, Acros Organics, UK). Fenton digestion was initiated with 20 mL of hydrogen peroxide ($H_2O_2$, 30%, Fisher Scientific, UK) and the beaker was shaken at 110 rpm for 12 hours. The digested solution was filtered again using the same filter mesh, which was sonicated for another 10 minutes.

Particles were rinsed into the same beaker with 20–40 mL of HPLC water. The final solution was diluted to 50 mL, homogenized, and stored in a screw-top bottle under refrigeration until analysis.

#### 6.2.3.2 Nile red staining- Fluorescence microscopy

Subsamples (10–20 mL of 50 mL) of the extracted solution were filtered through baked glass fibre filters (Θ = 0.7 µm, dia. 47 mm, Cytiva Whatman GF/F). While on the filtration setup, ~3 mL of 0.5% Nile Red (99%, Acros Organics, UK) in hexane was applied, left for 10 minutes, rinsed with hexane, and air-dried. Filters were analysed at 470 nm using a green filter set (emission 524/50 nm) on a Zeiss Axio Zoom.V16 microscope (Phan Le et al, 2025, see Chapter 2). Images were captured in green fluorescence and bright-field modes at 50x magnification and processed in Fiji-ImageJ using Gaussian blur and thresholding before automatic particle analysis (SI).

### 6.2.4 Nanoplastic analysis

#### 6.2.4.1 Nanoplastic extraction

3 g of soil were placed in a 20 mL prebaked glass vial with 15 mL of 30% $H_2O_2$ and digested overnight in an orbital shaker at 300 rpm and 40 °C (model...). The vial was vortexed for one minute and allowed to settle for another minute, during which heavier particles settled while nanoparticles remained suspended due to Brownian motion (Gigault et al., 2018; Hassan et al., 2014). The suspension was drawn into a 10 mL PP Luer-slip syringe (Labsolute) fitted with a 1 µm PTFE syringe filter (Chromafil Xtra PTFE-100/25, Macherey-Nagel, Germany) and vacuum filtered through an Anodisc filter (Θ= 0.02 µm, dia. 25 mm, with PP support ring, Whatman™ Cytiva, Germany). The filter was dried overnight in a 40 °C oven and then carefully cracked into 3–4 pieces using ultra-fine tweezers, subsampling 70–80% of the total surface area while avoiding the PP support ring. The filter pieces were placed in three 10 mL glass vials sealed with perforated PTFE discs (in-house production) under aluminium screw caps (VWR).

#### 6.2.4.2 Thermal desorption proton transfer reaction time of flight mass spectrometry

NPs analysis was performed using a PTR8000 PTR-MS (IONICON Analytik) following established methods (Materić et al., 2020). The thermal desorption (TD) program consisted of a 35 °C hold for 30 seconds, a ramp of 40 °C/min to 360°C, and a 3-minute plateau at 360 °C. The PTR parameters were as follows: TOF pressure = $2.6 \times 10^{-7}$ mbar, drift pressure = 2.9 mbar, drift temperature = 90°C, and inlet temperature = 180°C. The reduced electric field strength in the drift tube (E/N), where E is the electric field and N is the gas number density, was set to 119.52 Td (1 Td = $10^{-17}$ V.cm²) for the proton transfer reaction. Data extraction utilized PTRviewer 3.4.5. to integrate mass spectra and calculate concentrations in ppb based on ion counts, instrument parameters, and known PTR kinetics. Mass spectra were integrated over 7 minutes, beginning when the TD unit reached 200 °C, and the 40 highest-intensity ions were used for fingerprinting. Polymers were identified and quantified using reference spectra (**Table** S5) and calibrations as

described previously allowing analysis of 6 polymer types including polyethylene (PE), polypropylene (PP), polyethylene terephthalate (PET), polystyrene (PS), polyvinyl chloride (PVC) and tyre-wear particles (TWP) (Materić et al., 2020, 2022).

## 6.2.5 Quality assurance and quality control

### 6.2.5.1 Measures to prevent contamination

Strict quality control measures were implemented to prevent contamination from air, clothing, chemicals, or tools. Non-plastic equipment was rinsed twice with HPLC-grade water and ethanol before and between uses and covered with pre-baked aluminium foil. Stainless-steel filters, glass fibre filters, and non-volumetric glassware were incinerated at 500 °C for 4 hours prior to use. Sample handling was performed in a cleaned laminar flow hood, with personnel wearing 100% cotton lab coats and nitrile gloves. Reagents, including $ZnCl_2$, 30% $H_2O_2$, and 0.05M $FeSO_4$ solution, were filtered through PC filters ($\Theta$=0.2 µm) before use.

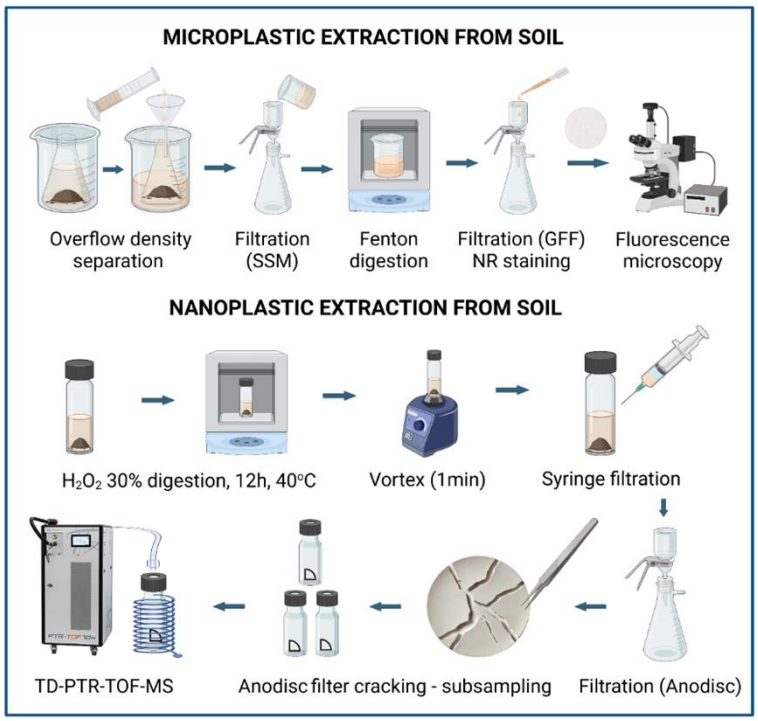


**Figure 6.2.** Workflow for MPs and NPs extraction from soil

### 6.2.5.2 Limit of detection

Procedural blanks, following the same processes as samples, were included in each batch. Samples with concentrations below the method limit of detection (MLODs), calculated as the mean procedural blank contamination plus three standard deviations, were excluded from analysis.

For MPs analysis, six procedural blanks starting with $ZnCl_2$ solution yielded 235 ± 130 MPs dia. >10 µm and 68 ± 38 MPs dia. >20 µm, with MLODs being 620 and 180 particles, respectively. This corresponds to MLODs of 15.6 MPs/g for dia. >10 µm and 4.5 MPs/g for dia. >20 µm, considering 40 g of soil per sample.

For NPs analysis, in addition to procedural blanks (PBs, 30% $H_2O_2$, n = 7), system blanks (SBs, n=39 clean, baked vials) were analysed three times: at the start, after every three samples, and at the end of each measurement day. These SBs were used to correct for instrument background and to establish the instrument limit of detection $LOD_{TD\text{-}PTR\text{-}MS}$, calculated for each batch as ($3\sigma_{SB\text{-}ion}$). Only ion signals from samples and procedural blanks that exceeded this instrument-specific threshold were considered for further analysis.

Following background correction, polymer fingerprinting was performed on batch-wise SB-corrected ion signals (ppb) from both samples and procedural blanks. Sample polymer concentrations were further refined batch-wise using method detection limits (MLODs) to determine the final plastic concentrations. MLODs, which accounts for the entire analytical workflow—including sample preparation, extraction, and instrumental analysis—was determined as (+ $3\sigma_{PB}$). The MLODs were identified as 74.4 ng/g for PP, 47.7 ng/g for PVC, 31.7 ng/g for PS, and 77.8 ng/g for TWPs, considering 3 g of soil per sample. No PE or PET was detected in the procedural blanks.

#### 6.2.5.3 Method recovery

For the MPs extraction method, recovery was tested by spiking 0.04 mg of monodisperse PS spheres (diameter: 10.07 µm, density: 1.05 g/cm³; Microparticles GmbH, Germany), equivalent to $7.2\times10^4$ PS particles, into two baked soil samples (500 °C). The samples underwent the complete extraction method, as described above, to evaluate overall recovery. The recovery rate for PS sphere dia. 10.07 µm was 23.0±8.9 %.

For the NPs extraction method, 2000 ng of PS spheres (dia. 500 nm, Microparticles GmbH, Germany) was spiked into two soil samples, which were then subjected to the full extraction process described above to assess overall recovery. Additionally, 300 ng of PS NPs as spiked directly onto the Anodisc filter after the cracking step, followed by drying at 40 °C before TD-PTR-MS analysis, to evaluate the thermal desorption and ionization efficiency of the method alone, without accounting for potential particle losses during soil extraction.

### 6.2.6 Lagrangian dispersion modelling

To understand the potential contributing sources, we used the Lagrangian particle dispersion model FLEXPART version 11 (FPv11) (Bakels et al., 2024) driven with ERA5 assimilated meteorological analyses (Hersbach et al., 2020) with 137 vertical levels, an hourly temporal resolution and a 0.5°x 0.5° spatial one. This version is suited to atmospheric NPs dispersion because it considers non-spherical shapes (e.g., fibres and fragments) (Tatsii et al., 2023). Here, we consider that the modelled NPs are fragments defined as cylinders with diameters of base of 1 µm and an aspect ratio of 3, 50 and 100 (that defines the length of the cylinder).

We simulate deposition amount using a feature in FLEXPART that reconstructs separately wet and dry deposition at the receptor for backward simulations (Eckhardt et al., 2017). Wet deposition was reconstructed after releasing computational particles at the receptor at altitudes of 0–20 km above sea level and wet removal was calculated using

different coefficients for in-cloud and below-cloud scavenging. For dry deposition, computational particles were released at 0–30 m at the same receptor point, as this shallow layer is equal to the height of the layer in which, in forward mode, particles are subject to dry deposition. All released particles represent a unity deposition amount, which was converted immediately (i.e., upon release of a particle) to atmospheric concentrations using the deposition intensity as characterized by either the dry deposition velocity or wet scavenging rate.

Considering that it is uncertain whether the detected NPs at the surface of the soil is due to direct atmospheric deposition, or they had been initially deposited on the snow ending at the surface of the soil after snow melting, we simulated wet and dry deposition for each month during three years prior to sampling, namely 2020-2023. Simulations of each monthly release extended over 50 days backward in time, sufficient to include most NPs emissions arriving at the station, given the long lifetime of atmospheric NPs (Evangeliou et al., 2020). The tracking includes gravitational settling (Tatsii et al., 2023), dry and wet deposition of aerosols (Grythe et al., 2017), turbulence (Cassiani et al., 2014), unresolved mesoscale motions (Stohl et al., 2005) and deep convection (Forster et al., 2005). The produced footprint emission sensitivity (or NPs deposition sensitivity) expresses the probability of any emission occurring in each grid-cell to reach the receptor.

## 6.3 Results

### 6.3.1 Microplastics concentration in Antarctica soil

Only one sample (sample 39, **Figure** 1) exhibited MPs concentrations exceeding the method's MLODs, with concentrations after procedural planks subtraction of 11.4 MPs/g for a threshold of 10 µm and 4.7 MPs/g for a threshold of 20 µm. The MPs displayed diverse shapes (Figure 6.3.), including irregular fragments and elongated fibres, with fibres-like particles (aspect ratio >3) accounting for 7.6 %. Particle sizes ranged from 3.5 µm (lower detection limit) to ~ 300 µm.

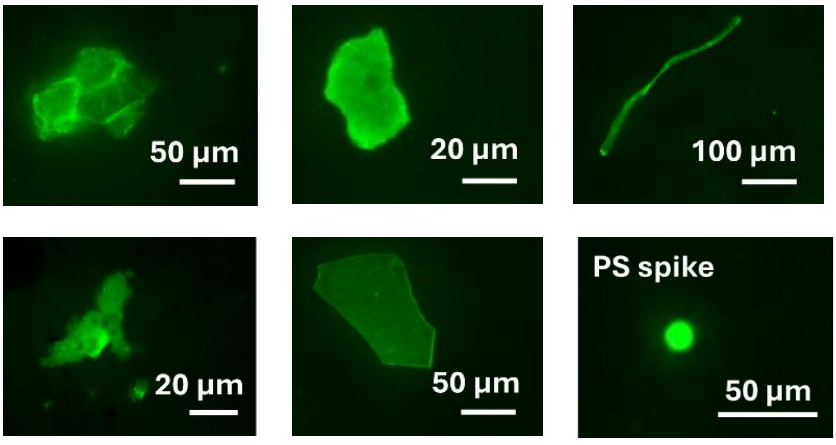


**Figure 6.3.** Morphological diversity of MPs visualized under GFP Filter fluorescence microscopy using Nile Red staining.

### 6.3.2 Nanoplastic concentration in Antarctica soil

A wide variation in NPs concentrations (sizes ranging from 20 nm to 1 µm) was observed across the samples, with concentrations after procedural blank subtraction ranging from 0 to 295.0 ng/g. Some samples (such as 63, 1, and 35-DS; **Figure** 6.1.) exhibited high NPs concentrations exceeding 200 ng/g, while others (including 4, 6, 13, 29, 52, 18, and 45; **Figure** 6.1.), showed minimal or negligible levels (<MLODs). The plastic composition also varied significantly among the samples. Sample 63 recorded the highest NPs concentration at 295 ng/g, predominantly composed of PP (61.9 %), followed by TWP (16.2 %), PE (13.8 %), PS (6.9 %), and PET (1.2 %); in contrast, samples 15 and 39 were dominated by PE, accounting for 96.3 % and 53.1 %, respectively, with smaller contributions from PP and/or PS (**Figure** 6.4.). Samples 49, 25, 1, and 35 were primarily composed of tyre particles, accounting for 39.7, 90.6, 38.1, and 44.3 %, respectively (**Figure** 6.4.). Overall, PP accounted for the largest proportion of NPs across all sites (40 %), followed by TWP (28 %), PE (15 %), PS (9 %), and smaller contributions from PET and PVC. Importantly, no significant difference in NPs concentrations was found between Wright and Taylor Valleys (t-test, p = 0.775).

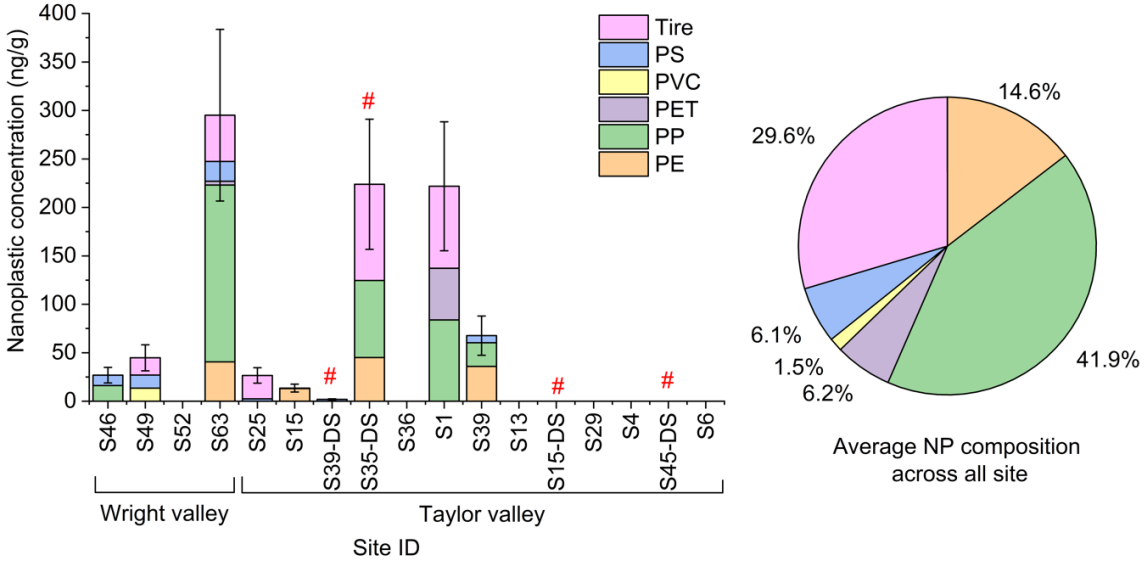


**Figure 6.4.** NPs concentration (ng/g) and composition across different sites in Taylor and Wright Valleys. The bar chart illustrates NPs concentrations at individual sampling sites (Site ID; see **Figure** 6.1.), categorized by polymer type. The # symbol indicates sites where deeper soil samples were collected. Uncertainty bars represent general PTR-MS quantification associated uncertainty of 30%. The pie chart shows the overall NPs composition across all sites.

Subsurface and deep soil samples generally exhibited much lower NPs concentrations compared to topsoil (0–10 cm). For instance, Sample 39 subsurface soil (S39-DS, >20 cm) recorded a NPs concentration of 3.9 ng/g, which is lower than its corresponding topsoil (sample 39), which measured 67.6 ng/g. Similarly, sample 15 deep soil (15-DS, >40 cm) had NPs concentrations <MLD, whereas its topsoil counterpart (sample 15) recorded 30.0 ng/g. Sample 45 deep soil (S45-DS, >40 cm) showed no detectable plastics,

while sample 35 deep soil (S35-DS, 30–40 cm) exhibited a relatively high concentration of 223.8 ng/g. Unfortunately, no topsoil samples were available for comparison with samples 45-DS and 35-DS.

The thermal desorption and ionization efficiency was 53.1 ± 2.8% for PS-spiked procedural blanks, in agreement with previously published data (Materić et al., 2020). Spiked samples exhibited similar ionization efficiency and strong mass spectral signals, indicating that matrix effects had only a minor influence on polymer identification.

A substantial difference in recovery was observed depending on whether the 500 nm PS particles were spiked before or after the syringe filtration step using a 1 µm membrane filter. When samples were spiked onto cracked Anodisks in the final step before thermal desorption—i.e., after 1 µm filtration—the recovery reached 84% (corrected for ionization efficiency). In contrast, when spiking was performed prior to 1 µm filtration, recovery dropped dramatically to 5.8% (corrected for ionization efficiency). This significant reduction is likely due to the retention or clogging of relatively large 500 nm PS particles by the syringe filter.

However, in actual environmental samples, the recovery is expected to be much higher, as the filtration effect should not impact the smaller nanoplastics typically present in remote locations. These results highlight a limitation of the current extraction method: it is biased toward detecting smaller nanoplastics, and therefore likely underestimates the concentration of larger particles (e.g., >500 nm).

Spiking procedural blanks prior to 1 µm filtration resulted in a recovery of 6.8%, which is slightly higher than the 5.8% recovery observed for spiked samples, although the difference is not statistically significant. The improved recovery in blanks may be attributed to matrix effects, but a more detailed investigation is beyond the scope of this study.

Due to the lack of other nanoplastic standards [34] and the time constraints of the project, recovery was assessed only for 500 nm PS particles. No recovery data were obtained for other polymer types or particle size fractions.

### 6.3.3 Potential plastic emission sources

The modelled footprint emission sensitivity for the deposited NPs mass is shown in **Figure** 5 for the receptor in Antarctica (white diamond sign). The calculated footprints express the probability of any unit gridded emission (kg $s^{-1}$) to reach and deposit at the receptor. When multiplied with any emission inventory the integral over the whole area gives the total simulated deposition flux (mg $m^{-2}$ $month^{-1}$). In general, the sources which are in the central part of Antarctica would have the highest impact to the measured mass at Taylor and Wright valleys. However, considering that there are no NPs sources in this region, there is potential for turbulent-induced resuspension of previously deposited NPs from snow-free regions of central Antarctica, transport from the surface of the ocean from bubble bursting or from the southernmost continents (**Figure** 6.5.). **Figure** S1 shows the monthly footprints of deposited NPs at the receptors averaged over three years prior to sampling (2020-2023). It is noteworthy that there are great differences in source regions between the Antarctic summer and all other months. From November to February (Antarctic summer, left panel in **Figure** 6.5.w), the emission sensitivity is largely

confined to Antarctica. On the contrary, from March to October, the Southern Ocean is an important source region, together with New Zealand and the southern tip of South America. Therefore, in general, we expect greater deposition during the Antarctic Winter due to the higher potential for long-range transport to Antarctica during this season.

In the present study, we have measured NPs in surface (and deep) soil during the Antarctic summer 2023 at two snow-free valleys. This means that the origin of NPs could be direct, resulting from long-range transport and deposition from South America or New Zealand, or indirect, if NPs had been deposited on snow and ice in Antarctic winter and migrated to the soil following snow melt during Antarctic summer. Although the source of the measured NPs is likely due to direct transport, during the Antarctic summer there may be some redistribution of NPs, as previously deposited NPs might have been resuspended from bare soil after snow melted, or from the numerous regional research stations. However, determining which of these two assumptions holds true remains challenging without consistent and systematic measurements of atmospheric and deposited NPs, as well as direct assessments of NPs in Antarctic soils.

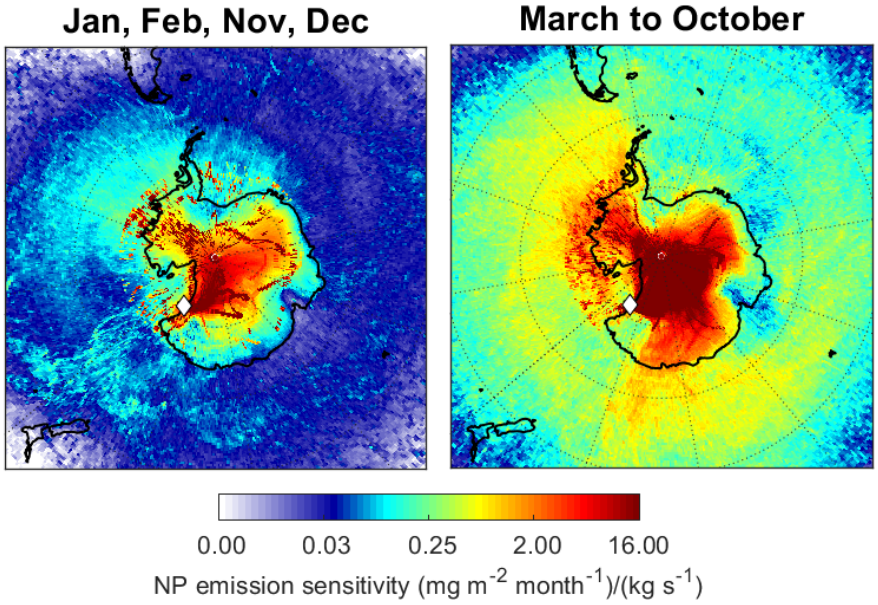


**Figure 6.5.** Footprint emission sensitivity for deposited NPs in Antarctic summer (left) and in all other months (right) expressed in mg $m^2$ $month^{-1}$ per kg $s^{-1}$. At each grid cell, the colours show the simulated accumulated monthly deposition flux ($mg/m^2$) at the receptor (white diamond) for a unit emission source (kg $s^{-1}$) in this respective grid cell.

## 6.4 Discussion

### 6.4.1 Occurrence of microplastics in Antarctica

MPs concentrations in the McMurdo Dry Valleys are low, with only one sample exceeding the MLDs. Assuming undetected sites have 0 MPs/g, the average concentrations are 0.6 ± 2.68 MPs/g for particles ≥10 µm and 0.26 ± 1.10 MPs/g for

particles ≥20 µm. While no prior studies have reported MPs concentrations in the McMurdo Dry Valleys or Southern Victoria Land, our findings fall within the same ranges to soil MPs concentrations in other Antarctic regions. For instance, soils in the Thala Hills, East Antarctica, contain 66–1933 particles/kg, as determined by manual digital microscopy (Kukharchyk et al., 2024). Similarly, research on the Fildes Peninsula reports an average of 13.6 particles/50 mL (range from 4–37 particles/50 mL) for particles ≥20 µm using FTIR (Perfetti-Bolaño et al., 2022), which translates to approximately 0.23 MPs/g, ranging from 0.067 to 0.617 MPs/g, assuming a soil density of 1.2 g/mL.

Discrepancies between studies may be due to methodological differences in sampling and analysis. For example, the Fildes Peninsula study sampled only the top 1 cm of soil (Perfetti-Bolaño et al., 2022), while the Thala Hills study sampled depths of 15–20 cm (Kukharchyk et al., 2024). This difference underscores the potential for MPs infiltrating deeper soil layers via meltwater, which may have been overlooked in studies that focused exclusively on topsoil. Furthermore, the lack of reporting on the MLODs or MLDs in these studies raises questions about whether MPs detected across all sites were thoroughly tested against secondary contamination. In contrast, in our study, most MPs concentration were <MLDs, suggesting stricter detection thresholds. Geographical factors, such as proximity to research activities, ship traffic, and ocean currents, may also explain the higher MPs concentrations observed in those studies compared to ours. Furthermore, Antarctic soils are highly diverse, with significant variability even within individual oases, influencing the accumulation and migration of pollutants (Abakumov, 2010; Goryachkin et al., 2019; Mergelov, 2014), including MPs and NPs.

Notably, this study focused on analysing MPs larger than 10 µm due to analytical challenges, such as increased matrix interference, which can lead to a higher incidence of false positives. Consequently, the particle fraction between 1–10 µm was not included. However, a study by Allen et al. (Allen et al., 2021) on atmospheric samples found that, on average, 51 % of MPs particles were in the smaller size fraction (≤10 µm) with a range of 21–74 % (±17 %). Another study found nearly all MPs (96 % ±0.1 %) were ≤20 µm in aerodynamic diameter (Allen et al., 2021). Future analyses could build on these findings by employing advanced techniques such as Raman spectroscopy, correlative SEM/Raman and QCL-FTIR (sensitive to MPs ≥ ~5 µm), to quantify MPs in the 1–10 µm range. Additionally, optimizing mass-based techniques with a relevant filtration setup could provide complementary mass quantification of plastics within this size range. Addressing this size gap would provide a more comprehensive understanding of atmospheric MPs, particularly if smaller particles significantly contribute to deposition, complementing the insights on NPs already provided in this study.

### 6.4.2 Occurrence of nanoplastics in Antarctica

NPs concentrations in the McMurdo Dry Valleys soils averaged 60.6 ng/g, with a median of 3.9 ng/g. The highest NPs concentration (20 nm–1 µm), 295 ng/g, was recorded at site 63, while MPs (≥10 µm) were detected only at site 39. This lack of overlap suggests that NPs may primarily originate from alternative sources, such as atmospheric deposition—a pathway more prevalent for NPs than MPs—rather than from MPs fragmentation. We suppose that the extreme conditions in the McMurdo Dry Valleys, characterized by low temperatures, minimal moisture, and limited microbial activity, likely inhibit the breakdown of MPs into NPs. However, further research is needed to fully understand the

fate, behaviour, and fragmentation processes of micro- and NPs in such unique environments. Additionally, the discrete nature of MPs and NPs contributes to their heterogeneous distribution, complicating accurate detection and quantification, particularly at low concentrations. Obtaining representative samples that truly reflect contamination levels remains a significant challenge. As such, interpreting environmental data requires caution, given the potential for uncertainties and errors introduced during sampling and analysis.

NPs concentrations in Antarctic soil have not been reported to date; however, NPs have been detected in other remote locations using TD-PTR-MS. For instance, at the high-altitude Alpine Sonnblick Observatory, melted surface snow contained an average NPs concentration of 46.5 ng/mL, with PP and PET being the dominant polymers (29.5 and 15.1 ng/mL, respectively) (Materić et al., 2021). In high-altitude Alpine glaciers, NPs were detected at concentrations ranging from 2–80 ng/mL, with TWP (41 %), PS (28 %), and PE (12 %) as the major contributors (Jurkschat et al., 2025). Similarly, in Greenland, a 14 m firn core revealed an average NPs concentration of 13.2 ng/mL, comprising PE (6.5 ng/mL), PET (2.7 ng/mL), PS, PVC (both 0.11 ng/mL), PP (0.57 ng/mL), and TWP (3.2 ng/mL) (Materić et al., 2022). While the most abundant NPs polymers vary across locations—likely due to differences in transport mechanisms and proximity to sources—the same key polymers (PE, PP, PS, PET, and TWPs) consistently dominate globally.

Closer to the McMurdo Dry Valleys, a study from McMurdo Sound Sea ice (70–80 km away from our study sites) found an average NPs concentration of 52.3 ng/mL using TD-PTR-MS (Materić et al., 2022). Atmospheric deposition, driven by wind transport, likely contributes to similar NPs concentrations in both soil and ice. Shared environmental and anthropogenic influences, such as scientific activities and tourism, may also explain these patterns. However, notable differences exist in accumulation and retention mechanisms between soil and ice. For instance, NPs in sea ice predominantly included PE, PP, and PET (38 and 20.7 ng/mL at the top of the ice core, respectively) (Materić et al., 2022), while soil samples also contained additional polymers such as tyre rubber, PVC, and PS. The absence of these polymers in sea ice could result from selective incorporation during ice formation, interactions with biogenic materials, or the exclusion of impurities like salts (Materić et al., 2022). Variability in sampling locations and methodologies further complicates direct comparisons, underscoring the need for careful interpretation of NPs data.

PP was the most abundant NPs in our study, accounting for 40 % of the total NPs mass. PP has also been identified as the dominant polymer in Alpine melted surface snow (Materić et al., 2020) and Southern Ocean Sea ice (Kelly, Anna et al., 2024). As one of the most widely used plastics, PP represented 19.3% of global plastic production in 2021 and is commonly used in packaging, household goods, automotive components, and textiles. TWP (24 %) and PE (15 %) were the next most abundant NPs, followed by PS and PET. Tyre-derived NPs, primarily composed of styrene-butadiene-styrene (SBS)—a durable and cost-effective thermoplastic elastomer—are widely produced. A global analysis of tyre and brake wear MPs transport has illustrated that these vehicle-related MPs are transported long distances from the land and ocean surface, with 30–34 % of tyre/brake wear MPs atmospherically transported and deposited in the world's oceans (Evangeliou et al., 2020). Beside atmospheric transport, Munari et al. reported TWP

debris near scientific bases in Terra Nova Bay (Ross Sea, Antarctica), linking these particles to anthropogenic (Munari et al., 2017). Besides, PET accounted for 5 % of the NPs mass in this study. As a widely used material in textiles and bottles, PET is a significant urban MPs and NPs pollutant and has been frequently detected in Arctic seawater, snow, and ice (Aves et al., 2022; Cincinelli et al., 2017a; Materić et al., 2022).

NPs tend to accumulate in the topsoil, with their vertical migration driven by mechanisms such as advection, where percolating water transports NPs through soil pores (Hou et al., 2020; Jiang, Y. et al., 2021). Except for our study, no other field evidence currently confirms the presence of NPs in deeper soil layers. However, laboratory experiments have demonstrated NPs vertical transport, influenced by various factors, including the physicochemical properties of the plastic (Hou et al., 2020; Jiang, Y. et al., 2021), the characteristics of the porous media (He et al., 2020; Tan et al., 2021), and solution chemistry (e.g., pH, ionic strength, and dissolved organic matter content) (Hou et al., 2020; Liu, Jin et al., 2019; Tan et al., 2021). For instance, Zhang et al. found that in quartz sand columns, PS-NPs transport in saturated porous media increased with higher input concentrations and larger media particle sizes, as larger particles created wider pore spaces, reducing resistance, and facilitating particle movement (Zhang, Mingzhi et al., 2023). In our McMurdo Dry Valleys soils, atmospheric deposition contributes to the accumulation of NPs in surface layers. Over time, surface disturbances, such as wind erosion and meltwater infiltration, may gradually drive these particles deeper. This process is particularly pronounced given that the soil in this study have a very low organic carbon content and a coarse texture, which provides larger pore spaces that facilitate NPs movement.

## 6.4.3 Source of microplastics and nanoplastics to Antarctica

MPs and NPs in Antarctica likely originate from both local and long-range sources and are distributed around the continent through a cycle of entrainment and deposition. Local inputs include the breakdown of plastic equipment at research stations, fibres shed from researchers' clothing, and improper waste disposal. Long-range transport mechanisms involve ocean currents (Fraser et al., 2018), ocean-to-atmosphere exchange (Allen et al., 2020) and atmospheric transport over varying distances (Evangeliou et al., 2020). Recent atmospheric transport modelling suggests Antarctica is a net importer of MPs, with fluxes from mismanaged plastic waste in the ocean transferring to the atmosphere at the Antarctic coast likely surpassing direct anthropogenic sources of MPs on the continent (Brahney et al., 2020d).

### 6.4.3.1 Long-range atmospheric transport

Long-range atmospheric transport (LRAT) significantly contributes to the deposition of MPs and NPs in remote regions, including Antarctica. Particles with aerodynamic size ranging from 100–1000 nm, can travel extensive distances through the atmosphere, occasionally covering entire hemispheres (Damoah et al., 2004). Studies have shown that even larger particles (>75 μm) can remain airborne for extended periods and be deposited thousands of kilometres from their sources, providing strong evidence of LRAT (Jeong et al., 2014; Van Der Does et al.; Varga et al., 2021). While evidence for the LRAT of NPs remains limited, more data exists for MPs. A field study detected 0.09–0.66 MPs/m³ (dia. <50 μm, including PE, PP, PS, PET, PVC) in free-tropospheric aerosols at Pic du Midi, with modelling confirming their intercontinental and trans-oceanic transport,

demonstrating the global dispersal of aerosolized MPs Allen et al., 2021). A hemispheric-scale analysis of airborne MPs along a cruise path from the mid-Northern Hemisphere to Antarctica reported concentrations ranging from 0.020 to 0.048 MPs/m³, with an average of 0.035 MPs/m³, containing rayon, PE, PP, PET, etc (Chen, Q. et al., 2023b). In the Atlantic Ocean atmosphere, MPs concentrations ranged from below MLODs to 51.75 ng/m³, depending on polymer types including PE, PP, polyisoprene (PI) and PS (Caracci et al., 2023). In Antarctica, studies on MPs presence in snow and glaciers (Aves et al., 2022; González-Pleiter et al., 2021), supported by backward air mass trajectories, suggest that MPs originate from both local, current, and past activities and are likely deposited via wind transport (González-Pleiter et al., 2021). Aves et al. identified transport over distances of up to 6,000 km, with air masses passing through the Amundsen or Ross Seas and occasionally from the Weddell Sea (Aves et al., 2022).

Key factors influencing MPs and NPs transport, such as wet and dry deposition rates, triboelectric effects, particle interactions, and atmospheric conditions (e.g., humidity, temperature, acidity, precipitation, and surface vegetation), remain largely unquantified (Allen et al., 2021). Recent studies have tentatively explored in-cloud and below-cloud scavenging coefficients for tyre and brake wear MPs transport, relying on statistical assumptions due to limited physical parameterization (Evangeliou et al., 2020). Additionally, MPs characteristics such as size and shape also significantly affect transport dynamics (Chen et al., 2023b; Tatsii et al., 2023). For example, Chen et al. provided the first measurements of MPs concentrations from the mid-Northern Hemisphere to Antarctica, showing that fibres are transported more efficiently than fragments, with behaviour similar to non-plastic particles (Chen et al., 2023b). Future research should prioritize characterizing and parameterizing MPs transport mechanisms, focusing on drivers of entrainment, deposition, and long-range transport. Improved modelling and particle dispersion analyses are crucial for advancing our understanding of MPs sources and atmospheric pathways.

#### 6.4.3.2 Possible local sources of microplastics and nanoplastics

Scientific activities and tourism, despite being regulated under the Antarctic Treaty, are significant contributors to MPs and NPs contamination in Antarctica. Research stations such as Marble Point, Ross Island, Scott Base (New Zealand), and McMurdo Station (US) are located within 20–100 km of our sampling sites (**Figure** 1). McMurdo Station accommodates up to 1,200 people during summer and around 150 in winter, while Scott Base hosts 86 people in summer and 11 in winter (COMNAP, 2017). This may also explain why, during the Antarctic summer, plastics are more locally sourced within the continent (**Figure** 4). Plastic products used at these stations, including building materials, marker flags, safety equipment, and tyre rubber, along with wear and weathering from clothing and outdoor equipment, likely contribute to MPs and NPs contamination. These plastics fragment under environmental exposure, accelerated by the Antarctic ozone hole's enhanced ultraviolet flux (Williamson et al., 2019). Additionally, MPs discharges from sewage plants (Cincinelli et al., 2017b; Waller et al., 2017a) and legacy pollution from poorly managed waste and dumpsites exacerbate contamination: 52 % of Antarctic research stations lack wastewater treatment, contributing to widespread contamination, with approximately 18.2 million person-days recorded per decade (Waller et al., 2017a).

Melting sea ice act as secondary sources of NPs and MPs, releasing previously trapped plastics during melting, providing a direct pathway into adjacent terrestrial and aquatic ecosystems (Peeken et al., 2018). The retreat of Antarctic glaciers due to climate change is likely to mirror this process, reintroducing legacy pollution into the McMurdo Dry Valleys. Once deposited, strong Antarctic winds can redistribute MPs across vast areas, further amplifying their spread. Bergmann et al. found that MPs could be transported across frozen landscapes by wind (Bergmann et al.), a process that may similarly occur in Antarctica's polar desert regions as pointed out in **Figure** 5.

## 6.4.4 Analytical limitations of the present study

### 6.4.4.1 Measurement of microplastic

The recovery rate of MP sphere dia. 10 um using this method was estimated at 23.0±8.9 %, with potential losses attributed to procedural inefficiencies (e.g., during density separation, organic digestion with fenton and other step like rinsing, loss thorough filter mesh, etc.) these are particularly relevant given the small size of the plastics sphere compare to previous recovery reporting using larger MP (e.g., 100um). Density separation using the overflow method was employed due to the simplicity of the apparatus, which utilized only incinerated glass materials to avoid plastic components (e.g., centrifuge tubes or PVC separation kits). This approach minimized plastic usage, thereby reducing the risk of cross-contamination, and lowering the MLODs. Although density separation using a glass funnel effectively minimizes plastic usage, it was not employed in this study because the gravelly nature of the soil samples could block the funnel. While the overflow setup has been tested for larger MPs (Crutchett & Bornt, 2024a), it may result in incomplete density separation, leading to the potential loss of particles as small as 10 µm during the overflow process. The oxidative digestion process using Fenton's reagent may also fragment MPs into particles smaller than the size cut-off of 10 µm.

While fluorescence microscopy is a useful tool, it has limitations, including its inability to chemically identify polymer types, which reduces the method's specificity. Furthermore, certain types of MPs, such as black particles or those with highly rigid or less hydrophobic surfaces, may not stain effectively with Nile Red, leading to their under-detection ( Phan Le et al., 2025, see Chapter 2). False-positive results also remain a concern when residual organic matter persists after extraction. However, in this study, the organic matter content of the soil samples was extremely low, ranging from 0.03 to 0.2 %, significantly reducing the likelihood of false-positive results, though not eliminating them entirely.

### 6.4.4.2 Measurement of nanoplastics

This study is among the first to establish an extraction and analytical protocol using TD-PTR-MS for NPs in soil. Although numerous methods exist for NPs analysis, only a few, including pyrolysis gas chromatography mass spectrometry (Py-GC–MS) and TD-PTR-MS, have been applied to environmental samples. Py-GC–MS has been used to detect NPs in seawater (PVC, PET, PS) (Ter Halle et al., 2017), beach sand (PS, PVC) (Davranche et al., 2020), and agricultural soil (PE, PS, PVC) (Wahl et al., 2021), with the latter being the first and only study to investigate NPs in soil, to the best of our knowledge. However, these studies are limited to detection, lacking quantification, with unreported

MLDs and recovery rates (Wahl et al., 2021). Additionally, Py-GC–MS is highly sensitive to organic impurities, requiring extensive pre-treatment for samples rich in organic matter, such as soil, sediment, and biological materials (Davranche et al., 2020; Wahl et al., 2021).

NPs analysis using TD-PTR-MS, on the other hand, has been rigorously tested for reliability in minimizing artefacts, addressing both false positives and false negatives. Common natural polymers, including cellulose and humic acids, were analysed and showed no matches with any of the plastics investigated (PE, PET, PS, PP, PVC, and TWPs) (Materić et al., 2021). To test for false negatives, PS was spiked into a mixture of these natural polymers, and a positive fingerprint match was obtained, demonstrating that the presence of natural polymers does not significantly interfere with NPs detection (Materić et al., 2021). These results confirm the robustness and accuracy of TD-PTR-MS.

Our protocol achieved a no significant difference between the recovery of PS-spiked samples compared to the PS-spiked procedural blank, demonstrating its effectiveness in extracting NPs from soil. $H_2O_2$ solution was used as the extraction medium with subsequent vertexing and settling, leveraging the Brownian motion of NPs, and proved generally sufficient for NPs recovery. However, it is important to note that the NPs recovery rate is influenced by several factors, including NPs size and other physiochemical characteristics, spiking conditions, and soil properties. For instance, when NPs spike undergo multiple wet-dry cycles with soil or are exposed to increased soil organic matter and clay content, these conditions might enhance homo- and heterogeneous aggregation with NPs, potentially altering recovery outcomes.

In our study, significant particle loss likely occurred due to NPs either becoming trapped in the 1 µm PP syringe filter or adhering to glassware and the filtration apparatus. Additionally, incomplete ionization and thermal desorption during TD-PTR-MS analysis further contributed to lower recovery rates. Specifically, the chemical ionization of thermally desorbed plastic vapours generates neutral molecules (e.g., $CO_2$) that are not detected by the method (Materić et al., 2020, 2022), resulting in a TD-PTR-MS efficiency of 44.8 %. Optimization of key parameters, including filtration systems, ionization efficiency, and thermal desorption, is essential to improve the detection and quantification of NPs in soil using TD-PTR-MS.

## 6.5 Conclusions

This study confirms the presence of both MPs and NPs in Antarctic soil, using Nile Red-stained fluorescence microscopy for MPs and a newly developed TD-PTR-MS protocol for NPs in soil. Plastics were detected in both Taylor and Wright Valleys of the McMurdo Dry Valleys. MPs larger than 10 µm were identified at only one site, while NPs were found in topsoil and deep soils across multiple locations, with an average concentration of 60.6 ng/g soil. The primary polymers detected included PP, TWP and PE. Potential sources include local contributions from research stations and long-range transport, as suggested by back-trajectory modelling. While further refinement of NPs analytical protocols is necessary, this study addresses significant knowledge gaps regarding the occurrence of MPs and NPs in Antarctic soil. It highlights the value of remote regions as

indicators of global plastic contamination. Continued research is essential to unravel the transport pathways delivering plastics to Antarctica and to assess their environmental fate and potential impacts on this fragile and pristine ecosystem.

Our findings raise significant concerns for Antarctic ecosystem health, as MPs and NPs may be ingested by soil-dwelling organisms or enter terrestrial food webs. Polar ecosystems may be especially vulnerable, e.g., native invertebrates have slow growth, low metabolism, weak genetic differentiation, and limited detoxification capacity, reducing their adaptability (Clarke & Peck, 1991; Peck, 2002; Zane & Patarnello, 2000). These traits make them more susceptible to climate and chemical stressors—yet the impacts of MPs and NPs under such conditions remain poorly understood. Our data on MP and NP exposure in polar terrestrial ecosystems—including polymer abundance, composition and potential sources—offer a critical foundation for ecotoxicity studies, which currently rely on assumptions about environmentally relevant concentrations, polymer types, and other characteristics.

This study also underscores the urgent need for strengthened international collaboration to reduce global emissions, alongside stricter local waste management practices, to safeguard Antarctica's ecological integrity. Continued research is essential to better understand plastic transport pathways to Antarctica and to assess their environmental fate and potential impacts on this fragile ecosystem. Given the intensity of ocean warming and acidification in polar regions—and the associated rapid environmental changes—it is vital to couple MP and NP ecotoxicological research with future climate scenarios. Moreover, the cumulative effects of MPs and NPs with other pollutants must be considered to fully understand their combined impacts

**Acknowledgements:** FLEXPART model simulations are cross-atmospheric research infrastructure services provided by ATMO-ACCESS (EU grant agreement No 101008004). The computations/simulations were performed on resources provided by Sigma2 - the National Infrastructure for High Performance Computing and Data Storage in Norway. This work is part of the PNRA 2018/D3.01 SENECA project (PNRA 2018 n° 00253 linea D, prot.73633/ 2019, SENECA PROJECT: Source and origin of greenhouses gases in Antarctica).

**Funding:** This work was supported by the European Union's Horizon 2020, SOPLAS, with grant agreement No. 55334. NE and SE are funded by the Norwegian Research Council (NFR) project MAGIC (Airborne Microplastic Detection, Origin, Transport and Global Radiative Impact, Project No.: 334086).

**Author contributions:** Conceptualization of the study was completed by QN.PL, D.M, C.Z., C.H. and J.Q. Methodology development for MPs and NPs analysis was undertaken by QN.PL. and D.M. Soil sampling and analysis were carried out by L.R., A.S., F.F. and C.Z. Investigation was undertaken by QN.PL. and D.M. Atmospheric deposition modelling was completed by N.E. and S.E. Funding was acquired by J.Q. and C.H. Supervision of study was led by C.H., J.Q., B.S. and L.A. The original draft was completed by QN.PL. with review and editing completed by all authors.

**Competing interests:** The authors declare that they have noncompeting interests.

# References


Abakumov, E. V. (2010). Particle-size distribution in soils of west antarctica. Eurasian Soil Science, 43(3), 297. doi:10.1134/s1064229310030075

Allen, S., Allen, D., Baladima, F., Phoenix, V. R., Thomas, J. L., Le Roux, G., et al. (2021). Evidence of free tropospheric and long-range transport of microplastic at pic du midi observatory. Nature Communications, 12(1) doi:10.1038/s41467-021-27454-7

Allen, S., Allen, D., Moss, K., Le Roux, G., Phoenix, V. R., & Sonke, J. E. (2020). Examination of the ocean as a source for atmospheric microplastics. Plos One, 15(5), e0232746. Retrieved from https://doi.org/10.1371/journal.pone.0232746

Anfuso, G., Bolívar-Anillo, H. J., Asensio-Montesinos, F., Portantiolo Manzolli, R., Portz, L., & Villate Daza, D. A. (2020). Beach litter distribution in admiralty bay, king george island, antarctica. Marine Pollution Bulletin, 160 doi:10.1016/j.marpolbul.2020.111657

Au, S. Y., Bruce, T. F., Bridges, W. C., & Klaine, S. J. (2015). Responses of hyalella azteca to acute and chronic microplastic exposures. Environmental Toxicology and Chemistry, 34(11), 2564. doi:10.1002/etc.3093

Aves, A. R., Revell, L. E., Gaw, S., Ruffell, H., Schuddeboom, A., Wotherspoon, N. E., et al. (2022). First evidence of microplastics in antarctic snow. The Cryosphere, 16(6), 2127. doi:10.5194/tc-16-2127-2022

Bakels, L., Tatsii, D., Tipka, A., Thompson, R., Dütsch, M., Blaschek, M., et al. (2024). FLEXPART version 11: Improved accuracy, efficiency, and flexibility. Geoscientific Model Development, 17(21), 7595. doi:10.5194/gmd-17-7595-2024

Barnes, D. K. A., Morley, S. A., Bell, J., Brewin, P., Brigden, K., Collins, M., et al. (2018). Marine plastics threaten giant atlantic marine protected areas. Current Biology, 28(19), R1137. doi:10.1016/j.cub.2018.08.064

Barnes, D. K. A., Galgani, F., Thompson, R. C., & Barlaz, M. (2009). Accumulation and fragmentation of plastic debris in global environments. Philosophical Transactions of the Royal Society B: Biological Sciences, 364(1526), 1985. doi:10.1098/rstb.2008.0205

Barrett, J. E., Virginia, R. A., Lyons, W. B., Mcknight, D. M., Priscu, J. C., Doran, P. T., et al. (2007). Biogeochemical stoichiometry of antarctic dry valley ecosystems. Journal of Geophysical Research: Biogeosciences, 112(G1) doi:10.1029/2005jg000141

Bergmann, M., Mützel, S., Primpke, S., Tekman, M. B., Trachsel, J., & Gerdts, G. White and wonderful? microplastics prevail in snow from the alps to the arctic.

Bessa, F., Ratcliffe, N., Otero, V., Sobral, P., Marques, J. C., Waluda, C. M., et al. (2019). Microplastics in gentoo penguins from the antarctic region. Scientific Reports, 9(1) doi:10.1038/s41598-019-50621-2

Bockheim, J. G. (1997). Properties and classification of cold desert soils from antarctica. Soil Science Society of America Journal, 61(1), 224. doi:10.2136/sssaj1997.03615995006100010031x

Brahney, J., Mahowald, N., Prank, M., Cornwell, G., Klimont, Z., Matsui, H., et al. (2020a). Constraining the atmospheric limb of the plastic cycle doi:10.1073/pnas.2020719118/-/DCSupplemental

Brahney, J., Mahowald, N., Prank, M., Cornwell, G., Klimont, Z., Matsui, H., et al. (2020b). Constraining the atmospheric limb of the plastic cycle doi:10.1073/pnas.2020719118/-/DCSupplemental

Campbell, I. B., & Claridge, G. G. C. (1987). Antarctica: Soils, weathering processes and environment. New York: Elsevier Science Publishing Company Inc.

Cassiani, M., Stohl, A., & Brioude, J. (2014). Lagrangian stochastic modelling of dispersion in the convective boundary layer with skewed turbulence conditions and a vertical density gradient: Formulation and implementation in the FLEXPART model. Boundary-Layer Meteorology, 154(3), 367. doi:10.1007/s10546-014-9976-5

Chen, Q., Shi, G., Revell, L. E., Zhang, J., Zuo, C., Wang, D., et al. (2023). Long-range atmospheric transport of microplastics across the southern hemisphere. Nature Communications, 14(1) doi:10.1038/s41467-023-43695-0

Cincinelli, A., Scopetani, C., Chelazzi, D., Lombardini, E., Martellini, T., Katsoyiannis, A., et al. (2017a). Microplastic in the surface waters of the ross sea (antarctica): Occurrence, distribution and characterization by FTIR. Chemosphere, 175, 391. doi:10.1016/j.chemosphere.2017.02.024

Cincinelli, A., Scopetani, C., Chelazzi, D., Lombardini, E., Martellini, T., Katsoyiannis, A., et al. (2017b). Microplastic in the surface waters of the ross sea (antarctica): Occurrence, distribution and characterization by FTIR. Chemosphere, 175, 391–400. doi:10.1016/j.chemosphere.2017.02.024

Cole, M., Lindeque, P., Fileman, E., Halsband, C., Goodhead, R., Moger, J., et al. (2013). Microplastic ingestion by zooplankton. Environmental Science &Amp; Technology, 47(12), 6646. doi:10.1021/es400663f

COMNAP. (2017). Antarctic_Station_Catalogue

Consoli, V., Ruggiero, L., Tondello, A., Squartini, A., Plaza, C., Sciarra, A., et al. Soil organic carbon and microbial community distribution in permafrost soils from antarctica (in preparation). Unpublished manuscript.

Convey, P., Barnes, D., & Morton, A. A. (2002). Debris accumulation on oceanic island shores of the scotia arc, antarctica. Polar Biology, 25(8), 612. doi:10.1007/s00300-002-0391-x

Crutchett, T. W., & Bornt, K. R. (2024a). A simple overflow density separation method that recovers >95% of dense microplastics from sediment. MethodsX, 12, 102638. doi:10.1016/j.mex.2024.102638

Crutchett, T. W., & Bornt, K. R. (2024b). A simple overflow density separation method that recovers >95% of dense microplastics from sediment. MethodsX, 12 doi:10.1016/j.mex.2024.102638

Cunningham, E. M., Ehlers, S. M., Dick, J. T. A., Sigwart, J. D., Linse, K., Dick, J. J., et al. (2020). High abundances of microplastic pollution in deep-sea sediments: Evidence from antarctica and the Southern Ocean American Chemical Society (ACS). doi:10.1021/acs.est.0c03441

da Costa, J. P., Santos, P. S. M., Duarte, A. C., & Rocha-Santos, T. (2016). (Nano)plastics in the environment – sources, fates and effects. Science of the Total Environment, 566-567, 15–26. doi:10.1016/j.scitotenv.2016.05.041

Damoah, R., Spichtinger, N., Forster, C., James, P., Mattis, I., Wandinger, U., et al. (2004). Around the world in 17 days -hemispheric-scale transport of forest fire smoke from russia in may 2003

David K.A. Barnes, Adam Walters, & Leandra Gonçalves. Macroplastics at sea around antarctica. Marine Environmental Research, 70(2), 250–252. doi:https://doi.org/10.1016/j.marenvres.2010.05.006

Davranche, M., Lory, C., Juge, C. L., Blancho, F., Dia, A., Grassl, B., et al. (2020). Nanoplastics on the coast exposed to the north atlantic gyre: Evidence and traceability. NanoImpact, 20, 100262. doi:10.1016/j.impact.2020.100262

Durante, C. A., Santos-Neto, E. B., Azevedo, A., Crespo, E. A., & Lailson-Brito, J. (2016). POPs in the south latin america: Bioaccumulation of DDT, PCB, HCB, HCH and mirex in blubber of common dolphin (delphinus delphis) and fraser's dolphin (lagenodelphis hosei) from argentina. Science of the Total Environment, 572, 352. doi:10.1016/j.scitotenv.2016.07.176

Eckhardt, S., Cassiani, M., Evangeliou, N., Sollum, E., Pisso, I., & Stohl, A. (2017). Source–receptor matrix calculation for deposited mass with the lagrangian particle dispersion model FLEXPART v10.2 in backward mode. Geoscientific Model Development, 10(12), 4605. doi:10.5194/gmd-10-4605-2017

Evangeliou, N., Grythe, H., Klimont, Z., Heyes, C., Eckhardt, S., Lopez-Aparicio, S., et al. (2020). Atmospheric transport is a major pathway of microplastics to remote regions. Nature Communications, 11(1) doi:10.1038/s41467-020-17201-9

Forster, C., Stohl, A., & Seibert, P. (2005). Parameterization of convective transport in a lagrangian particle dispersion model and its evaluation American Meteorological Society. doi:10.1175/jam2470.1

Fountain, A. G., Nylen, T. H., Monaghan, A., Basagic, H. J., & Bromwich, D. (2009). Snow in the McMurdo dry valleys, antarctica. International Journal of Climatology, 30(5), 633. doi:10.1002/joc.1933

Fraser, C. I., Morrison, A. K., Hogg, A. M., Macaya, E. C., van Sebille, E., Ryan, P. G., et al. (2018). Antarctica's ecological isolation will be broken by storm-driven dispersal and warming. Nature Climate Change, 8(8), 704–708. doi:10.1038/s41558-018-0209-7

Gigault, J., Halle, A. T., Baudrimont, M., Pascal, P., Gauffre, F., Phi, T., et al. (2018). Current opinion: What is a nanoplastic? Environmental Pollution, 235, 1030. doi:10.1016/j.envpol.2018.01.024

González-Pleiter, M., Edo, C., Velázquez, D., Casero-Chamorro, M. C., Leganés, F., Quesada, A., et al. (2020). First detection of microplastics in the freshwater of an antarctic specially protected area. Marine Pollution Bulletin, 161 doi:10.1016/j.marpolbul.2020.111811

González-Pleiter, M., Lacerot, G., Edo, C., Pablo Lozoya, J., Leganés, F., Fernández-Piñas, F., et al. (2021). A pilot study about microplastics and mesoplastics in an antarctic glacier. The Cryosphere, 15(6), 2531. doi:10.5194/tc-15-2531-2021

Goordial, J., Davila, A., Lacelle, D., Pollard, W., Marinova, M. M., Greer, C. W., et al. (2025). Nearing the cold-arid limits of microbial life in permafrost of an upper dry valley, antarctica. The ISME Journal, 10(7), 1613. doi:10.1038/ismej.2015.239

Goryachkin, S. V., Mergelov, N. S., & Targulian, V. O. (2019). Extreme pedology: Elements of theory and methodological approaches. Eurasian Soil Science, 52(1), 1. doi:10.1134/s1064229319010046

Grythe, H., Kristiansen, N. I., Groot Zwaaftink, C. D., Eckhardt, S., Ström, J., Tunved, P., et al. (2017). A new aerosol wet removal scheme for the lagrangian particle model FLEXPART v10. Geoscientific Model Development, 10(4), 1447. doi:10.5194/gmd-10-1447-2017

Hassan, P. A., Rana, S., & Verma, G. (2014). Making sense of brownian motion: Colloid characterization by dynamic light scattering. Langmuir, 31(1), 3. doi:10.1021/la501789z

He, L., Rong, H., Wu, D., Li, M., Wang, C., & Tong, M. (2020). Influence of biofilm on the transport and deposition behaviors of nano- and micro-plastic particles in quartz sand. Water Research, 178, 115808. doi:10.1016/j.watres.2020.115808

Hersbach, H., Bell, B., Berrisford, P., Hirahara, S., Horányi, A., Muñoz-Sabater, J., et al. (2020). The ERA5 global reanalysis. Quarterly Journal of the Royal Meteorological Society, 146(730), 1999–2049. doi:10.1002/qj.3803

Horton, A. A., & Barnes, D. K. A. (2020). Microplastic pollution in a rapidly changing world: Implications for remote and vulnerable marine ecosystems. Science of the Total Environment, 738 doi:10.1016/j.scitotenv.2020.140349

Hou, J., Xu, X., Lan, L., Miao, L., Xu, Y., You, G., et al. (2020). Transport behavior of micro polyethylene particles in saturated quartz sand: Impacts of input concentration and physicochemical factors. Environmental Pollution, 263, 114499. doi:10.1016/j.envpol.2020.114499

Isobe, A., Uchiyama-Matsumoto, K., Uchida, K., & Tokai, T. (2016a). Microplastics in the southern ocean. Marine Pollution Bulletin, 114(1), 623. doi:10.1016/j.marpolbul.2016.09.037

Isobe, A., Uchiyama-Matsumoto, K., Uchida, K., & Tokai, T. (2016b). Microplastics in the southern ocean. Marine Pollution Bulletin, 114(1), 623. doi:10.1016/j.marpolbul.2016.09.037

Jeong, G. Y., Kim, J. Y., Seo, J., Kim, G. M., Jin, H. C., & Chun, Y. (2014). Long-range transport of giant particles in asian dust identified by physical, mineralogical, and meteorological analysis. Atmospheric Chemistry and Physics, 14(1), 505. doi:10.5194/acp-14-505-2014

Jiang, Y., Yin, X., Xi, X., Guan, D., Sun, H., & Wang, N. (2021). Effect of surfactants on the transport of polyethylene and polypropylene microplastics in porous media. Water Research, 196, 117016. doi:10.1016/j.watres.2021.117016

Jones, N. R., de Jersey, A. M., Lavers, J. L., Rodemann, T., & Rivers-Auty, J. (2024). Identifying laboratory sources of microplastic and nanoplastic contamination from the air, water, and consumables. Journal of Hazardous Materials, 465, 133276. doi:10.1016/j.jhazmat.2023.133276

Jurkschat, L., Gill, A. J., Milner, R., Holzinger, R., Evangeliou, N., Eckhardt, S., et al. (2025). Using a citizen science approach to assess nanoplastics pollution in remote high-altitude glaciers Springer Science and Business Media LLC. doi:10.1038/s41598-024-84210-9

Kelly, A., Lannuzel, D., Rodemann, T., Meiners, K. M., & Auman, H. J. (2020). Microplastic contamination in east antarctic sea ice. Marine Pollution Bulletin, 154 doi:10.1016/j.marpolbul.2020.111130

Kelly, A., Rodemann, T., Meiners, K. M., Auman, H. J., Moreau, S., Fripiat, F., et al. (2024). Microplastics in Southern Ocean sea ice: A pan-antarctic perspective. Water Emerging Contaminants &Amp; Nanoplastics, 3(4) doi:10.20517/wecn.2024.66

Kukharchyk, T. I., Kakareka, S. V., & Rabychyn, K. O. (2024). Microplastics in soils of the thala hills, east antarctica. Eurasian Soil Science, 57(3), 502. doi:10.1134/s1064229323603025

Lacerda, A. L. D. F., Rodrigues, L. D. S., Van Sebille, E., Rodrigues, F. L., Ribeiro, L., Secchi, E. R., et al. (2019). Plastics in sea surface waters around the antarctic peninsula. Scientific Reports, 9(1) doi:10.1038/s41598-019-40311-4

Levy, J. (2012). How big are the McMurdo dry valleys? estimating ice-free area using landsat image data. Antarctic Science, 25(1), 119. doi:10.1017/s0954102012000727

Liu, J., Zhang, T., Tian, L., Liu, X., Qi, Z., Ma, Y., et al. (2019). Aging significantly affects mobility and contaminant-mobilizing ability of nanoplastics in saturated loamy sand American Chemical Society (ACS). doi:10.1021/acs.est.9b00787

Liu, K., Wu, T., Wang, X., Song, Z., Zong, C., Wei, N., et al. (2019). Consistent transport of terrestrial microplastics to the ocean through atmosphere. Environmental Science &Amp; Technology, 53(18), 10612. doi:10.1021/acs.est.9b03427

Materić, D., Kasper-Giebl, A., Kau, D., Anten, M., Greilinger, M., Ludewig, E., et al. (2020). Micro- and nanoplastics in alpine snow: A new method for chemical identification and (semi)quantification in the nanogram range. Environmental Science &Amp; Technology, 54(4), 2353. doi:10.1021/acs.est.9b07540

Materić, D., Kjær, H. A., Vallelonga, P., Tison, J., Röckmann, T., & Holzinger, R. (2022). Nanoplastics measurements in northern and southern polar ice. Environmental Research, 208 doi:10.1016/j.envres.2022.112741

Materić, D., Ludewig, E., Brunner, D., Röckmann, T., & Holzinger, R. (2021). Nanoplastics transport to the remote, high-altitude alps. Environmental Pollution, 288 doi:10.1016/j.envpol.2021.117697

Mergelov, N. S. (2014). Soils of wet valleys in the larsemann hills and vestfold hills oases (princess elizabeth land, east antarctica). Eurasian Soil Science, 47(9), 845. doi:10.1134/s1064229314090099

Munari, C., Infantini, V., Scoponi, M., Rastelli, E., Corinaldesi, C., & Mistri, M. (2017). Microplastics in the sediments of terra nova bay (ross sea, antarctica). Marine Pollution Bulletin, 122(1-2), 161. doi:10.1016/j.marpolbul.2017.06.039

Peeken, I., Primpke, S., Beyer, B., Gütermann, J., Katlein, C., Krumpen, T., et al. (2018). Arctic sea ice is an important temporal sink and means of transport for microplastic. Nature Communications, 9(1) doi:10.1038/s41467-018-03825-5

Perfetti-Bolaño, A., Araneda, A., Muñoz, K., & Barra, R. O. (2022). Occurrence and distribution of microplastics in soils and intertidal sediments at fildes bay, maritime antarctica. Frontiers in Marine Science, 8 doi:10.3389/fmars.2021.774055

Peter A. Conovitz, Diane M. Mcknight, Lee H. Macdonald, Andrew G. Fountain, & Harold R. House. (1998). Glaciers of the mcmurdo dry valleys, southern victoria land, antarctica. Ecosystem dynamics in a polar desert: The mcmurdo dry valleys, antarctica, volume 72

Quynh Nhu Phan Le, Crispin Halsall, Stoyana Peneva, Olivia Wrigley, Melanie Braun, Wulf Amelung, et al. Towards quality-assured measurements of microplastics in soil using fluorescence microscopy. Unpublished manuscript.

Reed, S., Clark, M., Thompson, R., & Hughes, K. A. (2018). Microplastics in marine sediments near rothera research station, antarctica. Marine Pollution Bulletin, 133, 460. doi:10.1016/j.marpolbul.2018.05.068

Rodrigues, J. P., Duarte, A. C., Santos-Echeandía, J., & Rocha-Santos, T. (2018). Significance of interactions between microplastics and POPs in the marine environment: A critical overview. TrAC Trends in Analytical Chemistry, 111, 252. doi:10.1016/j.trac.2018.11.038

Sander, M., Costa, E., Balbão, T. C., Carneiro, A. P., & Santos, C. (2009). Debris recorded in ice free areas of an antarctic specially managed area (ASMA): Admiralty bay, king george island, antarctic peninsula. Neotropical Biology and Conservation, 4(1), 36. doi:10.4013/nbc.2009.41.05

Sfriso, A. A., Tomio, Y., Rosso, B., Gambaro, A., Sfriso, A., Corami, F., et al. (2020). Microplastic accumulation in benthic invertebrates in terra nova bay (ross sea, antarctica). Environment International, 137 doi:10.1016/j.envint.2020.105587

Stohl, A., Forster, C., Frank, A., Seibert, P., & Wotawa, G. (2005). Technical note: The lagrangian particle dispersion model FLEXPART version 6.2.

Tan, M., Liu, L., Zhang, M., Liu, Y., & Li, C. (2021). Effects of solution chemistry and humic acid on the transport of polystyrene microplastics in manganese oxides coated sand. Journal of Hazardous Materials, 413, 125410. doi:10.1016/j.jhazmat.2021.125410

Tatsii, D., Bucci, S., Bhowmick, T., Guettler, J., Bakels, L., Bagheri, G., et al. (2023). Shape matters: Long-range transport of microplastic **fibres** in the atmosphere American Chemical Society (ACS). doi:10.1021/acs.est.3c08209

Ter Halle, A., Jeanneau, L., Martignac, M., Jardé, E., Pedrono, B., Brach, L., et al. (2017). Nanoplastic in the north atlantic subtropical gyre. Environmental Science & Technology, 51(23), 13689–13697. doi:10.1021/acs.est.7b03667

Van Der Does, M., Knippertz, P., Zschenderlein, P., Giles Harrison, R., & Stuut, J. W. The mysterious long-range transport of giant mineral dust particles

Varga, G., Dagsson-Waldhauserová, P., Gresina, F., & Helgadottir, A. (2021). Saharan dust and giant quartz particle transport towards iceland. Scientific Reports, 11(1) doi:10.1038/s41598-021-91481-z

Wahl, A., Le Juge, C., Davranche, M., El Hadri, H., Grassl, B., Reynaud, S., et al. (2021). Nanoplastic occurrence in a soil amended with plastic debris. Chemosphere, 262, 127784. doi:10.1016/j.chemosphere.2020.127784

Waller, C. L., Griffiths, H. J., Waluda, C. M., Thorpe, S. E., Loaiza, I., Moreno, B., et al. (2017a). Microplastics in the antarctic marine system: An emerging area of research. Science of the Total Environment, 598, 220–227. doi:10.1016/j.scitotenv.2017.03.283

Williamson, C. E., Neale, P. J., Hylander, S., Rose, K. C., Figueroa, F. L., Robinson, S. A., et al. (2019). The interactive effects of stratospheric ozone depletion, UV radiation, and climate change on aquatic ecosystems. Photochemical &Amp; Photobiological Sciences, 18(3), 717. doi:10.1039/c8pp90062k

Wright, S. L., Thompson, R. C., & Galloway, T. S. (2013). The physical impacts of microplastics on marine organisms: A review. Environmental Pollution, 178, 483. doi:10.1016/j.envpol.2013.02.031

Zeglin, L. H., Sinsabaugh, R. L., Barrett, J. E., Gooseff, M. N., & Takacs-Vesbach, C. D. (2009). Landscape distribution of microbial activity in the McMurdo dry valleys: Linked biotic processes, hydrology, and geochemistry in a cold desert ecosystem. Ecosystems, 12(4), 562. doi:10.1007/s10021-009-9242-8

Zhang, M., Hou, J., Wu, J., Miao, L., & Zeng, Y. (2023). Effects of input concentration, media particle size, and flow rate on fate of polystyrene nanoplastics in saturated porous media. Science of the Total Environment, 881, 163237. doi:10.1016/j.scitotenv.2023.163237

# Supporting information

## First evidence of nanoplastic in Antarctica soil

Quynh Nhu Phan Le[a], Nikolaos Evangeliou[b], Crispin Halsall[a], John Quinton[a], Ben W.J. Surridge[a], Lorna Ashton[c], Sabine Eckhardt[b], Livio Ruggiero[d], Alessandra Sciarra[e], Fabio Florindo[e], Claudio Zaccone[f,e,*], Dušan Materić[g*]

[a] Lancaster Environment Centre, Lancaster University, Lancaster LA1 4YQ, United Kingdom

[b] Stiftelsen NILU (former Norwegian Institute for Air Research), Instituttveien 18, 2007 Kjeller, Norway

[c] Department of Chemistry, Lancaster University, Lancaster, LA1 4YQ, United Kingdom

[d] Italian Institute for Environmental Protection and Research, Roma, Italy

[e] Istituto Nazionale di Geofisica e Vulcanologia, Via Vigna Murata 605, 00143 Roma, Italy

[f] Department of Biotechnology, University of Verona, Strada Le Grazie 15, 37134 Verona, Italy

[g] Department for Analytical Chemistry, Helmoltz Centre for Environmental Research – UFZ, Permoserstraße 15, 04318 Leipzig, Germany

**Table S1: Soil sampling: site description**

| Dry valley | Site | Site ID | Sampling description | | | | | |
|---|---|---|---|---|---|---|---|---|
| | | | X | Y | Lat | Lon | Date | Time |
| Taylor Valley | ANT23_TV-1-S_0-10 | 1 | 459412 | 1386379 | -77,593776 | 163,307423 | 14-Jan-23 | 10:30 |
| | ANT23_TV-2-S_0-10 | 4 | 459789 | 1385975 | -77,597492 | 163,322654 | 14-Jan-23 | 12:28 |
| | ANT23_TV-3-S_0-10 | 6 | 459940 | 1385873 | -77,598444 | 163,328828 | 14-Jan-23 | 13:30 |
| | ANT23_TV-5-S_0-10 | 13 | 459430 | 1386825 | -77,589786 | 163.308709 | 14-Jan-23 | 16:10 |
| | ANT23_TV-6-S_0-10 | 15 | 460911 | 1384527 | -77.610745 | 163.367751 | 26-Jan-23 | 11:00 |
| | ANT23_TV-9-S_0-10 | 25 | 460661 | 1386082 | -77.596754 | 163.359133 | 26-Jan-23 | 16:20 |
| | ANT23_TV-10-S_0-10 | 29 | 457846 | 1387257 | -77.585500 | 163.243254 | 27-Jan-23 | 11:10 |
| | ANT23_TV-12-S_0-10 | 36 | 458477 | 1385037 | -77.605551 | 163.266802 | 27-Jan-23 | 14:25 |
| | ANT23_TV-13-S_0-10 | 39 | 461075 | 1386781 | -77.590596 | 163.377199 | 28-Jan-23 | |
| Wright Valley | ANT23_WR-1-S_0-10 | 46 | 443171 | 1402825 | -77.441493 | 162.658143 | 08-Jan-23 | |
| | ANT23_WR-2-S_0-10 | 49 | 442838 | 1402543 | -77.443899 | 162.643969 | 08-Jan-23 | |
| | ANT23_WR-3-S_0-10 | 52 | 443168 | 1402601 | -77.443498 | 162.657651 | 08-Jan-23 | |
| | ANT23_WR-7-S_0-10 | 63 | 444346 | 1403147 | -77.439026 | 162.707030 | 09-Jan-23 | |
| Deep soil | Deep soil ANT23_TV-13-S_>20 | 41 | 461075 | 1386781 | -77.590596 | 163.377199 | 28-Jan-23 | |
| | Deep soil ANT23_TV-14-S_>40 | 45 | 462690 | 1387061 | -77.588480 | 163.444805 | 28-Jan-23 | 12:00 |
| | Deep soil ANT23_TV-6-S_40 | 18 | 460911 | 1384527 | -77.610745 | 163.367751 | 26-Jan-23 | 11:00 |
| | Deep soil ANT23_TV-11-S_30-40 | 35 | 458419 | 1385573 | -77.600735 | 163.265044 | 27-Jan-23 | 12:50 |

**Table S2: Soil characterisation of samples collected from Wright valley and Taylor Valley**

| Sample Name | Sample ID | Clay [%] <2 µm | Silt [%] 2-50 µm | Organic Carbon [%] |
|---|---|---|---|---|
| ANT23_TV-1-S_0-10 | 1 | 0.9 | 2.0 | 0.10 |
| ANT23_TV-2-S_0-10 | 4 | 2.7 | 17.0 | 0.13 |
| ANT_TV-3-S_0-10 | 6 | 1.5 | 9.9 | 0.10 |
| ANT23_TV-5-S_0-10 | 13 | 7.1 | 49.9 | 0.17 |
| ANT23_TV-6-S_0-10 | 15 | 1.3 | 5.3 | 0.09 |
| ANT23_TV-9-S_0-10 | 25 | 2.8 | 5.5 | 0.15 |
| ANT23_TV-10-S_0-10 | 29 | 5.3 | 12.8 | 0.13 |
| ANT23_TV-12-S_0-10 | 36 | 1.9 | 7.8 | 0.11 |
| ANT23_TV-13-S_0-10 | 39 | 0.7 | 3.7 | 0.08 |
| ANT23_TV-14-S_0-10 | 42 | 0.3 | 0.9 | 0.07 |
| ANT_WR-1-S_0-10 | 46 | 1.4 | 6.5 | 0.06 |
| ANT_WR-2-S_0-10 | 49 | 0.8 | 2.6 | 0.05 |
| ANT_WR-2-S_0-10 | 52 | 0.1 | 0.3 | 0.03 |
| ANT_WR-6-S_0-10 | 63 | 0.2 | 1.6 | 0.04 |

**Table S*3*: Microplastic concentration in procedural blanks**

| Blank | Total no. particles >=3.508 um | No. particles >=10um | No. particles >=20um | Total Volume (ml) | Volume taken (ml) | Total MPs in aqueous (>3um, extrapolated) | Total MPs in aqueous (>10um, extrapolated) | Total MPs in aqueous (>20um, extrapolated) |
|---|---|---|---|---|---|---|---|---|
| Blank 1 | 117 | 68 | 21 | 50 | 10 | 585 | 340 | 105 |
| Blank 2 | 190 | 78 | 21 | 50 | 10 | 950 | 390 | 105 |
| Blank 3 | 48 | 48 | 16 | 50 | 10 | 240 | 240 | 80 |
| Blank 4 | 37 | 22 | 5 | 50 | 10 | 185 | 110 | 25 |
| Blank 5 | 32 | 11 | 4 | 50 | 10 | 160 | 55 | 20 |
| Blank 6 | 124 | 55 | 15 | 50 | 10 | 620 | 275 | 75 |
| Average | | | | | | 456.7 | 235.0 | 68.3 |
| Standard deviation | | | | | | 314.7 | 130.2 | 37.6 |
| MLODs | | | | | | 1400.9 | 625.5 | 181.2 |

**Table S4: Microplastic concentration in samples.**

| Sample | Total no. particles >=3.508 um | No. particles >=10um | No. particles >=20um | Total Volume (ml) | Volume taken (ml) | Total MPs in aqueous (>3um, extrapolated) | Total MPs in aqueous (>10um, extrapolated) | Total MPs in aqueous (>20um, extrapolated) | Mass of soil (g) | MPs (>10 um) concentration after blank correction | MPs (>10 um) concentration after blank correction |
|---|---|---|---|---|---|---|---|---|---|---|---|
| 1 | 120 | 64 | 21 | 50 | 20 | 300 | 160 | 52.5 | 40.02 | <MLODs | <MLODs |
| 4 | 105 | 47 | 18 | 50 | 20 | 262.5 | 117.5 | 45 | 40 | <MLODs | <MLODs |
| 6 | 46 | 29 | 12 | 50 | 20 | 115 | 72.5 | 30 | 39.53 | <MLODs | <MLODs |
| 9 | 22 | 12 | 6 | 50 | 20 | 55 | 30 | 15 | 40.09 | <MLODs | <MLODs |
| 13 | 47 | 33 | 11 | 50 | 10 | 235 | 165 | 55 | 30.04 | <MLODs | <MLODs |
| 22 | 83 | 43 | 14 | 100 | 20 | 415 | 215 | 70 | 31.51 | <MLODs | <MLODs |
| 25 | 283 | 188 | 38 | 50 | 20 | 707.5 | 470 | 95 | 40.05 | <MLODs | <MLODs |
| 29 | 281 | 160 | 56 | 50 | 20 | 702.5 | 400 | 140 | 40.08 | <MLODs | <MLODs |
| 32 | 23 | 14 | 9 | 50 | 20 | 57.5 | 35 | 22.5 | 11.07 | <MLODs | <MLODs |
| 36 | 85 | 53 | 18 | 50 | 20 | 212.5 | 132.5 | 45 | 40.01 | <MLODs | <MLODs |
| 39 | 523 | 276 | 102 | 50 | 20 | 1307.5 | 690 | 255 | 40.04 | 11.4 | 4.7 |
| 42 | 249 | 151 | 17 | 50 | 20 | 622.5 | 377.5 | 42.5 | 41.5 | <MLODs | <MLODs |
| 46 | 83 | 43 | 16 | 100 | 20 | 415 | 215 | 80 | 40.04 | <MLODs | <MLODs |
| 49 | 31 | 18 | 10 | 50 | 5 | 310 | 180 | 100 | 40.19 | <MLODs | <MLODs |
| 52 | 278 | 133 | 45 | 50 | 20 | 695 | 332.5 | 112.5 | 40.05 | <MLODs | <MLODs |
| 55 | 131 | 63 | 28 | 50 | 20 | 327.5 | 157.5 | 70 | 25.7 | <MLODs | <MLODs |
| 58 | 174 | 97 | 38 | 50 | 20 | 435 | 242.5 | 95 | 23.22 | <MLODs | <MLODs |

| | | | | | | | | | | | |
|---|---|---|---|---|---|---|---|---|---|---|---|
| 60 | 118 | 54 | 15 | 50 | 20 | 295 | 135 | 37.5 | 8.17 | <MLODs | <MLODs |
| 63 | 131 | 64 | 27 | 50 | 20 | 327.5 | 160 | 67.5 | 40.07 | <MLODs | <MLODs |

**Table** S5: NPs TD-PTR-MS spectral library

| Rank [Int] | PE [m/z] | PE-LD [m/z] | PET [m/z] | PP [m/z] | PPC [m/z] | PS [m/z] | PVC [m/z] | Tire [m/z] | PE [m/z] | LDPE [m/z] |
|---|---|---|---|---|---|---|---|---|---|---|
| 1 | 101.059 | 101.059 | 149.03 | 101.059 | 101.059 | 105.065 | 107.049 | 107.048 | 101.059 | 101.059 |
| 2 | 121.064 | 113.058 | 123.044 | 123.113 | 123.113 | 107.049 | 129.089 | 123.042 | 121.064 | 113.058 |
| 3 | 113.057 | 115.074 | 181.083 | 109.099 | 113.057 | 121.064 | 149.03 | 101.058 | 113.057 | 115.074 |
| 4 | 115.075 | 111.075 | 105.034 | 113.057 | 109.099 | 123.044 | 121.064 | 111.046 | 115.075 | 111.075 |
| 5 | 125.058 | 125.058 | 151.032 | 111.075 | 125.094 | 117.087 | 123.044 | 109.097 | 125.058 | 125.058 |
| 6 | 111.075 | 123.045 | 167.034 | 195.154 | 111.075 | 106.072 | 257.246 | 105.033 | 111.075 | 123.045 |
| 7 | 129.089 | 129.088 | 121.064 | 125.094 | 115.075 | 133.064 | 131.084 | 121.098 | 129.089 | 129.088 |
| 8 | 123.044 | 139.106 | 150.036 | 115.075 | 139.106 | 108.053 | 133.064 | 113.058 | 123.044 | 139.106 |
| 9 | 131.084 | 109.096 | 193.049 | 121.1 | 141.089 | 103.041 | 143.084 | 135.041 | 131.084 | 109.096 |
| 10 | 149.03 | 127.075 | 124.047 | 207.109 | 121.1 | 209.096 | 105.065 | 133.059 | 149.03 | 127.075 |
| 11 | 153.093 | 153.093 | 175.039 | 141.089 | 129.089 | 207.109 | 155.08 | 139.078 | 153.093 | 153.093 |
| 12 | 207.109 | 103.073 | 165.09 | 139.106 | 167.138 | 149.03 | 181.1 | 125.093 | 207.109 | 103.073 |
| 13 | 195.154 | 149.031 | 131.084 | 153.093 | 153.093 | 119.083 | 135.046 | 119.079 | 195.154 | 149.031 |
| 14 | 109.099 | 143.105 | 195.119 | 129.089 | 195.154 | 131.104 | 101.024 | 127.074 | 109.099 | 143.105 |
| 15 | 141.089 | 141.089 | 139.04 | 167.138 | 127.105 | 145.105 | 130.073 | 108.053 | 141.089 | 141.089 |
| 16 | 127.075 | 157.119 | 137.06 | 107.082 | 137.122 | 118.063 | 108.053 | 137.058 | 127.075 | 157.119 |
| 17 | 139.077 | 137.061 | 106.036 | 137.122 | 107.082 | 223.166 | 157.094 | 115.074 | 139.077 | 137.061 |
| 18 | 137.06 | 155.102 | 257.246 | 127.105 | 151.138 | 104.076 | 183.082 | 307.128 | 137.06 | 155.102 |
| 19 | 103.073 | 171.137 | 125.024 | 151.138 | 143.105 | 135.046 | 117.087 | 157.091 | 103.073 | 171.137 |
| 20 | 165.09 | 151.073 | 191.094 | 149.123 | 149.123 | 124.047 | 119.083 | 153.088 | 165.09 | 151.073 |
| 21 | 107.049 | 107.05 | 147.043 | 165.146 | 165.146 | 129.089 | 167.083 | 124.045 | 107.049 | 107.05 |
| 22 | 117.087 | 181.122 | 163.043 | 223.166 | 163.14 | 221.108 | 285.277 | 147.076 | 117.087 | 181.122 |
| 23 | 171.139 | 185.155 | 133.031 | 135.079 | 102.064 | 143.084 | 147.043 | 151.08 | 171.139 | 185.155 |

| | | | | | | | | | | |
|---|---|---|---|---|---|---|---|---|---|---|
| 24 | 143.105 | 135.076 | 179.105 | 163.14 | 155.104 | 109.029 | 215.084 | 141.088 | 143.105 | 135.076 |
| 25 | 181.123 | 167.138 | 119.048 | 143.105 | 223.166 | 219.114 | 199.077 | 129.089 | 181.123 | 167.138 |
| 26 | 155.104 | 199.17 | 285.277 | 102.064 | 311.296 | 115.075 | 115.018 | 167.091 | 155.104 | 199.17 |
| 27 | 135.079 | 169.119 | 177.056 | 155.104 | 181.123 | 181.123 | 173.124 | 117.056 | 135.079 | 169.119 |
| 28 | 157.12 | 117.088 | 173.124 | 181.123 | 183.137 | 237.08 | 179.065 | 122.037 | 157.12 | 117.088 |
| 29 | 203.086 | 121.091 | 199.077 | 197.15 | 197.15 | 134.067 | 150.036 | 100.041 | 203.086 | 121.091 |
| 30 | 199.17 | 165.087 | 122.034 | 183.137 | 135.079 | 211.093 | 141.056 | 161.059 | 199.17 | 165.087 |
| 31 | 167.138 | 195.137 | 168.036 | 179.132 | 179.132 | 205.098 | 113.024 | 131.069 | 167.138 | 195.137 |
| 32 | 151.083 | 213.185 | 176.044 | 124.119 | 227.203 | 195.154 | 159.044 | 145.089 | 151.083 | 213.185 |
| 33 | 169.119 | 147.05 | 109.029 | 311.296 | 124.119 | 235.067 | 109.029 | 143.073 | 169.119 | 147.05 |
| 34 | 201.099 | 183.136 | 148.044 | 193.121 | 207.17 | 233.121 | 161.063 | 159.107 | 201.099 | 183.136 |
| 35 | 183.137 | 227.202 | 152.064 | 191.164 | 269.25 | 122.061 | 128.044 | 155.103 | 183.137 | 227.202 |
| 36 | 185.155 | 131.103 | 194.051 | 209.152 | 191.164 | 183.082 | 169.096 | 106.038 | 185.155 | 131.103 |
| 37 | 197.15 | 209.151 | 219.049 | 177.135 | 185.155 | 147.081 | 258.248 | 207.106 | 197.15 | 209.151 |
| 38 | 215.084 | 197.151 | 107.049 | 227.203 | 193.121 | 193.098 | 111.045 | 195.117 | 215.084 | 197.151 |
| 39 | 147.043 | 163.067 | 141.056 | 279.231 | 209.152 | 132.086 | 125.024 | 185.141 | 147.043 | 163.067 |
| 40 | 209.152 | 102.063 | 182.057 | 225.184 | 177.135 | 249.076 | 124.047 | 110.103 | 209.152 | 102.063 |

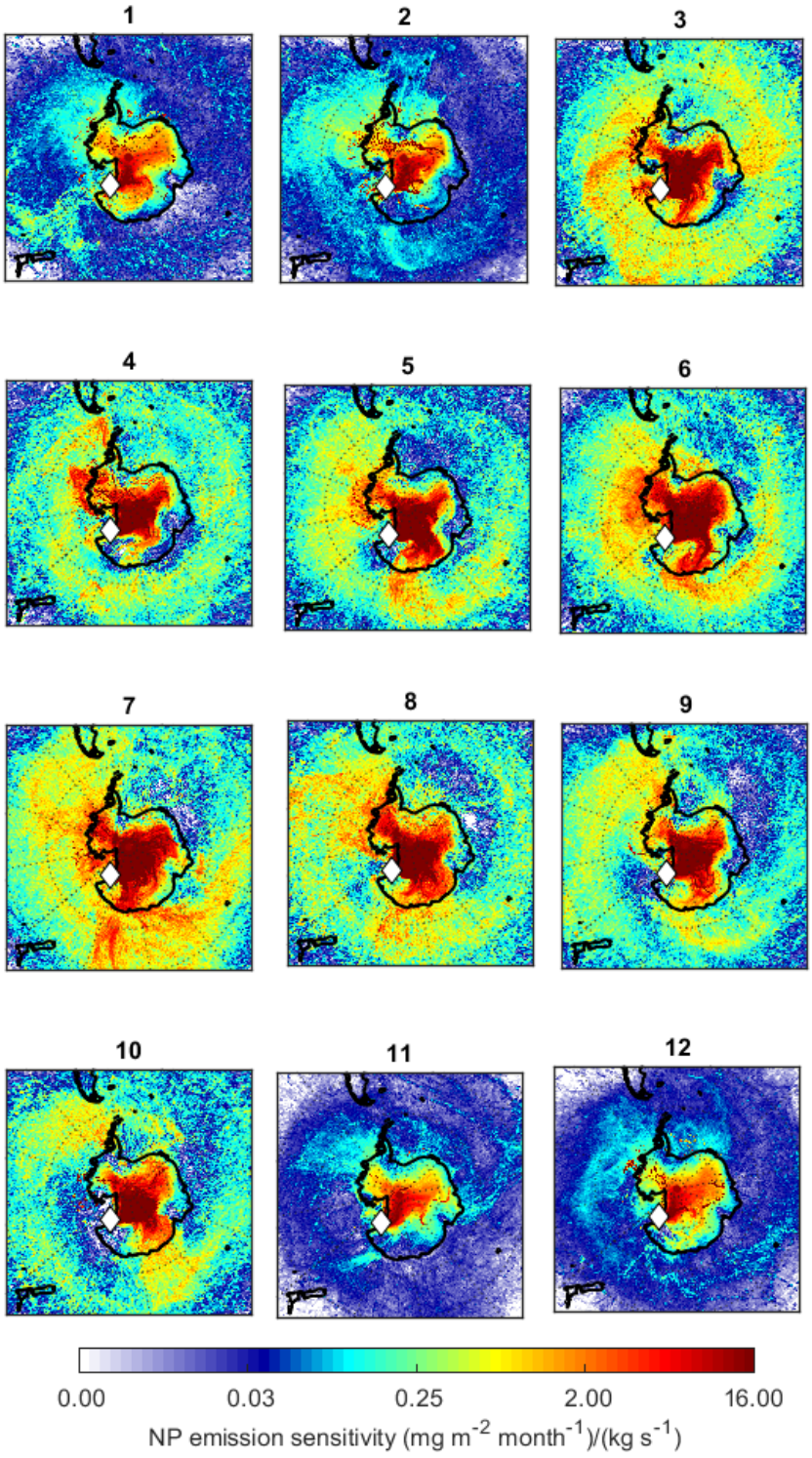


**Figure S1:** Monthly footprint emission sensitivity for deposited NPs in Antarctic.

# 7 Conclusion

## 7.1 Synopsis of the results

This PhD study initially focuses on developing and optimizing analytical protocols for the analysis of micro- and nanoplastics in soil. Subsequently, the study aims to investigate and provide field evidence for potential sources of plastics in soil, including agricultural applications of organic soil amendments such as sewage sludge and anaerobic digestate derived from animal manure, as well as the long-range atmospheric transport of microplastics. Depending on specific research questions and study objectives, different methods were selected and optimized accordingly. These include fluorescence microscopy, Fourier-transform infrared (FTIR) spectroscopy, and Raman spectroscopy for microplastics analysis. For nanoplastics, a highly sensitive thermal desorption proton transfer reaction mass spectrometry (TD-PTR-MS) method was developed, enabling the detection of nanoplastics even in the most pristine environments.

In **chapter 2**, the Nile Red staining-fluorescence microscopy method was developed and tested as a quick, user-friendly, and high-throughput approach for analyzing microplastics. Additionally, a digital image analysis tool was created using ImageJ, enabling automatic quantification of fluorescent particles and minimizing false positives caused by interference from the organic matrix. The method was tested on a wide range of commercial microplastics and various soil types, including clay, loam, and sandy soils, demonstrating its efficiency and applicability for analysing microplastics in complex soil matrices. Recovery rates were shown to vary depending on the polymer and soil types. Key soil characteristics, such as organic matter and clay content, significantly complicate the analysis of MPs. Additionally, plastics prone to degradation, such as biodegradable plastics, are difficult to extract and are often detected at levels lower than their true abundance.

In **chapter 3**, most commonly used methods for microplastic analysis including digital microscopy, fluorescence microscopy, Fourier-transformed infrared and Raman micro-spectroscopies, pyrolysis gas chromatography coupled with mass spectrometry, and quantitative proton nuclear magnetic resonance spectroscopy, each employing tailored extraction protocols were compared for their effectiveness when analysing a ranges of microplastics in different soil types, using the same materials as Chapter 2. This revealed significant impacts of extraction and analytical methods on recovery rates. Fluorescence microscopy was particularly effective for detecting small conventional plastics, while proton nuclear magnetic resonance spectroscopy excelled in analysing biodegradable MPs. Organic matter and clay in the soil matrix were identified as key complicating factors.

In **chapter 4 and 5**, the Nile Red staining fluorescence microscopy method was applied alongside Fourier-transform infrared (FTIR) spectroscopy to investigate the occurrence of microplastics in sewage sludge, anaerobic digestate, and soils receiving these amendments. High microplastics content was observed in both sewage sludge and

anaerobic digestate, with significantly higher microplastics concentrations in soils amended with these materials compared to non-amended background soils. Notably, the microplastics concentrations in amended soils exceeded the theoretically expected values based on the microplastics content in the amendments and their application rates. This discrepancy suggests the presence of additional sources of microplastics, such as atmospheric deposition, surface runoff, or the potential degradation of plastics over time. A comparison of methods revealed comparable particle counts between FTIR spectroscopy and fluorescence microscopy. However, closer alignment of results identified a significant level of mismatched findings, highlighting the occurrence of both false positives and false negatives in each method. These findings emphasize the importance of employing complementary techniques to enhance the accuracy and reliability of microplastics analysis.

In **chapter 6,** a method was developed for extracting nanoplastics from remote soil for subsequent analysis using the highly sensitive TD-PTR-MS. Plastics concentrations of up to 300 ng/g of soil were detected across sites in Antarctica's inland soil. Nanoplastics were also identified in deeper soil layers (>20 cm depth), albeit at much lower concentrations than in the topsoil, providing evidence of their infiltration into subsurface layers. To investigate potential sources, Lagrangian dispersion modelling was utilized, revealing distinct seasonal patterns of plastic deposition in Antarctica. These patterns highlighted contributions from both local sources and long-range atmospheric transport, along with oceanic input. This study emphasizes the critical role of remote Antarctic locations as a "barometer" for monitoring global background contamination and sheds light on the complex interplay of local and distant sources contributing to nanoplastics in polar soils.

## 7.2 Concluding remarks

### 7.2.1 Environmental aspects: sources and behaviour of plastic in soil

Microplastics (MPs) and nanoplastics (NPs) are ubiquitous environmental pollutants. Soils serve as the largest reservoirs of plastic contamination, with agricultural practices recognized as the primary contributors. Additionally, atmospheric deposition is emerging as a significant, though less studied, source of plastic contamination. This PhD research confirms the presence of MPs in agricultural soils, particularly in the UK, following the application of common organic amendments such as sewage sludge and anaerobic digestates derived from animal manure.

Our study revealed significantly higher concentrations of MPs in UK agricultural soils compared to previous reports. This discrepancy is attributed to the advanced analytical methods employed, which allowed the identification of smaller plastic particles—down to 25 µm—within complex soil matrices and organic amendments. The findings suggest that plastics deposited in soils through agricultural practices persist and undergo fragmentation over time. Notably, MPs from highly contaminated sewage sludge were found to remain detectable in soils even after a decade, with their composition evolving depending on the source and environmental interactions.

Significant levels of MPs were also detected in non-agricultural soils, suggesting additional inputs from surface runoff and atmospheric deposition. Field evidence and modelling from this research further support atmospheric transport and deposition as a major pathway for plastic contamination. This is exemplified by the detection of MPs in

the most remote and pristine soils of Antarctica, highlighting the global scale of atmospheric plastic transport.

| Method | Particle Information | Mass Information | Analysis Time | Advantages | Disadvantages |
|---|---|---|---|---|---|
| **Digital Microscopy** | Yes (≥ 200–300 µm, reliably) | No | Not specified | - Provides particle size, shape, and morphology<br>- Easy to use and cost-effective<br>- Fast with machine learning integration | - Prone to false positives/negatives<br>- Cannot identify polymer types |
| **Fluorescent Microscopy** | Yes (≥ 10–20 µm, reliably) | No | ~15 minutes per sample | - Provides particle size, shape, and morphology<br>- Easy to use and cost-effective<br>- Fast with digital image analysis or machine learning | - Prone to false positives/negatives<br>- Fluorescence depends on plastic properties (e.g., hydrophobicity, rigidity, color)<br>- Cannot identify polymer types |
| **FPA-µ-FTIR** | Yes (≥ 11 µm; QCL-FTIR down to 5 µm) | No* | 3–4 hours (3.5X objective) | - Provides particle size, shape, and morphology<br>- Identifies polymer types and occasionally additives | - Time-consuming<br>- Requires expert knowledge and advanced spectral libraries<br>- Plastic thickness and color may affect spectral accuracy |
| **µ-Raman Spectroscopy** | Yes (≥ 0.5–1 µm)** | No* | 8–10 hours per sample | - Provides particle size, shape, and morphology<br>- Identifies polymer types and occasionally additives | - Highly time-consuming<br>- Requires expert knowledge and spectral libraries<br>- Interference from additives (e.g. colorants)<br>- Difficult to standardize settings (laser power, exposure)<br>- Fluorescence from organic matter can obscure plastics |
| **Py-GC/MS** | No | Yes | Not specified | - Identifies polymer types and additives | - Time-consuming<br>- Requires expert knowledge and spectral libraries |

| | | | | | |
|---|---|---|---|---|---|
| | | | | - Provides chemical composition | - Risk of false positives due to low m/z fragment selection |
| **TD-PTR-MS** | No | Yes | ~15 minutes per sample | - Identifies polymer types and additives<br>- Fast and highly sensitive<br>- Produces large m/z fragments, reducing false positives | - Requires expert knowledge and spectral interpretation<br>- Prone to false negatives due to incomplete desorption or ionization |

* Mass conversion from particle information (surface area, plastics density based on typical density when known plastics types) are possible, however, the accuracy need to be further investigate, especially when volume of particle cant be obtained unless using 3D analysis, etc.

** For soil samples, this method can reliably measure down to 10um due to matrix interference

The findings of this research provide critical data for advancing future modelling studies, informing public policy, and guiding environmental monitoring and reporting. Addressing the dual sources of plastic contamination—agricultural practices and atmospheric pathways—will be essential for developing effective mitigation strategies.

In summary, this study emphasizes the widespread presence and persistence of MPs in diverse soil environments, including those in remote regions like Antarctica. These results underscore the importance of integrated approaches that consider both agricultural and atmospheric contributions to tackle MPs contamination comprehensively.

### 7.2.2 Analytical aspect: challenges and advance

In this PhD research, commonly used analytical methods—including Fourier Transform Infrared (FTIR) spectroscopy, Raman spectroscopy, fluorescence microscopy, pyrolysis-GC/MS, digital microscopy, Nuclear Magnetic Resonance (NMR), and Thermal Desorption Proton Transfer Reaction Mass Spectrometry (TD-PTR-MS)—were adapted, optimized, and tested to evaluate their recovery of plastics from a range of soil matrices. Some of these methods (including FTIR, Raman, fluorescence microscopy, and TD-PTR-MS) were further applied to investigate the occurrence of plastics in soils, aiming to enhance the understanding of their sources and pathways, and demonstrating their applicability to real environmental samples.

This research highlighted that each method possesses specific strengths and limitations, emphasizing the importance of aligning the analytical approach with the research objectives.

### Key takeaways and recommendations

Extracting microplastics (MPs) and nanoplastics (NPs) from complex soil matrices remains a significant challenge. The process requires careful balancing to avoid false positives while minimizing plastic degradation during extraction. Despite advancements, current techniques cannot fully achieve this balance, highlighting the need for further refinement.

From the author's perspective, while standardized methodologies for the analysis of microplastics (MPs) have been established for water matrices (e.g., ISO 5667-27:2025), achieving similar standards for the analysis of MPs—and especially nanoplastics (NPs)—in soils remains a distant goal. Ongoing efforts aim to develop new methods and refine existing analytical techniques. While methods like FTIR and Py-GC/MS may eventually be adopted as standardized techniques due to their accessibility and versatility, the complexity of plastic analysis underscores that a single method is insufficient. Instead, a complementary range of methods is essential to provide a comprehensive understanding of plastics in the environment (e.g., combining mass-based and particle-based techniques to integrate data on mass and particle count).

To ensure data comparability and usability for stakeholders—particularly for risk assessments and data reporting—studies on plastics must adhere to stringent quality assurance and quality control (QA/QC) protocols. These include reporting method recovery and limits of detection/sensitivity, using validated methodologies to minimize

bias and error, and ensuring transparency and reproducibility in data collection and interpretation.

A key priority is the development of plastic standards: Universal standards for MPs and NPs analysis across a wide range of polymers are essential. A recommendation for this would be to produce mixtures of the most commonly used plastics within consistent size ranges. These standards should include a variety of particle sizes and shapes to ensure comprehensive analysis and applicability across different studies.

## 7.3 Future research

### 7.3.1 Analytical advancement

Mass-based approaches, such as pyrolysis-GC/MS, TD-PTR-MS coupled with cascade filtration, and advanced techniques like field-flow fractionation or electrophoresis, offer significant potential to provide particle size data while delivering mass information. Although many of these techniques are still in the testing phase and not yet widely applied to environmental samples, their promise is evident. Combining these methods with techniques that characterize shape and morphology, such as SEM or TEM, could provide a highly robust characterization of plastics.

An important yet underexplored aspect of this study is the investigation of plastic additives and associated chemicals, which play a critical role in shaping plastic toxicity. Understanding their co-occurrence and interactions with plastics is essential to advancing future research. However, this remains a significant challenge due to the lack of comprehensive data on additives, particularly for untargeted analyses. A recent report on the global plastic treaty identified that, out of 17,000 chemicals, poorly defined chemicals and mixtures account for one-fourth of all plastic chemicals (Wagner et al 2024). This substantial gap indicates that many additives are missing from current analytical libraries, leading to incomplete and fragmented data. Furthermore, the analysis of micro- and nanoplastics and their additives is often conducted in isolation, with limited integration across studies. A more holistic approach is crucial to comprehensively understand the relationships between plastics and their additives, especially regarding their fate, degradation, leaching, and sorption processes.

### 7.3.2 Environmental aspects

Our findings provide clear evidence of plastic contamination in soils, primarily through the application of sewage sludge and anaerobic digestate as organic soil amendments. However, the long-term fate and impacts of these amendment-derived micro- and nanoplastics remain poorly understood. Most existing studies focus on pristine, lab-aged plastics, which may behave very differently from plastics originating in sewage sludge and digestate treatments. These treatment processes introduce complex chemical and physical alterations to the plastics, affecting properties such as surface charge, functional groups, microbial colonization, and the sorption of pollutants from these organic matrices.

Similarly, plastics transported over long distances are subjected to UV radiation and other environmental processes that induce significant physical and chemical transformations. These changes further complicate the understanding of their environmental impacts.

Key unanswered questions include the pollutants released during plastic degradation and their environmental interactions, the persistence and mobility of plastics in soil and water systems, and their impacts on microorganisms, nutrient cycles, and soil health. Additionally, the behaviour of plastics during atmospheric transport, their influence on climate processes like cloud formation and weather patterns, and the cumulative effects of plastics, additives, and by-products on ecosystems and global systems remain critical areas for investigation.

A deeper understanding of these questions is crucial for assessing the full environmental and ecological impacts of micro- and nanoplastics. Future research should prioritize real-world scenarios, such as plastics derived from sewage sludge and digestate treatments, to overcome the limitations of lab-based studies and bridge the gap between controlled experiments and environmental complexities.

## 7.4 Addressing plastic contamination in agricultural soils

Soil and water health are essential for food security, carbon cycling, and biodiversity. However, increasing plastic contamination in agricultural soils poses serious risks to crop productivity, soil quality, and ecosystem stability. To mitigate these impacts, targeted policies and solutions must be implemented, focusing on prevention, regulation, and sustainable practices. Key actions haven been implemented and proposed (UNEP, 2022), including:

- Uniform standards for biosolids: Establish strict regulations to prevent MPs, NPs, and toxins from entering crops, groundwater, and waterways via sewage sludge and digestate.
- Improved product design: Promote innovations to reduce MPs shedding from textiles, packaging, and consumer products, particularly those entering wastewater.
- Consumer awareness: Educate the public on the environmental impact of plastics and promote sustainable choices through clear labelling and awareness campaigns.
- Mandatory MPs filters: Require washing machines and industrial laundries to install MPs filters, preventing wastewater contamination.
- Regulating biodegradable agricultural products: Enforce stricter standards (e.g., EU Regulation 2019/1009) to ensure biodegradable products do not leave harmful residues.
- Recycling agricultural plastics: Improve the collection, recycling, and repurposing of agricultural plastics like mulch films and irrigation pipes.
- Advancing biodegradable plastics: Invest in R&D for affordable, zero-residue biodegradable plastics that fully decompose without toxic by-products.
- Nature-based farming practices: Encourage organic farming, reduced synthetic inputs, and agroecological approaches to minimize plastic contamination.

Given the uncertainties surrounding the long-term impacts of MPs and NPs, the precautionary principle should guide immediate action. Prioritizing cost-effective removal mechanisms in wastewater treatment, adopting more sustainable soil management practices, and conducting full life cycle assessments are essential steps to balance ecological preservation with agricultural productivity.

By addressing these challenges through coordinated research, policy, and public engagement, we can develop impactful and long-term solutions to safeguard soil health, water quality, and overall environmental sustainability while mitigating the risks of plastic contamination in agricultural systems.

## References

UNEP (2022). Plastics in Agriculture – An Environmental Challenge. United Nations Environment Programme. Foresight Brief 029. Nairobi.

Martin Wagner, Laura Monclús, Hans Peter H. Arp, Ksenia J. Groh, Mari E. Løseth, Jane Muncke, Zhanyun Wang, Raoul Wolf, Lisa Zimmermann (2024) State of the science on plastic chemicals - Identifying and addressing chemicals and polymers of concern, http://dx.doi.org/10.5281/zenodo.10701706.

# 8 Appendices

Appendix 1 Plastic input and dynamic in industrial composting ..... 2

Appendix 2 Unravelling the plasticsphere-soil and plasticplane microbiome of plastic mulch residues in agricultural soils..... 13

Waste Management 193 (2025) 283–292

Contents lists available at ScienceDirect

Waste Management

journal homepage: www.elsevier.com/locate/wasman

Research Paper

# Plastic input and dynamics in industrial composting

Stoyana Peneva [a,d], Quynh Nhu Phan Le [b], Davi R. Munhoz [c], Olivia Wrigley [d], Giovana P.F. Macan [e,f], Heidi Doose [g], Wulf Amelung [d,h], Melanie Braun [d,*]

[a] Wessling GmbH, Am Umweltpark 1, Bochum, 44793, Germany
[b] Lancaster Environment Centre, Lancaster University, Lancaster LA1 4YQ, UK
[c] Soil Physics and Land Management Group, Wageningen University & Research, P.O. Box 47, 6700 AA Wa-geningen, the Netherlands
[d] Institute for Crop Science and Resource Conservation (INRES) - Soil Science and Soil Ecology, University of Bonn, Nussallee 13, 53115 Bonn, Germany
[e] Institute for Sustainable Agriculture – Spanish National Research Council (IAS-CSIC), Avda Menéndez Pidal S/N, 14004 Cordoba, Spain
[f] Department of Agronomy, University of Córdoba, 14014 Córdoba, Spain
[g] Wessling Consulting Engineering GmbH & Co.KG, Feodor-Lynen Straße 23, Hannover, 30625, Germany
[h] Agrosphere Institute (IBG-3), Forschungszentrum Jülich GmbH, Wilhelm-Johnen-Str., 52425 Jülich, Germany

ARTICLE INFO

*Keywords:*
Composting
Microplastic pollution
Irrigation water
Fragmentation
Biowaste

ABSTRACT

Green and biowaste, processed within large facilities into compost, is a key fertilizer for agricultural and horticultural soils. However, due to improper waste disposal of plastic, its residues often remain or even lead to the formation of microplastics (1 μm – 5 mm, MiPs) in the final compost product. To better understand the processes, we first quantified 'macroplastics' (> 20 mm, MaPs) input via biowaste collection into an industrial composting plant, and, then determined MiP concentrations at five stages during the composting process (before and after shredding and screening processes), and in the water used for irrigation. The total concentrations of MaPs in the biowaste collected from four different German districts ranged from 0.36 to 1.95 kg ton$^{-1}$ biowaste, with polyethylene (PE) and polypropylene (PP) representing the most abundant types. The "non-foil" and "foil" plastics occurred in similar amounts (0.51 ± 0.1 kg ton$^{-1}$ biowaste), with an average load of 0.08 ± 0.01 items kg$^{-1}$ and 0.05 ± 0.01 items kg$^{-1}$, respectively. Only 0.3 ± 0.1 kg MaP t$^{-1}$ biowaste was biodegradable plastic. Compost treatment by shredding tripled the total number of MaPs and MiPs to 33 items kg$^{-1}$, indicating an enrichment of particles during the process and potential fragmentation. Noticeably, a substantial amount of small MiPs (up to 22,714 ± 2,975 particles L$^{-1}$) were found in the rainwater used for compost moistening, being thus an additional, generally overlooked plastic source for compost. Our results highlight that reducing plastic input via biowaste is key for minimizing MiP contamination of compost.

## 1. Introduction

Plastic production increased by 4 % from 2020 to 2021, resulting in 390 Mt produced globally, nevertheless, proper recycling and disposal of plastics are often insufficient (PlasticsEurope, report 2022). Consequently, plastic items are found also in biowaste, and, if not removed during composting – in compost (Van den Zee and Molenveld, 2020; Edo et al., 2022; Braun et al., 2021; Laforsch et al., 2023). However, the dynamics of plastics within a compost facility, i.e., the plastic input by biowaste, as well as their removal or enrichment during different steps of composting, are still unclear.

Biowaste, including green waste, is often sold as compost after respective treatment in large composting companies. In agriculture, as well as in gardening horticulture, compost is used as an important organic fertilizer and soil amendment, as it improves soil quality and fertility, and additionally supports a circular economy (Siebert and Kehres, 2008; Viaene et al., 2016; Colombini et al., 2022). The EU compost production equals 17.3 million tons per year, with Germany being the largest compost producer. Around 14 million tons of this compost are derived from green and biowaste, and about 85 % of the final compost is reused as a fertilizer (European Compost Network (ECN) report, 2019). However, the biowaste used for compost production may contain macroplastics (MaPs, >20 mm), mesoplastics (MePs, 5 mm – 20 mm), and microplastics (MiPs, 1 μm – 5 mm). Especially kitchen waste tends to be the most polluted (Ricci and Centemero, 2018, Friege and Eger, 2022). If biowaste is not separated by type at the source or plastic

* Corresponding author.
*E-mail address:* melanie.braun@uni-bonn.de (M. Braun).

https://doi.org/10.1016/j.wasman.2024.11.043
Received 12 June 2024; Received in revised form 18 October 2024; Accepted 27 November 2024
Available online 17 December 2024

is not properly removed before composting, these plastic particles might enrich the final product or break down to smaller sizes, i.e., forming further MiPs or even submicron plastic particles (<1 μm). Hence, compost application was identified as a principal input pathway of plastics into agricultural soils (Kumar et al., 2020; Sajjad et al., 2022; Porterfield et al., 2023; Braun et al., 2021; 2023).

Municipalities and operators of composting facilities pursue different strategies for collecting unmixed biowaste and removing foreign matter, including plastics. Typically, after collecting, green and biowaste undergo sorting, shredding, and sieving stages, preparing it for subsequent decomposition (Edo et al., 2022). This decomposition occurs under certain humidity and temperature conditions for a predetermined period through the activity of microorganisms (Diaz et al., 2007). Simultaneously, European regulations govern the acceptable presence of foreign materials in the final compost product, such as metals, glass and plastics. The compost cannot be commercialized if it contains more than 0.5 % foreign matter (dry weight, dw), larger than 2 mm. The regulations aim to reduce the plastic content to 0.25 g $kg^{-1}$ dw from July 2026 onwards (*Bundesgütegemeinschaft Kompost* (BGK), Federal Quality Association for Compost, 2021; ECN, 2021; ECN, Germany, 2023).

Steiner et al. (2023) screened 14 waste treatment plants with anaerobic and aerobic treatments for the presence of plastics. The authors highlighted that final sieving efficiently reduced the number of MaPs and MePs but lacked efficiency for smaller MiPs. In aerobic facilities, the final product contained plastic fragments (mainly polyethylene (PE)) over 5 mm and between 1–5 mm, i.e., 101 and 21 items $kg^{-1}$ dw, respectively. Conversely, anaerobic digestion produced liquid fertilizer with up to 10,000 particles of 10–1000 μm, raising more environmental concerns. In another study, placed 5x5 cm plastic pieces (PE, polypropylene (PP), polylactic acid (PLA), and polystyrene (PS)) in compost piles generated17 to 52 MiP particles during composting (>50 μm, Sholokhova et al., 2023). Although recent studies underscore the possibility of plastic fragmentation in composting facilities (e.g., Groß et al., 2024), there is little information available on the true plastic inputs; i.e., potential correlations of plastic input and plastic load of biowaste and composted material during the different steps of compost production. Especially, the contamination of the irrigation water during the composting process with MiP has not been evaluated, yet.

Here, we aimed to better understand the input and dynamics of plastics during composting. We hypothesized that i) most large plastic items entering the compost facility would be effectively removed after composting. Further, we assumed that ii) there will be a relative enrichment of small MiPs during the composting process, i.e., every treatment step during composting will reduce the size of plastic particles but increase the number of such small particles that the sieves cannot separate. Finally, we hypothesized that iii) the composting process will lead to an additional MiP contamination in the water used to irrigate the compost. To test these hypotheses, we monitored the plastic content, starting with the fresh waste throughout the whole composting process in a large industrial composting facility in Germany, processing biowaste. In detail, we determined the content of large plastic items in the incoming biowaste and analyzed the plastic content after each treatment step and in finished compost (i.e., at six sampling points) as well as in the irrigation water before and after composting.

## 2. Materials and methods

### 2.1. Compost facility

The experiment was carried out at a facility using tunnel composting

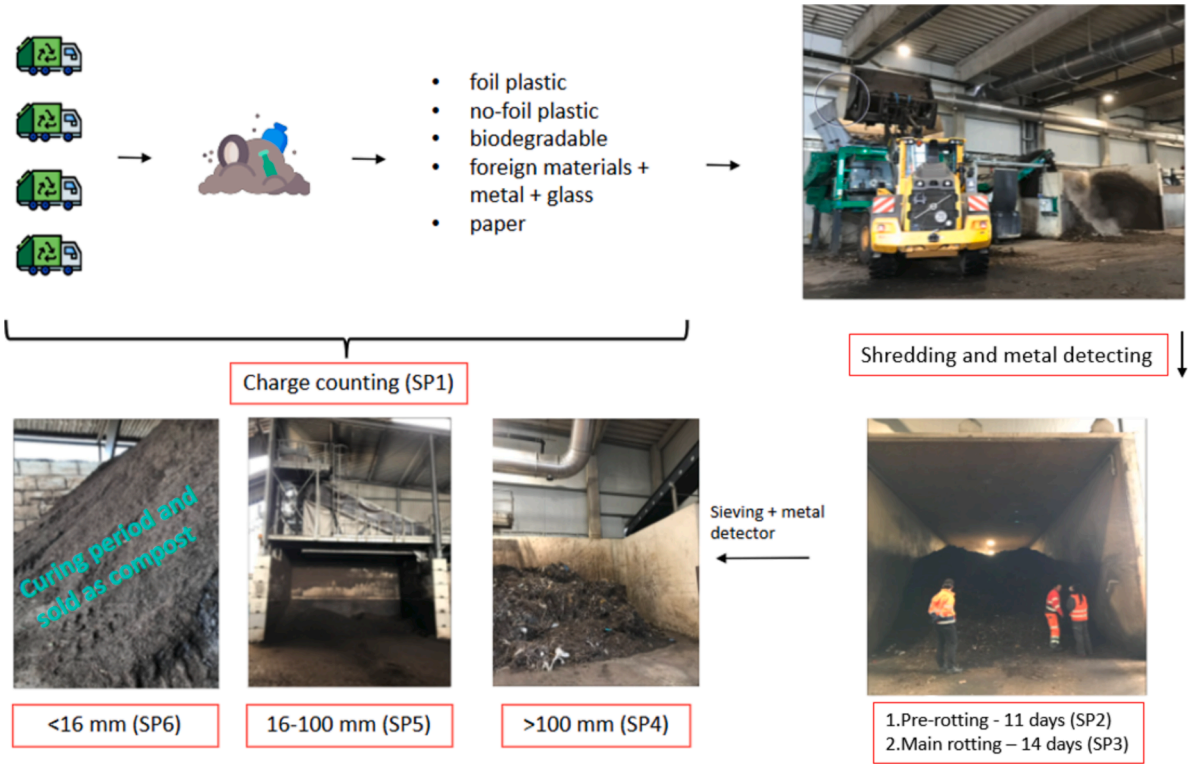


**Fig. 1.** Schematic representation of the composting process, with each sampling point (SP) distinctly underlined and squared in red, corresponding to the fractions collected for macroplastics, mesoplastics and microplastics. Following the arrows from left to right, charge counting (SP1) is done for quality control by carefully searching for foreign materials within the initial biowaste. Subsequently, the waste undergoes shredding and metal detection before entering a tunnel for pre-rotting (11 days, SP2). This is followed by a round of decompacting and main composting (14 days, SP3). At the end of the main rotting, the compost is sieved into three fractions (SP4-SP6) and ferrous metals are removed again. The fraction > 100 mm (SP4) is disposed of in most cases. The final fraction, <16 mm (SP6), is marketed and serves as a valuable soil amendment and organic fertilizer (the icons for the image are taken from www.flaticon.com). (For interpretation of the references to color in this figure legend, the reader is referred to the web version of this article.)

(annual input quantity: 30.000 tons of organic waste, consisting of around 98 % biowaste and around 2 % of green waste), producing around 7.000 tons of compost per year.

The organic and green waste was first shredded and subjected to ferrous metal separation via a conveyor belt (Fig. 1, sampling point 1 (SP1), Figure S1). A wheel loader then transported it into a tunnel, for pre-rotting under controlled pressurized ventilation (spigot system) and irrigation via a sprinkler system for 11 days (Fig. 1, SP2, Figure S1). The temperature development is measured directly within the rotting material and indirectly within the exhaust air. In addition, the direct temperature measurement (core temperature) serves as proof of hygiene (Figure S2). Excess water that escapes from the organic material during the rotting process (process water) is drained into a collecting tank via a channel system on the tunnel floor. After pre-rotting, the rotting material is transported out of the tunnel with a wheel loader, loosened, and mixed in a decompactor. A wheel loader then conveys the material into another tunnel for main rotting (duration: 14 days, Fig. 1, SP3; temperature reaching 70 °C after the second day, decreasing to 30 °C at the end of the process; Figure S2). The waste is then de-compacted again using wheel loaders and roughly fractionated using star sieves. Here the fraction > 100 mm is separated (Fig. 1, SP4), which is either fed back into the composting cycle as a feedstock or disposed of (incineration), depending on the foreign matter content.

A conveyor carries the fraction < 100 mm to the fine processing hall, where a second metal removal is conducted before the composted material is divided into two fractions through a flip-flow screen: 16 to 100 mm (Fig. 1, SP5) and < 16 mm (Fig. 1, SP6).

## 2.2. Sampling

### 2.2.1. Charge counting (incoming biowaste) for plastics > 20 mm and other foreign matter (SP1)

To identify the income of plastic items > 20 mm and other foreign matter via the collected biowaste, we conducted a so-called batch analysis (*Chargenanalyse*) for 4 different trucks from four districts ("District 1–4", Table 1), with three of them feeding the plant for later sampling (SP1). A "batch" corresponds to a sample quantity of 2x250 kg, representing the contents of a collection vehicle and helps to allocate possible waste contamination to specific collection areas (Figure S3). This procedure follows the BGK (2021) method for "Batch analysis", mirroring the company's process as well as guidelines for foreign materials treatment indicated in ECN, 2021. In addition, we analyzed a fifth sample (1 × 500 kg) as an additional reference after initial shredding.

When the collection truck arrived the biowaste was unloaded and carefully mixed using an excavator. Then, two sampling units, each 250 kg of biowaste, were taken and sorted manually (Figure S3) by careful examination and separation to identify foreign matter larger than 20 mm (foreign materials < 20 mm are disregarded at this stage). The foreign matter > 20 mm was categorized by visual inspection into seven main categories: 1) foil plastics, 2) no foil plastics, 3) biodegradable plastics, 4) glass, 5) metal, 6) other foreign materials and 7) paper (Figure S4). For simplification, we combined categories 4–6 (glass, metal, and other foreign materials) into one category (Table 1). The first differentiation of plastics was based on physical appearance, i.e., plastics were categorized as foil (as plastic bags) or non-foil (like pieces from plastic boxes). Biodegradable plastics were identified by their green color and labeling that indicated biodegradability (Figure S4).

The foreign material content was calculated for each category after BGK (2021) manual (Table 1, BGK, 2021); plastic types were assessed by Attenuated Total Reflectance Fourier Transform Infrared (ATR-FTIR, Supplementary Materials).

Following the composting facility's practice, we wanted to account for the initial amount of plastics in representative amounts of biowaste, as those are considered major contributor for the creation of MiPs throughout the composting process (Van Wijnen et al., 2019). Additionally, as homogenization of the incoming waste was not possible and hence also no reliable MiP analysis, MiP monitoring started directly after the first homogenization (SP2, after shredding).

### 2.2.2. Pre-rotting for 11 days (SP2-3)

We collected each 3×10 L of the waste material after shredding and pre-rotting (Fig. 1, SP2) and of the material after pre-rotting and de-compacting (SP3).

### 2.2.3. Main rotting for 14 days, sieving and curing (SP4-6)

We collected 3x10 L of each of the three different final fractions (>100 mm, 16–100 mm, and < 16 mm) after main rotting (Fig. 1, SP4, 5 and 6).

### 2.2.4. Irrigation and processing water

Rainwater, collected after draining from the rooftop of the composting facility, was stored in a large concrete tank (Figure S5, A). The roof, as well as all connecting pipes, from the roof to the collection container and from the container to the nozzles in the composting tunnels, consist of plastic.

The excess water that escapes during the decomposition process is drained into a collection shaft through channels located at the bottom of the tunnels. The excess water from the biofilter is also collected in this shaft. From there, the process water is pumped into a storage tank (Figure S5, B and C) made of concrete.

To elucidate if the irrigation water is contaminated during the composting process, we collected each 2x1 L of rainwater (used for the main rotting process), and processed water (more information in Supplementary Materials, Water sample collection).

## 2.3. Plastic analyses

The plastics > 20 mm collected during the batch analysis were

**Table 1**
Mass distribution of paper and foreign matter categories, including plastic, extrapolated from 2x250 kg, of four districts (delivered by four trucks) were examined. The last sample is a composite sample of the entire tunnel input of 1x500 kg.

| | Foil Plastics | No-foil Plastics | Biodegradable Plastics | Other foreign Materials | Paper | Location |
|---|---|---|---|---|---|---|
| **kg plastic ton$^{-1}$ biowaste** | | | | | | |
| **Truck 1** | 0.36 | 0.48 | 0.16 | 6.88 | 37.28 | District 1 |
| **Truck 2** | 0.24 | 0.12 | 0 | 5.44 | n.a. | District 2 |
| **Truck 3** | 0.48 | 0.44 | 0.32 | 3.12 | n.a. | District 3 |
| **Truck 4** | 0.94 | 1.01 | 0.50 | 16.02 | 47.00 | District 4 |
| **Mean (±SE)** | **0.5 ± 0.15** | **0.51 ± 0.18** | **0.25 ± 0.1** | **7.8 ± 2.8** | **42.14 ± 4.86** | |
| **Number of items ton$^{-1}$ waste (mean)** | 84 | 50 | 2 | n.a. | n.a. | |
| **kg plastic ton$^{-1}$ biowaste** | | | | | | |
| **Shredded composite** | 2.1 | 2.1 | 0.52 | 24.44 | n.a. | Tunnel entry |
| **Number of items ton$^{-1}$ waste** | 296 | 152 | 6 | n.a. | n.a. | Tunnel entry |

n.a.* – non analysed

cleaned using water and ethanol, cut into pieces and positioned on adhesive tape for ATR-FTIR analysis. We identified 9 groups of plastics types (Fig. 2A), based on frequency in their appearance: 1) PE, 2) PP, 3) polyamide (PA, mostly nylon), 4) polyester (PES, mostly polyethylene terephthalate (PET)), 5) acrylates, 6) copolymers, used often to improve performance compared to conventional plastics (those that could have been identified and including ethylene methyl methacrylate (EMMA), polyester:nylon 75:25, polyester:elastane 82:18, nylon:elastane 83:17, rayon:pet 80:20, cotton:PEPP, etc., 7) others (including plastics with only a few representatives, such as varnish, PS, PVC or additives), and 8) unidentified (with either lower than 50 % hit quality (HQ) index or too dirty surfaces to confirm the finding from the ATR-FTIR characterization) and 9) biodegradable (more information in Supplementary materials, "ATR-FTIR and Raman Microscopy analysis").

The five fractions of waste material and compost (SP2-6) were dried, sieved according to MeP and MiP size limits (5 mm, 1 mm, and 500 μm, Fig. 2B, Table 2) and analyzed via ATR-FTIR (Figure S6).

For the compost fraction, <16 mm, we conducted wet sieving and comprehensive analysis, crucial as this fraction is marketed as compost (Supplementary Materials, Final compost fraction analysis).

The water samples were also analyzed with μ-Raman (each 1 L was processed and placed on a whole filter with particles > 150 μm and 20 % of the filter for particles 6 – 150 μm), following an extraction protocol with density separation via NaCl (density of 1.2 g $cm^{-3}$), enzymatic steps (including enzymes cellulase/amylase solution for 3 days at 50 °C, lipase for 1 day at 45 °C and protease for 1 day at 45 °C) and Fenton reagent reaction (Peneva et al. unpublished data).

**Table 2**
Number of items found per kg of green and biowaste/compost dry weight after visual inspection and extrapolation, divided into size groups of macroplastics (MaPs), mesoplastics (MePs) and microplastics (MiPs). For the final compost fraction"<16 mm" both dry and wet sieving were applied. For the other fractions, only dry sieving was applied. "-" indicates that no plastics within this size range were found.

| | | MaP/ MeP> 5 mm | Large MiP 1 – 5 mm | Small MiP 0.5 – 1 mm | Total |
|---|---|---|---|---|---|
| Pre-rotting | Before pre-rotting (SP2) | 2 ± 2 | 10 ± 5 | – | 12 ± 5 |
| | After pre-rotting (SP3) | 9 ± 10 | 0 ± 0 | – | 9 ± 6 |
| After main rotting | > 100 mm (SP4) | 7 ± 3 | 10 ± 4 | – | 17 ± 3 |
| | 16–100 mm (SP5) | 8 ± 6 | 33 ± 38 | – | 41 ± 18 |
| | < 16 mm, dry (SP6) | 26 ± 7 | 7 ± 4 | – | 33 ± 13 |
| | < 16 mm, wet (SP6) | 2 ± 3 | 11 ± 2 | 2 ± 3 | 15 ± 6 |

## 3. Results

### 3.1. Charge counting – in search for > 20 mm plastics and foreign materials (SP1)

Paper was the most frequently found material, followed by other foreign materials and conventional plastics. The lowest amounts of foreign matter could be attributed to biodegradable plastics (Table 1). Although paper is not considered foreign material according to the

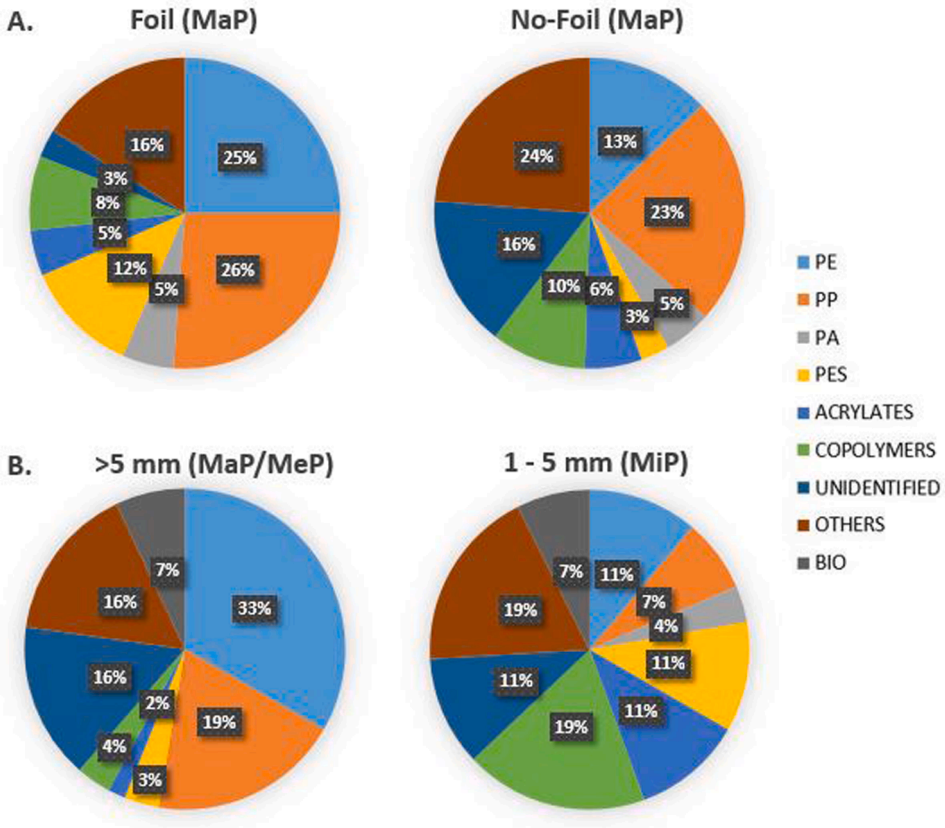


**Fig. 2.** .Pie chart, representing the composition of the plastics found in the biowaste during charge counting of biowaste from 4 districts (A), charge counting fraction > 20 mm, for both categories "foil" (on the left) and "no foil" and (B) all characterized macro and mesoplastics (MaPs/MePs) and microplastics (MiPs) found throughout the composting process.

"Batch analysis" method (BGK, 2021), we decided to examine it in two batches and found 42.14 ± 4.86 kg paper ton$^{-1}$ biowaste (Table 1).

The plastic content in the "Truck 4″ exceeded that of the other three, underscoring the heterogeneity and varying amounts of foreign materials entering the composting plant, particularly plastic. On average, the plastic foils amounted to 0.5 ± 0.15 kg ton$^{-1}$ biowaste, while "no-foil" plastics contributed to 0.51 ± 0.18 kg ton$^{-1}$ biowaste, indicating a similar presence of foil and no-foil plastics in a 1:1 ratio (Table 1). The lowest plastic content was found for truck 2 (0.36 kg t$^{-1}$ biowaste, equaling 0.04 % of plastic in the biowaste). The tunnel entry carried the largest share of overall foreign materials with 4.2 kg plastic t$^{-1}$ biowaste (sum of foil and no foil plastics), equaling 0.42 % of plastic in the biowaste.

The charge analysis of 2.5 tons of biowaste revealed a total of 500 items of both "foil" and "no-foil" plastics, but only 7 items from plastics were classified as biodegradable. Of those 500 items, 269 were found in the four trucks, with 168 "foil" and 101 "non-foil" items, whereas the rest 224 was found in the shredded composite from the tunnel (with 148 "foil" and 76 "no-foil" items). Approximately half of the plastic items were PE and PP, 122 and 134 items, respectively (Table S1). For "foil"-type plastics, PP constituted 26 %, followed by PE (25 %), others (16 %), and PES (12 %, Fig. 2A), with unidentified plastic items weighing only 3 % of the total plastic. In contrast, for the "no-foil" category, others (24 %) and PP (23 %) had the largest percentage (% of plastic weight), followed by acrylates (16 %), PE (13 %), and copolymers (11 %, Fig. 2A), while PES made up the smallest percentage (3 %).

PP corresponds to almost the same percentage, 26 % and 23 %, in the "foil" and "no-foil" plastic categories, respectively. Interestingly, there were no plastic bottles in the total 2.5 tons checked. Bags and snack food wrappers were some of the most common representatives in the "foil" category of plastics.

In the section copolymers, biodegradable plastics were included, as ATR-FTIR analysis always resulted in a mixture of plastics. These biodegradable plastics were identified either as polyethylene: acrylate copolymer, or polyester. For this plastic category, the hit quality was always under 60 %, which restricted the accurate conclusion of their composition. Noteworthy, all foreign materials had elevated contents in the shredded composite, though it remains uncertain whether this indicated the formation of smaller, more abundant foreign items by the shredding, or simply a remaining sample heterogeneity when taking aliquots for analyses.

### 3.2. Pre-rotting and main rotting (SP2-6)

In this part, we focused on assessing MaPs, MePs, and MiPs in the green and biowaste, during and after composting (Table 2). The five fractions yielded wet weight between 2.57 and 4.14 kg; the moisture content varied from 15 % to 45 % (Table S2).

The total plastic load increased after the main rotting (SP4-6) and was largest in the fraction 16–100 mm (SP5), followed by < 16 mm (SP6) sold as compost (Table 2). Plastics found in different fractions comprised mainly MaP/MeP (>5 mm) and large MiPs (1–5 mm), while small MiP (0.5–1 mm) were only found at SP6 (Table 2). The largest number of plastics within the category > 5 mm was observed for SP3 and SP6, with 9 ± 10 and 26 ± 7 items kg$^{-1}$ dw, respectively. SP5 showed the largest number of large MiP (33 ± 38 items kg$^{-1}$ dw), i.e., at least about 3 times larger than in any other fraction. Yet, an elevated number of large MiPs kg$^{-1}$ dw was also found in the waste fractions at SP2 and SP4. A slow but steady 3-fold concentration increase of total plastics is visible from the pre-rotting to the final fraction, starting with total of 12 ± 5 items kg$^{-1}$ dw to 33 ± 13 items kg$^{-1}$ dw, respectively (Table 2). The majority of large MiP items was thus also found at the final SP5 and SP6 fractions (Table 2 and Table S3).

The composition of MaPs/MePs and MiPs (identified by ATR-FTIR; Table S4, Fig. 2B, Fig. 3A and 3B) was categorized according to categories of "Batch analysis". Since most plastic items were found in size groups of ">5 mm" and "1–5 mm", only those two were illustrated in Fig. 2B and Table S3. The data showed significant variation in polymer composition between the two main size categories MaP/MeP (>5 mm), and large MiP (1–5 mm). For MaP/MeP, PE emerged as the most abundant polymer type across the five fractions, followed by PP, whereas biodegradable polymers exhibited the lowest abundance (Fig. 2B, Fig. 3A and 3B). Conversely, PE and PP were less frequently detected within MiPs, with "acrylates'' and "others" emerging as the predominant polymer types (Fig. 2B and Fig. 3B). Notably, PA was the least abundant polymer and was nonexistent in size of MaP/MeP. Other items with minor abundance were either not identified (appearing as PS foam, 2 items) or Aluminium oxalate (likely as part of cellophane), whereas the biodegradable plastics comprised poly-2-hydroxyethyl methacrylate at SP2. At SP3, the copolymer was identified as PE-co-vinyl acetate, but with a minute HQ of 29 %.

The composition of the plastics changed at SP4: for the ">100 mm" fraction all four items categorized as PES visually looked like biodegradable MiPs, one plastic was recognized as styrene-allyl, and the rest three plastics as vinyl chloride, as parexyl, and as butyl hydroxide. For the fraction "16–100 mm" (SP5), the unidentified plastic visually looked like plush or plaster and was not identified according to the library spectra. The two biodegradable ones were identified as PES; however, due to the obvious physical alterations we sorted them as biodegradable. The copolymer there was identified as styrene-acrylonitrile resin (SAN).

At all sampling points, in the size of MaP/MeP, PE was the most abundant polymer type representing 25 % of plastics in the initial biowaste and 29 % in the last processing step at SP6 (Tables S1 and S4). Other plastic types like PP, PA, copolymers, and Acrylates had a higher

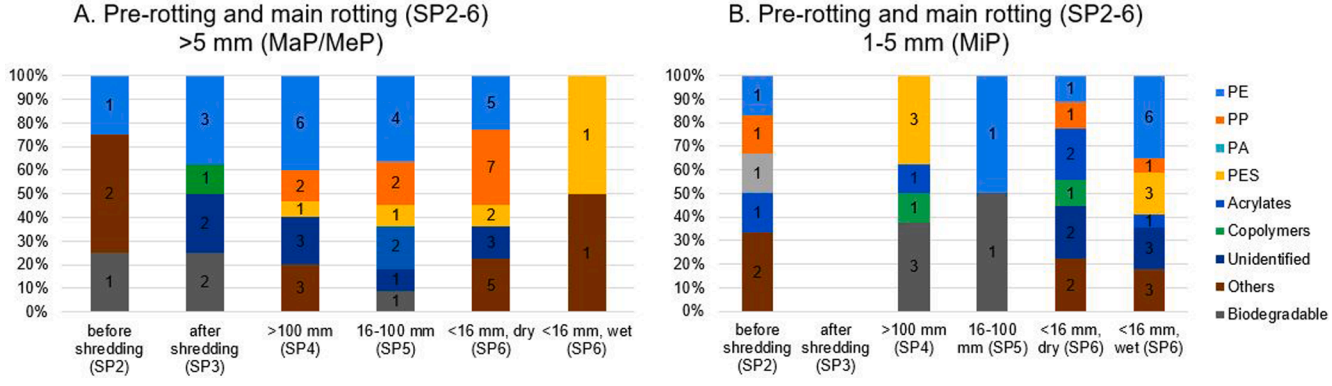


**Fig. 3.** Stacked bar chart representing the number of plastics (inside of the stacks), their type (as a legend with colors) and the representative percentage (on the y-axis) found in the five fractions of bio and green waste and compost analyzed, for macroplastics/mesoplastics (MaP/MeP), >5mm (A.) and microplastics (MiP, 1–5 mm (B.)). (For interpretation of the references to color in this figure legend, the reader is referred to the web version of this article.)

percentage at SP1 than in the final analyzed waste fractions. On the other hand, PES, unidentified and biodegradable plastics showed the opposite trend (Table S1 and S4). Noteworthy, none of the factions created by the composting plant for plastic sizes of > 5 mm contained PA (Fig. 2B and Fig. 3A).

### 3.3. Additional extraction and detection of small MiPs of 20–500 μm and > 500 – 1000 μm from compost fraction < 16 mm

From the 500—1000 μm MiPs, only 3 to 50 % of particles selected under the stereomicroscope could be identified via Raman spectroscopy. Likely due to some remaining organic material, identification of smaller-sized MiPs was difficult, despite strong signals at 1600 $cm^{-1}$, 2884 to 2904 $cm^{-1}$, and 3070 $cm^{-1}$ observed for many of the particles, typically associated with plastic spectra. From the total number of 12 identified plastic particles in the 15 g dw of compost, polybutylene adipate terephthalate (PBAT), represented 42 %, followed by PE and PS with 16 % and finally PP, PVC and Nylon with 8 %. Thus, after extrapolation, for the 500–1000 μm MiPs this resulted in 800 ± 529 items $kg^{-1}$ dw compost. For the smaller size-fraction, 20–500 μm, from the 10 on average items selected in 5 g of dw compost under the stereomicroscope, only 1 appeared as biodegradable. However, this particle could not be identified via Raman spectroscopy, preventing any definitive conclusion.

### 3.4. Water samples analysis

Three main polymer types were identified in high quantities for the rainwater: PE was most abundant with 22,714 ± 2,976 items $L^{-1}$, followed by PA and PP with 3,108 ± 748 and 686 ± 398 items $L^{-1}$, respectively (Fig. 4). The same pattern was observed for the process water, though the numbers of plastic items were lower with 13,864 ± 3,866 items $L^{-1}$ for PE; 617 ± 28 items $L^{-1}$ for PA; 497 ± 197 items $L^{-1}$ for PP, respectively (Fig. 4). The size range for those MiPs had been set from 6 to 150 μm, yet, all particles found were in the size of 6–70 μm. Additionally, we found 35 ± 0.4 and 100 ± 0.6 larger MiP items (150 – 600 μm) per L of rain and processed water, respectively.

## 4. Discussion

### 4.1. Charge counting – searching for > 20 mm plastics and foreign materials (SP1)

Paper dominated in the biowaste inputs, likely reflecting that paper, being compostable, is organic and considered biodegradable. For hygienic reasons, biowaste in Germany is frequently pre-collected in small paper bags or wrapped in paper before being placed in the organic waste bin for collection. Also paper absorbs much more moisture from biowaste than plastic and, therefore, has a higher wet weight. After composting, and unlike plastics, the paper was largely degraded.

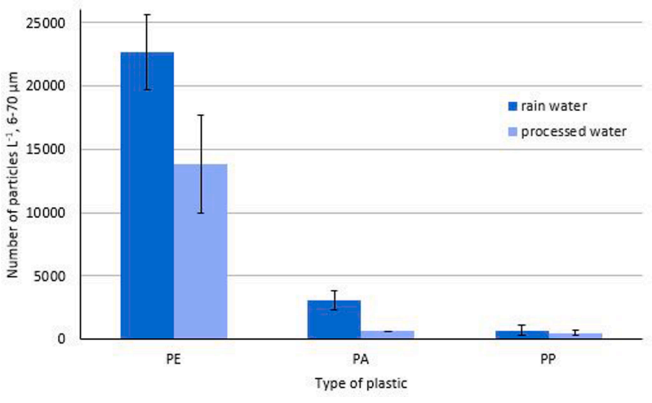


**Fig. 4.** Number of small microplastics (6 to 70 μm) of polyethylene (PE), polyamide (PA) and polypropylene (PP) found in rainwater (used for irrigation) and processed water (after irrigation). Data is presented as means ± standard deviation.

The biowaste input typically maintained a 1:1 gravimetric ratio of "foil" to "no foil" plastic contaminations, except once where foil dominated. Also Colombini et al. (2022) reported that plastic films constituted up to 80 % of compost contaminations. In line with Van den Zee and Molenveld (2020), half of the plastics can be categorized as "flexible packaging." Despite equal weight distribution in our study, the category "foil" comprised 316 items, while "no-foil" had 177 items in the 2.5 tons, respectively. This discrepancy underscores the importance of considering both weight and quantity metrics when analyzing plastic abundance, as weight-based assessments ignore particle size information and hence may not accurately capture material distribution. The higher item numbers in the "foil" category are attributed to the intrinsic weight differences between foil and non-foil materials, with foil materials being lighter. Our data also suggest that the easier fragmentation of "foil" structures contributes to their larger item numbers compared to "no foil" pieces.

The percentage of PE in the "foil"-type was nearly two times larger than in the "no-foil"-type category. That aligns with the common use of PE in plastic bags and wrappings (López and Serna, 2022). For instance, all collection trucks had paper/plastic bags frequently used in bakeries and baking sections in big supermarkets. Given that this packaging is primarily composed of paper, with only a small portion being plastic, it may often be mistakenly disposed of in biowaste. When a piece consisted of a mixture of different materials, mostly bags from bakery shops where paper and plastic were abundant, we carefully separated the respective components. In those cases, the plastic parts of pieces were categorized as part of the foil group due to their foil-like form. The paper from these bags was not included in the paper group during charge counting, which only accounted for fully paper-based items like boxes made entirely of paper.

Polypropylene, in turn, is equally found in both "foil" and "no foil" plastics, with double amount in "no-foil" in comparison with PE, likely reflecting that PP is commonly used in food packaging, such as boxes for food deliveries. The same trend was observed by Van den Zee and Molenveld (2020), with PET being the second most commonly found rigid plastic type. Additionally, PP is a common component of fruit stickers, another significant plastic contaminant in compost (EPA, 2022; Groß et al., 2024). Besides, we found meat packages still unopened, and, occasionally, also small toys, rubber gloves and plant pots.

PE was the most frequently detected plastic type in compost reported by Edo et al. (2022), Colombini et al. (2022) and Van den Zee and Molenveld (2020), accounting for 35 %, 71 % and 29 % of all plastic items respectively. Interestingly, both Edo et al. (2022) and Colombini et al. (2022) found PS as the second most abundant plastic type, whereas here PS was rather rarely detected (3 items per ton), and, thus, included in the "others" category. Additionally, we found many other plastic items lacking clear identification likely due to a layer of grease on their surface, which could not be completely removed even after meticulous sample cleaning. Also, Van den Zee and Molenveld (2020) could not identify 17 % of the plastic items due to their altered surfaces when investigating plastic loads in a composting facility in the Netherlands. Van den Zee and colleagues reported 21 % of biodegradable bags in green and biowaste samples, in contrary to our results, with less than 1 % of the plastic items being biodegradable bags.

According to the Biowaste Ordinance, cities and districts have the option of restricting the list of authorized input materials in their waste bylaws. In many nationwide statutes, as in the statutes for this composting plant, the use of biodegradable plastic collection bags is expressly prohibited. This is presumably why relatively few such bags were found in the organic waste. A German team of researchers, who initiated in 2019 a project called BabbA (Biologisch abbaubare Beutel in der Bioabfallverwertung) found that composts contain significant

amounts of biodegradable MiPs smaller than 1 mm, which can persist in the soil over extended periods (Forberger et al., 2023). Their final report highlights paper bags as a promising alternative to biodegradable bags and calls for a critical revision of current standards for compostable materials. Other research groups summarized that it can take up to 18 weeks until 85–99 % of biodegradable plastics are fully degraded (Le et al., 2023). However, this depends, besides on the composting conditions, strongly on the type of biodegradable polymers used to create the blend, i.e., polylactic acid-poly(hydroxyalkanoate) PLA-PHA based biodegradables can be > 95 % degraded in just 4 weeks (Sintim et al., 2020). Noteworthy, the remaining parts from biodegradable bags were very easily broken once touched and tried to be placed under the ATR-FTIR (Van den Zee and Molenveld, 2020).

Our study neither aimed at reporting typical variations in plastic inputs between different composting plants nor accurately assessing in-situ variations. Instead, we aimed to report realistic contaminations by sampling large volumes. We found 272 plastic items (comprising foil, no foil, and biodegradable plastics) within 2 tons of biowaste, corresponding to 136 items per $t^{-1}$ of biowaste. Some larger plastic items were found after the sieving, shredding, and rotting stages (SP2-5), underscoring difficulties in their effective removal throughout the process and/or their transformation into smaller sizes during shredding. That highlights the need to reduce plastic inputs by optimizing top-down policymaking.

### 4.2. Plastic loads (> 500 μm) throughout the composting process and in final compost (SP2-6)

The threefold increase of cumulative MaPs/MePs and MiPs from the initial stage throughout the composting process supports the hypothesis that plastics enrich with weight loss of other organics during composting. Furthermore, large plastic items likely underwent shredding (SP2), facilitating fragmentation and hence the formation of secondary MiPs (Gui et al., 2021; Sholokhova et al., 2023). Reported numbers of large MiPs in the end-product are lower than reported by Weithman et al. (2018) and Braun et al. (2020). The authors found 24 items $kg^{-1}$ dw and an average of 21 ± 31 items $kg^{-1}$ dw, respectively. Other studies found 310 to 410 items $kg^{-1}$ dw to 2,533 ± 457 items $kg^{-1}$ dw, with sizes of 1–5 mm and 0.05–5 mm, respectively (Premasiri, 2021; Gui et al., 2021), thus underscoring the complexity and variability in MiP distribution within composting facilities. In contrast, reported MeP/MaP numbers were higher than the numbers of MaPs routinely collected by the facility, with mean values of 2–4 items $kg^{-1}$ (unpublished data of the composting facility), which were confirmed by an earlier study (Braun et al., 2021). Varying results point to a high heterogeneity of plastic loads within the compost, letting us assume that the found 26 ± 7 items reflect rather maximal loads.

Here, we focused on quantifying plastics and MaPs loads from the incoming organic waste, examining 2 tons across four trucks and a shredded composite from the tunnel, however, this represents only 1.1 % of the total 180 tons in the tunnel. Additionally, we observed a high heterogeneity, especially for large plastics. Different numbers may also be due to differences in the methodologies used: when using wet sieving for the final biowaste fraction, we found about 50 % more plastic items in the < 16 mm fraction.

However, for obtaining representative measurements an adequate sampling strategy is key. For future studies, increasing replicates (including the number of subsamples used for one composite sample), also from different seasons across the year, could reduce the uncertainties. Particularly since plastic contamination is likely higher during the colder months compared to spring and summer when unpackaged fruits and vegetables are more readily available and consumed in larger quantities (Adam et al., 2024). Although there are similarities between studies from different countries, such as the prevalence of foil-like plastics and the dominance of PE (Colombini et al., 2022, Edo et al., 2022), national regulations vary, which can add to differences in findings among different countries or even continents.

A key challenge remaining is the lack of a standardized methodology for MiP extraction from complex organic matrices such as compost, digests, and food waste (Porterfield et al., 2023). We are confident that the detected MiP load was not affected by sampling or sample processing, because strict contamination precautions were taken, using, e.g., only non-plastic materials, and because the processed lab blanks did not point at significant MiP loads.

Overall the composition of the plastic types found was diverse, with PE dominating MaPs/MePs (Fig. 2B and Fig. 3A), while no specific plastic type dominated within MiPs.

On the other hand, PS, for example, was hardly detected and hence categorized under “others” in the fresh biowaste (SP1). However, after pre- and main-rotting, we identified a total of 9 PS items within the total 11.9 kg dw (SP2-6, Table S2), with 0.3 items $kg^{-1}$ and 0.4 items $kg^{-1}$ falling within the size range of MaP/MeP and MiP, respectively, pointing to a slight increase throughout the composting process. Notably, expanded PS has a very low density (0.01–0.05 g $cm^{-3}$) and a large potential to generate numerous MiPs (British Plastic Federation). In this case, the paradox between particle number and mass is evident, as PS can produce a significant number of MiPs with minimal weight. Gui et al. (2021) highlight the rapid fragmentation of expanded PS, generating 53 MiP particles from a single item within 30 days of composting, surpassing the formation rates of PE and PP, which only produce 9 and 5 MiP items, respectively. As we observed a low abundance of PS in our experiment, we can relate this to the changing trends in plastic usage. With regulations like the EU’s ban on single-use plastics (DIRECTIVE (EU) 2019/904), the decrease in single-use PS, commonly used in food and beverage containers, may explain the observed trend. We believe that this shift in consumer behavior aligns with the ongoing efforts to reduce plastic pollution.

Overall, the total count of MaPs/MePs and MiPs in the final fractions “16–100 mm” (SP5) and “<16 mm” (SP6) surpasses that in the fractions taken after pre-rotting (SP 2–4) by two to three times, which may be attributed to the steps of shredding and composting (Gui et al.,2021; Sholokhova et al., 2023).

In principle, there might be an additional source of MiP: atmospheric deposition (Kernchen et al., 2022; O’Brien et al., 2023). To account for such processes, we analyzed MiP loads in rainwater from the rooftop. It likely contained both atmospheric deposition from rather long-distance transport, as well as from the blown-out material of the composting facility itself.

### 4.3. Small MiPs (500–1000 μm) in final compost and water samples

In general, the selection of small MiPs under a microscope, a widely employed method for plastic particle recognition, can introduce a potential source of error (Mariano et al., 2021), especially when organic matter is still present in the sample. This was evidenced by the relatively low number of identified items and by a notable occurrence of false positives as only between 3 and 50 % of selected items could be identified as plastic. Also, extracting MiPs from high-organic matter content soils or compost is challenging, with varying success reported in the literature (Hurley et al., 2018; Braun et al., 2023). To address challenges in extracting MiPs smaller than 1 mm from organic matrices like compost, thermoanalytical methods, such as TED-GC-MS, can support the analysis, providing mass-based concentration for single polymer types (Wiesner et al., 2023).

In the final compost, we found 800 ± 529 items $kg^{-1}$ dw compost, of small MiPs (500–1000 μm). In comparison, Van Schothorst et al. (2021) analyzed MiPs in the size range of 0.03 to 2 mm by applying 30 mL of distilled water to 5 g of compost, followed by centrifugation. This method allowed them to identify 1,253 ± 561 items per kg of compost made of green cuttings, using a microscope and a hot plate at 130 °C. Further, Edo et al. (2021) employed a two-step protocol and identified 1,357 out of 1,532 particles as synthetic polymers, with the most

common sizes ranging from 150 to 700 μm. In contrast, Steiner et al. (2022) utilized a seven-step enzymatic-oxidative digestion protocol for MiPs (10–1000 μm) in liquid fertilizer, ending with density separation using $ZnCl_2$ and subsequent dilution in filtered water to avoid matrix interference during FTIR analysis. They found between 6,000 and 12,000 particles $L^{-1}$ of liquid fertilizer. The high variation in MiP loads reported by different studies might result from differences in methodology, including the number of steps, reagents used, and particle size ranges analyzed. However, the results might also point to the high heterogeneity of MiP loads within the compost, as already observed by other studies (Braun et al., 2021).

Surprisingly, we discovered MiP items in both process water and rainwater. The high numbers in the rainwater suggest significant contamination by atmospheric deposition (Kernchen et al., 2022), likely due to wind-driven distribution of MiPs, especially as rainwater is stored under the rooftop, even if the containers are closed (Wei et al., 2023). This rooftop consists of a plastic foil roof, and all the pipes connecting the rooftop to the collection container and from there to the nozzles used for compost irrigation are made of plastic, despite the container itself being non-plastic (See Supplementary Materials, Water samples Collection). Hence, any abrasion process from the roof, if there were any, might have contributed to the contamination of rainwater if blown around with the wind. Moreover, in the process water, the MiPs could originate from the compost itself. The big floods in Germany, which may also have transported plastics around, even into the plant, had passed since 9 months. Another input source for the rainwater could be the nearby motorway.

In addition to these potential contamination sources, it is important to consider the possibility of false positives arising from Raman measurements and a potential overestimation of very small-sized MiPs, common in spectroscopic techniques, that could explain the observed high numbers, especially for particles below 10 μm (Xu et al., 2019).

As the process water after being used to irrigate the compost, contains significantly fewer MiPs than the rainwater, we assume that a large part of these MiPs are filtered by the compost. Hence, we must refute our initial hypothesis, that the irrigation water is contaminated by MiPs during composting. Instead, we conclude that the irrigation water is an additional source for small MiPs during composting, which has been overlooked so far.

## 5. Future implications

Market acceptance of compost and digestion products hinges on users' expectations that these products are free, or nearly free, of foreign substances, particularly plastics, to ensure high-quality organic fertilization. In the future, it remains crucial to develop strategies for reducing the plastic load in compost. This could include more strict regulations, such as limiting plastic contamination in composts. The EU, for instance, permits up to 0.3 % dry weight impurity for plastic, metal, and glass (larger than 2 mm), whereas Germany enforces stricter standards (0.1 % dry weight for particles larger than 1 mm).

However, to reduce the plastic load of compost, the key strategy must be to minimize the plastic input via waste collection into composting facilities, i.e., preventing improper waste disposal in organic bins, and not to leave the burden of purifying the materials to the plant. The contamination of household organic waste, particularly with plastics, has increased in recent years (BGK, 2024). The German Federal Quality Association for Compost (BGK) attributes this to declining public awareness regarding separate waste collection systems and inadequate identification and elimination of foreign material sources. The problem is that during waste collection, single collected bins can pollute a whole batch of waste. To prevent existing plastic contaminations some composting facilities already use a system to recognize foreign matter during the collection of biowaste. Contaminated garbage cans can so directly be excluded. In addition to these measures, ensuring correct use and disposal of biodegradable plastic is crutial. Biodergadable plastic, used as a bin liner for collection of biowaste is becoming more and more popular, although their complete degradation during composting is still under discussion (Flury et al., 2021). An approach to better account for incomplete degradation under various disposal conditions, is the calibration of the actual biodegradability in standards. Further, the provision of biodegradability certificates on biodergadable plastics with clear disposal instructions is recommended to ensure proper end-of-life management (Yu et al., 2024). Encouraging the collection of source-separated green and biowaste, combined with public education and better marketing, can further enhance the purity of compost (Fricke et al., 2017). Expanding the organic waste bin system, as seen in Germany since 2015, could also be a helpful measure (Friege and Eger, 2022). Public education via social media and awareness campaigns as well as regular compliance checks are essential to reduce the plastic contamination of compost (BGK, 2024; Habermann, 2022).

Although our study confirmed that final compost contains plastics, even when applying high MeP/MaP contents, resulting in a total mean amount of 833 items $kg^{-1}$, this plastic content is substantially lower than plastic values of sludge where 1,000 to 24,000 items $kg^{-1}$ are found (Bläsing and Amelung, 2018). Considering now compost application rates, which vary widely from 7 to 35 t/ha annually (BioAbfV, 2013, WRAP, 2015), the plastic contents found in this study (mean: 833 items $kg^{-1}$), a plowing depth of 30 cm and a soil bulk density of 1.4, a one-time compost application of 7 and 35 t would result in soil plastic contents of 1.39 to 27.77 plastic items per kg soil, respectively. Twenty years of annual compost application would result in soil plastic contents of 27.8 to 139 plastic items per kg soil, which are considerably lower than reported for soils under plastic mulching or soils under sludge application, most of them having concentrations larger than 1000 items per kg (van den Berg et al., 2020, Büks and Kaupenjohann, 2020, Harms et al., 2021, van Schotthorst et al., 2021, Wrigley and Braun et al., 2024).

## 6. Conclusions

Here, we investigated the presence and composition of MaPs, MePs and MiPs in fresh biowaste and at different stages throughout the composting process within a German composting facility, following national and state regulations. The analysis included biowaste batch analysis, pre- and main rotting assessments, and collection of irrigating water – before and after composting. The results revealed varying MiP loads in different compost fractions, with PE and PP standing out as the most widespread plastics. We found with up to 1.95 kg per ton large amounts of MaPs in biowaste, highlighting the role of improper waste separation as an entry route for plastics in composting facilities. During the composting process, total plastics became enriched by a factor of three, which might be caused by the fragmentation of large plastic items into smaller ones. Moreover, we could identify irrigation water as an additional source for especially small MiPs. The latter presents, thus, a still under-examined source of a plastic cycle within the industrial compost plant.

## CRediT authorship contribution statement

**Stoyana Peneva:** Writing – original draft, Validation, Methodology, Formal analysis, Data curation. **Quynh Nhu Phan Le:** Writing – review & editing, Formal analysis. **Davi R. Munhoz:** Writing – review & editing, Data curation. **Olivia Wrigley:** Writing – review & editing, Formal analysis, Data curation. **Giovana P.F. Macan:** Writing – review & editing, Data curation. **Heidi Doose:** Writing – review & editing. **Wulf Amelung:** Writing – review & editing, Supervision, Conceptualization. **Melanie Braun:** Writing – review & editing, Supervision, Data curation, Conceptualization.

## Declaration of competing interest

The authors declare that they have no known competing financial

interests or personal relationships that could have appeared to influence the work reported in this paper.

## Acknowledgements

This work was funded by the European Union's Horizon 2020, ITN SOPLAS, with grant agreement No. 55334 to the main author. The authors thank the composting facility for supporting this study and Wessling GmbH for collecting the water samples and collecting the data needed for their further analysis. We also thank Flora Wille for helping with collecting and cleaning the samples from stage 1 of the process.

## Appendix A. Supplementary material

Supplementary data to this article can be found online at https://doi.org/10.1016/j.wasman.2024.11.043.

## Data availability

Data will be made available on request.

## References

BGK, 2024. Kunststsoffe in komposten und Gärresten, Bundesgütegemeinschaft Kompost Cologne, Germany.
BioAbfV, 2013. Verwertung von Bioabfällen auf landwirtschaftlich, forstwirtschaftlich und gärtnerisch genutzten Böden (Bioabfallverordnung). VHE, Kompost https://www. vhe.de/kompost/kompostprodukte/kompost/.
Bläsing, M., Amelung, W., 2018. Plastics in soil: analytical methods and possible sources. Sci. Total Environ. 612, 422–435. https://doi.org/10.1016/j.scitotenv.2017.08.086.
Braun, M., Mail, M., Heyse, R., Amelung, W., 2021. Plastic in compost: prevalence and potential input into agricultural and horticultural soils. Sci. Total Environ. 760, 143335. https://doi.org/10.1016/j.scitotenv.2020.143335.
Braun, M., Mail, M., Krupp, A.E., Amelung, W., 2023. Microplastic contamination of soil: Are input pathways by compost overridden by littering?, 158889 Sci. Total Environ. 855. https://doi.org/10.1016/j.scitotenv.2022.158889.
British Plastic Federation. Retrieved from https://www.bpf.co.uk/plastipedia/polymers/expanded-and-extruded-polystyrene-eps-xps.
Büks, F., Kaupenjohann, M., 2020. Global concentrations of microplastics in soils – a review. SOIL 6, 649–662. https://doi.org/10.5194/soil-6-649-2020.
Bundesgütegemeinschaft (BGK). (2021). https://www.kompost.de/publikationen/themen/positionen/methoden/methoden.
Colombini, G., Rumpel, C., Houot, S., Biron, P., Dignac, M.F., 2022. A long-term field experiment confirms the necessity of improving biowaste sorting to decrease coarse microplastic inputs in compost amended soils. Environ. Pollut. 315, 120369. https://doi.org/10.1016/j.envpol.2022.120369.
Diaz, L.F., Savage, G.M., Eggerth, L.L., Chiumenti, A., 2007. Compost science and technology. In: Waste Management Series, Vol. 8. Elsevier, pp. 67–87. https://doi.org/10.1016/S1478-7482(07)80008-X.
Edo, C., Fernández-Piñas, F., Rosal, R., 2022. Microplastics identification and quantification in the composted organic fraction of municipal solid waste. Sci. Total Environ. 813, 151902. https://doi.org/10.1016/j.scitotenv.2021.151902.
European Compost Network (ECN) report. (2019). https://www.compostnetwork.info/download/ecn-status-report-2019/.
European Compost Network (ECN), 2021. Position paper. Retrieved from https://www.compostnetwork.info/ecn-position-paper-published/.
European Compost Network (ECN), 2023. Country report: Germany. Retrieved from https://www.compostnetwork.info/download/country-report-germany-2023/.
Flury, M., Narayan, R., 2021. Biodegradable plastic as an integral part of the solution to plastic waste pollution of the environment. Current Opinion in Green and Sustainable Chemistry 30, 100490.
Forberger, J., Freitag, R., Laforsch, C., Kandeler, E., Geyer, J., Kröner, U., Möller, J., 2023. BabbA - Biologisch Abbaubare Beutel in Der Bioabfallverwertung. https://doi.org/10.24406/publica-2127.
Fricke, K., Heußner, C., Hüttner, A., Turk, T., 2017. Recycling of Biowaste: Experience with Collection, Digestion, and Quality in Germany. In: Maletz, R., Dornack, C., Ziyang, L. (eds) Source Separation and Recycling. The Handbook of Environmental Chemistry, vol 63. Springer, Cham. doi: 10.1007/698_2017_34.
Friege, H., Eger, Y., 2022. Best practice for bio-waste collection as a prerequisite for high-quality compost. Waste Manage. Res. 40 (1), 104–110. https://doi.org/10.1177/0734242X211033714.
Groß, M., Mail, M., Wrigley, O., Debastiani, R., Scherer, T., Amelung, W., Braun, M., 2024. Plastic fruit stickers in industrial composting—surface and structural alterations revealed by electron microscopy and computed tomography. Environ. Sci. Tech. 58 (16), 7124–7132. https://doi.org/10.1021/acs.est.3c08734.
Gui, J., Sun, Y., Wang, J., Chen, X., Zhang, S., Wu, D., 2021. Microplastics in composting of rural domestic waste: abundance, characteristics, and release from the surface of macroplastics. Environ. Pollut. (Barking, Essex : 1987), 274, 116553. doi: 10.1016/j.envpol.2021.116553.
Habermann, P.-M., 2022. Innovative Öffentlichkeitsarbeit und Bioab fallaufbereitung zur Sicherstellung einer hochwertigen Kompostqualität [Innovative public relations work and biowaste processing to ensure high-quality compost]. Bundesgütegemeinschaft Kompost e. V., Witzenhausen, Germany.
Harms, Ivy Kaye, Diekötter, Tim, Troegel, Saskia, Lenz, Mark, Amount, distribution and composition of large microplastics in typical agricultural soils in Northern Germany, Sci. Total Environ. 758 (2021) 143615, ISSN 0048-9697, doi: 10.1016/j.scitotenv.2020.143615.
Hurley, R.R., Lusher, A.L., Olsen, M., Nizzetto, L., 2018. Validation of a method for extracting microplastics from complex, organic-rich, environmental matrices. Environ. Sci. Tech. 52 (13), 7409–7417. https://doi.org/10.1021/acs.est.8b01517.
Kernchen, S., Löder, M.G.J., Fischer, F., Fischer, D., Moses, S.R., Georgi, C., Nölscher, A. C., Held, A., Laforsch, C., 2022. Airborne microplastic concentrations and deposition across the Weser River catchment. Sci. Total Environ. 818, 151812. https://doi.org/10.1016/j.scitotenv.2021.151812.
Kumar, M., Xiong, X., He, M., Tsang, D.C.W., Gupta, J., Khan, E., Bolan, N.S., 2020. Microplastics as pollutants in agricultural soils. Environ. Pollut. 265, 114980. https://doi.org/10.1016/j.envpol.2020.114980.
Laforsch, C., Kandeler, E., Geyer, J., Kröner, U., Pagel, H., Steiner, T., Forberger, J., Freitag, R., Löder, M., Bayha, A., Gromer, G., Möller, J., 2023. BabbA - Biologisch abbaurbare Beutel in der Bioabfallverwertung, Projektbericht - Abschlussbericht. https://pudi.lubw.de/detailseite/-/publication/10553.
Le, V.-R., Nguyen, M.-K., Nguyen, H.-L., Lin, C., Rakib, M.R.J., Thai, V.-A., Le, V.-G., Malafaia, G., Idris, A.M., 2023. Organic composts as a vehicle for the entry of microplastics into the environment: a comprehensive review. Sci. Total Environ. 892, 164758. https://doi.org/10.1016/j.scitotenv.2023.164758.
López, G.I.D., Serna, E.A., 2022. The dilemma of plastic bags and their substitutes: a review on LCA studies. Sustain. Prod. Consumpt. 30, 107–116. https://doi.org/10.1016/j.spc.2021.11.021.
Mariano, S., Tacconi, S., Fidaleo, M., Rossi, M., Dini, L., 2021. Micro and nanoplastics identification: classic methods and innovative detection techniques. Front. Toxicol. 3, 636640. https://doi.org/10.3389/ftox.2021.636640.
PlasticsEurope, 2022. Plastics – the facts. Retrieved from https://plasticseurope.org/wp-content/uploads/2022/10/PE-PLASTICS-THE-FACTS_V7-Tue_19-10-1.pdf.
Porterfield, K.K., Hobson, S.A., Deborah, A.N., Niles, M.T., Roy, E.D., 2023. Microplastic in compost, digestates, and food wastes: a review. J. Environ. Qual. 52 (2), 225–240. https://doi.org/10.1002/jeq2.20450.
Premasiri, M.R.P.H., 2021. Microplastics in freshwater, terrestrial and marine ecosystems in the western Sri Lanka: an assessment of rivers, compost and beach sediment. In: Department of Natural Resources and Environmental Management. Sabaragamuwa University of Sri Lanka.
Ricci, M.J., Centemero, M., 2018. Separate collection of food waste and rejects. In: Müll und Abfall. Erich Schmidt Verlag GmbH & Co. KG, Berlin, pp.340–343.
Sajjad, M., Huang, Q., Khan, S., Amjad Khan, M., Liu, Y., Wang, J., Guo, G., 2022. Microplastics in the soil environment: a critical review. Environ. Technol. Innov. 27, 102408. https://doi.org/10.1016/j.eti.2022.102408.
Sholokhova, A., Denafas, G., Ceponkus, J., Kriukiene, R., 2023. Microplastics release from conventional plastics during real open windrow composting. Sustainability 15 (1), 758. https://doi.org/10.3390/su15010758.
Siebert, S., Kehres, B., 2008. Agricultural humus management using high quality compost. CODIS 2008, Compost and Digestate: Sustainability, Benefits and Impacts for the Environment and Plant Production.
Sintim, H.Y., Bary, A.I., Hayes, D.G., Wadsworth, L.C., Anunciado, M.B., English, M.E., Flury, M., 2020. In situ degradation of biodegradable plastic mulch films in compost and agricultural soils, 138668 Sci. Total Environ. 727. https://doi.org/10.1016/j.scitotenv.2020.138668.
Steiner, T., Möller, J.N., Löder, M.G.J., et al., 2023. Microplastic contamination of composts and liquid fertilizers from municipal biowaste treatment plants: effects of the operating conditions. Waste Biomass Valorization 14, 873–887. https://doi.org/10.1007/s12649-022-01870-2.
van den Berg, Pim, Huerta-Lwanga, Esperanza, Corradini, Fabio, Geissen, Violette, 2020. Sewage sludge application as a vehicle for microplastics in eastern Spanish agricultural soils, Environmental Pollution, 261(2020) 114198, ISSN 0269-7491, 10.1016/j.envpol.2020.114198.
Van den Zee, M., Molenveld, K., 2020. The fate of (compostable) plastic products in a full scale industrial organic waste treatment facility. (Report / Wageningen Food & Biobased Research; No. 2020). Wageningen Food & Biobased Research. doi: 10.18174/514397.
van Schothorst, B., Beriot, N., Huerta Lwanga, E., Geissen, V., 2021. Sources of light density microplastic related to two agricultural practices: the use of compost and plastic mulch. Environments 8 (4), 36. https://doi.org/10.3390/environments8040036.
Viaene, J., Van Lancker, J., Vandecasteele, B., Willekens, K., Bijttebier, J., Ruysschaert, G., De Neve, S., Reubens, B., 2016. Opportunities and barriers to on-farm composting and compost application: a case study from northwestern Europe. Waste Manage. 48, 181–192. https://doi.org/10.1016/j.wasman.2015.09.021.
Wei, L., Yue, Q., Chen, G., Wang, J., 2023. Microplastics in rainwater/stormwater environments: influencing factors, sources, transport, fate, and removal techniques. TrAC Trends Anal. Chem. 165, 117147. https://doi.org/10.1016/j.trac.2023.117147.
Wiesner, Y., Bednarz, M., Braun, U., Bannick, C.G., Ricking, M., Altmann, K., 2023. A promising approach to monitor microplastic masses in composts. Front. Environ. Chem. 4, 1281558. https://doi.org/10.3389/fenvc.2023.1281558.
WRAP, 2015. Using Compost in Agriculture and Field Horticulture-Compost Information Package 1. Waste and Resources Action Programme.

Wrigley, O., Braun, M., Amelung, W., 2024. Global soil microplastic assessment in different land-use systems is largely determined by the method of analysis: A meta-analysis. Sci. Total Environ. 957, 177226. https://doi.org/10.1016/j.scitotenv.2024.177226. Advance online publication.

Xu, Jun-Li, Thomas, Kevin V., Luo Zisheng, Gowen Aoife A., 2019. FTIR and Raman imaging for microplastics analysis: State of the art, challenges and prospects. TrAC Trend Anal. Chem. 119 (2019) 115629, ISSN 0165-9936, doi: 10.1016/j.trac.2019.115629.

Yu, Y., Flury, M., 2024. Unlocking the potentials of biodegradable plastics with proper management and evaluation at environmentally relevant concentrations. npj Materials Sustainability 2 (1), 9.

Applied Soil Ecology 206 (2025) 105900

Contents lists available at ScienceDirect

Applied Soil Ecology

journal homepage: www.elsevier.com/locate/apsoil

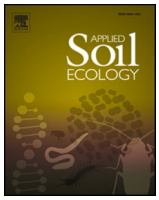

Research paper

# Unravelling the plastisphere-soil and plasticplane microbiome of plastic mulch residues in agricultural soils☆

Giovana P.F. Macan [a,b,*], Manuel Anguita-Maeso [a,c], Concepción Olivares-García [a], Quynh Nhu Phan Le [d], Crispin Halsall [d], Blanca B. Landa [a,**]

[a] Institute for Sustainable Agriculture, Spanish National Research Council (IAS-CSIC), 14004 Córdoba, Spain
[b] Programa de Doctorado de Ingeniería Agraria, Alimentaria, Forestal y de Desarrollo Rural Sostenible, Universidad de Córdoba, Córdoba, Spain
[c] Department of Biology, University of North Carolina at Chapel Hill, NC-27599 Chapel Hill, USA
[d] Lancaster Environment Centre, Lancaster University, Lancaster LA1 4YQ, UK

ARTICLE INFO

*Keywords:*
Agricultural fields
Core bacteria
Environmental pollution
Microbial diversity
Plastisphere
Soil health

ABSTRACT

Advances in molecular techniques have recently uncovered microbial communities associated with plastic debris. The term 'plastisphere', was originally used for microbial communities on marine plastic. In terrestrial systems, this term has been extended to the plastic-soil interface, encompassing microbes from the surrounding soil. Although some studies have revealed differences in microbial composition and diversity between plastisphere and bulk soil, high-resolution spatial analyses of microbial communities on the immediate plastic surface (plasticplane) and in the attached soil (plastisphere-soil), are still lacking. In this study, a methodology was developed to disentangle the bacterial populations associated with the plastisphere-soil of weathered plastic mulch from agricultural fields from those on the plasticplane by using culture-based and High-Throughput sequencing approaches. A significantly higher number of colony-forming units were cultured from the plastisphere-soil compared to the plasticplane. Main genera isolated from the plasticplane by culturing included *Arthrobacter, Pseudarthrobacter, Priestia, Massilia, Microbacterium, Bacillus*, and *Kocuria* genera, some of which are known plastic-degraders. High-throughput sequencing analysis revealed higher bacterial richness in plastisphere-soil, while beta diversity showed main significant differences among field plots. Core taxa significantly associated to the plasticplane included *Bacillus*, *Sphingomonas*, *Nocardioides,* and *Solirubrobacter*. This study provides a pioneering description of a methodology to differentially analyze microbial communities at different soil-plastic interfaces, particularly on a small spatial scale using samples from plastic mulch residues in agricultural soils. This methodology may lay a foundation for future research to isolate and identify microbial plastic degraders, contributing to efforts against mitigating plastic pollution.

## 1. Introduction

The use of plastic mulch plays an important role in crop production by improving water-use efficiency and soil temperature, decreasing weed pressure, and providing higher yields and earlier harvests. However, associated drawbacks, including its disposal and environmental pollution, have gained significant attention in recent years (FAO, 2021; Zhang et al., 2020). The process of removing plastic mulch from the soil is considered a time-consuming and laborious activity. Frequently, the complete retrieval of this plastic is not achievable, leading to a significant accumulation of plastic debris in the soils that can be further fragmented, resulting in one of the major sources of microplastic (particles smaller than 5 mm) pollution in agricultural soils (Bläsing and Amelung, 2018; FAO, 2021; Huang et al., 2020; van Schothorst et al., 2021). Available studies have already highlighted notable levels of macro- and microplastic pollution in agricultural fields continuously exposed to plastic mulch worldwide. This reveals a pervasive and persistent issue, raising concerns about the potential effects on soil

☆ This article is part of a special issue entitled: Soil Health II-ADV & CHLG published in Applied Soil Ecology.

* Correspondence to: G.P.F. Macan, Programa de Doctorado de Ingeniería Agraria, Alimentaria, Forestal y de Desarrollo Rural Sostenible, Universidad de Córdoba, Córdoba, Spain.
** Corresponding author.
*E-mail addresses:* gprado@ias.csic.es (G.P.F. Macan), blanca.landa@csic.es (B.B. Landa).

https://doi.org/10.1016/j.apsoil.2025.105900
Received 12 October 2024; Received in revised form 13 January 2025; Accepted 20 January 2025
Available online 28 January 2025

health and ecosystem services, and consequently, it emphasizes the need for further research in this field (Huang et al.,2020; Meng et al., 2023; Van Schothorst et al.,2021; Ya et al., 2022).

Microbial communities are crucial for ecosystem functionality, with soil microorganisms playing key roles in nutrient cycling, organic matter decomposition, soil structure maintenance, and regulation of soil-borne pathogens (Garbeva et al., 2004; Saccá et al., 2017). Current molecular techniques including High-Throughput Sequencing (HTS) combined with advanced microscopy have recently unveiled the occurrence of diverse microbial communities associated with different plastic debris from different environments (Amaral-Zettler et al., 2020; Luo et al., 2023; Schlundt et al., 2020; Vethaak and Leslie, 2016; Zettler et al., 2013). Zettler et al. (2013) first introduced the term 'plastisphere' to describe the unique microbial community colonizing plastic marine debris. However, the application of this term to terrestrial environments necessitates careful consideration to avoid potential confusion or misinterpretation. While the term is sometimes used in strict adherence to its original definition, referring specifically to the microbial communities closely associated with plastic surfaces, in other instances, it is applied more broadly, akin to the concept of the 'rhizosphere'. This broader usage encompasses the entire soil-plastic interface, thus including both microbes attached to the plastic and those in the interacting soil (Rüthi et al., 2020). This expanded interpretation serves to highlight the complex interactions within the plastisphere in terrestrial ecosystems.

Given the persistent nature of plastic contaminants and their increasing accumulation in the environment, assessing and comparing the microbial communities associated with plastic particles to those living on natural soil particles is of significant interest. However, it must be taken into consideration the fact that plastic are anthropogenic materials, chemically and physically distinct from natural soil particles (De Souza Machado et al., 2018). Thus, the microbial community residing on the plastic surface can differentiate from the one found in the attached soil. In this context, our study aims to develop a methodology that allows to distinguish the main compartments that microbes can occupy in terrestrial agroecosystems polluted with plastics. Therefore, we propose the adoption of the term 'plastisphere-soil' to describe the soil zone directly influenced by plastic. Additionally, we suggest using 'plasticplane' as a more specific term to describe the surface of the plastic where specific microbial colonization can also occur akin to the concept of "rhizoplane" terminology, broadly adopted in soil microbiology studies (Foster, 1986; Li et al., 2023a; Mwajita et al., 2013; Wieland et al., 2001).

Most previous research has focused on evaluating the microbial communities colonizing plastic surfaces in comparison to bulk soil, reporting notable differences in composition, diversity, and richness compared to those associated with plastic debris (Gkoutselis et al., 2021; Yu et al., 2021). However, it is crucial to consider the extreme heterogeneity of soils. Most studies on the plastisphere have come from aquatic environments, which are more homogeneous, making it reasonable to compare microbial communities attached to plastic surfaces with those in bulk, non-influenced regions. In contrast, soil ecosystems are highly heterogeneous, and observed differences in microbial communities may simply be attributed to natural spatial constraints.

As emphasized by Rillig et al. (2023), there is still a lack of information on plastisphere microbial communities at the microscale, where the compartmentalized and heterogeneous nature of soil must not be overlooked. This highlights the importance of this research, which isolated and compared microbial communities across adjacent plastic-associated microenvironments at a small spatial scale, using both culture-dependent and culture-independent approaches.

Plastic mulch debris was collected from agricultural fields, providing a more realistic perspective compared to traditional laboratory experiments. A methodology was developed to differentiate the recovery of the microbial communities associated with the soil adhering to the plastic (referred to as plastisphere-soil) and those closely associated with the plastic surface itself (termed plasticplane). This study has also identified core microbial taxa consistently associated with plastic mulch debris, as well as isolated bacteria species that could be further evaluated for their potential to degrade polymer-based materials contributing to global efforts to mitigate plastic pollution.

## 2. Material and methods

### 2.1. Study site and field sampling

Weathered plastic mulch debris was collected from five agricultural fields located at Baza (Granada), southern Spain (Fig. S1). The fields were characterized by intensive horticultural production and historical use of plastic at least twice a year over the last ten years. At each sampling site, a total of ten weathered plastic mulch debris samples measuring from 5 to 10 × 5–10 cm, were randomly collected from the topsoil. Samples were gently shaken to remove the loosely attached soil particles, placed in sampling bags, and stored at 4 °C until further analysis.

### 2.2. Plastic characterization by Raman and Fourier infrared (FTIR) spectroscopy

Prior to chemical characterization, plastic films were thoroughly washed with warm water (40 °C), followed by a 20-min ultrasonication in deionized water. Subsequently, the films were rinsed and wiped using cotton wool in distilled water and 70 % isopropanol to remove residual soil and potential bio-contaminants.

The chemical characterization of the plastic film surfaces was performed using Raman and FTIR. FTIR is especially sensitive to observing oxidative products resulting from weathering, while Raman spectra can provide insights into the polymer backbone, crystallinity, and the presence of inorganic additives undetectable by FTIR.

Raman analysis was performed using a Renishaw InVia microspectrometer (Renishaw plc, New Mills, Wotton under Edge, UK) equipped with a 532 nm laser (15 mW at the sample) and a 50× objective lens (numerical aperture NA 0.50). Raman spectra were collected in the 100–3500 $cm^{-1}$ range using a 2400 lines per millimeter grating, resulting in a spectral resolution of approximately 1 $cm^{-1}$. All measurements were conducted with 5 accumulations at 5 % laser power. After collection, each spectrum underwent cosmic ray removal (Wire 4.2), baseline correction, and normalization at the 2851 $cm^{-1}$ in Spectragryph version 1.2.15. Given the heterogeneous nature of the plastic surface, spectra were collected at ten different positions on each plastic sample. The fraction of trans ($\alpha_t$) and amorphous ($\alpha_a$) conformers were calculated using $I_{1298}$ and $I_{1305}$ intensities of the Raman bands at 1298 and 1305 $cm^{-1}$, respectively according to Hiejima et al. (2018).

Alongside Raman spectroscopy, a Cary 630 FTIR (Agilent Technologies Inc., Danbury, CT, USA) with an attenuated total reflection (ATR accessory, diamond substrate) was used to identify plastics and potential weathering effects on the polymer surface functional groups (penetration depth~ 2 μm at 1700 $cm^{-1}$). FTIR spectra were gathered in the 650–4000 $cm^{-1}$ range, with 64 accumulated scans and a 2 $cm^{-1}$ spectral resolution. After collection, each spectrum underwent baseline correction and normalization at the 2912 $cm^{-1}$ peak in Spectragryph.

### 2.3. Assessment of microbial communities associated with plastic mulch debris

To assess and distinguish the microbial community of the plastisphere-soil (PPh) from the one tightly attached to the plastic surface (plasticplane (PPl)) the collected plastic samples were subjected to sequential washing steps (Fig. S2) by using a modified protocol mimicking those developed to sample and isolate rhizosphere and rhizoplane bacteria (Barillot et al., 2013).

Plastic mulch samples collected from each field were cut into small

pieces (2 × 1.5 cm) with sterile scissors and pooled into a single composite sample. A total of 50 mg of composite plastic samples was placed in a falcon tube containing 10 mL of sterile distilled water. Collectively, three replicates of plastic samples were processed per field plot. Falcon tubes were softly shaken for two min at 250 rpm in a horizontal rotatory shaker, obtaining a first suspension that contained the attached soil fraction (plastisphere-soil). From this soil suspension, 1-mL aliquots were taken for isolation of cultivable bacteria whereas 1.5-mL aliquots were taken for DNA extraction. Specifically, the 1.5-mL aliquots were centrifuged at 14,000 rpm for 1 min. Then, the supernatant was discarded, and this process was repeated six times to recover a soil pellet that was stored at −20 °C until DNA extraction.

On the other hand, the washed plastic pieces from the first suspension were subjected to a second intermediate washing step (Fig. S2). Plastic debris was recovered and transferred to another falcon tube that was shaken for 2 min with 20 mL of sterile water. Then, the washed plastic mulch films (plasticplane) were transferred to a new 15-mL tube with 5 mL of sterile water, and it was sonicated for 5 min and vigorously vortexed for 2 min. A 1-mL aliquot of the resulting suspension, containing bacteria from the plasticplane, was taken for isolation of cultivable bacteria (see below), whereas the washed plastics were transferred to a 2-mL tube and kept at −20 °C until DNA extraction.

Additionally, samples from the plastic surfaces at each consecutive washing step were observed under a stereomicroscope (Leica, M165C, Leica Microsystems, Germany) to assess the efficacy of the washing process in removing soil particles attached to the plastic surfaces, and the same washed pieces were subjected to SEM-EDX analysis described below to corroborate the efficacy of the different washing steps to differentiate plastisphere-soil and plasticplane interfaces.

#### 2.3.1. Isolation and characterization of culturable bacteria

Aliquots of plastisphere-soil and plasticplane suspensions were subjected to serial dilutions and 100-µl aliquots were plated in triplicate on R2A (Difco, Detroit, MI, USA) agar plates which contains yeast extract (0.5 g $L^{-1}$), proteose peptone No. 3 (0.5 g $L^{-1}$), casamino acids (0.5 g $L^{-1}$), dextrose (0.5 g $L^{-1}$), soluble starch (0.5 g $L^{-1}$), sodium pyruvate (0.3 g $L^{-1}$), dipotassium phosphate (0.3 g $L^{-1}$), magnesium sulfate (0.05 g $L^{-1}$), and agar (15 g $L^{-1}$), with a final pH of 7.2.

The number of colonies forming units (CFU) was assessed after a 2-day incubation period at 28 °C. Subsequently, a representative number of distinct colonies from the plasticplane were selected based on morphology (color, shape, margin, and texture). Then, selected colonies were isolated and purified (three cloning steps) and kept in 40 % glycerol stocks at −80 °C.

For bacteria identification, DNA was extracted using the DNeasy kit (QIAGEN, Madrid, Spain). The near-complete 16S rDNA gene was amplified using 8f (5′-AGAGTTTGATCCTGGCTCAG-3′) and 1492r (5′-ACGGCTACCTTGTTACGACTT-3′) primers (Weisburg et al., 1991) following the protocol outlined in Anguita-Maeso et al. (2022). Amplicons were sequenced by Sanger sequencing with the same primers used for the PCR at STABvida sequencing facilities (Caparica, Portugal). Sequences were assembled and manually corrected using DNASTAR software version 15.3.0.66 (Madison, WI, USA). The identification of isolates to the genus/species level was carried out by comparing their sequences with reference 16S rRNA gene sequences in the GenBank "nt" database using the BLAST algorithm as described by Altschul et al. (1997).

#### 2.3.2. DNA extraction and 16S rRNA gene amplicon library preparation

DNA from plastisphere-soil and plasticplane samples was extracted using the DNeasy PowerSoil Kit (QIAGEN, Hilden, Germany) following the manufacturer's instructions with small modifications. Briefly, samples were homogenized with the lysis buffer for 7 min at 50 pulses $s^{-1}$ with the Tissuelyser LT (QIAGEN) and then were incubated for 1 h at 60 °C to increase cell lysis. DNA was eluted in a final volume of 50 µL of sterilized distilled water and its purity was determined using a NanoDrop®156 ND-1000 UV–Vis spectrophotometer (Thermo Fisher Scientific, Inc., Waltham, MA, USA). This DNA was used as a template for amplicon library preparation as described previously in Anguita-Maeso et al. (2022). Shortly, the V5-V6 region of the bacterial 16S rRNA gene was amplified with the primers 799F (5′- AACMGGATTAGATACCCKG-3′) and 1115R (5'-AGGGTTGCGCTCGTTG-3′). Barcodes indexes were added to the amplicons using Fluidigm barcodes (Access Array Barcode Library for Illumina® Sequencers kit). Next, barcoded PCR products were purified by using Agencourt AMPure XP (Beckman Coulter Inc., Brea, CA, USA), following the manufacturer's instructions. Purified PCR products were quantified by using the Quant-iT™ PicoGreen™ dsDNA Assay Kit (Thermo Fisher Scientific) and a TECAN SAFIRE microplate reader (Tecan Group, Männedorf, Switzerland). Equimolecular amounts from each individual sample were added to a single tube; the pooled library was quantified by using a 2100 Bioanalyzer (Agilent, Santa Clara, CA, USA), and was purified again if primer dimers were still evident. Finally, the library was sequenced on the Illumina MiSeq platform (V2; PE 2× 250 bp) at the Genomics Unit at the Madrid Science Park Foundation, Madrid, Spain. The ZymoBIOMICS microbial standard (Zymo Research Corp., Irvine, CA, USA) and water (no template DNA) were used as internal positive and negative controls, respectively, for library construction and sequencing. Raw sequence data have been submitted to the NCBI database Sequence Read Archive (SRA) submission portal under BioProject accession number PRJNA1172085.

### 2.4. Scanning electron microscopy-energy dispersive X-ray analysis (SEM-EDX) of plastic surfaces

Scanning electron microscopy-energy dispersive X-ray analysis (SEM-EDX) was utilized to evaluate the plastic surface morphology, determine the elemental composition of the plastic, and assess the efficacy of the washing steps in removing soil particles adhered to the plastic. Distinctly plastic mulch samples were chosen from each sampling site. These samples underwent fixation with 2 % glutaraldehyde, dehydration through an ethanol series, and gold coating. The scanning electron microscopy analysis was conducted using a JEOL JSM 7800 F scanning microscope (JEOL Ltd., Peabody, MA, USA) equipped with energy-dispersive X-ray spectrometer (EDX) at Central Service of Research Support (SCAI) of the University of Cordoba, Spain.

### 2.5. Statistical and bioinformatics analysis

Statistical analysis of culturable bacteria was performed using R statistical software (R Core Team, 2013). The significant effect of field location and soil-plastic habitat was tested using a factorial analysis of variance (ANOVA) followed by Tukey's multiple comparison test ($P < 0.05$). The Shapiro-Wilk test was used to determine whether the data were normally distributed whereas the homogeneity of variance was tested using Levene's test. Data from bacteria enumeration were log-transformed to fulfill the assumptions of homogeneity and normality.

TrimGalore v.0.6.6 tool was employed for quality control and adapter trimming of the demultiplexed raw fastq files. In this process, the first 10 bp of all reads were trimmed, and a truncation length of 240 base pairs for forward bacterial reads and 200 base pairs for reverse bacterial reads was applied to achieve a satisfactory Phred quality score ($Q > 30$). Subsequently, the high-quality reads underwent analysis using the DADA2 method to identify the amplicon sequence variants (ASVs) present in the samples (Callahan et al., 2016). Taxonomic classification was carried out using the Silva SSU v.138 database, and singleton ASVs were excluded from taxonomy assignment and statistical analysis. Differences in bacterial communities were assessed using alpha-diversity indexes (Richness and Shannon) at the ASV level. The non-parametric Scheirer–Ray–Hare test ($P < 0.05$), implemented with the rcompanion v.2.4.1 package in R (Mangiafico, 2022), was employed to evaluate the effects of the sampled field and habitat (plastisphere-soil or plasticplane)

and their interaction on alpha-diversity indexes. Beta-diversity was determined through principal coordinate analysis (PCoA) of weighted UniFrac distance matrices. Additionally, the Permutational multivariate analysis of variance using distance matrices (ADONIS function) from the vegan package in R (with 999 permutations) was employed to test the effects ($P < 0.05$) of the sampled plot, habitat, and their interaction. To achieve parity in the total number of counts between samples, alpha- and beta-diversity analyses were performed after resampling the abundance values to the minimum number of reads observed. Moreover, a linear discriminant analysis effect size (LEfSe) (Segata et al., 2011), based on the microbiomeMarker package in R (Cao et al., 2022), was employed to identify differences in microbiota composition at the genus level among the various treatments ($P < 0.05$).

## 3. Results

### 3.1. Plastic characterization

The most representative spectra, showcasing the overall plastic composition and the influences of weathering is shown in Fig. 1. Both Raman and FTIR analyses confirmed that the plastic mulch collected from the five fields was composed of polyethylene (Table S1).

Raman spectra analysis of the plastic samples displayed distinct peaks corresponding to the native bonds in the LDPE polymer, found in the C—C stretching (1040–1200 $cm^{-1}$), -$CH_2$- twisting and bending (1300–1500 $cm^{-1}$), and C—H stretching (2800–3000 $cm^{-1}$) regions (Fig. 1). The latter is sensitive to subtle structural changes due to intermolecular interactions and crystallinity. The peaks at 2882 and 2851 $cm^{-1}$ indicated the presence of LDPE's amorphous and crystalline regions, respectively. Plastic samples from Field 1 had a significant decrease in the intensity of the 2882 $cm^{-1}$ peak relative to the 2851 $cm^{-1}$ peak, compared to the plastic samples obtained from other fields, indicating its lower crystallinity.

Additional Raman signals linked to LDPE's crystallinity appeared at peaks 1305 and 1298 $cm^{-1}$, associated with the $CH_2$ twisting modes of the amorphous and trans (consecutive trans chains) conformers, respectively (Meier, 2002). The highest amorphous fraction was found in the plastic samples from Field 1, being 45.39 ± 0.03 %, while the fractions obtained from Fields 3, 4, and 5 were 36.4 ± 0.1 %, 33.19 ± 0.06 %, and 34.28 ± 0.06 % respectively. Field 2 was excluded from the calculations due to a broad additive band at 1360 $cm^{-1}$. Often, plastic degradation, especially due to photodegradation, results in increased crystallinity (decreased amorphous phase), leading to material embrittlement and fragmentation.

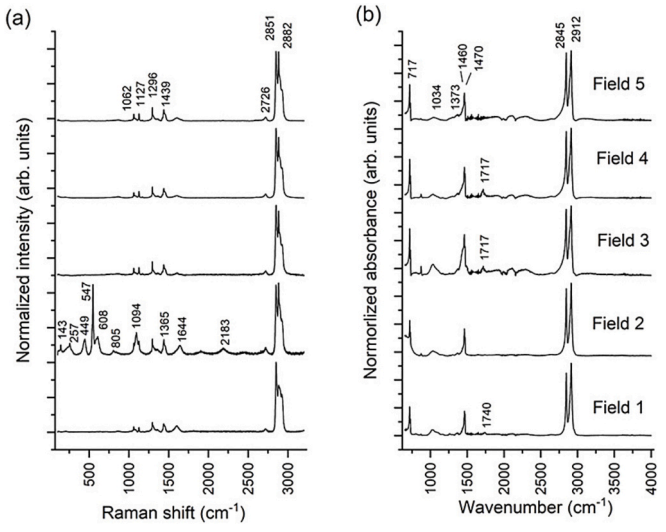


**Fig. 1.** Characterization of the plastic film samples from each of the fields. A. Normalized Raman spectra. B. Normalized FTIR spectra.

The lower Raman spectral region (100–600 $cm^{-1}$) indicated the presence of inorganic compounds. In this case, the presence of titanium oxide ($TiO_2$) and the blue pigment Lazurite-a sodium silico aluminate in a sulfur matrix were confirmed in plastic samples from Field 2 (Fig. S3 A). This was evidenced by the presence of bands corresponding to anatase $TiO_2$ (143 $cm^{-1}$) and rutile $TiO_2$ (233, 442, 610 $cm^{-1}$), and the characteristic bands of Lazurite (257, 547, 805, 1094, 1644, and 2183 $cm^{-1}$, (Fig. S3 B). These findings align with the SEM-EDX data, which also revealed the presence of titanium (0.12%wt), silicon (2.76%wt), calcium (1.87%wt), sulfur (0.15%wt), and aluminum (1.01%wt) in plastic samples from Field 2, while no sulfur and titanium were detected in plastics from other fields (Table S2).

Interestingly, plastic samples from Fields 1, 3, and 4 exhibited a noticeable presence of carbonyl (C=O) groups in their FTIR spectra, potentially formed during plastic oxidation. Samples from Field 3 and Field 4 displayed unique peaks due to ketone carbonyl at 1717 $cm^{-1}$, while those from Field 1 showed a peak due to ester carbonyl at 1740 $cm^{-1}$. The carbonyl index, a common indicator of oxidation level, which is calculated as the ratio of peak intensity between 1717 (or 1740) $cm^{-1}$ and 1465 $cm^{-1}$, was 0.13, 0.20, and 0.28 for samples from Fields 1, 3, and 4, respectively, indicating a higher concentration of carbonyl in plastic samples from Field 4.

### 3.2. Microscopic evaluation of plastic surface: Scanning electron microscopy and optical microscope analysis

Visual inspection using light images from a stereomicroscope (Figs. S4 A and B) and SEM (Fig. S4 C) was performed to assess the efficacy of the sequential washing steps in removing soil particles from the plastic surface and enabling independent sampling of plastisphere-soil and plasticplane-associated microorganisms. The image shows the condition of the plastic surface immediately after field sampling and after each successive washing steps described in Fig. S2.

Initial attempts revealed that even after two washing steps, some soil particles remained, which could lead to misleading results in the differential extraction of microorganisms associated with the soil particles rather than the plastic surface. Therefore, an additional washing step was introduced to remove the soil particles more effectively (Fig. S2). This modification included in our protocol ensured a clear distinction between the plastisphere-soil and plastic-plane compartments, facilitating more accurate characterization of their respective microbial communities.

### 3.3. Characterization of the culturable bacterial population

Both plastic-debris compartments (plastisphere-soil and plastic-plane) and location (field) factors significantly affected the population density of culturable bacteria ($P < 0.001$) (Fig. 2). The bacterial density found on the plastisphere-soil was significantly greater than that obtained on the plastic surface for all sampled fields. Thus, the bacterial density isolated from the plastisphere-soil fraction ranged from log 7.1 to log 7.7 CFU $g^{-1}$ plastic, whereas the bacterial population on the plastic surface ranged from log 6.2 to 6.9 CFU $g^{-1}$ plastic.

A total of 74 bacteria from the plasticplane were isolated, cultivated, and taxonomically identified by 16S rRNA gene sequencing. Isolated bacteria were assigned to four phyla, five classes, six orders, nine families, and 19 genera (Table S3A). The most abundant genera included *Arthrobacter* (16.2 % of isolates) followed by *Priestia* (14.9 % of isolates), *Pseudarthrobacter* (13.5 % of isolates), *Massilia* and *Microbacterium* (9,5 % each), *Bacillus* (8,1 %) and *Kokuria* (6.8 %) (Table S3B). On the other hand, less frequent bacteria included *Frondihabitans, Lysinibacillus, Nocardioides, Paenarthrobacter, Paenibacillus, Planococcus, Planomicrobium, Rossellomorea,* and *Rufibacter*. Plasticplane samples from Fields 3 and 5 showed a higher diversity of bacterial genera (8 and 10 respectively), whereas in those from the remaining field plots, a total of

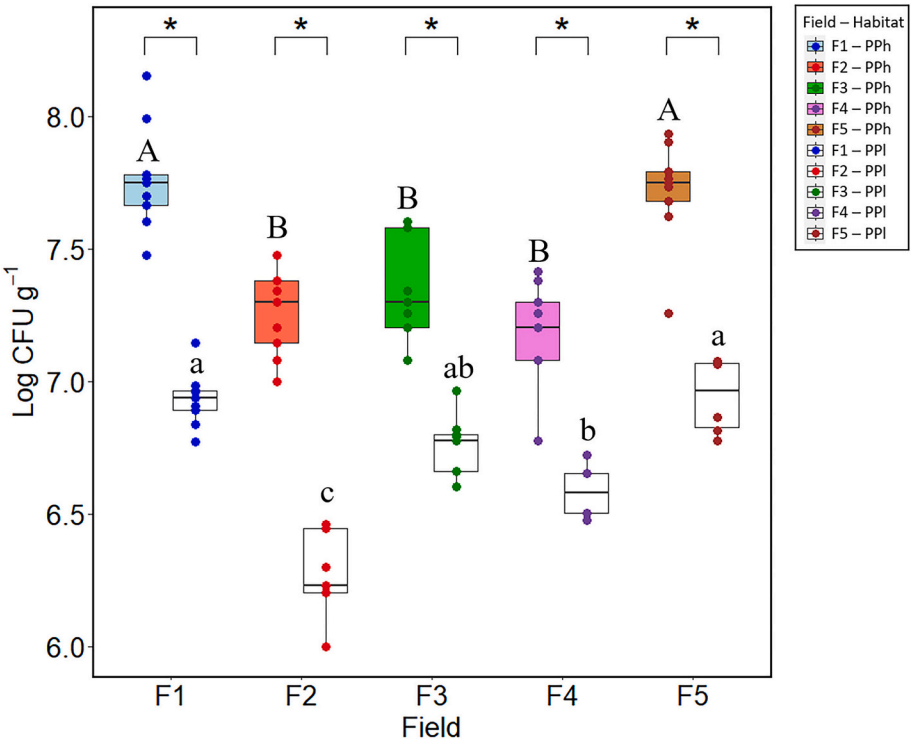


**Fig. 2.** Bacterial population density (log of the mean CFU g$^{-1}$) in the plastisphere-soil (PPh) and plasticplane (PPl) of plastic mulch debris sampled in different field plots. Means followed by different letters are significantly different ($P < 0.001$) according to Tukey Test. Uppercase letters are related to the plastisphere, while lowercase letters are related to the plasticplane. The asterisks indicate significant ($P < 0.001$) differences between the sampled plastic-associated compartments (plastisphere soil, PPh and plasticplane, PPl) at each field plot.

seven bacterial genera were identified.

### 3.4. Composition and diversity of bacterial communities in the plastisphere-soil and plasticplane

Illumina sequencing yielded a total of 351,265 good-quality reads after removal of chimeras, unassigned, or mitochondrial reads. A total of 1701 amplicon sequence variants (ASVs) were identified among all treatments, with 1682 ASVs being retained for alpha- and beta-diversity analysis after rarefying all data to the minimum number of reads and singleton removal. The Scheirer–Ray–Hare test indicated significant differences ($P < 0.05$) for the Richness and Shannon alpha-diversity indices according to the field plot ($H = 19.63$, $P = 0.001$, and $H = 21.54$, $P = 0.001$, respectively) whereas plastic -associated compartments resulted significant for Richness ($H = 4.13$, $P = 0.04$), but not for Shannon ($H = 3.25$, $P = 0.07$) diversity. Furthermore, there was no

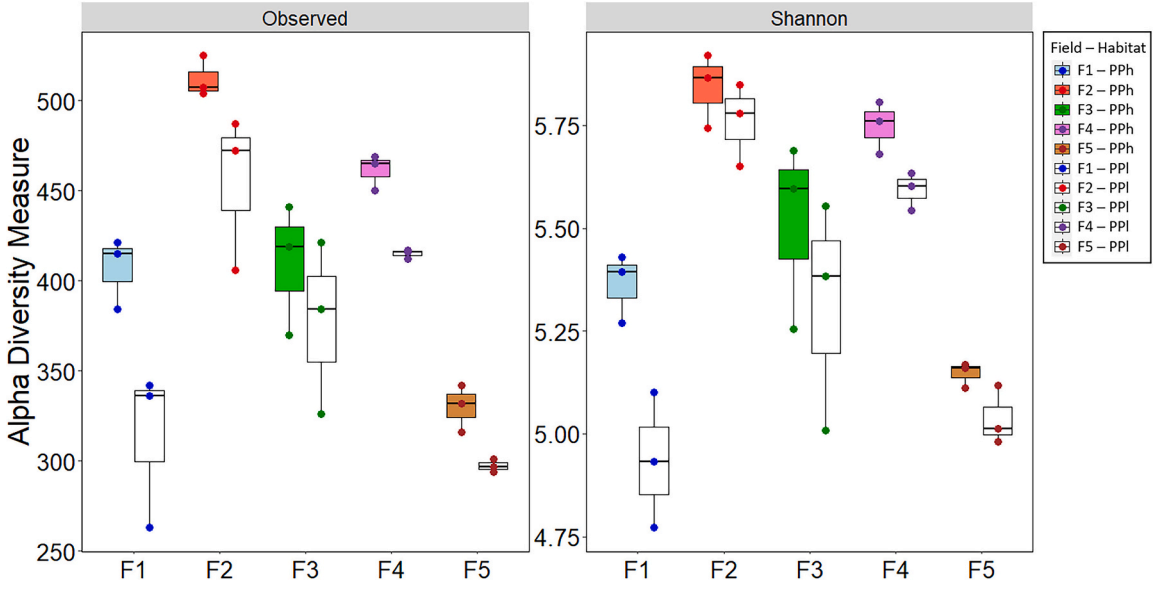


**Fig. 3.** Boxplots of Richness (observed) and Shannon diversity indices for bacterial communities at ASV level in the plastisphere soil (PPh) or plasticplane (PPl) compartments of plastic mulch debris sampled at different field locations. The boxes represent the interquartile range, while the horizontal line within the box defines the median and whiskers represent the lowest and highest values of four values for each treatment combination.

significant interaction between the plastic fraction and field plot for both alpha-diversity indices ($H < 0.77$, $P > 0.94$) (Fig. 3).

Principal coordinate analysis of beta-diversity weighted UniFrac distances differentiated bacterial communities mainly according to the field location. Thus, there was a clear tendency to group bacterial communities according to the sampled field along Axis 1, which explained 49.9 % of the variation (Fig. 4). In fact, ADONIS analysis supported the results described above and indicated a significant main effect of the field plot ($R^2 = 0.79$, $P < 0.001$). However, the bacterial habitat (plastisphere-soil or plasticplane) resulted not significant ($R^2 = 0.01$, $P > 0.196$) nor their interaction ($R^2 = 0.03$, $P > 0.424$).

A total of 24 phyla, 60 classes, 173 orders, 321 families, and 723 genera of bacteria were taxonomically identified by illumine sequencing. Most abundant bacterial genera in all the plastisphere-soil samples belonged to *Bacillus* (23.3 %), *Nocardioides* (11.7 %), *Planomicrobium* (10.4), *Blastococcus* (10.1 %) and *Streptomyces* (8.5 %) genera, whereas those from plasticplane included *Blastococcus* (15.6 %), *Sphingomonas* (10.7 %), *Arthrobacter* (10.1 %), *Bacillus* (9.3 %) and *Hymenobacter* (7.4 %). In Field 1 and 2, there was a prevalence of *Bacillus* (41.3 % and 51.8 %, respectively), whereas, in Fields 3 and 4, *Blastococcus* was the dominant genus (18.9 % and 30.7 %, respectively) (Fig. 5).

In line with these results, Linear Discriminant Analysis Effect Size (LEfSe) analysis was used to identify key bacterial genera differentially associated with the plasticplane or plastisphere-soil fractions of plastic mulch debris sampled at different field locations. Globally, LEfSe identified a bacterial enrichment of *Skermanella* and Class_ASV511 enriched in the plastisphere-soil (Fig. S5). However, when applying LEfSe to each field independently, field plot F2 showed a higher number of differentially abundant genera. In particular, genera such as *Polycyclovorans*, *Sphingomonas,* and *Cellvibrio*, were enriched in the plasticplane, while genera such as *Arthrobacter, Planomicrobium*, and *Skermanella* were significantly more abundant in the plastisphere-soil than in the plasticplane (Fig. 6).

### 3.5. Core community analysis

The Venn Diagram (Fig. S6) analysis revealed the shared and unique bacterial genera in the different plastic-associated habitats. Notably, in all evaluated fields, between 62.5 % and 88.4 % of the bacterial genera were shared between both habitats. Interestingly, on plastic debris recovered from field plots F3 and F5, approximately 13 % of bacterial genera were exclusively found on the plasticplane, while in the other fields, these values were lower.

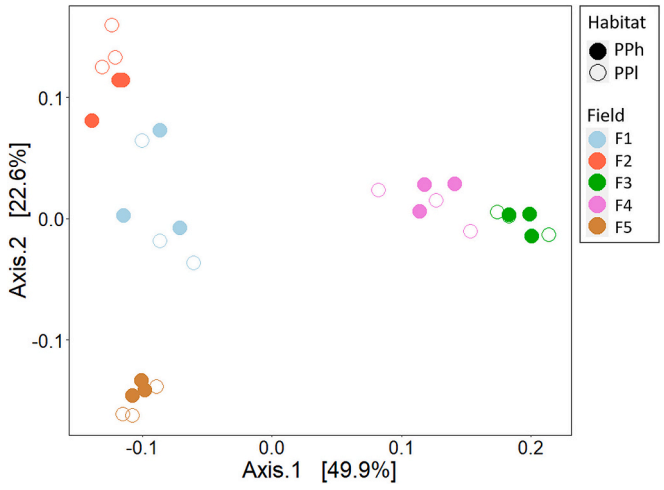


**Fig. 4.** Principal Coordinates Analysis (PCoA) of bacterial communities based on Weighted UniFrac distances at the ASV taxonomic level in the plastisphere (PPh) or plasticplane (PPl) compartments of plastic mulch debris sampled at different field locations. Points are colored by field location and shaped by habitat type.

The core microbial taxa consistently found only in the plastisphere-soil of all evaluated samples recovered from the different fields were represented by 220 bacterial ASVs, while 79 ASVs represented the core taxa on the plasticplane (Fig. 7). The majority of bacteria consistently found on the plasticplane belonged to the genera *Bacillus*, *Sphingomonas*, *Nocardioides,* and *Solirubrobacter*. A complete list identifying the core plasticplane bacterial community can be found in Supplementary Table S4.

## 4. Discussion

While some studies have compared the plastisphere microbiome with bulk soil, highlighting significant differences in their microbial community composition and structure, there is still a need for a more comprehensive understanding of microbial communities at a finer spatial definition within the plastic-soil interface (Bandopadhyay et al., 2020; Gkoutselis et al., 2021; Rillig et al., 2023; Rüthi et al., 2020). This study addresses this gap by developing a methodology to differentially sample and compare the bacterial community composition and diversity of plastic surfaces (plasticplane) with those found on natural soil particles interacting with this anthropogenic material (plastisphere-soil).

Polyethylene polymers are commonly regarded as recalcitrant materials, known for their resistance to degradation (Brown et al., 2022; El-Sherif et al., 2022). However, research suggests that weathered polyethylene plastics, previously exposed to UV radiation, can be colonized and undergo partial metabolism facilitated by specific microbial taxa capable of secreting enzymes such as esterase, lipases, peroxidases, and oxidoreductases (El-Sherif et al., 2022; Sharma and Neelam, 2023). Consequently, it was expected that, as observed, the microbial community richness on the surface of weathered polyethylene might experience a reduction or selection of specific bacterial taxa compared to soil particles. This difference can be attributed to the easily assimilated carbon sources provided by the associated organic matter in soil particles, contrasting with the resistant nature of polyethylene, which is not considered a straightforward or efficient carbon source for most bacteria. Interestingly, these results are similar to those described for the rhizosphere soil and rhizoplane-root interfaces, where the secretion of root exudates favors the growth of specific bacteria that are better adapted to this environment, leading to a decrease in overall bacterial richness (Philippot et al., 2013).

Furthermore, our results revealed similarities in the microbial communities' composition retrieved according to the field of origin of the plastic debris. Thus, the tendency to group bacterial communities according to the sampled field, and the observed similarities between Fields 3 and 4, which are geographically closer to each other, highlight the role of environmental and geographic constraints in shaping the soil microbial community at the plastic-soil interface. Additionally, the plastic debris collected from Field 2 exhibited a higher number of differentially abundant taxa on the plasticplane compared to the plastisphere-soil. Interestingly, this plastic was unique in its color, appearing light grey instead of the commonly found black plastic mulch of the remaining field sites. Analysis of the plastic's chemical properties by SEM-EDX and Raman spectroscopy revealed the presence of titanium dioxide ($TiO_2$) on this specific mulch film, a pigment commonly found in white plastics due to its high light scattering efficiency, inertness, thermal stability, dispersibility, and cost-effectiveness (Puglisi et al., 2019; Turner and Filella, 2023).

Some previous studies have demonstrated the effects of $TiO_2$ on soil bacterial communities (Ge et al., 2011, 2012, 2013). Ge et al. (2012), for instance, found that the presence of this chemical compound can significantly reduce certain bacterial genera, including *Actinoplanes, Balneimonas, Blastococcus, Bradyrhizobium*, and *Skermanella.* The toxicity of this material to some bacteria can be related to oxidative damage to bacterial cell walls, leading to membrane disorganization and permeability. Our results also indicate a reduction in the *Blastococcus* genus on

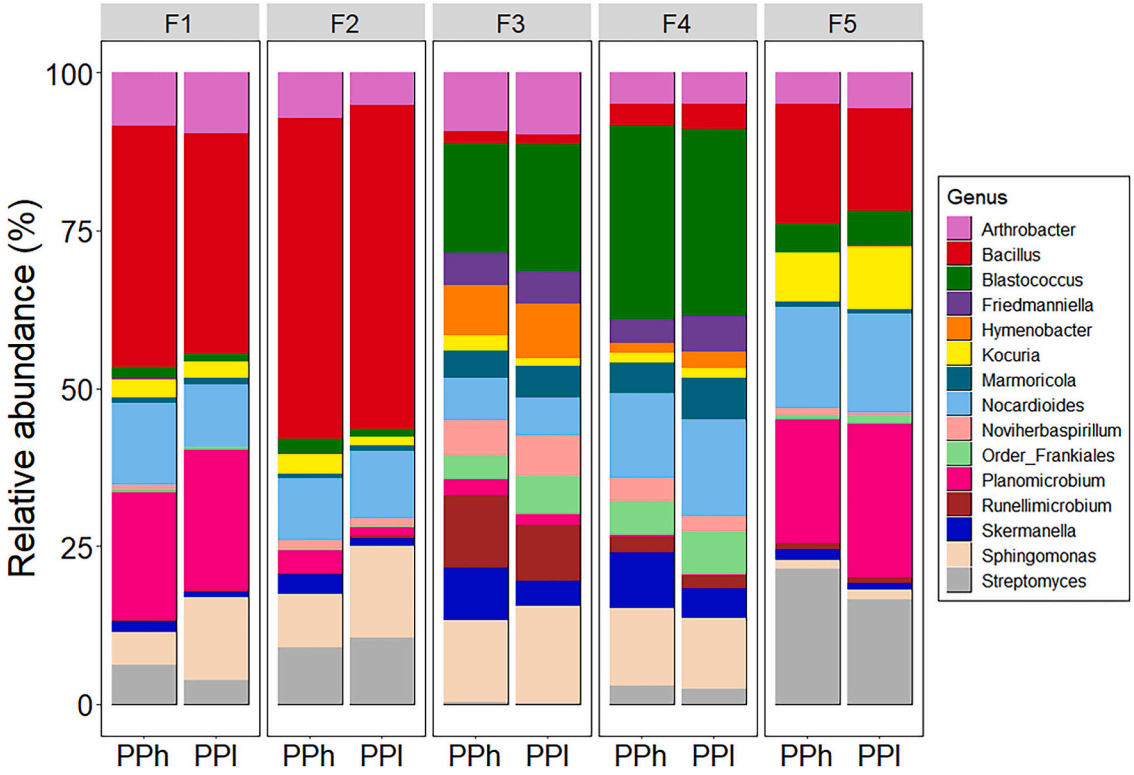


**Fig. 5.** Barplots showing the relative abundance of the 15 most abundant bacterial taxa at the genus level in the plastisphere (PPh) and plasticplane (PPl) compartments of plastic mulch debris sampled at different field plots (F1 to F5).

the plastic surface compared to the plastisphere-soil. In contrast, the genera *Polycyclovarans* and *Cellvibrio* were enriched on the plasticplane compared to the plasticphere. These findings suggest that plastic additives and dyes may influence the assemblage of plastic-associated bacterial communities, underscoring the need for further research focusing on this topic.

Differing from most contaminants found in the soil, plastic debris represents a potential threat to the soil environment as it constitutes an external anthropogenic particle with a distinct shape, size, and volume compared to natural soil particles (Rillig et al., 2023). Additionally, it contains a series of additives, such as pigments, plasticizers, and antioxidants, which can leach over time and could interact with the microbial community (Macan et al., 2024). Furthermore, these materials can adsorb contaminants such as pesticides commonly applied in agricultural fields, as well as heavy metals (Li et al., 2023b; Rillig et al., 2023). Consequently, all these factors may play a role in selecting specific taxa more adapted to colonize the plasticplane.

Isolating, cultivating, and identifying key species from the plasticplane is particularly noteworthy, as they present promising candidates for further assessments as plastic degraders. Both molecular and culturable methods revealed a prevalent presence of *Arthrobacter* genus in plastic-soil interface. Numerous reports in the literature highlight its significant role in degrading various carbon sources, emphasizing its active hydrolytic enzyme production and the ability to break down persistent conventional plastics (Gobbetti and Rizzello, 2014; Han et al., 2020). Furthermore, members of the *Priestia* genus were isolated and cultured from the majority of plasticplane samples. This genus is recognized as an environmental bacterium extensively used in biotechnology and bioremediation due to its ability to produce several enzymes (Dhaka et al., 2022; Shwed et al., 2021). Other culturable bacterial genera isolated and identified, such as *Bacillus, Terribacillus, Paenibacillus, and Kocuria*, have also been previously associated with plastics according to existing literature and could be further explored as key genera in plastic biodegradation assays (Anwar et al., 2016; Bardají et al., 2019; Harshvardhan and Jha, 2013; Vidal-Verdú et al., 2022). More specifically, *Priestia megaterium* and *Bacillus pumilus,* for instance, were some of the cultivated and identified species in this study which have also been previously isolated from the plastic debris and assessed for their biodegradation abilities on a range of polymer types such as polyethylene (PE), polypropylene (PP) and also poly(lactic acid) (PLA) and poly(3-hydroxybutyrate) (PHB) biodegradation (Jeszeová et al., 2018; Sangeetha Devi et al., 2019; Takaku et al., 2006; Wróbel et al., 2023).

HTS of 16S rRNA gene allowed the identification of a high diversity of bacteria, many of which were not isolated by using cultured-based approaches. The results showed that certain bacterial taxa, including species from the genus *Bacillus, Sphingomonas, Nocardioides, Solirubrobacter, Nitrosospira,* and *Paenibacillus*, were consistently present on the plasticplane of all plastic samples recovered from the different fields. This analysis identified these taxa as core genera associated with the plastic surface of LDPE-based plastic mulches. *Bacillus*, for instance, emerged as one of the most dominant genera in the core plasticplane. The literature indicates that this genus is considered a prominent bacterial taxon involved in plastic biodegradation (Priya et al., 2022). Specific *Bacillus* species have been evaluated for their plastic degradation abilities, including LDPE, in different studies. For instance, Yao et al. (2022) observed a 3.49 % and 2.82 % weight loss of LDPE films after exposure to different *Bacillus* strains, after 30 days of incubation. Moreover, *Nocardioide* is a taxon characterized by its ability to thrive under low-nutrient conditions, being able to degrade a range of pollutants as a source of carbon and nitrogen (Ma et al., 2023; Zhao et al., 2023). *Nitrospira* spp. have also been recently isolated and assessed as potential degrader of various plastic materials, including LDPE, while *Paenibacillus* and *Sphingomonas* have also been previously characterized as key taxa of the plastisphere-associated microbiome (Bardají et al., 2019; Di Pippo et al., 2020; *P.* Wang et al., 2023; Wu et al., 2022).

It should be remarked that, in this study, assessments were conducted using commercial samples of environmental relevance collected

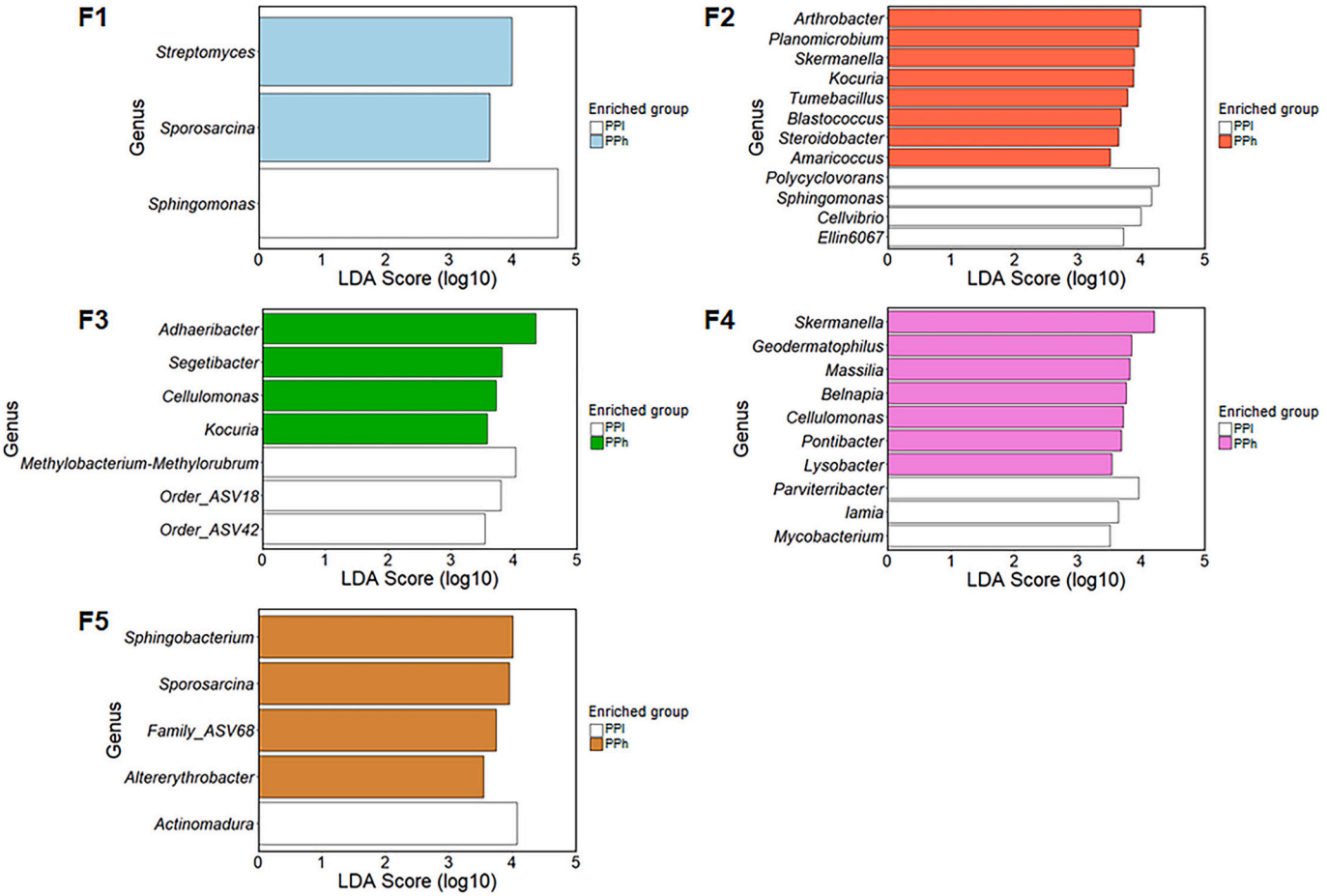


**Fig. 6.** Linear discriminant analysis Effect Size (LEfSe) analysis of differentially enriched bacterial genera present in the plastisphere-soil (PPh) or plasticplane (PPl) compartments of plastic mulch debris sampled at different field locations. Horizontal bars represent the effect size for each taxon. Only significant taxa ($P < 0.05$) with a LDA Score (log10) higher than 3.5 are shown.

from the natural environment, offering a more realistic perspective compared to laboratory incubation experiments. Additionally, all the assessed plastic samples were characterized as polyethylene. Further studies should also be conducted considering a wider range of plastic types (e.g., biodegradable plastic mulches), and in a more diverse range of agricultural fields. Biodegradable plastic mulch, for instance, is starting to be widely adopted in the field as an alternative to conventional LDPE plastic and it could play a more prominent role in shaping the microbial community by selecting specific taxa able to metabolize it and thus having a greater interference in the soil microbial communities (Zhang et al., 2024). Bandopadhyay et al. (2020), for instance, showed that some bacterial genera such as *Methylobacterium, Arthrobacter*, and *Sphingomonas* were enriched on biodegradable plastic mulch in comparison to conventional LDPE mulches.

## 5. Conclusion

This study has significantly contributed to expanding our understanding of the plastic-associated microbial communities in agricultural systems. It stands by providing a detailed methodology to disentangle the microbial communities at the soil-plastic interface, particularly at a small spatial scale, through the distinct assessment of the 'plasticplane' and 'plastisphere' microbiomes.

This research focused on developing a methodology to unravel and compare the assemblage of the plasticplane and plastisphere-soil microbiome, emphasizing taxonomic profiling, with less attention given to functional characterization. Nevertheless, this methodology could be applied to develop further research focusing on functional approaches, which can offer valuable insights into microbial mechanisms, metabolic activities, and enzymatic functions associated with plastic biodegradation.

Our findings reveal that the plastic surface can host taxa that are consistently present on the plasticplane across different field sites. This suggests the existence of a core microbial community with a strong affinity for plastic surfaces, regardless of the specific field site. Moreover, it has been shown that geographical constraints can play a significant role in shaping both the microbial community of the soil and therefore that of the plastic interacting with it. Additives can also influence the associated microbial community, prompting the need for further detailed evaluations.

Finally, this study serves as a foundational basis for future research, particularly in the characterization of potential microbial degraders. Thus, some key bacterial genera closely associated with the plastic debris identified in this study included *Bacillus, Nocardioides, Solirubrobacter,* and *Sphingomonas*. These taxa could be pivotal in assessing their ability to degrade not only LDPE plastics but also various other polymer-based materials, thereby contributing to the global effort to tackle plastic pollution.

## CRediT authorship contribution statement

**Giovana P.F. Macan:** Writing – review & editing, Writing – original draft, Visualization, Validation, Methodology, Investigation, Formal analysis, Data curation, Conceptualization. **Manuel Anguita-Maeso:** Writing – review & editing, Writing – original draft, Visualization, Validation, Methodology, Formal analysis, Data curation,

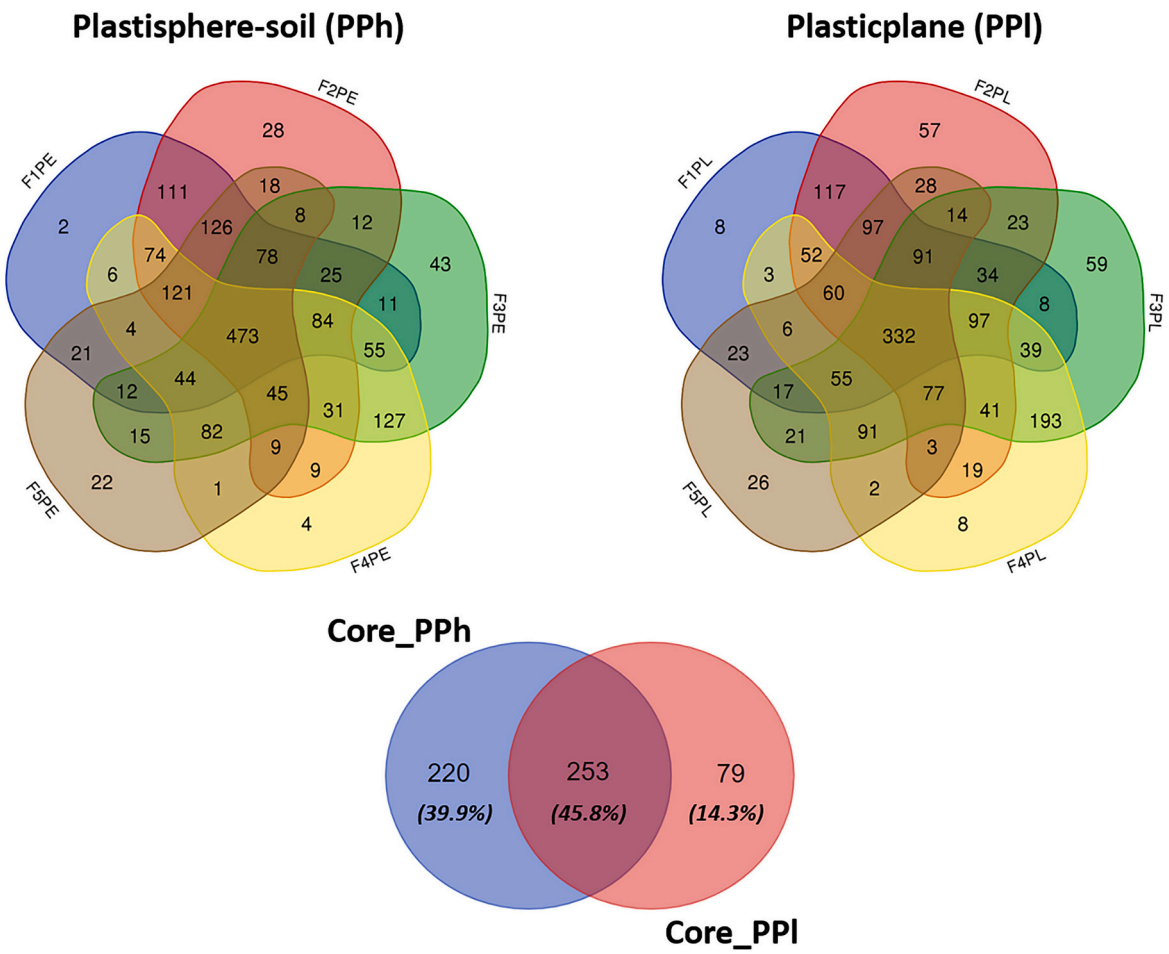


**Fig. 7.** Venn diagrams comparing the observed shared and unique ASVs on the plastisphere soil (PPh) and plasticplane (PPl) found in each of the evaluated field plots and plastic compartments. Colors represent the field from which the samples were collected, and the numbers represent the number of shared or unique ASVs found.

Conceptualization. **Concepción Olivares-García:** Methodology, Data curation. **Quynh Nhu Phan Le:** Writing – review & editing, Methodology, Data curation. **Crispin Halsall:** Writing – review & editing, Supervision, Project administration, Funding acquisition. **Blanca B. Landa:** Writing – review & editing, Writing – original draft, Supervision, Project administration, Funding acquisition, Formal analysis, Conceptualization.

## Declaration of competing interest

The authors declare that they have no known competing financial interests or personal relationships that could have appeared to influence the work reported in this paper.

## Acknowledgements

We would like to acknowledge the financial support from the European Union's Horizon 2020 research and innovation programme under the Marie Skłodowska-Curie grant agreement No 955334 SOPLAS and the Qualifica Project QUAL21-023IAS, Consejeria de Universidad, Investigación y Inovación-Junta de Andalucía. We also thank Pablo Castillo and Ilenia Clavero-Camacho for providing their stereomicroscope and for their assistance with its use and image analysis, respectively.

## Appendix A. Supplementary data

Supplementary data to this article can be found online at https://doi.org/10.1016/j.apsoil.2025.105900.

## Data availability

Data will be made available on request.

## References

Altschul, S.F., Madden, T.L., Schäffer, A.A., Zhang, J., Zhang, Z., Miller, W., Lipman, D.J., 1997. Gapped Blast and PSI-Blast: a new generation of protein database search programs. Nucleic Acids Res. 25, 3389–3402. https://doi.org/10.1093/nar/25.17.3389.

Amaral-Zettler, L.A., Zettler, E.R., Mincer, T.J., 2020. Ecology of the plastisphere. Nat. Rev. Microbiol. 18, 139–151. https://doi.org/10.1038/s41579-019-0308-0.

Anguita-Maeso, M., Haro, C., Navas-Cortés, J.A., Landa, B.B., 2022. Primer choice and xylem-microbiome-extraction method are important determinants in assessing xylem bacterial community in olive trees. Plants 11, 1320. https://doi.org/10.3390/plants11101320.

Anwar, M.S., Kapri, A., Chaudhry, V., Mishra, A., Ansari, M.W., Souche, Y., Nautiyal, C. S., Zaidi, M.G.H., Goel, R., 2016. Response of indigenously developed bacterial consortia in progressive degradation of polyvinyl chloride. Protoplasma 253, 1023–1032. https://doi.org/10.1007/s00709-015-0855-9.

Bandopadhyay, S., Liquet y González, J.E., Henderson, K.B., Anunciado, M.B., Hayes, D. G., DeBruyn, J.M., 2020. Soil microbial communities associated with biodegradable plastic mulch films. Front. Microbiol. 11, 587074. https://doi.org/10.3389/FMICB.2020.587074.

Bardají, D.K.R., Furlan, J.P.R., Stehling, E.G., 2019. Isolation of a polyethylene degrading Paenibacillus sp. from a landfill in Brazil. Arch. Microbiol. 201, 699–704. https://doi.org/10.1007/s00203-019-01637-9.

Barillot, C.D.C., Sarde, C.O., Bert, V., Tarnaud, E., Cochet, N., 2013. A standardized method for the sampling of rhizosphere and rhizoplan soil bacteria associated to a herbaceous root system. Ann. Microbiol. 63, 471–476. https://doi.org/10.1007/s13213-012-0491-y.

Bläsing, M., Amelung, W., 2018. Plastics in soil: analytical methods and possible sources. Sci. Total Environ. 612, 422–435. https://doi.org/10.1016/j.scitotenv.2017.08.086.
Brown, R.W., Chadwick, D.R., Thornton, H., Marshall, M.R., Bei, S., Distaso, M.A., Bargiela, R., Marsden, K.A., Clode, P.L., Murphy, D.V., Pagella, S., Jones, D.L., 2022. Field application of pure polyethylene microplastic has no significant short-term effect on soil biological quality and function. Soil Biol. Biochem. 165, 108496. https://doi.org/10.1016/j.soilbio.2021.108496.
Callahan, B.J., McMurdie, P.J., Rosen, M.J., Han, A.W., Johnson, A.J.A., Holmes, S.P., 2016. DADA2: high-resolution sample inference from Illumina amplicon data. Nat. Methods. 13, 581–583. https://doi.org/10.1038/nmeth.3869.
Cao, Y., Dong, Q., Wang, D., Zhang, P., Liu, Y., Niu, C., 2022. MicrobiomeMarker: an R/Bioconductor package for microbiome marker identification and visualization. Bioinformatics 38, 4027–4029. https://doi.org/10.1093/bioinformatics/btac438.
De Souza Machado, A.A., Lau, C.W., Till, J., Kloas, W., Lehmann, A., Becker, R., Rillig, M. C., 2018. Impacts of microplastics on the soil biophysical environment. Environ. Sci. Tech. 52, 9656–9665. https://doi.org/10.1021/acs.est.8b02212.
Dhaka, V., Singh, S., Ramamurthy, P.C., Samuel, J., Naik, Swamy Sunil Kumar, T., Khasnabis, S., Prasad, R., & Singh, J., 2022. Biological degradation of polyethylene terephthalate by rhizobacteria. Environ. Sci. Pollut. Res. 30, 116488–116497. https://doi.org/10.1007/s11356-022-20324-9.
Di Pippo, F., Venezia, C., Sighicelli, M., Pietrelli, L., Di Vito, S., Nuglio, S., Rossetti, S., 2020. Microplastic-associated biofilms in lentic Italian ecosystems. Water Res. 187, 116429. https://doi.org/10.1016/j.watres.2020.116429.
El-Sherif, D.M., Eloffy, M.G., Elmesery, A., Abouzid, M., Gad, M., El-Seedi, H.R., Brinkmann, M., Wang, K., Al Naggar, Y., 2022. Environmental risk, toxicity, and biodegradation of polyethylene: a review. Environ. Sci. Pollut. Res. 29, 81166–81182. https://doi.org/10.1007/s11356-022-23382-1.
FAO, 2021. Assessment of Agricultural Plastics and their Sustainability: A Call for Action. UN Food and Agriculture Organization (FAO), Rome. https://www.fao.org/policy-support/tools-and-publications/resources-details/en/c/1460015/ (accessed 24 Jun 2024).
Foster, R.C., 1986. The ultrastructure of the rhizoplane and rhizosphere. Annu. Rev. Phytopathol. 24, 211–234. https://doi.org/10.1146/annurev.py.24.090186.001235.
Garbeva, P., Van Veen, Van Elsas, J.D., 2004. Microbial diversity in soil: selection of microbial populations by plant and soil type and implications for disease suppressiveness. Annu. Rev. Phytopathol. 42, 243–270. https://doi.org/10.1146/annurev.phyto.42.012604.135455.
Ge, Y., Schimel, J.P., Holden, P.A., 2011. Evidence for negative effects of TiO2 and ZnO nanoparticles on soil bacterial communities. Environ. Sci. Tech. 45, 1659–1664. https://doi.org/10.1021/es103040t.
Ge, Y., Schimel, J.P., Holdena, P.A., 2012. Identification of soil bacteria susceptible to TiO2 and ZnO nanoparticles. Appl. Environ. Microbiol. 78, 6749–6758. https://doi.org/10.1128/AEM.00941-12.
Ge, Y., Priester, J.H., Van De Werfhorst, L.C., Schimel, J.P., Holden, P.A., 2013. Potential mechanisms and environmental controls of TiO2 nanoparticle effects on soil bacterial communities. Environ. Sci. Tech. 47, 14411–14417. https://doi.org/10.1021/es403385c.
Gkoutselis, G., Rohrbach, S., Harjes, J., Obst, M., Brachmann, A., Horn, M.A., Rambold, G., 2021. Microplastics accumulate fungal pathogens in terrestrial ecosystems. Sci. Rep. 11, 13214. https://doi.org/10.1038/s41598-021-92405-7.
Gobbetti, M., Rizzello, C.G., 2014. Arthrobacter. In: Batt, C.A., Tortorello, M.L. (Eds.), Encyclopedia of Food Microbiology. Academic Press, Cambridge, MA, pp. 69–76. https://doi.org/10.1016/B978-0-12-384730-0.00009-4.
Han, Y.N., Wei, M., Han, F., Fang, C., Wang, D., Zhong, Y.J., Li, F.M., 2020. Greater biofilm formation and increased biodegradation of polyethylene film by a microbial consortium of Arthrobacter sp. and Streptomyces sp. Microorganisms 8, 1979. https://doi.org/10.3390/microorganisms8121979.
Harshvardhan, K., Jha, B., 2013. Biodegradation of low-density polyethylene by marine bacteria from pelagic waters, Arabian Sea. India. Mar. Pollut. Bull. 77, 100–106. https://doi.org/10.1016/j.marpolbul.2013.10.025.
Hiejima, Y., Kida, T., Takeda, K., Igarashi, T., Nitta, K., hei., 2018. Microscopic structural changes during photodegradation of low-density polyethylene detected by Raman spectroscopy. Polym. Degrad. Stab. 150, 67–72. https://doi.org/10.1016/j.polymdegradstab. 2018.02.010.
Huang, Y., Liu, Q., Jia, W., Yan, C., Wang, J., 2020. Agricultural plastic mulching as a source of microplastics in the terrestrial environment. Environ. Pollut. 260, 114096. https://doi.org/10.1016/j.envpol.2020.114096.
Jeszeová, L., Puškárová, A., Bučková, M., Kraková, L., Grivalský, T., Danko, M., Mosnáčková, K., Chmela, Š., Pangallo, D., 2018. Microbial communities responsible for the degradation of poly(lactic acid)/poly(3-hydroxybutyrate) blend mulches in soil burial respirometric tests. World J. Microbiol. Biotechnol. 34, 1–12. https://doi.org/10.1007/s11274-018-2483-y.
Li, K., Jia, W., Xu, L., Zhang, M., Huang, Y., 2023b. The plastisphere of biodegradable and conventional microplastics from residues exhibit distinct microbial structure, network and function in plastic-mulching farmland. J. Hazard. Mater. 442, 130011. https://doi.org/10.1016/j.jhazmat.2022.130011.
Li, Y., Hou, Y., Hou, Q., Long, M., Yang, Y., Wang, Z., Liao, Y., 2023a. Long-term plastic mulching decreases rhizoplane soil carbon sequestration by decreasing microbial anabolism. Sci. Total Environ. 868, 161713. https://doi.org/10.1016/j.scitotenv.2023.161713.
Luo, G., Zhu, Q., Jin, T., Peng, J., Zuo, N., Zhang, H., Geng, M., Huang, Y., Han, Y., Tian, C., Yang, Y., Fei, J., 2023. Crop types and irrigation regimes as drivers of plastisphere bacterial communities in plastic-mulching croplands of subtropical China. Appl. Soil Ecol. 182, 104696. https://doi.org/10.1016/j.apsoil.2022.104696.
Ma, Y., Wang, J., Liu, Y., Wang, X., Zhang, B., Zhang, W., Chen, T., Liu, G., Xue, L., Cui, X., 2023. Nocardioides: "specialists" for hard-to-degrade pollutants in the environment. Molecules 28, 7433. https://doi.org/10.3390/molecules28217433.
Macan, G.P.F., Munhoz, D.R., Willems, L.A.J., Monkley, C., Lloyd, C.E.M., Hageman, J., Geissen, V., Landa, B.B., Harkes, P., 2024. Macro- and microplastics leachates: characterization and impact on seed germination. J. Hazard. Mater. 480, 136013. https://doi.org/10.1016/J.JHAZMAT.2024.136013.
Mangiafico, S., 2022. Rcompanion: functions to support extension education program evaluation. R Package Version 2.4.13 [Computer software]. https://CRAN.R-project.org/package=rcompanion.
Meier, R.J., 2002. Studying the length of trans conformational sequences in polyethylene using Raman spectroscopy: a computational study. Polymer 43, 517–522. https://doi.org/10.1016/S0032-3861(01)00416-5.
Meng, F., Harkes, P., van Steenbrugge, J.J.M., Geissen, V., 2023. Effects of microplastics on common bean rhizosphere bacterial communities. Appl. Soil Ecol. 181, 104649. https://doi.org/10.1016/j.apsoil.2022.104649.
Mwajita, M.R., Murage, H., Tani, A., Kahangi, E.M., 2013. Evaluation of rhizosphere, rhizoplane and phyllosphere bacteria and fungi isolated from rice in Kenya for plant growth promoters. SpringerPlus 2, 1–9. https://doi.org/10.1186/2193-1801-2-606.
Philippot, L., Raaijmakers, J.M., Lemanceau, P., Van der Putten, W.H., 2013. Going back to the roots: the microbial ecology of the rhizosphere. Nat. Rev. Microbiol. 11, 789–799. https://doi.org/10.1038/nrmicro3109.
Priya, A., Dutta, K., Daverey, A., 2022. A comprehensive biotechnological and molecular insight into plastic degradation by microbial community. J. Chem. Technol. Biotechnol. 97, 381–390. https://doi.org/10.1002/JCTB.6675.
Puglisi, E., Romaniello, F., Galletti, S., Boccaleri, E., Frache, A., Cocconcelli, P.S., 2019. Selective bacterial colonization processes on polyethylene waste samples in an abandoned landfill site. Sci. Rep. 9, 14138. https://doi.org/10.1038/s41598-019-50740-w.
R Core Team, 2013. R: A Language and Environment for Statistical Computing.
Rillig, M.C., Kim, S.W., Zhu, Y.G., 2023. The soil plastisphere. Nat. Rev. Microbiol. 22, 64–74. https://doi.org/10.1038/s41579-023-00967-2.
Rüthi, J., Bölsterli, D., Pardi-Comensoli, L., Brunner, I., Frey, B., 2020. The "Plastisphere" of biodegradable plastics is characterized by specific microbial taxa of alpine and Arctic soils. Front. Environ. Sci. 8, 173. https://doi.org/10.3389/fenvs.2020.562263.
Saccá, M.L., Caracciolo, A.B., Lenola, M.Di, Grenni, P., Saccá, M.L., Caracciolo, A.B., Lenola, M., Di, Grenni, 2017. Ecosystem services provided by soil microorganisms. In: Lukac, M., Grenni, P., Gamboni, M. (Eds.), Soil Biological Communities and Ecosystem Resilience. Springer, Cham, pp. 9–24. https://doi.org/10.1007/978-3-319-63336-7_2.
Sangeetha Devi, R., Ramya, R., Kannan, K., Robert Antony, A., Rajesh Kannan, V., 2019. Investigation of biodegradation potentials of high density polyethylene degrading marine bacteria isolated from the coastal regions of Tamil Nadu, India. Mar. Pollut. Bull. 138, 549–560. https://doi.org/10.1016/j.marpolbul.2018.12.001.
Schlundt, C., Mark Welch, J.L., Knochel, A.M., Zettler, E.R., Amaral-Zettler, L.A., 2020. Spatial structure in the "Plastisphere": molecular resources for imaging microscopic communities on plastic marine debris. Mol. Ecol. Resour. 20, 620–634. https://doi.org/10.1111/1755-0998.13119.
Segata, N., Izard, J., Waldron, L., Gevers, D., Miropolsky, L., Garrett, W.S., Huttenhower, C., 2011. Metagenomic biomarker discovery and explanation. Genome Biol. 12, 1–18. https://doi.org/10.1186/gb-2011-12-6-r60.
Sharma, H., Neelam, D.K., 2023. Understanding challenges associated with plastic and bacterial approach toward plastic degradation. J. Basic Microbiol. 63, 292–307. https://doi.org/10.1002/jobm.202200428.
Shwed, P.S., Crosthwait, J., Weedmark, K., Hoover, E., Dussault, F., 2021. Complete genome sequences of Priestia megaterium type and clinical strains feature complex plasmid arrays. Microbiol. Resour. Announc. 10, 10-1128. https://doi.org/10.1128/mra.00403-21.
Takaku, H., Kimoto, A., Kodaira, S., Nashimoto, M., Takagi, M., 2006. Isolation of a gram-positive poly(3-hydroxybutyrate) (PHB)-degrading bacterium from compost, and cloning and characterization of a gene encoding PHB depolymerase of Bacillus megaterium N-18-25-9. FEMS Microbiol. Lett. 264, 152–159. https://doi.org/10.1111/J.1574-6968.2006.00448.X.
Turner, A., Filella, M., 2023. The role of titanium dioxide on the behaviour and fate of plastics in the aquatic environment. Sci. Total Environ. 869, 161727. https://doi.org/10.1016/j.scitotenv.2023.161727.
van Schothorst, B., Beriot, N., Huerta Lwanga, E., Geissen, V., 2021.. Sources of light density microplastic related to two agricultural practices: the use of compost and plastic mulch. Environments 8, 36. https://doi.org/10.3390/environments8040036.
Vethaak, A.D., Leslie, H.A., 2016. Plastic debris is a human health issue. Environ. Sci. Tech. 50, 6825–6826. https://doi.org/10.1021/acs.est.6b02569.
Vidal-Verdú, À., Latorre-Pérez, A., Molina-Menor, E., Baixeras, J., Peretó, J., Porcar, M., 2022. Living in a bottle: Bacteria from sediment-associated Mediterranean waste and potential growth on polyethylene terephthalate. MicrobiologyOpen 11, e1259. https://doi.org/10.1002/mbo3.1259.
Wang, P., Liu, J., Han, S., Wang, Y., Duan, Y., Liu, T., Hou, L., Zhang, Z., Li, L., Lin, Y., 2023. Polyethylene mulching film degrading bacteria within the plastisphere: co-culture of plastic degrading strains screened by bacterial community succession. J. Hazard. Mater. 442, 130045. https://doi.org/10.1016/j.jhazmat.2022.130045.
Weisburg, W.G., Barns, S.M., Pelletier, D.A., Lane, D.J., 1991. 16S ribosomal DNA amplification for phylogenetic study. J. Bacteriol. 173, 697–703. https://doi.org/10.1128/jb.173.2.697-703.1991.
Wieland, G., Neumann, R., Backhaus, H., 2001. Variation of microbial communities in soil, rhizosphere, and rhizoplane in response to crop species, soil type, and crop

development. Appl. Environ. Microbiol. 67, 5849–5854. https://doi.org/10.1128/AEM.67.12.5849-5854.2001.

Wróbel, M., Szymańska, S., Kowalkowski, T., Hrynkiewicz, K., 2023. Selection of microorganisms capable of polyethylene (PE) and polypropylene (PP) degradation. Microbiol. Res. 267, 127251. https://doi.org/10.1016/j.micres.2022.127251.

Wu, C., Ma, Y., Wang, D., Shan, Y., Song, X., Hu, H., Ren, X., Ma, X., Cui, J., Ma, Y., 2022. Integrated microbiology and metabolomics analysis reveal plastic mulch film residue affects soil microorganisms and their metabolic functions. J. Hazard. Mater. 423, 127258. https://doi.org/10.1016/j.jhazmat.2021.127258.

Ya, H., Xing, Y., Zhang, T., Lv, M., Jiang, B., 2022. LDPE microplastics affect soil microbial community and form a unique plastisphere on microplastics. Appl. Soil Ecol. 180, 104623. https://doi.org/10.1016/j.apsoil.2022.104623.

Yao, Z., Seong, H.J., Jang, Y.S., 2022. Degradation of low density polyethylene by Bacillus species. Appl. Biol. Chem. 65, 1–9. https://doi.org/10.1186/s13765-022-00753-3.

Yu, H., Zhang, Y., Tan, W., 2021. The "neighbor avoidance effect" of microplastics on bacterial and fungal diversity and communities in different soil horizons. Environ. Sci. and Ecotechnol. 8, 100121. https://doi.org/10.1016/j.ese.2021.100121.

Zettler, E.R., Mincer, T.J., Amaral-Zettler, L.A., 2013. Life in the "plastisphere": microbial communities on plastic marine debris. Environ. Sci. Tech. 47, 7137–7146. https://doi.org/10.1021/es401288x.

Zhang, D., Ng, E.L., Hu, W., Wang, H., Galaviz, P., Yang, H., Sun, W., Li, C., Ma, X., Fu, B., Zhao, P., Zhang, F., Jin, S., Zhou, M., Du, L., Peng, C., Zhang, X., Xu, Z., Xi, B., Liu, H., 2020. Plastic pollution in croplands threatens long-term food security. Glob. Chang. Biol. 26, 3356–3367. https://doi.org/10.1111/gcb.15043.

Zhang, Y., Ma, J., Song, Y.Q., Li, G., O'Connor, P., 2024. Stronger deterministic processes shape the plastisphere microbiota of biodegradable microplastics compared to non-biodegradable microplastics in farmland soil. Appl. Soil Ecol. 196, 105312. https://doi.org/10.1016/j.apsoil.2024.105312.

Zhao, S., Liu, R., Wang, J., Lv, S., Zhang, B., Dong, C., Shao, Z., 2023. Biodegradation of polyethylene terephthalate (PET) by diverse marine bacteria in deep-sea sediments. Environ. Microbiol. 25, 2719–2731. https://doi.org/10.1111/1462-2920.16460.